Sloshing in rectangular tanks and interaction with ship motions

Dr.ing. thesis

Olav Rognebakke

Trondheim, February 14, 2002

Department of Marine Hydrodynamics
Faculty of Engineering Science and Technology
Norwegian University of Science and Technology

URN:NBN:no-2322

Abstract

Sloshing is a violent resonant free surface flow in a container. The main objective of this thesis has been to study sloshing in rectangular and prismatic tanks. The tank may be excited by a harmonic motion or it may move with a ship in waves. In the latter case, the coupled ship motions and sloshing problem is investigated. A nonlinear analytically based sloshing model is used in the sloshing calculations. Experiments have been conductedand collected data are utilized in the validation of the sloshing model and computations of interaction between sloshing and ship dynamics. Tank roof impacts are studied. Energy in the impact jet is dissipated and this leads to damping of the sloshing motion. An iterative procedure is applied to incorporate the effect of energy dissipation in the calculations. Damping of the sloshing motion is an important parameter around resonance for the coupled ship motion and sloshing system.

The sloshing model is based on a nonlinear modal theory analysis of two-dimensional nonlinear sloshing of an incompressible fluid with irrotational flow in a rectangular tank. Infinite tank roof height and no overturning waves are assumed. The free surface is expressed as a Fourier series and the velocity potential is expanded in terms of the linear natural modes of the fluid motion. The infinite-dimensional modal system is approximated and the result is a finite set of ordinary differential equations in time for generalized coordinates (Fourier coefficients) of the free surface. This theory is not valid for small water depth or when water impacts heavily on the tank roof. The proposed method has a high computational efficiency, facilitates simulations of a coupled vehicle-fluid system and has been extensively validated for forced motions.

Experiments with a smooth, rectangular tank excited by forced harmonic horizontal oscillations have been performed and the results are used to validate the analytical sloshing model. Transients and associated nonlinear modulation of the waves, beating, are important due to the low level of damping of the fluid motion. The measured parameters are the motion of the tank and the free surface elevation at three positions. Pictures and video are used to study local flow details and the dynamics of the flow. At excitation periods in the vicinity of the first natural period for the fluid motion in the tank, even small motion amplitudes lead to violent sloshing and impacts between the rising water surface and the tank roof.

Impacts cause high pressures and forces. The effect of slamming in the tank is included by a local analysis interacting with the nonlinear sloshing model. A Wagner based method is used

to find the flow induced by slamming. Hydroelastic effects are ignored. The hypothesis that the kinetic and potential energy in the jet flow caused by the impact is dissipated when the jet flow hits the free surface, enables a rational calculation of the damping effect of impacts on the sloshing flow. The Wagner approach requires a small angle between the impacting free surface and the tank roof. A correction by a similarity solution, or alternatively, by a generalization of Wagner's theory valid for larger angles is applied when this is not the case. Since analytically based methods are used, fluid impact load predictions are robust.

A coupled ship motion and sloshing system is studied both experimentally and theoretically. Two-dimensional experiments on a box-shaped ship section excited by regular beam sea have been conducted. The section contains two tanks and can only move in sway. Fluid motion inside the tanks has a large effect on the sway motion response of the section. Simulations of a corresponding system are performed by assuming a mainly linear external flow and applying the nonlinear sloshing model. The linear external hydrodynamic loads due to body motion are expressed in terms of a convolution integral representing the history of the fluid motion. A detailed numerical study of how to accurately incorporate the convolution integral is presented. A good agreement between experimental and numerical sway motion of the ship section is reported. The calculated coupled motion is sensitive to the damping of the sloshing motion in a certain frequency range where the coupled sloshing and ship motions cause resonant ship motions. A quasi-linear frequency domain analysis is used to explain this by introducing the sloshing loads as a frequency dependent spring.

Acknowledgements

This work has been carried out under the supervision of Professor Odd M. Faltinsen at the Department of Marine Hydrodynamics, Norwegian University of Science and Technology. He has shown great interest in this work, and I am sincerely grateful for all the attention, both professional and personal, he has shown me. A tight schedule notwithstanding, he has always found time to contribute with new ideas and solutions.

I am indebted to Florus Korbijn for his help in arranging the experiments conducted at Det Norske Veritas, Høvik. Florus has an impressive physical understanding of sloshing and our discussions during my many stays at DNV have been fruitful. The Department of Hydrodynamics and Stability at DNV has been most helpful in providing an office desk and PC whenever I asked for it.

A special thank goes to Professor Bjørnar Pettersen, Guttorm Grytøyr and Pål Lader who all inspired me to start this Dr.ing. study .

It has been great fun to discuss various topics with Rolf Baarholm. Particularly I appreciate us working together in preparing for exams during the first two years.

I have enjoyed every bit of this study. The Department of Marine Hydrodynamics and Department of Marine Structures are characterized by a friendly and pleasant atmosphere. I extend my deepest gratitude towards the staff and my fellow Dr.ing. students for being their excellent selves and helping to create and maintain this nice environment. I especially want to thank Gro S. Baarholm, Eirik Byklum, Svein Ersdal, Arne Fredheim, Marilena Greco, Herbjørn Haslum, Odd Kristensen, Marit Ronæss and Rune Tønnesen.

My love and gratitude goes to Hanne Wist. Her love, support and encouragement have provided me with more energy than ever.

This work was supported financially by the Research Council of Norway.

Contents

Chapter 1

Introduction

Sloshing is a violent resonant free surface flow with strong nonlinear behaviour in a partially filled container. Sloshing in ship tanks is of prime interest in this study . Ideal fluid effects dominate the global motion, so that the fluid can be considered incompressible and the flow irrotational. However,this does not mean that dissipative non-potential flow is unimportant. The fluid motion inside a tank has according to potential flow theory an infinite number of natural periods. The main focus is on excitation with frequency content in the vicinity of the highest natural period. The corresponding linear mode of motion for a rectangular tank is an anti-symmetric standing wave with wave length twice the tank length. Lateral and angular tank motions cause the largest fluid response in the frequency range of interest.

The tank shape, the level of filling and the characteristics of the tank motion, for example amplitude and frequency content, make up the principal parameters that determine the nature of the free surface flow. The relative importance of the different parameters depends on the characteristics of the flow, i.e. the response. There is a dramatic difference between sloshing in a shallow liquid condition and higher filling level conditions. For small ratios between fluid depth and tank length and an excitation frequency around resonance, a hydraulic jump or bore, which travels back and forth in the tank, is formed. When the steep front of the bore hits the tank wall, an impact occurs and a thin vertical jet shoots upwards. This effect is referred to as run-up along the wall. When the liquid depth is non-shallow, the free surface motion resembles a standing wave.

Swirling or rotational flow is a special feature of three-dimensional flow and is caused by an instability of the anti-symmetric lateral sloshing mode. A motion of the tank normal to the undisturbed free surface may excite symmetric modes, but since the highest sloshing period is of prime interest, vertical tank excitation is of secondary importance.

Sloshing must be considered for almost any moving vehicle or structure containing a fluid with a free surface. The design of both the container and supporting structure will therefore be influenced.

Resonant free surface flows in tanks in aircrafts, missiles and rockets have been the focus of much research. For these vehicles, sloshing will have a strong influence on the dynamic stability. Sloshing in separators on-board floating oil and gas production platforms will affect the efficiency of gravity separators. Structures fixed onshore may be exposed to sloshing if an earthquake occurs (Fischer and Rammerstorfer (1999)). Large scale sloshing in a lake with steep sides may be the result of a landslide or earthquake. Under dam construction such circumstances should be factors to investigate. Large scale sloshing may also occur in harbours. Bruun (1976) presents modes of free oscillation with corresponding eigenperiods in semi-enclosed basins of different geometrical shapes. Shallow water sloshing in a container can be used to dampen out wind induced motions of tall buildings. A tuned liquid damper, TLD, is a well known concept in the civil engineering world (Fujino et al. (1992); Modi and Seto (1997)).

Ocean-going vessels experience wave induced motions, and thus sloshing is likely to be excited. Figure 1.1 from Faltinsen, Olsen, Abramson, and Bass (1974) illustrates a family of sway acceleration spectra corresponding to several sea state conditions which may occur. The figure also shows that differently sized tanks with different filling levels yield peak response amplitudes within the range of sway periods to be expected. An increased tank size increases the highest natural period of the fluid flow. As a consequence, higher sea states and larger ship motions excite sloshing around resonance. Figure 1.2 gives the natural period of the first sloshing mode for a rectangular tank (Olsen (1976)). In general the severity of sloshing is a function of the configuration of internal structures obstructing the flow in the tank. Internal structures act as dampers of the fluid motions.

Sloshing has always been an important design criterion for oil tankers, even if partial filling is rare in actual operation. Environmental concerns have led to requirements about double hull tankers. Ship owners try to avoid internal structures in cargo tanks for cleaning reasons. The resulting wide and smooth oil tanks increase the probability of severe sloshing. Sloshing is also of concern for Floating Production Storage and Offloading (FPSO) units and shuttle tankers. The severity of sloshing is connected to possible filling height restrictions for oil tankers, gas carriers, shuttle tankers and FPSOs. Often, operators require no restrictions on filling heights to achieve loading flexibility. Since ballast exchange is required outside the port for a bulk carrier, there are possibilities for sloshing damages. Particularly the hatch cover is vulnerable. Hansen (1976) reports damages due to sloshing in bulk carriers, combination Oil-Bulk-Ore (OBO) carriers and LNG carriers. These are characterized by large and smooth tanks. Partial fillings in LNG carriers are a consequence of gas boil-off during operation.

A ship carrying liquid cargo in partially filled tanks in waves may experience violent sloshing. The ship motions excite sloshing, which in return affects the ship motions. Ships equipped with anti-rolling tanks (ARTs) utilize this effect.

FPSOs sometimes have several partially filled tanks during operation. The wave induced motions and loads on these ships will then be influenced by the dynamic motion of the fluid in the tanks. Since ship motions can strongly affect the wavedrift forces and moments, sloshing may also

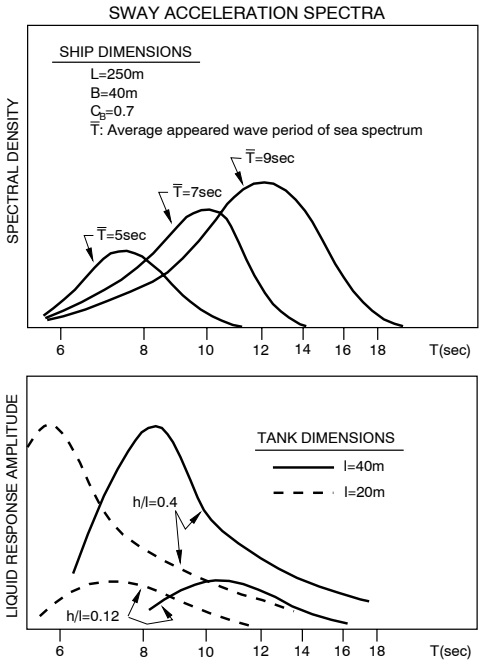

Figure 1.1: Ship motion and transfer function of sloshing response (lateral force) versus period of oscillation (Faltinsen et al. (1974))

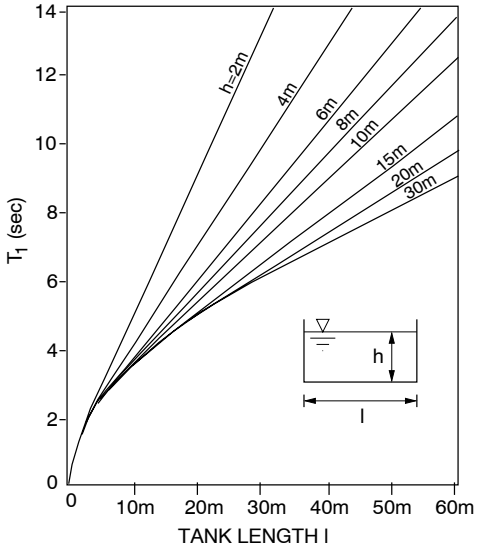

Figure 1.2: First mode natural sloshing periods for a rectangular tank (Olsen (1976))

matter in a station-keeping analysis.

The hydrodynamic loading inside a tank can be classified either as impact loads or 'dynamic', non-impulsive, loads. In this context dynamic loads mean loads that have dominant time variations on the time scale of the sloshing period, while impact loads may last only from 10^{-3} to 10^{-2} seconds. Sloshing loads are of significance for both fatigue and ultimate strength. Figure 1.3 lists different load categories. This figure is based on a discussion of loading types presented by Olsen (1976), as a part of a seminar on sloshing held by Det Norske Veritas.

Local structural response due to fluid impact is an important response variable. Loads on possible internal structures must be considered. Some internal structures like a horizontal stringer on the wall or web-frame at the tank roof, may be in and out of the fluid so that impact loads as well as dynamic loads may matter. Hydroelastic effects are sometimes of importance for impact loads. Total dynamic loads on the tank are of interest in order to estimate tank support reactions and possible global interaction with ship dynamics.

The importance of different physical parameters varies with the type of flow in the tank. As previously mentioned, global fluid motion is dominated by potential flow effects, which have the main influence on the magnitude of the integrated force. Viscosity is of minor importance since the main effect is normally concentrated in thin boundary layers along the tank boundaries. The

boundary layer is often laminar in model scale and turbulent in full scale. If internal structures obstructing the flow are present, flow separation occurs, and rotational flow and turbulence will matter. A turbulent wake behind an internal structural part may interact with another internal structure. Breaking waves and overturning of the free surface due to run-up along the walls or due to fluid impact on the tank roof may cause important dissipation and damping of the global flow. As a part of this study, a high level of sensitivity of the response of a coupled ship motion and sloshing system to the damping of internal fluid flow is reported in a frequency range in the

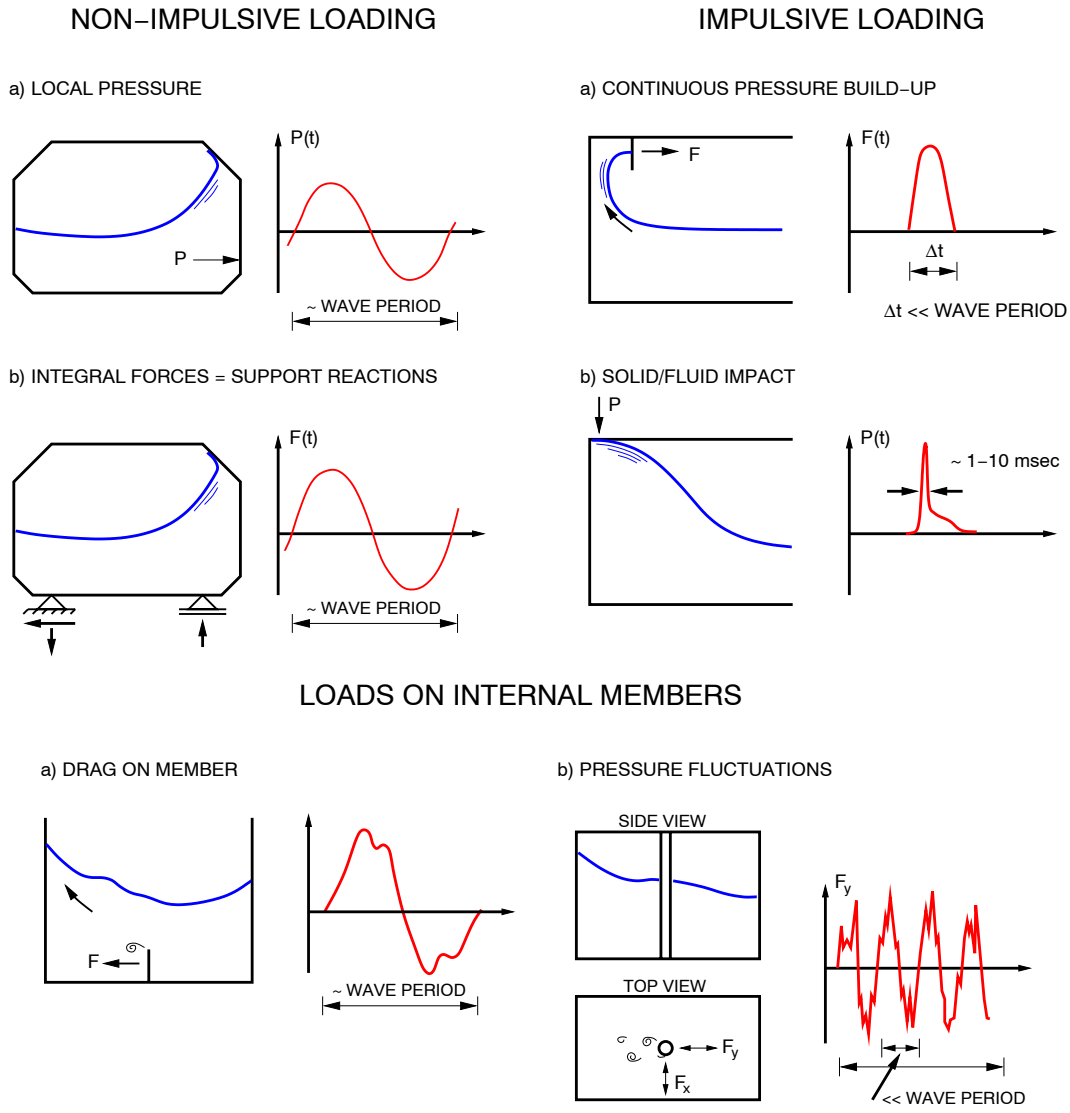

Figure 1.3: Examples of sloshing loads (Olsen (1976))

vicinity of the natural period for the sway motion, which is a result of the sloshing dynamics.

Different physical effects occur during slamming. An air (or gas) cushion may be formed between the fluid and body surface if the initial local impact angle is small. Compressibility influences the airflow which again influences the fluid flow. The air cushion generates air bubbles when it collapses. The ullage pressure influences the presence and behaviour of air bubbles. Local hydrodynamic effects can cause vibrations that trigger ventilation and cavitation. However, when analyzing slamming, one must always have the structural reaction in mind. In a situation where the structural response is caused by physical phenomena that occur on a small time scale relative to the highest local structural natural period, a hydroelastic analysis is essential.

1.1 Properties of linear and nonlinear analytical sloshing models

The classical linear sloshing solution provides the important linear eigenperiod of the free surface motion inside the tank. Unfortunately, the linear solution predicts an infinite free surface motion amplitude at resonance, and cannot be used to find accurate estimates for motion amplitudes and forces in the vicinity of the first linear eigenperiod.

The second order solution presented in Paper 2 exhibits the same behaviour, since the linear solution is an integral part. The response is the same order as the excitation. A solution based on a different ordering scheme is needed to get reasonable results close to resonance.

Faltinsen (1974) presents a nonlinear theory of 2-D steady-state sloshing in rectangular tanks, based on the work of Moiseyev (1958). It is assumed that the excitation period is in the vicinity of the highest (first) linear eigenperiod and that the first eigenmode dominates and is of order $\mathcal{O}(\epsilon^{1/3})$. Here ϵ characterizes the amplitude of the forced horizontal and/or rotational motion of the tank. The solution is found to $\mathcal{O}(\epsilon)$. The final solution resembles the solution of Duffing's equation, see Fig. 1.4. A is the amplitude of the primary sloshing mode and l is the length of the tank. T_1 is the first linear eigenperiod and T_* is the period where the upper stable branch tends to infinity. There may be either one, two or three real values for the amplitude of the primary sloshing mode for a given period of excitation. If three solutions occur, only two are stable. What solution the physical system selects depends on how the period is approached. If in Fig. 1.4 the excitation starts with a low period that is slowly increased, the response will follow the stable upper branch. For some value larger than the period corresponding to the turning point, a jump occurs and the solution is found from the lower stable branch. The period where this jump occurs is dependent on the level of damping in the system, and it cannot be predicted by a model with no damping included. When a large period is the starting point and the period is slowly decreased, the solution follows the lower stable branch until the turning point where it jumps to the upper stable branch.

The largest sloshing response does in general not occur for an excitation period equal to the first linear eigenperiod.

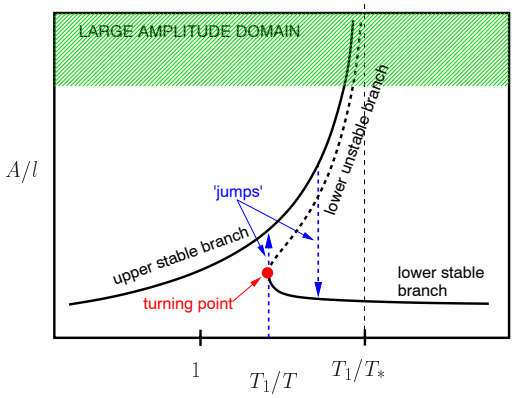

Figure 1.4: Schematic amplitude-frequency response for nonlinear sloshing. A is the amplitude of the primary sloshing mode and l is the length of the tank. T_1 is the first linear eigenperiod and T_* is the period where the upper stable branch tends to infinity

In the third order solution, a special situation arise for a certain filling level, $h/l \approx 0.34$. An infinite response is predicted for a period equal to the first linear eigenperiod. A t this critical filling level the system changes behaviour. When $h/l < 0.34$ a higher excitation amplitude leads to a higher jump frequency and the response behaves like a so-called 'hard-spring'. For a higher filling the response changes to a 'soft-spring'.

As long as the primary mode dominates, the nonlinear analytical methods used throughout this thesis work have similar properties as described above. The branches differ from diagrams obtained by Faltinsen's theory only in the large amplitude domain and far aw ay from the first linear eigenperiod. The differences are due to the asymptotic restriction on the value of the excitation period that is present in Faltinsen's theory. A similar restriction does not apply for the new nonlinear theory in Paper 3. In the multimodal approach, the critical depth is a function of both the filling level and period of excitation.

Figure 1.5 shows the amplitude-frequency response for nonlinear sloshing due to sway excitation when the sloshing model presen tedin Paper 3 is applied. The curve denoted 'O' sho ws the frequency of free nonlinear sloshing as a functiontheofsloshing amplitude. The steady-state amplitude of the sloshing mode is found from from the low er branch P_- or the upper branch P_+ for $|\eta_2/l| = 0.04$.

F altinsen'stheory and the multimodal method of Paper 3 assumes that the primary sloshing mode is dominant. When the depth becomes small with respect to the tank length, more and more modes matter. This is always true for $h/l < 0.24$ and is caused by secondary resonance. Nonlinearities associated with higher harmonic loading excite resonant motions for higher modes. Since the differences betw eenthe linear natural periods decrease with filling lev el, this effect becomes more pronounced with a decreasing depth.

The secondary parametric resonance that can occur for small depths implies that asymptotic

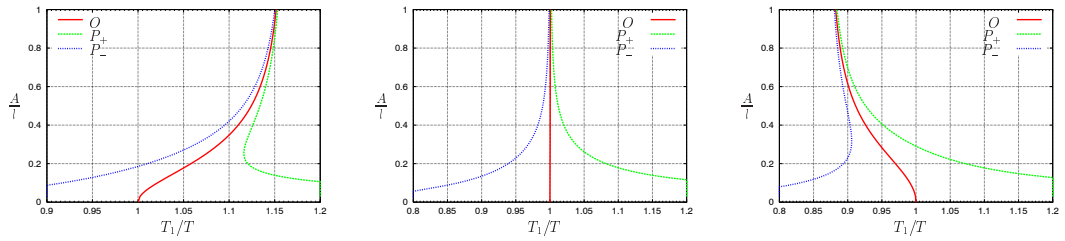

(a) $h/l = 0.25$ (b) Critical depth: $h/l = 0.339$ (c) $h/l = 0.495$

Figure 1.5: Amplitude-frequency response for nonlinear sloshing due to sway excitation. $|\eta_2|/l = 0.04$. A is the amplitude of the primary sloshing mode and l is the length of the tank

theories where one mode is assumed dominant are not applicable for shallow water sloshing.

When initial v aluelinear and nonlinear analytical methods are used to calculate the sloshing response in a smooth tank that has a filling level $h/l > \approx 0.24$ and is excited harmonically in the horizontal direction, the wav es sho w a strong modulation, or beating, if transients are introduced in the start-up of the simulation.

A rectangular smooth tank has an extremely low level of damping in the case of non-shallow sloshing. The damping is mainly associated with dissipation of energy in the viscous boundary layer along the tank wall. A different situation is seen for shallow water sloshing, $h/l < \approx 0.2$. Local wave overturning and breaking, run-up and generation of spray give important contributions to dissipation. Experiments sho w that for small fluid depths steady-state oscillations may be obtained in as few as 2-3 oscillations when the tank is excited by a regular oscillatory motion, while for large depths more than 100 cycles may be necessary to reach this state.

Figure 1.6 shows the free surface elevation at one side of a rectangular tank that is harmonically excited in sw aywith a period $T = 1.11T_1$ where T_1 is the first linear eigenperiod. The ratio betw eenthe filling height and tank length is $h/l = 0.4$ which means non-shallow fluid depth. The dimensionless sway amplitude is $|\eta_2|/l = 0.02$.

Two different sets of initial conditions are used. These are thought to be most representative for the real initial conditions in the sloshing experiments that have been conducted as a part of this w ork. The 'zero' condition implies that the initial free surface is at rest at its mean position. The 'impulse' condition is based on impulse conservation and in this case the free surface is at its mean position but has a given v ertical velocity. The transient beating behaviour is observed for simulations where a linear and a nonlinear sloshing model with no damping is used. Figures 1.6(a) and 1.6(b) show that the envelope is the same regardless of initial conditions and model used, and one may conclude that a change of the initial conditions has a small influence on the response. How ever, a smooth start-up of the system by for instance using a ramp function for the excitation amplitude, decreases the energy contents of the system at the first linear eigenperiod, and the beating effect is diminished. When steady-state sloshing results are sought for a smooth tank, a careful start-up is necessary to avoid a long simulation time or the use of a high artificial

damping.

Figure 1.6(c) shows results for simulations with the nonlinear sloshing model where 'zero' initial conditions are used. In one case a linear ramp function is used to increase the sway amplitude from zero to its maximum value o ver ten oscillation periods.A much smaller beating effect is the result.

Figure 1.6(d) presents the difference in free surface motion for a simulation without damping and a steady-state motion that is the result of a long simulation where damping has been introduced.

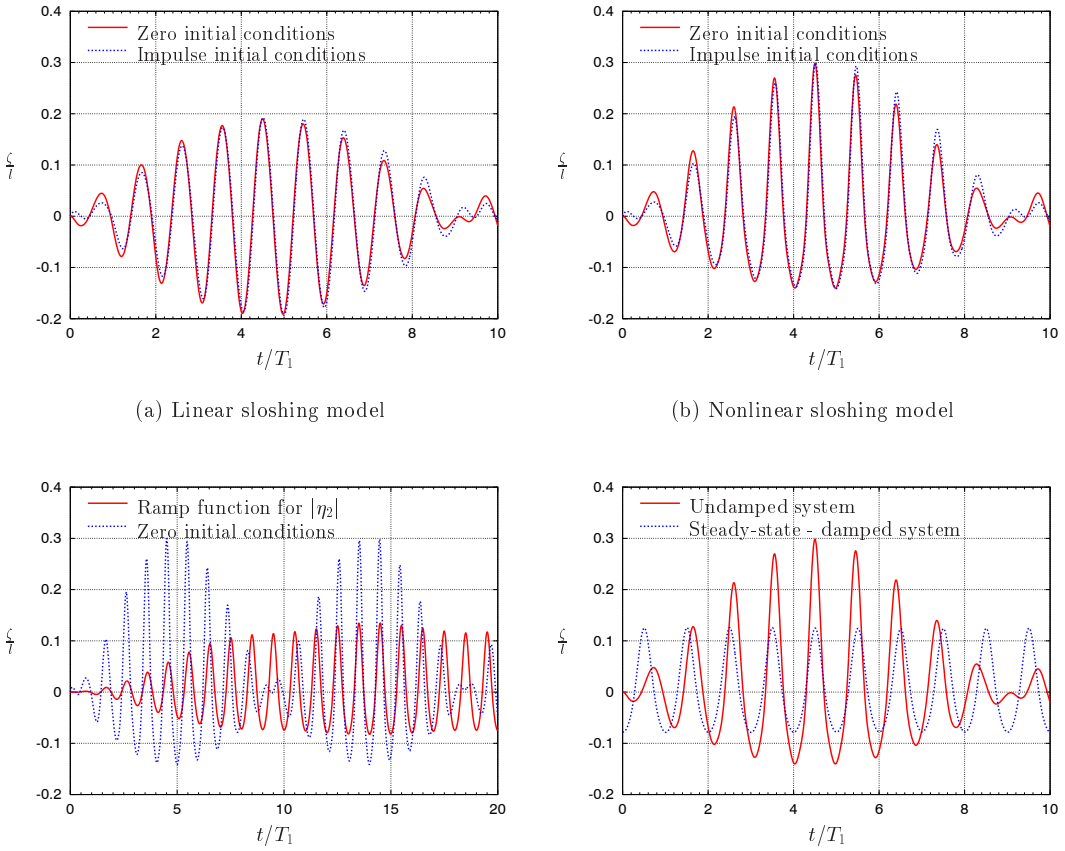

(a) Linear sloshing model

(b) Nonlinear sloshing model

(c) Smooth start-up

(d) Nonlinear sloshing model

Figure 1.6: F ree surface elev ation at the tank w allfor a rectangular tank excited b y regular horizontal motion. $h/l = 0.4$, $T_1/T = 0.9$ and $|\eta_2|/l = 0.02$

1.2 Historical Developments

Sloshing flows have been studied by a large number of researchers who have applied a wide spectrum of different analytical, numerical and experimental approaches. Inherently sloshing is difficult to predict theoretically because it is a highly nonlinear phenomenon with large fluid motions, wave breaking, spray and mixing of e.g. oil and air.

A good introductory text on the topic of sloshing is the Ph.D. thesis of Solaas (1995). She presents an extensive literature survey of analytical and numerical solutions to sloshing problems, as well as detailed comments on available model tests.

In general analytical solutions to sloshing problems are based on a potential flow assumption. A velocity potential is used to represent the flow in tanks of simple geometrical shapes. Linear analytical solutions exist for some tank configurations, and they supply the eigenfrequencies of the fluid motion. However, a numerical method like illustrated by Solaas (1995) can be used to predict linear eigenfrequencies and modes for any tank shape. When linear theory is used, fluid response can only be predicted accurately for frequencies away from resonance.

Moiseyev (1958) suggests a general nonlinear method based on potential flow for determination of free and forced oscillations of the liquid in generally shaped tanks. This has been the foundation for several analytical studies of sloshing. The forced oscillation frequency is close to the lowest natural frequency for the fluid motion. A characteristic length of the tank is $\mathcal{O}(1)$ and the depth of the fluid is either $\mathcal{O}(1)$ or infinite. The excitation is $\mathcal{O}(\epsilon)$, and the response is $\mathcal{O}(\epsilon^{1/3})$. Here, ϵ is a small parameter. The steady-state solution of the resulting nonlinear boundary-value problem for the velocity potential is found as a power series in $\epsilon^{1/3}$. The lowest mode is assumed dominant. Moiseyev does not carry out the derivation in details for specific tank geometries.

Abramson (1966) presents a comprehensive review of the studies of sloshing up to 1966. In this report, linear and nonlinear analytical solutions of sloshing in tanks of a variety of different geometries undergoing harmonic oscillations are shown. Linear solutions are presented for three-dimensional rectangular tanks, vertical cylindrical tanks of various compartmenting, horizontal cylindrical tanks, spherical, toroidal and conical tanks. The nonlinear theory of Moiseyev (1958) is included, as is the theory of Penney and Price (1952) for free oscillations in a two-dimensional tank of infinite depth.

Faltinsen (1974) uses the work of Moiseyev and derives a nonlinear analytical theory for sloshing in a two-dimensional rectangular rigid tank. The tank is forced to oscillate harmonically with small amplitudes in sway or roll in the vicinity of the lowest natural frequency for the fluid inside the tank. The power series for the velocity potential is found correctly to $\mathcal{O}(\epsilon)$. ϵ is the order of the response and it is expressed as the ratio of the sway amplitude to the tank lenght or the roll amplitude. The stability of the steady-state solution is studied, and theory and experiments are shown to compare well.

Solaas (1995), and Solaas and Faltinsen (1997) present a semi-analytical approach based on Moiseyev's perturbation method. This method uses a boundary element numerical method to determine the eigenfunctions and eigenvalues of the problem for tank shapes where these cannot be found analytically.

In Paper 3 in this thesis, Faltinsen et al. (2000) present an analytical approach to sloshing in rectangular tanks of finite water depth. The derivations are based on the Bateman-Luke variational principle and the use of the pressure in the Lagrangian of the Hamilton principle. The result is a system of nonlinear ordinary differential equations in time for the generalized coordinates of the free surface elevation. The procedure applies to any tank shape as long as the tank walls are vertical near the mean free surface. This method has been extensively validated for forced motions. The paper gives additional references on analytically based nonlinear sloshing methods.

Faltinsen and Timokha (2001) have generalized the method of Faltinsen et al. (2000). An adaptive procedure allows for different ordering of the modes describing the free surface. The result is a method that works for lower filling heights and higher excitation amplitudes. This work is described in more detail in Faltinsen and Rognebakke (2000), Paper 1. This method gives reliable results for a rectangular tank with a ratio between fluid depth h and tank length $h/l > \approx 0.24$. Faltinsen and Timokha (2002) have further developed the procedure to cover h/l down to 0.1. This procedure shows that contributions from many modes matter. These contributions are assumed of the same $\mathcal{O}(\epsilon^{1/4})$, which is also the order of the fluid depth. The authors point out that dissipation is of higher importance for the smallest fluid depths.

An analytical solution to shallow water sloshing, $h/l < 0.1$, is given in Verhagen and van Wijngaarden (1965). They study roll oscillations of a rectangular container. The shallow water sloshing is characterized by travelling waves and the formation of a hydraulic jump or bore. They apply a theory developed for one-dimensional gas flow to the fluid oscillations and thereby calculate the strength and the phase of the jump. The moment exerted on the container is also calculated. They report a good agreement between theoretical values and experimental results at the lowest resonance frequency for these quantities when $h/l = 0.075$.

Some recent publications that cover numerical methods relevant for the analysis of sloshing, are referred in the following. A brief introduction to the different methods is given.

The comparative study of the 13$^{\text{th}}$ ISSC (Moan and Berge (1997) with details in Cariou and Casella (1999)) shows that different numerical techniques may give quite different predictions of the free surface elevation. This indicates the numerical difficulties in modelling sloshing. A main drawback of computational fluid dynamics (CFD) for coupled sloshing and ship motions analysis is the limited computational efficiency. The ISSC study does not consider the use of computer resources. A time domain solution is necessary due to the importance of nonlinearities for sloshing. Long time simulations are also required to obtain probability density functions of response variables caused by sloshing.

The field equations governing the fluid flow may be the complete Navier-Stokes equations, the Euler equation or the Laplace equation when potential flow is assumed. The basic idea in numerical methods used to solve a partial differential equation is to discretize the given continuous problem with infinite degrees of freedom to obtain a discrete problem or system of equations with only a finite number of unknowns. These may be solved using a computer. A mesh, or a grid, is used in the discretization of the flow domain. Either an Eulerian or Lagrangian description, or a mixture of these, is used. In the Eulerian description, the grid is fixed relative to the reference frame and the fluid moves through the grid, as opposed to the Lagrangian description where the

coordinate system and the grid points move with the fluid. The type of grid is dependent on the method used to create an equivalent discrete form of the continuous field equations.

A finite difference method, FDM, uses a structured grid and flow variables are calculated for fixed discrete points within this grid using an Eulerian approach. Algebraic difference quotients replace the partial derivatives of the governing equations. The result is a system of algebraic equations for the unknown flow variables. Mitchell and Griffiths (1980) give a detailed description of the finite difference method.

The finite volume method, FVM, subdivides the spatial domain into a finite number of discrete contiguous control volumes. Considering an arbitrarily chosen volume, the goal is to calculate the values of the conserved variables averaged across the volume. The disretization of the governing equations is performed in two steps. First, an integration over each control volume is performed and secondly, the resulting cell boundary values are approximated. The advantage of the finite volume method over finite difference method is that the finite volume method does not require a structured mesh. Usually, a clear distinction between FDM and FVM is not made, and one may find a method described as a finite difference method using a control volume approach.

When studying free surface flows by FDM or FVM, some means of volume tracking method are usually applied. Rider and Kothe (1998) describe basic features of volume tracking methods. Initially, fluid volumes are initialized in each computational cell from a specified interface geometry. This task requires computing fluid volumes in each cell containing the interface, and exact interface information is discarded in favor of discrete volume data, usually retained as volume fractions. Mixed cells have a volume fraction between zero and one, and cells without interfaces have a volume fraction equal to zero or unity. Detailed interface information cannot be extracted until an interface is reconstructed. The principal constraint is local volume conservation. The interfaces are tracked by evolving fluid volumes forward in time with solutions of an advection equation. At any time in the solution, the exact interface location is not known, and a given distribution of volume data does not guarantee a unique interface. Interface geometry is found based on local volume data and a particular algorithm, and the interfaces are reconstructed. The reconstructed interface is then used to compute the volume fluxes necessary to integrate the volume evolution equations.

An early approach to surface tracking was the Marker and Cell, MAC, method. This method divides the fluid domain into cells. Initially, a system of marker particles are placed in the cells containing fluids. The particles are moved with the local flow. A cell without marker particles is considered to contain no fluid, and a cell with particles adjacent to an empty cell is called a surface cell.

A frequently used method of volume tracking in two and three dimensions is the Volume of Fluid, VOF, method. Hirt and Nichols (1981) give a thorough description of this method. VOF has all the basic features of a volume tracking method as described previously. The discrete volume data is a volume fraction and hence the VOF method provides more information than the MAC method and, in general, requires less storage. A clever reconstruction algorithm is the key to a successful method, and the original VOF has seen a lot of improvements by different authors over the years. Rider and Kothe (1998) present a new algorithm for the volume tracking of interfaces, as well as a summary of the pros and cons of other approaches. Rudman (1997)

also compares well known methods and proposes a new technique. He concludes that Youngs (1982) has the superior VOF algorithm in comparison with, among others, Hirt and Nichols (1981).

Sussman et al. (1998) present a level set approach for computing solutions to incompressible two-phase flow. The interface between the two fluids is considered to be sharp and is described as the zero level set of a smooth function. A set of equations for the level set function must be solved in addition to the equations governing the flow. The authors solve Navier-Stokes equations using a staggered mesh and compute flows involving air bubbles and water drops. Sethian (1996) gives a good introduction to the level set method. He explains that the core of level set methods is the shift in how one views moving boundaries; rethinking the Lagrangian geometric perspective and exchanging it for an Eulerian, initial value partial differential equation.

Solaas (1995) has studied sloshing by use of the commercial program FLOW-3D, developed by Flow Science, Inc. The program implements a combination of the SOLA finite difference scheme for solving Navier-Stokes equations and the VOF technique for tracking the free boundaries of the fluid. She reports a sensitivity of the results to the choice of numerical parameters and that lack of conservation of fluid mass can cause unphysical sloshing behaviour.

Armenio and La Rocca (1996) and Armenio (1997) study shallow water sloshing of water in rectangular open tanks by numerical analysis and experimental validation. They employ the Reynolds Averaged Navier Stokes Equations (RANSE). The RANSE is solved using a modified version of the MAC method, denoted SIMAC. The Navier-Stokes equations are solved in primitive variables on a non-uniform staggered Cartesian grid by means of a finite difference scheme.

Van Daalen et al. (1999) present numerical simulations of the water motion inside a free surface anti-roll tank using a Navier-Stokes solver based on the VOF method. Measured and calculated roll moment amplitudes and phases were found to be in good agreement for various combinations of motion and tank parameters. The studied filling heights represent shallow water conditions.

Kim (2001) has developed a Navier-Stokes solver based on the SOLA scheme with the assumption of the free surface as a single-valued function. He presents a special treatment of impacts between the free surface and the tank ceiling. A buffer zone is adopted where a mixed boundary condition of rigid wall and free surface is imposed before an impact. The calculated impact pressures depend on the size of the buffer zone, but a time-averaging technique is introduced and reduces the dependency. Calculated impact pressures agree well with experimental data. Kim ensures conservation of fluid mass by slightly moving the free surface for each time step. The global motion is not affected.

Finite element methods, FEM, use a different discretization process than a finite difference method. The given differential equation is reformulated as an equivalent variational problem. A given type of finite element discretization constructs a finite dimensional space. The solution of the problem is assumed a priori to have a prescribed functional behaviour over the elements. This function may, for instance, vary linearly between neighboring nodal points on the elements. The nodes are defined points on the element. The assumed solution is inserted into the differential equations, and, since this solution does not completely satisfy the differential equations, the

result is a residual. The final equation system for the unknowns is obtained by minimizing the residual in a weighted manner by multiplying with a weighting function and integrating the product over the computational domain. Boundary conditions are incorporated as known values at the nodal points on the elements. The grid does not have to be structured, and an advantage of finite element methods compared with finite difference methods is that complicated geometries and general boundary conditions can be handled relatively easily. Johnson (1987) has written an accessible book on FEM.

In contrast to FDM and FVM, it is customary in FEM to use a Lagrangian approach and let the node points and elements move with the flow. This may be a challenge for large deformations of the flow domain, since the elements can be distorted causing loss of accuracy. An adaptive regridding of the domain is a possible solution. Ramaswamy and Kawahara (1987) handle large free surface motions by adopting an arbitrary Lagrangian-Eulerian kinematic description, ALE, of the fluid domain. The nodal points can be placed independently of the fluid motion by using one of three options for the moving vertices: (1) they can flow with the fluid for Lagrangian computing, (2) they can remain fixed for Eulerian computing or (3) they can move in an arbitrarily prescribed way to give a continuous rezoning capability. Ramaswamy and Kawahara discuss stability and present results from numerical computations of, among others, a large amplitude sloshing case.

Okamoto and Kawahara (1990) present a Lagrangian finite element method that solves Navier-Stokes equations. They study a two-dimensional sloshing problem and compare calculated free surface elevation with video snapshots from experiments for a rectangular tank excited in the horizontal plane. They report a good agreement. The sloshing amplitude is small. Numerical calculations but no experimental values are presented for a tank with a multi-sloped wall. No convergence study with respect to element size or time step is shown. This work is based on Ramaswamy et al. (1986).

An interesting numerical technique is developed for the simulation of free surface flows and interfaces by Mashayek and Ashgriz (1995). A finite element method is used to calculate field variables and a Volume of Fluid method is applied in the advection of the fluid interfaces. Navier-Stokes equations govern the flow. Mashayek and Ashgriz find that this hybrid method can handle large surface deformations with accurate treatment of the boundary conditions. They apply this method on a collision of liquid drops and the study of instability and break-up of a capillary jet.

Wu et al. (1998) simulate sloshing waves in two- and three-dimensional tanks by using a finite element method based on fully nonlinear wave potential theory. A comparison between calculated results and published two-dimensional data validates the computer code. A very good agreement is found. An extensive set of results are presented for a rectangular tank undergoing translatory motion in more than one direction.

Boundary element methods, BEM, are based on a potential flow assumption, i.e. the effect of viscosity is neglected and the fluid is assumed incompressible and the flow irrotational. The flow is governed by Laplace equation. Green's second identity is applied. Singularities representing the velocity potential are distributed over the boundary of the fluid domain. In a nonlinear formulation, these singularities are infinite fluid sources and normal dipoles. The boundary

conditions are used to set up integral equations for the unknown singularity densities. These equations are solved numerically. In a nonlinear formulation, the elements must follow a moving boundary. Post-breaking flow is difficult to handle, and a careful treatment of the contact point, where the free surface intersects the tank wall, is imperative.

Other methods include spectral methods and the Smoothed Particle Hydrodynamics method, SPH. Ferrant and Le Touze (2001) use a pseudo-spectral method based on fully nonlinear potential theory to study sloshing. The velocity potential is expanded in series of the natural modes of the tank geometry. The presented results agree well with finite element analysis results by Wu et al. (1998) for a very shallow water case.

Landrini and Colagrossi at INSEAN, Italy, have used the SPH method described by Monaghan (1992) to calculate sloshing flows. They also use a high-order boundary element method to calculate the sloshing flow. The results compare well, and interestingly the SPH is able to calculate also after the occurrence of wavebreaking, when the BEM simulations stop. SPH can deal with large free surface deformation and even fragmentation. The SPH is a purely Lagrangian method, and the flow is described by flowing fluid particles. However, the physical properties of the computational particles are not related to a single point in space, but they are smeared or smoothed out over a region of space. Therefore, the name smoothed particles. At the heart of SPH is an interpolation method which allows any physical quantity to be expressed in terms of its value at a set of disordered points. A challenge with SPH is the treatment of the boundaries.

A validation of a numerical or analytical approach to sloshing flows relies on the availability of experimental data. Abramson (1966) gives experimental data for tanks of various shapes;rectangular, spherical and circular cylindrical tanks. These may be uncompartmented or with different compartmenting. Solaas (1995) has collected references to experimental works up to 1995.

Two experimental studies of sloshing were conducted as a part of this thesis work, and details will be given in the following.

1.3 Outline of Present Work

The work reported in this thesis concerns violent resonant fluid motion in ship tanks. The focus is on non-shallow sloshing in smooth rectangular or prismatic tanks. The workis limited to the study of two-dimensional flows. A nonlinear analytical sloshing model is selected for the analysis. Impact loads and energy dissipation due to impacts are studied by a local analysis. The sloshing model is implemented as a part of a linear time-domain seakeeping code to study the coupling of sloshing and ship motions. Experiments are conducted both for an isolated tank and a hull section with internal tanks moving in waves. Data collected from the experiments are used in validation of the computational results.

1.3.1 Experiments of sloshing in a rectangular tank

A series of experiments on two-dimensional sloshing in a smooth rectangular tank excited harmonically in the horizontal (sway) direction has been conducted by the author at Det Norske Veritas, in Høvik, Norway, during spring and early summer 1998. The experiments gave valuable insight into the physics of sloshing, as well as providing measurements of the free surface elevation for a wide frequency range around the first linear eigenperiod of the fluid motion for a variety of water filling levels. Video and pictures of the sloshing motion were taken and have proved to be a valuable source of information and a foundation for later discussions. Appendix E presents a description of the experiments including tables where the different combinations of parameters are shown. The emphasis is on the transient part of the flow. The duration of the recordings were not sufficient for the free surface motion to reach steady-state conditions for non-shallow fluid depths with a ratio between filling height and tank length $h/l > 0.24$. A typical recording included 30 oscillations, but some longer runs were done and these show transient behaviour after more than 100 cycles. A different situation is observed for $h/l = 0.17$ and $h/l = 0.12$, where steady-state oscillations in many cases were obtained after 2-3 oscillations periods. This indicates very large damping for small fluid depth. Tank roof impacts drastically reduce the time to reach steady-state for non-shallow fluid depth.

Figure 1.7 presents a number of pictures taken during the experiments. These are representative of the different free surface flows studied. Table 1.1 shows the parameters, which apply to specific pictures, and includes a short description of the flow. The parameter in column four, 'Effect', is a relative measure of the sway amplitude. This is explained in Appendix E. For larger filling levels, tank roof impacts occur when the top of what resembles a standing wave hits the roof. For a shallow water case, bores are formed and may result in impacts at the lower corners of the tank. As a consequence of this impact, a jet sometimes shoots upwards and hits the roof. For a low filling height, run-up is seen when the excitation period is away from the first natural period for the fluid in the tank. The angle between the free surface and the wall is small, and the upward velocity of the water at the intersection between the free surface and the wall is high.

1.3.2 Sloshing modelling

The sloshing experiments at DNV showed obvious nonlinearities of the free surface flow as well as modulation of the waves as a consequence of transient and forced oscillations. This led to the derivation of a second order initial value solution for sloshing in a smooth rectangular tank. The solution was found for only one set of initial conditions. The agreement with the experiments was better than for a linear solution, but there was an obvious need for a method including higher order terms. The solution was derived for a constant excitation period and was not suited for a later integration in a time domain seakeeping code. A general time domain solution is needed to handle unsteady excitation. Work was initiated to develop a nonlinear boundary element method.

Visiting scientist Alexander N. Timokha from Kiev, Ukraine, and Prof. Odd M. Faltinsen started the development of a multi-dimensional modal method by the time the second order solution was finished. The DNV experiments were used to validate this analytical approach, which proved to

be an excellent basis for further studies of sloshing. The modal method is a time domain solution that works with non-harmonic excitation. The work on a nonlinear BEM code was abandoned, but the initial work has later proved useful when working with the external fluid flow problem.

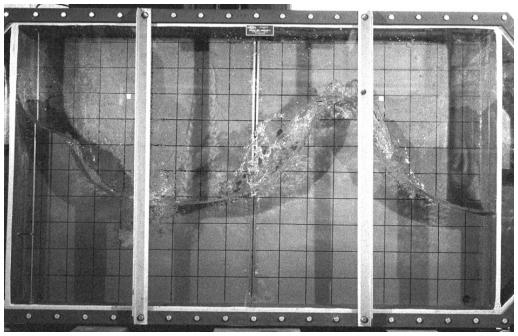

(a)

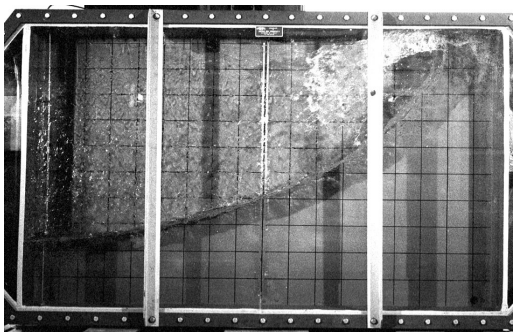

(b)

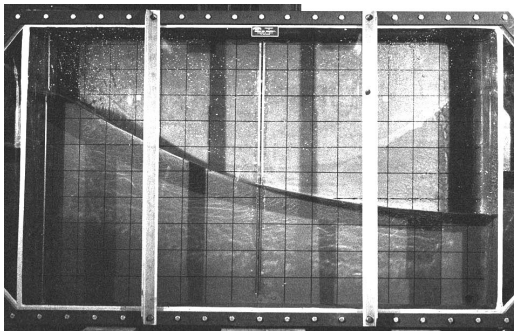

(c)

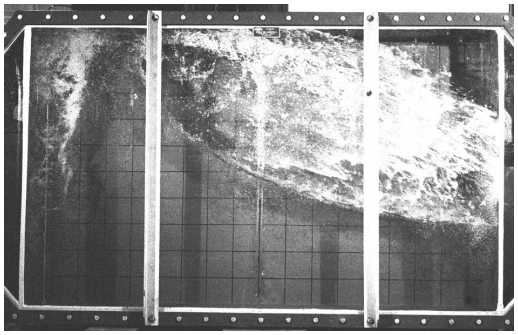

(d)

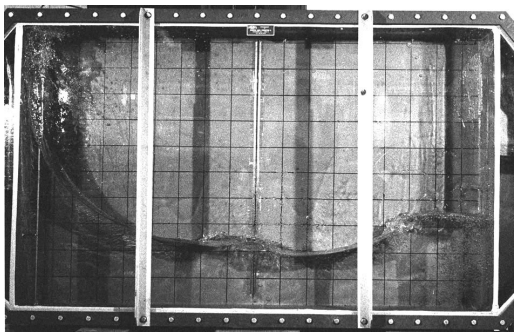

(e)

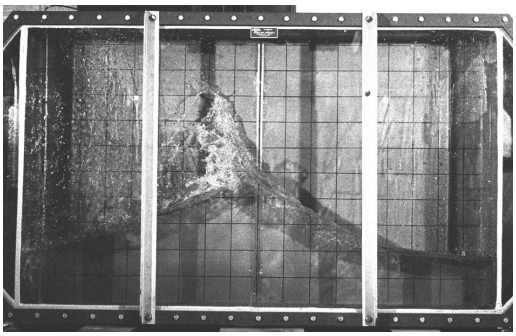

(f)

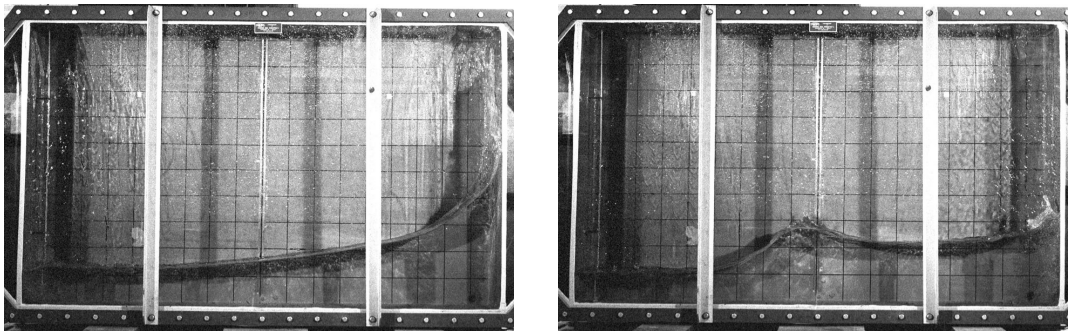

(g) (h)

Figure 1.7: Snapshots of sloshing

Table 1.1: Case description for the presented pictures of sloshing

Figure	**Filling level** [cm]	**Period** [s]	**Effect**	**Description**
1.7(a)	50	0.91	0.8	Near 3rd mode resonance, steep standing wave with spray at crests
1.7(b)	50	1.7	0.8	Close to 1st mode resonance, moderate tank roof impacts occur
1.7(c)	50	1.74	0.10	1st mode resonance, small excitation and no impacts. Smooth surface
1.7(d)	60	1.7	1.32	Close to 1st mode resonance, heavy impacts, cavity formed at impact corner, air-water mixture
1.7(e)	30	2.3	0.8	Dominant traveling wave - bore formation, vertical jet at tank wall
1.7(f)	30	2.3	0.8	Breaking bore causes spray
1.7(g)	20	2.1	0.8	Traveling bore impacts at lower corner and causes thin, fast vertical jet at the tank wall
1.7(h)	20	2.5	0.8	Traveling bore gives impacts at tank wall

Faltinsen and Timokha (2001) present a generalization of the multi-dimensional modal method. Some of the shortcomings of that method are addressed by the new adaptive multimodal approach. The improved method was adopted in the subsequent sloshing analysis. Validation shows that this method is applicable for non-small water depth; when the ratio between filling height and tank length $h/l > 0.24$.

1.3.3 Sloshing and slamming

When sloshing occurs in a partially filled tank, impacts between the water and structure are often a consequence. Impacts lead to high pressures and forces, and energy is dissipated in the resulting jets. A local analysis was used to model impact with the tank roof for both rectangular and chamfered tanks. An equivalent slamming problem has been constructed, and a generalization of Wagner's slamming theory (Wagner (1932)) was used. The coupling with the base flow calculated by the adaptive multimodal approach is obtained through the inclusion of a damping term and a modification of the generalized coordinates defining the base flow.

1.3.4 Sloshing and ship motions

When a computationally efficient and robust sloshing model including the effect of impacts was ready, the study of coupled sloshing and ship motions was a natural next step. Sloshing in the context of marine engineering usually happens when a tank is excited by ship motions. The sloshing induced forces will influence the ship motion.

The author performed a set of experiments at the wave flume of the Department of Marine Hydrodynamics, NTNU, during summer 2000. A rectangular hull section with two smooth, rectangular internal tanks was allowed to move in sway only along the flume on low friction bearings. The section was excited by regular waves for different wave frequencies, wave amplitudes and levels of water in the tanks. Selected conditions were such that the internal fluid motion did not cause tank roof impacts. Measurements include wave parameters and the sway motion of the section. The sloshing motion inside the tanks was captured on video. Figure 1.8 shows the experimental set-up.

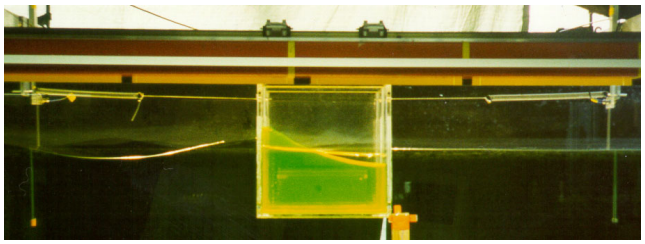

Figure 1.8: Experimental set-up for a study of coupled sloshing and ship motions

A commercial linear time and frequency domain seakeeping program was first used to represent the external flow in the study. A sloshing module was coded and included in the program. However, as the work proceeded, it became clear that the external fluid flow would have to be solved by a tailor-made program. A low order boundary element method based on Green's second identity with straight line elements of constant Rankine singularity density was applied. This method includes a convolution formulation in the equation of motion to properly handle non-harmonic/transient motions. Characteristics of the coupled system are the sway motion

and the generalized coordinates defining the internal fluid flow. A time domain simulation is used to evaluate the behaviour of the system.

1.4 Structure of the Thesis

The main part of this thesis consists of a collection of papers which the author has co-authored. The organization of the thesis this way, raises the need to address the fact that some of the papers are written in a condensed form. This is most obvious for the three extended abstracts presented at the International Workshop on Water Waves and Floating Bodies. It was therefore necessary to include a preface to each paper. The purpose of this is to elaborate on some parts of the presented material, sometimes by pointing to an appendix. The prefaces also serve to link the different papers and help to create a better reading experience.

The first paper is a keynote lecture presented by Prof. Faltinsen in Venice, Italy, in September 2000. This paper is a natural starting point, since it contains an extensive description of the nature of sloshing and the physical effects that are relevant when studying sloshing in ship tanks. Different means of modelling sloshing are presented, and the authors argue for the use of an analytically-based approach.

The rest of the papers are presented in the same order as the work they report was done.

1.5 Major Findings

The present study is limited to two-dimensional flows. The study covers experimental and theoretical investigations of sloshing, internal slamming in tanks and coupled ship motions and sloshing. The author has contributed to all parts of the included papers except for the theory described in Paper 3. The rest of this section presents a summary of the major findings reported in the papers.

Features of sloshing in smooth, rectangular tanks. The nonlinearity of sloshing is clearly observed in conducted model experiments. The experiments show modulation, or beating, of the free surface motion for non-shallow fluid depth. The modulation is explained by a frequency analysis. The transient start-up of the horizontal motion of the tank results in energy content at both the frequency corresponding to the excitation frequency and the eigenfrequency of the first anti-symmetric mode for the free surface. The level of damping in the tank is extremely low when no tank roof impact occurs, and the beating does not subside during a typical recording length of thirty excitation cycles. Impacts occur at the upper corners for high filling levels and at the lower part of the wall for a small fluid depth situation. A steady-state free surface motion is reached after a few excitation cycles when heavy or moderate impacts are observed. This indicates the large dissipation of energy caused by impacts. For small fluid depths, breaking bores and run-up cause jet formation and spray that contribute to dissipation, and the transient

part of the flow usually dies out almost immediately. Pictures and video render possible a detailed investigation of the impact flow. A large set of experimental data is collected.

Second order initial value solution of two-dimensional sloshing in rectangular tanks. An analytical solution based on a potential flow assumption is derived. The response is assumed to be of $\mathcal{O}(\epsilon)$ where the small parameter ϵ characterizes the order of magnitude of the forced sway amplitude relative to the length of the tank. The solution is of second order in ϵ. Initial values for the potential and its time derivative are, respectively, $\Phi = 0$ and $\partial\Phi/\partial t = 0$ on the mean free surface. The second order solution is able to capture some of the nonlinearities seen in the experiments, but there are still unexplained differences.

Experimental validation of sloshing models. The analytical sloshing models by Faltinsen et al. (2000), Paper 3, and Faltinsen and Timokha (2001) have been extensively validated for forced swaymotions of rectangular and prismatic tanks. A very good agreement between calculations and available experimental data is demonstrated for filling height/tank length ratios $h/l > \approx 0.24$.

Analysis of tank roof impacts. A method is developed to calculate impact pressures and forces when the free surface inside a tank hits the roof. The nonlinear sloshing theories by Faltinsen et al. (2000) and Faltinsen and Timokha (2001) are modified to include a local flow model, which combines the theory of Wagner (1932) with an infinite set of image potentials. The image system is of secondary importance. The slamming causes large loads on the vertical wall adjacent to the impact area in the tank roof. The horizontal slamming induced force is larger than the vertical slamming force acting on the tank roof. After the impact, the free surface is modified to account for the uprise due to slamming. The free surface correction is found to have a negligible effect.

Damping of sloshing due to tank roof impacts. When impacts occur in a smooth tank, experiments show that the dissipative effect of the impacts dominates relative to the energy loss in the viscous boundary layers. A robust method for estimating the damping effect of impacts on sloshing flow is developed based on the hypothesis that the kinetic and potential energy in the jet flow caused by the impact is dissipated when the jet flow impacts on the free surface. The energy loss is related to the mean total energy of the system, and an equivalent damping ratio is found. This is used to calculate the ambient sloshing flow to make sure that the lost energy is subtracted from the system. An iterative scheme is applied in the calculations. In simulations that are performed for a prismatic tank with chamfered roof, the estimated energy loss from the Wagner's analysis is corrected due to the large impact angle. A similarity solution, or alternatively, a generalization of Wagner's slamming theory valid for larger angles, is used to find the correction factor. The severity of impacts is drastically reduced in a chamfered tank relative to a rectangular tank. Violent sloshing with heavy impacts is possible to calculate when the impact damping model is utilized. Comparisons between theory and experiments show a satisfactory agreement.

Effect of sloshing on ship motions. Two-dimensional experiments on a box-shaped ship section excited by regular beam sea have been conducted. The section contains two smooth tanks and can only move in sway. Fluid motion inside the tanks has a large effect on the sway motion response of the section. The resonance frequency for the coupled system is different from the

eigenfrequencies of the dominant sloshing mode and the moored ship section without water in the tanks. Simulations of a corresponding system are performed by assuming a mainly linear external flow and applying the nonlinear sloshing model of Faltinsen and Timokha (2001). A good agreement between experiments and computations is reported. The calculated coupled motion is sensitive to the damping of the sloshing motion in the frequency range where the coupled sloshing and ship motions cause resonant ship motions. A quasi-linear frequency domain analysis is used to explain the sensitivity by introducing the sloshing loads as a frequency dependent spring. The comparison between calculations and experiments implies that the level of damping of the sloshing flow is higher than predicted by Keulegan (1958) for dissipation in a laminar boundary layer.

Paper 1

Sloshing

Faltinsen, O. M. and Rognebakke, O. F.
Int. Conf. on Ship and Shipping Research - NAV, Venice, Italy, 2000

Preface

This paper was prepared for a keynote lecture that Prof. Odd M. Faltinsen held at the International Conference on Ship and Shipping Research, NAV, Venice, Italy, September 2000. The paper represents a summary of our work on sloshing in two-dimensional rectangular and prismatic tanks.

The section on physical and mathematical modeling aims at providing a thorough discussion of sloshing in the context of marine engineering. The nature of sloshing is violent resonant fluid motion with strong nonlinearities. Sloshing often leads to fluid impacts on the structure, and hydroelastic effects may matter. The impacts result in wave breaking and spray formation and, as a consequence, energy is dissipated. The tanks may have a variety of geometrical shapes and filling levels. Internal structures in tanks experience dynamic loads and generally have a damping effect on the free surface flow. A set of criteria for selecting a sloshing model is listed, as are pros and cons of available numerical tools.

An analytically-based sloshing model is used in the study. This choice is founded on the need for a fast and robust method that facilitates coupling with ship dynamics. A basic method based on an infinite tank roof assumption is modified by including an artificial damping accounting for energy loss due to tank roof impacts. When steady-state motions are studied, an iterative procedure is followed when impacts occur. Appendix A contains a brief description of the program that has been developed.

The basic method is the adaptive multimodal approach developed by Faltinsen and Timokha (2001). This is a generalization of the multi-dimensional modal analysis presented in Faltinsen, Rognebakke, Lukovsky, and Timokha (2000), Paper 3. The difference between the two approaches is outlined in the following paper.

SLOSHING

Odd M. Faltinsen and Olav F. Rognebakke
Department of Marine Hydrodynamics
Norwegian University of Science and Technology
N-7491 Trondheim, Norway

ABSTRACT

Physical aspects of sloshing in ship tanks are discussed. The importance of hydroelasticity for small angles between impacting fluid and body surface is stressed. Performance requirements for numerical methods are presented. CFD methods are reviewed. The drawbacks are long simulation time, sensitivity to numerical parameters and general inability to predict impact loads and resulting structural response. An analytically based sloshing model is therefore recommended. Its drawbacks are that the tank has to be smooth with vertical sides at the free surface. Shallow fluid phenomena are excluded. The method consists of a basic method that assumes infinite tank roof height and a second part, which accounts for tank roof impact. The importance of tank roof impact damping on sloshing is demonstrated. Extensive validation of free surface elevation, total forces and moments for 2-D flow in rectangular and prismatic tanks are reported. This includes realistic motion excitation and studies close to critical depth 0.3374 times the tank breadth. Impact pressure predictions and demonstrations of the influence of the tank fluid motions on the global ship dynamics are presented.

URN:NBN:no-2322

INTRODUCTION

A partially filled tank will experience violent fluid motion when the ship motions contain energy in the vicinity of the highest natural period for the fluid motion inside the tank. Impact between the fluid and the tank roof is then likely to occur for larger filling ratios. The consequence is wave breaking, spray and mixing of air (or gas) and fluid. Actually, extreme cases with air bubbles everywhere in the fluid have been experimentally observed.

The resonant fluid motion has different main characteristics depending on the fluid depth and the three-dimensionality of the flow. Swirling (rotational) motion is a special feature of 3-D flow ([1],[2]). Our focus is on the highest sloshing period, 2-D flow and finite fluid depth. It implies that typical shallow water phenomena like travelling waves and hydraulic bores are excluded. However, this can for instance be studied by the method of [3]. This was done with satisfactory results for horizontal forces by Abramson et al. [2] for a 2-D nearly rectangular tank with fluid depth 0.12 times the breadth.

Since sloshing is a typical resonance phenomenon, it is not necessarily the most extreme ship motions or external wave loads that cause the most severe sloshing. This implies that external wave induced loads can in many practical cases be described by linear theory. However, nonlinearities must be accounted for in the tank fluid motions. Since it is the highest sloshing period (natural period) that is of prime interest, vertical tank excitation is of secondary importance.

Generally speaking the larger the tank size is and the less internal structures obstructing the flow in the tank are present, the more severe sloshing is. The reasons are: a) Increased tank size tends to increase the highest natural sloshing period and hence higher sea states and larger ship motions will excite the severe sloshing. b) Internal structures dampen the fluid motions.

[4] reported damages due to sloshing in bulk carriers, combination Oil-Bulk-Ore (OBO) carriers and LNG carriers. Large and smooth tanks characterized these. Partial fillings in LNG carriers are a consequence of boil-off of gas during operations. Sloshing has always been an important design criterion for oil tankers even if partial filling is rare in actual operation. Since environmental concerns have caused requirements about double hull tankers and ship owners avoid internal structures in cargo tanks to facilitate cleaning, this has lead to wide and smooth oil tanks that increase the probability of severe sloshing. Sloshing is also of concern for Floating Production Storage and Offloading (FPSO) units and shuttle tankers. However, this is for shuttle tankers only in a limited time during loading. Obviously the severity of sloshing is connected to possible filling height restrictions for oil tankers, gas carriers, shuttle tankers and FPSOs. Since ballast exchange is required outside the port for a bulk carrier, there are possibilities for slamming damages. Damage to the hatch cover is of particular concern.

The hydrodynamic loads occurring inside a tank are often classified as impact loads and “dynamic” loads. Impact loads are of course also dynamic loads. But in this context dynamic loads mean loads that have dominant time variations on the time scale of the sloshing period, while impact loads may only

URN:NBN:no-2322

last 10^{-2} to 10^{-3} seconds. Both resulting fatigue and ultimate strength are of concern.

Local structural response due to fluid impact (slamming) is an important response variable. But loads on possible internal stringers, web-frames, cross-ties, piping supports and equipment like LNG pump towers must also be considered. Since some internal structures like a web-frame at the tank roof may be out of the fluid at certain time intervals, impact as well as dynamic loads may matter. Dynamic pressures on the tank wall and bottom as well as total dynamic loads on the tank are also of interest. The latter is needed to estimate tank support reactions and possible global interactions with the ship dynamics. For instance, the horizontal but not the vertical support reaction is important for spherical LNG tanks. The use of anti-rolling tanks exemplifies that global interaction between the tank fluid motion and ship motion, i.e. rolling, can be strong. If several tanks are partially filled like it may be on a FPSO, global ship motions and wave bending moments may be strongly affected.

The following study will concentrate on numerical methods and validation, but starts out stating performance requirements of numerical methods and physical aspects of sloshing.

PHYSICAL AND MATHEMATICAL MODELING

A theoretical method has to be robust and time efficient. Long time simulations are needed to obtain statistical estimates of the tank response. This should ideally be coupled with the ship motions in a stochastic sea. Both impact and non-impact loads should be evaluated. Impact loads may require hydroelastic analysis. There is a variety of tank shapes. This includes rectangular, prismatic, tapered and spherical tanks as well as horizontal cylindrical tanks. The fluid may be oil, liquefied gas, water or heavy density cargoes like molasses and caustic soda. The fluid dynamic properties of the two last cargo types are not focused on in this context. Ideally one should be able to predict two phase flow due to strong mixing of air (or gas) with the fluid. However, this is not focused on. It is hard enough to predict one phase flow.

Internal structures obstructing the flow may be present. This causes flow separation and implies that Navier-Stokes equations have to be solved. The question of turbulence modeling arises, but may not be a dominant effect when flow separation from sharp corners occurs. The argument is that dominant scale effects due to difference between laminar and turbulent flow for separated flow past a blunt body is due to differences in separation line position (or point for 2-D flow). On the other hand the wake behind an internal structural part may interact with another internal structure, the free surface and the tank boundaries. A wake flow would in practice be turbulent. What turbulence model to use is still a research issue. Numerical simulations of flow separation from sharp corners require fine gridding in the vicinity of the corners. The main effect of viscosity for a smooth tank with conventional fluid like oil is normally concentrated in thin boundary layers along the tank boundaries. The boundary layer flow may be laminar in model scale, but is turbulent in full scale. But anyway the boundary layer flow has a small influence on tank response of

URN:NBN:no-2322

practical interest. It implies that Euler equations can be used for a smooth tank. Further compressibility of the fluid is of secondary importance. Anyway a smooth tank would give the most violent response and provide a conservative estimate if internal structures are present. It is also possible to provide estimates of the effect of internal structures in combination with potential flow. It assumes the cross-dimensions of the internal structures are small relative to fluid depth and tank breadth. The internal structures are then handled as appendages with Morison type calculations [5]. Equivalent damping of the fluid motion has to be introduced in a similar way as described later in connection with tank roof impact damping.

The previous discussion assumes a submerged internal structure. Some internal structures may be part of the time in and out of the fluid. Fluid impact becomes then part of the problem. The impact pressures can become very high. [2] reported full scale measured pressures up to 24 bar in an OBO tank. We will in the following text discuss fluid impact in a more general sense. Different physical effects occur during slamming. When the local angle between the fluid surface and the body surface is small before impact, an air (or gas) cushion may be formed between the body and the fluid. Compressibility influences the airflow. The airflow interacts with the fluid flow, which is influenced by the compressibility of the fluid. When the air cushion collapses, air bubbles are formed. Air bubbles may also be entrapped in the fluid from previous impacts. The ullage pressure influences the presence and behaviour of air bubbles. The large loads that can occur during impact when the angle between the fluid surface and body surface is small can cause important local dynamic hydroelastic effects. The vibrations can lead to subsequent cavitation and ventilation. The previously mentioned physical effects have different time scales. The important time scale from a structural point of view is when maximum stresses occur. This scale is given by the highest wet natural period (T_{n1}) for the local structure. Compressibility and the formation and collapse of an air cushion are important initially and normally in a time scale smaller than the time scale of when local maximum stresses occur. Hence, the effect on maximum local stress is generally small. The theoretical and experimental studies of wave impact on horizontal elastic plates of steel and aluminium presented by [6], [7], [8], [9] and [10] are relevant in this context. Significant dynamic hydroelastic effects were demonstrated. The physics can be explained as follows. The plate experiences a large force impulse during a small time relative to the highest natural period for the plate vibrations. (Structural inertia phase). This causes the space-averaged relative velocity between the elastic vibration velocity and the rigid body impact velocity V to be zero at the end of the initial phase. The plate then starts to vibrate as a free vibration with an initial vibration velocity V and zero deflection. Maximum strains occur during the free vibration phase. The details of the pressure distribution during the first initial phase are not important. Very large pressures that are sensitive to small changes in the physical conditions, may occur in this phase. This can be seen from the collection of measured maximum pressures during the tests. The measured maximum strains showed a very small scatter for given impact velocity and plate even if maximum pressure varied strongly. The largest measured pressure was approximately 80 bar for V equal to 6 m/s.

Fluid impact against a horizontal tank roof during sloshing has similarities with water impact of elastic plates. The tank roof impact will also cause hydroelastic vibrations in the tank wall adjacent to the impact area. [11] studied this by a hydroelastic beam theory. The effect of a chamfered tank roof was also investigated. This problem is similar to water entry of a wedge before the horizontal roof part is reached. The effect of hydroelasticity decreases with increasing deadrise angle of the wedge. The tank roof impact causes also damping of the fluid motions. This will be further discussed later in the text.

[12] studied the relative importance of hydroelasticity for an elastic hull with wedge-shaped cross-sections penetrating an initially calm water surface. A stiffened plating between two rigid transverse frames was examined. A parameter that is proportional to the ratio between the wetting time of the rigid wedge and the natural period of a longitudinal stiffener, was introduced to quantify the relative importance of hydroelasticity. We can associate the wetting time of the wedge with the duration of the loading. If we make an analogy to a simple mechanical system consisting of a mass and spring, then we know that the duration of the loading relative to the natural period characterizes dynamic effects. The wetting time depends on the impact velocity V and deadrise angle β. It means that the importance of hydroelasticity increases with increasing V and decreasing β. In practice we should be aware of hydroelastic effects when $\beta <\approx 5^\circ$.

The literature on sloshing contains many studies on slamming pressures. There is a strong tendency to focus on the high slamming pressures that can occur. Few seem to be aware of the importance of hydroelasticity. It is misleading to use physical pressures as parameter for structural response when the pressures become high and concentrated in time and space. What we are saying is that the structure needs time to react. The previous discussion on fluid impact has severe consequences for how sloshing should be numerically modeled.

It has become popular to use CFD to model sloshing. The problem has to be solved in the time domain due to the strong nonlinearities associated with the free surface conditions. There is a broad variety of numerical methods. The load committee of the 13th ISSC has provided a survey in 1997. Normally the Reynolds Averaged Navier Stokes equations (RANSE) are solved, but also Euler equations or potential flows for incompressible fluid are used. 2-D flow studies are most common. The field equations are numerically solved by either Finite Difference Methods (FDM), Finite Volume Methods (FVM) or Finite Element Methods (FEM). The use of Boundary Element Methods (BEM) is based on a velocity potential satisfying Laplace equation. Methods based on field discretization can handle nonlinear free surface motion by height function method, marker method, volume of fluid method or a level set technique.

More recently some meshless methods have been developed to deal with large deformations and even fragmentation of the free surface. Among these, Smoothed Particle Hydrodynamics (SPH) [13] is currently under testing for sloshing problems by Landrini and Colagrossi at INSEAN, Italy. A good agreement with BEM solutions up to breaking has been obtained. Long time simulation for cases with large excitation amplitudes show the ability to follow the post breaking behaviour.

What are then the disadvantages and advantages of using CFD? Advantages are that complex tank geometry, any fluid depth and general excitation may in principle be considered. A CFD method may provide good flow visualization, which is helpful in understanding the flow. Flow separation around internal structures can be simulated by a RANSE-code. A disadvantage is that the CFD methods are time consuming which makes statistical estimates of tank response variables difficult. Some methods may not be robust enough. For instance a Boundary Element Method based on mixed Eulerian-Lagrangian method breaks down when an overturning wave hits the free surface. Numerical problems may also arise with a BEM at the intersection between the free surface and the tank boundary. [14] discussed numerical problems associated with BEM and sloshing. If not sufficient care is shown, some of the methods may numerically loose or generate fluid mass on a long time scale. Since the highest natural period of the fluid motion is strongly dependent on fluid mass, this can result in an unphysical numerical simulation. This was demonstrated by Solaas [15] by using the commercial, multipurpose FLOW-3D code, developed by Flow Science, Inc. The method uses a combination of the SOLA finite difference scheme for solving Navier-Stokes equations and the Volume of Fluid (VOF) technique for tracing the free boundaries of the fluid. Kim [16] has presented a CFD method where conservation of fluid mass is satisfied. The amount of fluid in the tank is corrected for each time step by slightly moving the free surface. The correction is so small that the global motion is not affected.

It seems generally accepted that CFD codes have difficulties in predicting impact loads. This was also the conclusion of the load committee of 13th ISSC in 1997. A reason is rapid changes in time and space occurring even for relatively large local angles between the impacting free surface and the body surface ([17]). Few codes include hydroelasticity during impact. However, if doing so, the structural modeling requires also special care. [9] demonstrated the numerical difficulties in modeling hydroelastic impact of a horizontal beam. The complications are associated with the many structural modes that are initially excited and the very rapid change of the wetted body surface. More analytically based methods were therefore used to provide robust solutions.

There exist examples on satisfactory predictions of non-impact loading by CFD (f. ex. [15] and [18]). However the load committee of the 13th ISSC presented a comparative study by 12 different CFD codes belonging to different classification societies, a shipyard, research organizations and universities. The agreement in predicted free surface elevations in non-extreme cases was not convincing.

[15] illustrated the grid dependence and the sensitivity to parameters used in numerical differentiation and iteration procedures in the FLOW-3D code. The EPSADJ parameter gives an automatic adjustment of the convergence criterion in the pressure iteration algorithm in order to fulfill the continuity equation. The default value is 1.0, but a much smaller value had to be used for resonant fluid motion to satisfy mass conservation. But even so the results were not perfect. A case with EPSADJ=0.01 showed that the volume error was 4% after 30 oscillation periods. This illustrates also the problem of using a multipurpose program. The different main applications have different main important physical effects. The ALPHA parameter in FLOW-3D controls the weighting of the

advective flux terms in Navier-Stokes equation. ALPHA can be between 0 and 1. The default value is 1.0, which means fully upstream differencing and a first order approximation of the advective flux terms is used. ALPHA=0.0 means central differencing, but this gave a numerically unstable solution. It is difficult from a physical point of view to state that the default value ALPHA=1.0 should be used for sloshing. [15] demonstrated that there could be a large sensitivity to choice of parameters and grid size. Convergence studies by decreasing the grid size were performed. This gives a qualitative but not quantitative guidance on how to select grid size. The reasons are that convergence is dependent on the ALPHA parameter and that in some cases the results did not converge by decreasing grid size. There is of course also a limit to how small the grid size can be before the demand on computer resources gets too large.

Instead of developing a CFD code we have decided to develop a more analytically based method. The method is time efficient and seems easy to combine with the ship motions and external linear wave induced loads. The simulation time depends on the chosen approximate modal model and excitation parameters. Consider for instance a typical calculation of 100 forced motion oscillation periods presented later in the paper. This may take from 1 to 20 seconds on a Pentium-III 500. The numbers are based on non-optimized computer code. The fluid depth has to be finite. Our selected procedure applies to any tank shape as long as the tank walls are vertical near the mean free surface. Details have so far been developed for a rectangular 2-D tank and a vertical circular tank. Since irrotational fluid motion is assumed, internal structures causing flow separation can only be treated empirically by Morison type calculations. The basic method assumes infinite tank roof height. The effect of the tank roof impact is handled by generalizing Wagner's method [19]. Since analytically based methods are used, fluid impact load predictions are robust. The effect of hydroelasticity can be incorporated. The method will be described in more details in the next chapter.

ANALYTICALLY BASED SLOSHING MODEL

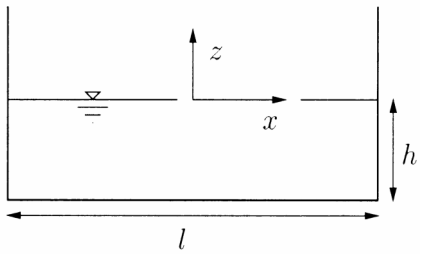

Figure 1: Coordinate system and tank dimensions

We describe first the basic method, which assumes infinite tank roof height. Details will be shown for 2-D flow and a rectangular rigid tank. The tank can have a general forced motion in surge (or sway), heave and pitch (or roll), but the main frequency component σ of the forced oscillation has to be in the vicinity of the lowest natural frequency σ_1 for the tank fluid motion. The fluid is incompressible and the flow is irrotational. The fluid depth and the breadth of the tank are h and l. The coordinate system (x, z) is fixed relative to the tank with origin in the mean free surface and the center of the tank (See Fig. 1). The procedure is based on a Bateman-Luke variational principle and use of the pressure in the Lagrangian of the Hamilton principle. This results in a system of nonlinear ordinary differential equations in

time. The unknowns are generalized coordinates β_i of the free surface elevation. The free surface elevation ζ is written as

$$\zeta = \sum_{i=1}^{N} \beta_i(t) \cos\left(\frac{\pi i(x+0.5l)}{l}\right) \tag{1}$$

Since Eq. 1 assumes ζ to be a single-valued function of x, it implies no overturning waves and vertical tank sides in the free surface. Further Eq. 1 does not permit travelling waves. The consequence is that shallow water conditions cannot be simulated. The forced oscillation amplitude is assumed small and of $O(\varepsilon)$. There exist different possibilities for how to order β_i, but it should reflect that the fluid response is lower order than $O(\varepsilon)$. This reflects that a strong amplification of the flow occurs due to a small excitation. However, in order to develop an asymptotic theory, we must assume ζ to be asymptotically small. The original method presented by Faltinsen et al. [20] assumed $\beta_i = O(\varepsilon^{i/3})$, $i = 1,3$. Higher order terms than ε are neglected in the nonlinear equations. The following system of nonlinear ordinary differential equations for the generalized coordinates describing the free surface are derived for forced motions

$$\begin{aligned}
&\left(\ddot{\beta}_1 + \sigma_1^2\beta_1\right) + d_1\left(\ddot{\beta}_1\beta_2 + \dot{\beta}_1\dot{\beta}_2\right) + d_2\left(\ddot{\beta}_1\beta_1^2 + \dot{\beta}_1^2\beta_1\right) \\
&\qquad + d_3\ddot{\beta}_2\beta_1 + P_1(\dot{v}_{0x} - S_1\dot{\omega} - g\psi) + Q_1\dot{v}_{0z}\beta_1 = 0 \\
&\left(\ddot{\beta}_2 + \sigma_2^2\beta_2\right) + d_4\ddot{\beta}_1\beta_1 + d_5\dot{\beta}_1^2 + Q_2\dot{v}_{0z}\beta_2 = 0 \\
&\left(\ddot{\beta}_3 + \sigma_3^2\beta_3\right) + d_6\ddot{\beta}_1\beta_2 + d_7\ddot{\beta}_1\beta_1^2 + d_8\ddot{\beta}_2\beta_1 + d_9\dot{\beta}_1\dot{\beta}_2 \\
&\qquad + d_{10}\dot{\beta}_1^2\beta_1 + P_3(\dot{v}_{0x} - S_3\dot{\omega} - g\psi) + Q_3\dot{v}_{0z}\beta_3 = 0 \\
&\ddot{\beta}_i + \sigma_i^2\beta_i + P_i(\dot{v}_{0x} - S_i\dot{\omega} - g\psi) + Q_i\dot{v}_{0z}\beta_i = 0, \quad i \geq 4
\end{aligned} \tag{2}$$

Here dots mean time derivatives. v_{0x} and v_{0z} are projections of translational velocity onto axes of Oxz, $\omega(t)$ and $\psi(t)$ are the angular velocity and angle of coordinate system $Oxyz$ with respect to an earth fixed coordinate system. Both v_{0x} and ω cannot be zero. g means acceleration of gravity. The calculation formulas for the coefficients σ_i, P_i, S_i, Q_i, $i \geq 1$ and d_j, $j = 1,\ldots,10$ are given in Faltinsen et al. [20]. σ_i means the natural frequencies. The equation system is solved numerically by a fourth order Runge-Kutta method.

Faltinsen & Timokha [21] found that the excitation amplitude had to be very small and that the depth should not be close to the critical value $h/l = 0.3374$ in order for Eqs. 2 to be valid. This was explained to be due to secondary resonance. An example of such mechanisms is as follows. Nonlinearities cause oscillations with frequency 2σ, where σ is the excitation frequency of the rigid body motion. If the second natural frequency σ_2 of the fluid is close to 2σ, secondary resonance will occur. The generalized coordinate β_2 will be amplified and can be of same order as β_1. Nonlinear interactions can also

cause resonant oscillations at the other natural frequencies. If the excitation amplitude is increased, the fluid response becomes large in an increased frequency domain around the first natural frequency. This increases the possibility that large nonlinearly excited resonance oscillations at a higher natural frequency can occur. Both the second and third mode associated with respectively β_2 and β_3 can be the same order as β_1. Since the amplification of the fluid motion is relatively larger at the critical depth than at other fluid depths, the upper bound of tank excitation amplitude where the theory of Faltinsen et al. [20] is applicable for critical depth is relatively small. An adaptive procedure that allows for different ordering of β_i is presented by Faltinsen & Timokha [21]. This worked for all excitation periods as long as $h/l > 0.24$. When $h/l < 0.24$, good agreement with experiments was documented in isolated cases for h/l down to 0.173.

When the water impacts on the tank roof, fluid damping is believed to occur. The hypothesis is that the kinetic and potential energy in the jet flow caused by the impact is dissipated when the jet flow later on impinges on the free surface. The latter process resembles rainfall on water. We will illustrate the procedure by the tank with chamfered tank roof shown in Fig. 3. The upper corner is one half part of a wedge. When the water reaches this corner, the problem is similar to water entry of a wedge. Rognebakke & Faltinsen [22] estimated the damping of sloshing due to tank roof impact, by first evaluating the potential and kinetic energy flux $\mathrm{d}E_{\mathrm{pot}}/\mathrm{d}t$ and $\mathrm{d}E_{\mathrm{kin}}/\mathrm{d}t$ into the jet caused by the impact. The ambient flow was based on [20], but [21] can also be used. This theory gives a time varying impact velocity and radius of curvature R of impacting surface. R has to be large, i.e. run-up cannot be considered. The Wagner theory is convenient to use because a time varying velocity, R and the change from the wedge part to the horizontal part of the roof can be analytically accounted for. The effect of the tank bottom and the opposite wall is negligible (Faltinsen & Rognebakke [23]). Since the Wagner theory overpredicts $\mathrm{d}E_{\mathrm{pot}}/\mathrm{d}t$ and $\mathrm{d}E_{\mathrm{kin}}/\mathrm{d}t$, a correction factor based on the similarity solution by Dobrovol'skaya [24] was introduced. An alternative is to use the generalized Wagner theory presented by Faltinsen [25]. The linear damping terms $2\xi\sigma_i\dot{\beta}_i$ are included in each of Eqs. 2. The damping is found as an equivalent damping so that the energy ΔE removed from the system during one full cycle is equal to the kinetic and potential energy lost in the impact, i.e. $\xi = \Delta E/(4\pi E)$. E is the total energy in the system, which is found from $\dot{E} = F_x v_{0x}$ for forced surge motion. Here F_x is the horizontal hydrodynamic force. An iterative procedure is followed. A simulation over one period is started with no damping. A first estimate of ξ is found. The simulation is repeated, which results in a new ΔE and thereafter a new ξ. This is done for iteration $i > 1$ as $0.5(\Delta E_i + \Delta E_{i-1})/E = 4\pi\xi$. Typically, 5 iterations are sufficient for convergence. The procedure conserves fluid mass, which is essential in sloshing problems. Further, when the basic method and the tank roof impact model are combined, overturning waves are accounted for through the impact model.

Faltinsen et al. [20] presented an extensive validation by comparing with experimental values of free surface elevation in a rectangular tank with 2-D flow. The tank was forced to oscillate in the horizontal direction in the cross-sectional plane with excitation frequency in the vicinity of the lowest natural frequency. It was demonstrated that it takes a very long time for transient fluid motion to die out when the fluid does not hit the tank roof in a smooth tank. This implies that damping is very low and that viscosity does not matter. Modulated (beating) waves occurred as a consequence of transient and forced oscillations. Strong nonlinearities were evident.

Faltinsen & Timokha [21] presented also an extensive validation for rectangular and prismatic tanks. Steady state values of horizontal force and roll moment amplitudes as well as free surface elevation were studied. The maximum forced surge harmonic oscillation amplitude $|\eta_1|$ was 0.1 times the breadth and the maximum forced harmonic pitch oscillation amplitude was 0.1 rad. We will present one example and at the same time compare with FLOW-3D calculated by [15] (Fig. 2).

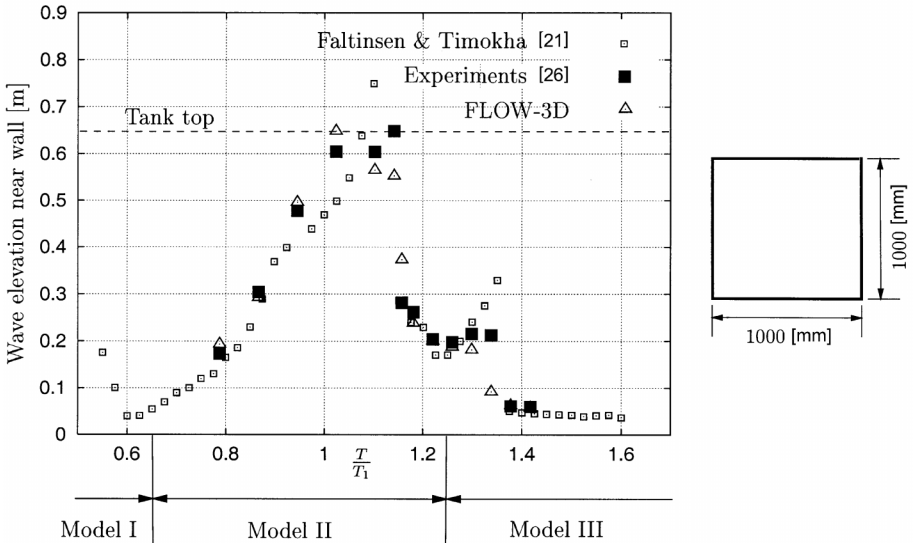

Figure 2: Steady-state maximum wave elevation near the wall vs. "forced period (T)-first natural period (T_1) ratio". Rectangular tank with $h/l = 0.35$, $|\eta_1| = 0.05l$

The fluid depth is 0.35 times the breadth, which is close to the critical depth. The grid size used in the FLOW-3D calculations was $\Delta x = \Delta z = 0.025$ m, where Δx and Δz are respectively the horizontal and vertical distance between adjacent grid points. This means a total of 40×40 elements. The ALPHA and EPSADJ parameters were respectively 0.5 and 1.0. Three different models were used in the adaptive multimodal approach by Faltinsen & Timokha [21]. These correspond to different ordering of the generalized free-surface coordinates β_i (See Eq. 1). The first stage of the analysis by [21] is to locate possible resonances for T/T_1 between 0.45 and 1.65. The primary resonances of the first and third mode occur at respectively $T/T_1 = 1$ and $T/T_1 = 0.55$. The secondary resonance of the second mode is predicted at $T/T_1 = 1.28$. The

secondary resonance of the third mode is at $T/T_1 = 1.55$. The positions of primary and secondary resonances are important for selection of model. The models are indicated as Model I,II and III. It was controlled that the models overlap with each other in a small frequency domain. Model I was used for $0.5 \le T/T_1 \le 0.65$. The expected resonances are due to primary excitation of the third and first mode. They have the same main frequency response σ. No secondary resonance is expected. This causes the relations $\beta_1 \approx \beta_3 = O(\varepsilon^{1/3})$. This means that the secondary modes have the main harmonic 2σ. Such modes are $\beta_2 \approx \beta_6 = O(\varepsilon^{2/3})$. Other modes (up to 9th) are considered as driven and having $O(\varepsilon)$. Model II was used for $0.6 \le T/T_1 \le 1.25$. The system is of third order in β_1 and β_2. It contains all the necessary terms in Eq. 2 as well as a theory considering $\beta_1 \approx \beta_2 = O(\varepsilon^{1/2})$. The modes β_3, β_4, β_5 and β_6 were included as driven. If the response is not too large, the modal system gives the same results as Eqs. 2. When $T/T_1 > 1.28$, the third mode response was assumed to have the same order as β_1 and β_2 (Model III). The reason is the influence of the secondary resonance of third mode at $T/T_1 = 1.55$. Model III was used for $1.28 \le T/T_1 \le 1.65$. The predicted values in Fig. 2 belong to different branches of the steady-state periodic solution. The concept of branches of the solutions was for instance extensively discussed by Faltinsen et al. [20]. There exist in their solution an upper and lower branch. The lower branch is divided into an upper and lower branch. The lower branch is divided into a stable and unstable sub-branch with a turning point between them. A jump in the solution will happen at an excitation period corresponding to the turning point. The results in Fig. 2 have two jumps, one around $T/T_1 = 1.1$ and the other one around $T/T_1 = 1.3$. Fig. 2 shows that the multimodal approach by Faltinsen & Timokha [21] agrees well with the experiments. No tank roof damping was included. Even if the steady-state free surface elevation did not hit the tank roof, impact would occur during the transient phase. The FLOW-3D calculations agree also well with the experiments. However, it should be noted that the results would depend on grid size and the ALPHA and EPSADJ parameters previously discussed.

Horizontal forced harmonic oscillations of the LNG tank in Fig. 3 will now be studied. Two-dimensional fluid motions occur. The mean fluid depth h is $0.4l$ where l is the tank breadth. The forced oscillation amplitude $|\eta_1|$ is $0.01l$. Fig. 3 shows numerical and experimental predictions of steady-state maximum horizontal force F as a function of the forced oscillation frequency σ. The lowest natural frequency σ_1 is 4.36 rad/s. Various fluids with different viscosity are used in the experiments. This has small influence on the non-dimensional force. There are two theoretical curves based on Faltinsen & Timokha [21]. One assumes infinite tank roof height and the other one accounts for tank roof damping. The impact-induced horizontal force is not included in the latter case. The effect of the two lower corners submerged in the fluid was neglected. The error in doing so is small ([21]). The previous described Model II and III were used for respectively $0.65 \le T/T_1 \le 1.3$ and $1.3 \le T/T_1 \le 1.65$. Results by FLOW-

3D published by [15] are also presented in Fig. 3. The grid size was $\Delta x = 0.0276$ m and $\Delta z = 0.02782$ m corresponding to 50×37 elements. The effect of the corners was accounted for. There are also shown two curves corresponding to ALPHA=1.0 and 0.5. In both cases EPSADJ=0.01 which is different from the value used in connection with Fig. 2. The presented results for ALPHA=1.0 and 0.5 are clearly different. The results obtained with the default value ALPHA=1.0 are furthest away from the experiments. The agreement between FLOW-3D and the experiments is fair. The results based on Faltinsen & Timokha [21] and accounting for tank roof impact are in good agreement with experiments. The simulations with infinite tank roof height give jumps between different solution branches at certain frequencies. These jumps disappear when tank roof impact damping is introduced.

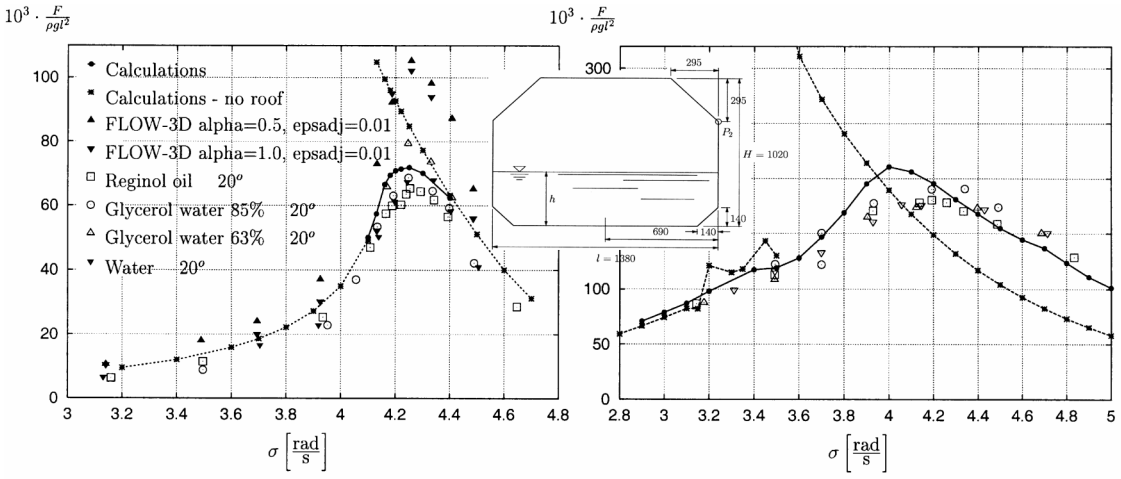

Figure 3: Maximum horizontal force F per unit length of LNG tank as a function of forced oscillation frequency σ. Forced surge amplitude $|\eta_1| = 0.01l$ (left) and $|\eta_1| = 0.1l$ (right). Mean fluid depth $h = 0.4l$. l=tank breadth, ρ=mass density of the fluid. Experiments by Abramson et al. [2]. Length dimensions in [mm]

Fig. 3 shows also comparisons between theory and experiments for the larger surge excitation amplitude $|\eta_1| = 0.1l$. This represents a realistic design excitation. Only the analytically based sloshing models are used. We note the significant effect of tank roof damping when $\sigma >\approx 3.5$ rad/s. Accounting for tank roof impact was not straightforward for $|\eta_1| = 0.1l$. Very violent motions occurred initially for 3.4rad/s < σ < 4.2rad/s. An artificial damping coefficient was therefore introduced in the transient phase. When the free surface motion reached a less violent state, our tank roof damping model was switched on. Fig. 3 demonstrates good agreement between theory and experiments. One may note that the sloshing force for $\sigma >\approx 4.0$ rad/s is larger when tank roof impact is included in the calculations. Examining the force expression will illuminate this. The horizontal hydrodynamic force for forced surge oscillations can according to [20] and [21] be written as

$$F_x = -m_l\left(\frac{\mathrm{d}v_{0x}}{\mathrm{d}t} + \frac{\mathrm{d}^2 x_C}{\mathrm{d}t^2}\right) \tag{3}$$

where m_l is the fluid mass and x_C is the instantaneous horizontal position of the mass-centre of the fluid relative to the tank fixed coordinate system. x_C is a function of the generalized coordinates β_i. Fig. 4 shows how the magnitude is increased and the phasing shifts for the term depending on x_C, when impact damping is accounted for. This leads to a larger total hydrodynamic force even if the free surface elevation is smaller.

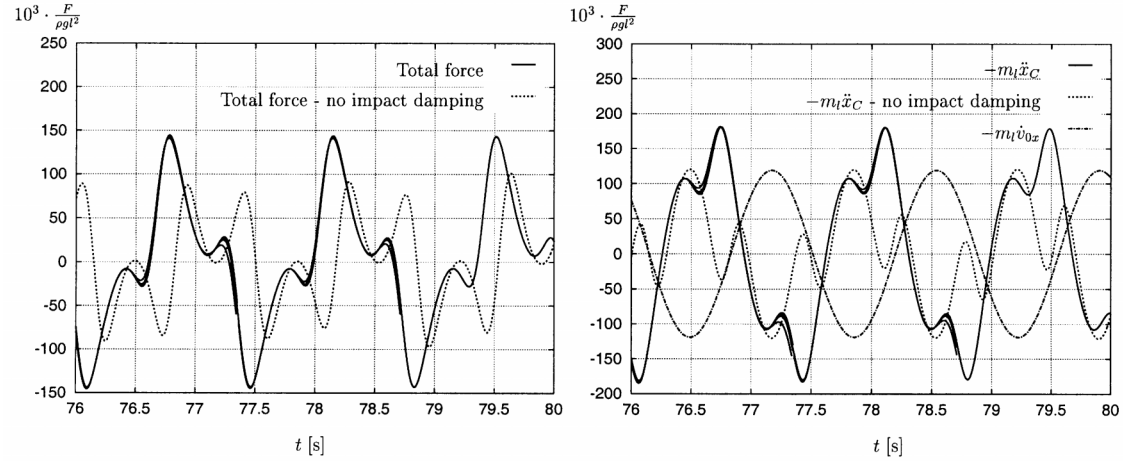

Figure 4: Contributions to the total horizontal hydrodynamic force F per unit length on the LNG tank shown in Fig. 3 for a forced sway frequency $\sigma = 4.6$ rad/s. $|\eta_1| = 0.1l$

The analytically based method provides a robust procedure for impact loads. However, this has to be validated for cases where impact pressures are relevant for local structural response. Abramson et al. [2] presented experimental slamming predictions for the LNG tank shown in Fig. 3. This included statistical distributions. The pressure transducer location is indicated as P_2 in Fig. 3. Viscosity seemed to be important when the forced surge amplitude $|\eta_1|$ was 0.01 times the tank breadth l, but not for $|\eta_1| = 0.1l$. Fig. 5 shows computed and experimental pressures for $|\eta_1| = 0.1l$. The computations are for steady state fluid motions. The experimental values are 10% exceedance limits for the pressure. The computed values would represent the most frequently occurring in a long time simulation. What the 10% exceedance level would be depends on the time series. We can very well realize the level of pressure shown in Fig. 5 in the transient phase of our computations. But we would need the complete time series in the experiments to make a quantitative estimate of the 10% exceedance limit. The way that the data by Abramson et al. [2] were presented, suggest that they meant that the process is stochastic. However, in our opinion this particular type of impact on a chamfered tank roof

URN:NBN:no-2322

is deterministic during harmonic excitation of the tank. Another matter is impact on a horizontal tank roof. In that case the impact pressure may very well have a stochastic behaviour, but as previously discussed, maximum pressure is then an irrelevant parameter for local structural response.

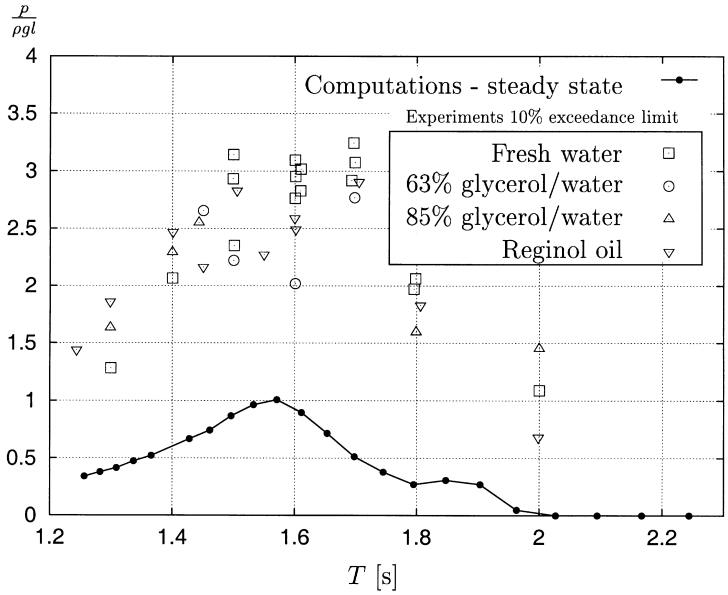

Figure 5: Measured [2] and calculated impact pressures p at the location P_2 in the LNG tank shown in Fig. 3. Presented as a function of forced oscillation period T. $|\eta_1| = 0.1l$

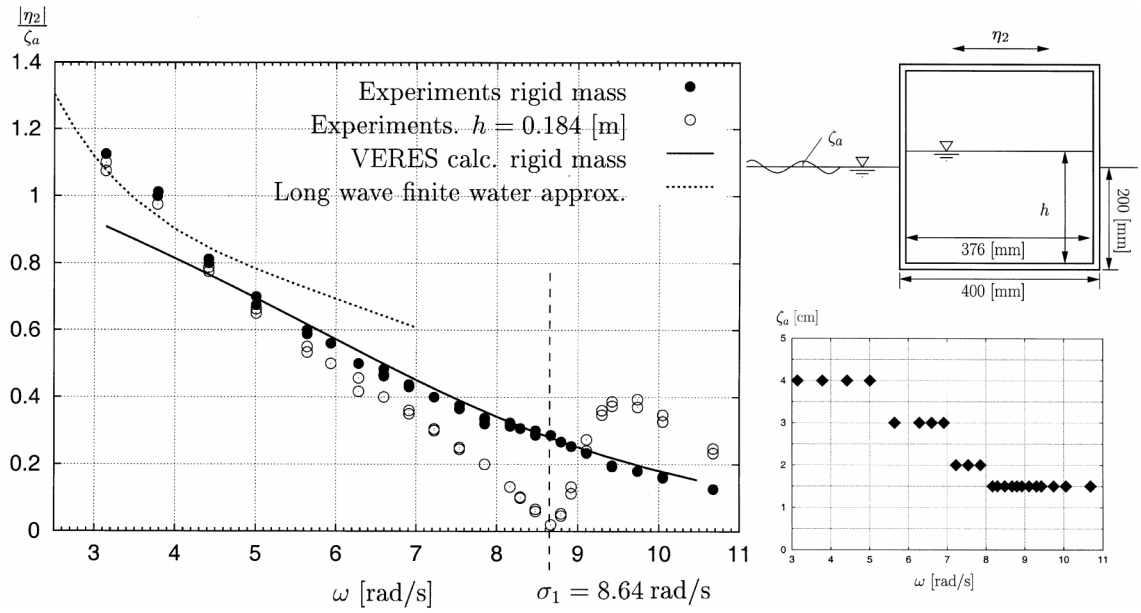

Figure 6: Sway amplitude $|\eta_2|$ of a rectangular ship section in regular beam sea. Waves with frequency ω. σ_1 is the first natural frequency of the fluid motion in the tanks for $h = 0.184$ m

The analytically based sloshing model facilitates coupling between fluid motion in the tank and wave induced ship motion. The predictions must be validated. Experimental 2-D studies with a ship cross-section containing two tanks have therefore been carried out at the wave flume of the Department of Marine Hydrodynamics at the Norwegian University of Science and Technology. The wave flume has an overall length of 13.5m and is 0.6m wide. It is equipped with an electronically operated, computer controlled, single flap wavemaker, calibrated for a water depth of 1.03m. The wavemaker has the ability to dampen out waves reflected by the model at the same time as new waves are generated. The rectangular ship section shown in Fig. 6 is free to move in sway. The draught is 0.20m, and the section is excited by regular beam waves with frequency ω. The length of the ship model is 0.596m. The weight of the model is adjusted to be equal to the buoyancy for both empty and half-filled tanks. The amplitude ζ_a of the incoming wave is lowered as the wave frequency increases. The relationship between ζ_a and ω is shown in Fig. 6. The model contains two identical tanks with an inner length l=0.376mm. The width of a tank is 0.15m, and the height is 0.388m. The section is prevented from drifting off by two springs with a total stiffness of 30.9 N/m.

Fig. 6 shows calculated and measured values for the sway amplitude $|\eta_2|$ of the section. The calculations have presently not been performed with fluid inside the tanks. The sway amplitude is normalized by the amplitude of the incoming wave.

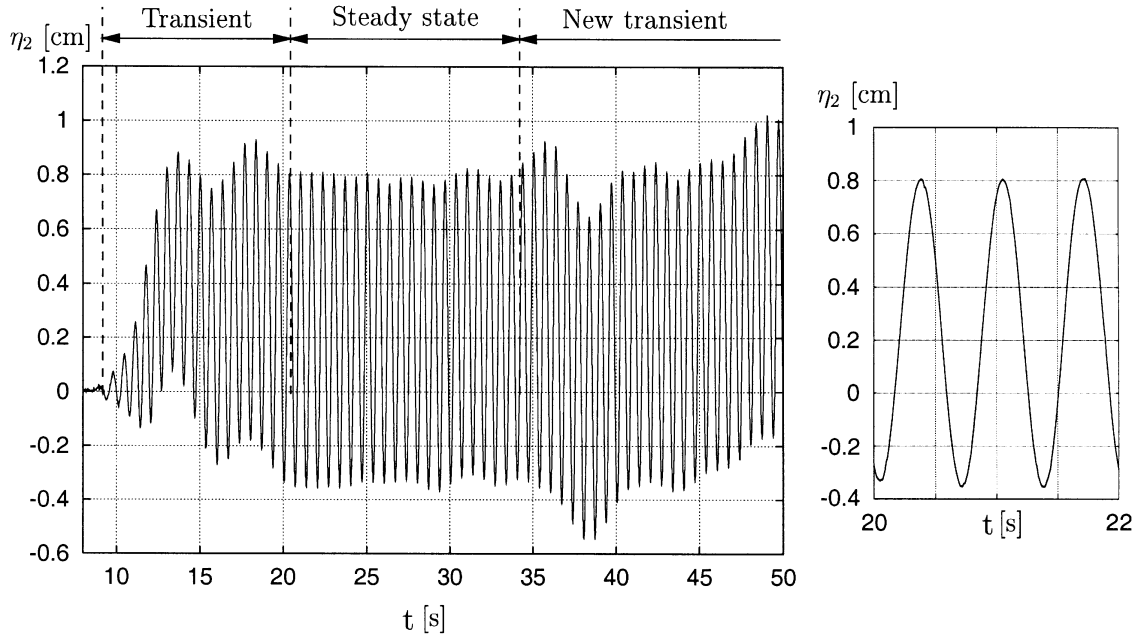

Figure 7: Example of time history of the sway motion of the ship section shown in Fig. 6 with fluid in the tanks. $\omega = 9.42$ rad/s and $\zeta_a = 0.015$ m

Fig. 7 shows a typical time history of the measured sway motion of the ship section. First there is a transient phase before the system reach a steady state. A beating period of approx. 5 seconds is evident during the transient phase. This is the eigenperiod for horizontal motion of the system consisting of the springs and the ship model without fluid in the tanks. A shift in mean position of the section occurs due to 2. order drift force. The steady state is ended when waves are reflected from the wavemaker and beach at the end of the wave flume and a second transient phase starts. The steady state motions show almost no trace of higher order harmonics. This indicates that the higher order part of the sloshing force is filtered out by the system. The experimental results for rigid mass agree well with the computed values from the linear seakeeping code VERES. In these computations, infinite water depth is assumed. This explains the discrepancy for low frequencies. Calculated results from long wavelength, finite water depth theory show better agreement when the wavelength is long compared to the water depth and section length.

We observe a large effect of the fluid motions inside the tanks for $\omega >\approx 7$ rad/s. Excitation with $\omega <\approx 9$ rad/s results in a lower sway response for half-filled tanks than for a rigid mass. The resulting force from the fluid motion in the tanks acts then against the sway excitation force. When $\omega \approx \sigma_n$ there is almost no sway motion. For $\omega >\approx 9$ rad/s the sway motion is increased due to the fluid in the tanks. This behaviour can be qualitatively explained by using a linear model for the sloshing. We then find that the phase of the horizontal sloshing force shifts 180° when the excitation frequency is changed from being slightly below to slightly above the first natural frequency. This is well known from linear dynamic systems.

CONCLUSIONS AND PERSPECTIVES

Sloshing represents violent fluid motion with strong nonlinearities during resonant motion in the vicinity of the highest natural period. The physical behaviour during impact is discussed. The importance of hydroelasticity for small angles between impacting fluid and body surface is stressed. The very high slamming pressures are then unimportant for the structural response.

CFD methods are reviewed. The drawbacks are long simulation time, sensitivity to numerical parameters and general inability to predict strong impact. An analytically based sloshing model is therefore recommended. Its drawbacks are that the tank has to be smooth with vertical sides at the free surface. Shallow fluid phenomena are excluded.

The importance of tank roof impact damping on sloshing is demonstrated. Extensive validation of free surface elevation, total forces and moments for 2-D flow in rectangular and prismatic tanks by the analytical method is reported. This includes realistic motion excitation and studies close to critical depth 0.3374 times the tank breadth.

The analytical method provides a robust way to predict impact pressures. However, this has to be validated for cases where impact pressures are relevant for local structural response. The study shows that steady-state impact pressures are clearly lower than would occur during a transient phase.

URN:NBN:no-2322

Experimental studies where hydroelasticity matters during impact are recommended.

The structure of the analytical method facilitates coupling with the ship dynamics. Experimental 2-D studies with a ship cross-section containing two tanks are presently performed. These show that the ship response can be strongly influenced by the fluid motion in the tanks. The next step is to perform a complete time domain solution of a ship by combining external linear wave loads with the nonlinear analytically based sloshing model for head and beam sea conditions.

The details of the analytically based method have to be developed for a ship tank with 3-D flow. A 3-D rectangular tank would represent a direct generalization of the 2-D method for a rectangular tank. Analysis can be used to the same extent. However, a tapered tank would require numerical methods to describe the linear eigenfunctions as a part of the solution procedure.

AKNOWLEDGEMENTS

The contributions from Dr. Hang Sub Urm from DNV concerning important sloshing problems are appreciated.

BIBLIOGRAPHY

[1] Abramson, M.N., Chu, W.H., Kana, D.D. : ”Some Studies of Nonlinear Lateral Sloshing in Rigid Containers”, *Journal of Applied Mechanics*, Vol. 33, No. 4, (1966).

[2] Abramson, M.N., Bass, R.G., Faltinsen, O.M., Olsen, H.A. : ”Liquid Slosh in LNG Carriers”, *10th Symp. on Naval Hydrodynamics, Boston*, (1974).

[3] Verhagen, J.H.G, and van Wijngaarden, L. : “Nonlinear Oscillations of Fluid in a Container” , *J. Fluid Mech.,* Vol. 22, Part. 4, (1965).

[4] Hansen, H.R. : ”Damage Experience, Potential Damages, Current Problems Involving Slosh Considerations”, *Seminar on Liquid Sloshing, Det Norske Veritas, Høvik, Norway,* (1976).

[5] Faltinsen, O.M. : ”Sea Loads on Ships and Offshore Structures”, *Cambridge University Press*, (1990).

[6] Faltinsen, O.M. : ”The Effect of Hydroelasticity on Slamming”, *Phil. Trans. R. Soc. Lond.*, A. 355, pp. 575-591, (1997).

[7] Faltinsen, O.M., Kvålsvold, J., and Aarsnes, J.V. : ”Wave Impact on a Horizontal Elastic Plate”, *J. Marine Science and Techn*., Vol. 2, No. 2, pp. 87-100, (1997).

[8] Haugen, E.M. : ”Hydroelastic Analysis of Slamming on Stiffened Plates with Application to Catamaran Wetdeck*”, Dr. Ing. thesis, Dept. Marine Hydrodyn., NTNU, Trondheim, Norway*, (1999).

[9] Kvålsvold, J. : “Hydroelastic Modelling of Wetdeck Slamming on Multihull Vessels”, *Dr. Ing. thesis, Dept. Marine Hydrodynamics, NTH, Trondheim, Norway*, MTA-Report 1994:100, (1994).

[10] Kvålsvold, J., Faltinsen, O.M., Aarsnes, J.V. : "Effect of Structural Elasticity on Slamming Against Wetdecks of Multihull Vessels", *Proc. PRADS'95, Korea, The Society of Naval Architects of Korea*, pp. 1.684-1699, (1995).
[11] Faltinsen, O.M. : "Slamming on Ships", Keynote lecture, *IMAM 2000, Naples, Italy*, (2000).
[12] Faltinsen, O.M. : "Water Entry of a Wedge by Hydroelastic Orthotropic Plate Theory" , *J. Ship Research*, Vol. 43, No. 3., pp. 180-193, (1999).
[13] Monaghan, J.J. : "Smoothed Particle Hydrodynamics", *Annu. Rev. Astron. Astrophys*, Vol. 30, pp. 543-74, (1992)
[14] Landrini, M., Grytøyr, G., Faltinsen, O.M. : "A B-Spline based BEM for Unsteady Free-Surface Flows", *J. Ship Research*, Vol. 13, No. 1, pp. 13-24, (1999).
[15] Solaas, F. : "Analytical and Numerical Studies of Sloshing", *Dr. Ing. thesis, Dept. Marine Hydrodynamics, NTNU, Trondheim, Norway*, (1995).
[16] Kim, Y. : "Numerical Simulation of Sloshing Flows with Impact Load", To be submitted
[17] Zhao, R., and Faltinsen, O.M. : "Water Entry of Two-Dimensional Bodies" , *J. Fluid Mech*., Vol. 246, pp. 593-612, (1993).
[18] Mikelis, N.E., Miller, J.K., Taylor, K.V. : "Sloshing in Partially Filled Liquid Tanks and Its Effect on Ship Motions" , *Numerical simulations and experimental verification, RINA, Spring meeting*, (1984).
[19] Wagner, H. : Über Stoss- und Gleitvorgänge an der Oberflache von Flussigkeiten", *Zeitschr. F. Angew. Math. und Mech*., 12, pp. 193-235, (1932).
[20] Faltinsen, O.M., Rognebakke, O.F., Lukovsky, I.A., Timokha, A.N. : "Multidimensional Modal Analysis of Nonlinear Sloshing in a Rectangular Tank with Finite Water Depth" , *J. Fluid Mech*., Vol. 407, pp. 201-234, (2000).
[21] Faltinsen, O.M, and Timokha, A.N. : "Adaptive Multimodel Approach to Nonlinear Sloshing in a Rectangular Tank" , To be published in J. Fluid Mech., (2000).
[22] Rognebakke, O.F., and Faltinsen, O.M. : "Damping of Sloshing due to Tank Roof Impact" , *15th Int. Workshop on Water Waves and Floating Bodies, Caesarea, Israel*, (2000).
[23] Faltinsen, O.M., and Rognebakke, O.F. : "Sloshing and Slamming in Tanks" , *Hydronav'99-Manouevring'99, Gdansk-Ostrada, Poland*, (1999).
[24] Dobrovol'skaya, Z.N. : "On Some Problems of Similarity Flow of Fluid with a Free Surface" , *J. Fluid Mech*., Vol. 36, pp. 805-829, (1969).
[25] Faltinsen, O.M. : "Water Entry of a Wedge with Finite Deadrise Angle", Submitted to J. Ship Research, (2000).
[26] Olsen, H., and Johnsen, K.R. : "Nonlinear Sloshing in Rectangular Tanks. A Pilot Study on the Applicability of Analytical Models", *Report No. 74-72-5*, Vol. 2, Det Norske Veritas, Høvik, Norway, (1975).

URN:NBN:no-2322

Paper 2

A second order initial value solution of two-dimensional sloshing in rectangular tanks

Rognebakke, O. F. and Faltinsen, O. M.

14th International Workshop on Water Waves and Floating Bodies, Port Huron, Michigan, USA, 1999

Preface

This extended abstract was presented at the 14th International Workshop on Water Waves and Floating Bodies in Port Huron, Michigan, USA. The motivation for this study was the findings from sloshing experiments carried out at the laboratory facilities of Det Norske Veritas at Høvik, Norway. A smooth rectangular tank was forced to move harmonically in sway. The purpose of the experiments was to get hands on experience with sloshing and to gain a better understanding of the physical effects involved.

A distinct feature of the sloshing motion was modulated ('beating') waves as a consequence of interaction between transient and forced oscillations of the free surface flow. A frequency analysis showed the presence of both the lowest natural frequency and the forced oscillation frequency Figure 2.1 illustrates the frequency analysis. A steady-state solution would not capture this behaviour. Nonlinear effects were clearly present in the experimental results.

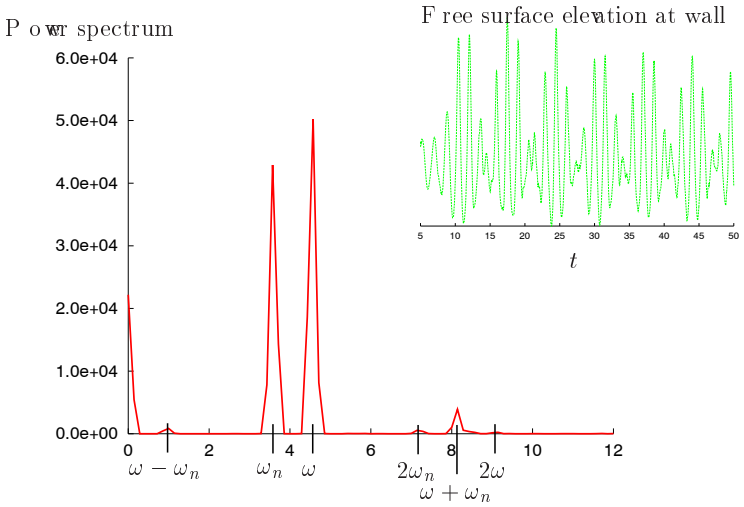

Figure 2.1: Powerspectrum of free surface elevation for rectangular tank forced to oscillate harmonically in sway with frequency ω. The first natural frequency of the fluid motion in the tank is ω_n

Faltinsen (1978) presents a linear initial value solution for two-dimensional sloshing in a harmonically oscillating rectangular tank. The idea was to extend this to second order in a small parameter ϵ that characterizes the order of magnitude of the forced sway amplitude relative to the tank length. The response is assumed to be $\mathcal{O}(\epsilon)$. Since the derivations were based on the linear solution, the same choice of a coordinate system fixed in space was applied. It may have been easier to adopt a coordinate system moving with the tank, as suggested by Prof. B. Molin at the workshop. This would result in homogeneous Neumann wall conditions for the second

order potential. Cointe, Molin, and Nays (1988) have developed an analytical solution for free oscillations of transient waves in a rectangular tank to second order.

The derivations are lengthy and only the final expression for the second order potential would fit in the four pages abstract. Appendix D presents the full derivation. The solution is found for only one set of initial conditions. Although the agreement with the experiments is better than for the linear solution, there is an obvious need for a method including higher order terms.

Alexander N. Timokha from Kiev, Ukraine, arrived at the Department of Marine Hydrodynamics by the time this abstract was finished, and work was initiated to develop a more general nonlinear solution.

A SECOND ORDER INITIAL VALUE SOLUTION OF TWO-DIMENSIONAL SLOSHING IN RECTANGULAR TANKS

Olav F. Rognebakke and Odd M. Faltinsen
Department of Marine Hydrodynamics
Norwegian University of Science and Technology
N-7491 Trondheim, Norway

Environmental concern has led to requirements about double bottoms and skin in new tankers. It is desirable to save steel, and this has led to wide oil tanks that can be smooth inside. The most violent fluid motions inside the tank occur in the vicinity of the highest natural period of the fluid motion. When the tank is smooth, viscous effects are not important and potential flow theory can be used. Nonlinear free surface effects are significant.

Experiments have been carried out with forced harmonic sway oscillations of a rectangular smooth tank. The oscillation frequencies are close to the lowest natural frequency of the fluid motion inside the tank. The results show a clear beating effect that does not die out. A frequency analysis shows the presence of both the lowest natural frequency and the forced oscillation frequency. This implies that a steady-state solution as presented by Faltinsen [1] and Solaas and Faltinsen [2] cannot be used. Nonlinear effects are clearly present in the experimental results. A theoretical solution is derived to explain the experimental findings. The response is assumed to be $\mathcal{O}(\epsilon)$, where the small parameter ϵ characterizes the order of magnitude of the forced sway amplitude relative to the breadth of the tank. A second-order solution in terms of ϵ is derived. This is not valid at resonance. It then seems necessary to assume that the response is of lower order than the excitation. The steady-state solution in [1] and [2] assumes the response to be $\mathcal{O}(\epsilon^{1/3})$. The fluid is assumed incompressible and the flow two-dimensional and irrotational so that there exists a velocity potential Φ_T satisfying the 2-D Laplace equation in the fluid domain. The rectangular tank is oscillating harmonically in sway. The coordinate system is shown in Fig. 1. The tank position relative to equilibrium is $\eta = \epsilon_0 \sin(\omega t)$. The first order potential Φ_1 satisfies the linearized free surface condition and the body boundary conditions on the side walls and the tank bottom. The transient is kept due to a very small damping. The level of damping can be estimated by the use of formulas given in Keulegan [3]. For the tank dimensions used in the experiments it will be less than 0.3% of the critical damping for a linear standing wave at the highest natural period. This means the amplitude is halved after ≈ 100 oscillation cycles. Since potential theory is used, the damping is zero. The initial conditions $\Phi_1 = 0$ and $\partial\Phi_1/\partial t = 0$ on the mean free surface are used. The first order potential is written as $\Phi_1 = \phi_1 + \phi_c$ where $\phi_c = Ax\cos(\omega t)$ is associated with the forced oscillation. The expression for ϕ_1 is

$$\phi_1 = \sum_{n=0}^{\infty} [A_n \cos(\omega_n t) + C_n \cos(\omega t)] \sin\left\{\frac{(2n+1)\pi}{2a}x\right\} \cosh\left\{\frac{(2n+1)\pi}{2a}(z+h)\right\} \qquad (1)$$

where

$$\omega_n^2 = g\frac{(2n+1)\pi}{2a}\tanh\left\{\frac{(2n+1)\pi}{2a}h\right\} \quad , \quad C_n = \frac{\omega K_n}{(\omega_n^2-\omega^2)} \quad , \quad A_n = -C_n - \frac{K_n}{\omega} \tag{2}$$

$$K_n = \frac{\omega A}{\cosh\left\{\frac{(2n+1)\pi h}{2a}\right\}}\frac{2}{a}\left(\frac{2a}{(2n+1)\pi}\right)^2(-1)^n \quad , \quad A = \epsilon_0\omega \tag{3}$$

The second order potential Φ_2 must satisfy the inhomogeneous free surface condition

$$\begin{aligned}\frac{\partial^2\Phi_2}{\partial t^2} + g\frac{\partial\Phi_2}{\partial z} &= -\frac{\partial}{\partial t}\left[\left(\frac{\partial\Phi_1}{\partial x}\right)^2 + \left(\frac{\partial\Phi_1}{\partial z}\right)^2\right] \\ &+ \frac{1}{g}\frac{\partial\Phi_1}{\partial t}\frac{\partial}{\partial z}\left(\frac{\partial^2\Phi_1}{\partial t^2} + g\frac{\partial\Phi_1}{\partial z}\right) \quad \text{on} \quad z=0\end{aligned} \tag{4}$$

the wall condition

$$\frac{\partial\Phi_2}{\partial x} = -\epsilon_0\sin(\omega t)\frac{\partial^2\Phi_1}{\partial x^2} \quad \text{on} \quad x = \pm a \tag{5}$$

and the bottom condition $\frac{\partial\Phi_2}{\partial z} = 0$ on $z = -h$. Further the second order part of the free surface elevation has to satisfy $\int_{-a}^{a}\zeta_2 \mathrm{d}x = 0$. Here

$$\zeta_2 = -\frac{1}{g}\left(\frac{\partial\Phi_2}{\partial t} + \frac{1}{2}[(\frac{\partial\Phi_1}{\partial x})^2 + (\frac{\partial\Phi_1}{\partial z})^2] + \zeta_1\frac{\partial^2\Phi_1}{\partial z\partial t}\right)\Bigg|_{z=0} \tag{6}$$

A possible solution for the second order potential is

$$\begin{aligned}\Phi_2 &= \sum_{n=1}^{\infty} P(t)_n\cos(\frac{n\pi x}{a})\cosh[\frac{n\pi(z+h)}{a}] + B(t) \\ &- \frac{\pi A}{4a\omega}(A_0\sin[(\omega+\omega_0)t] + A_0\sin[(\omega-\omega_0)t] \\ &+ C_0\sin(2\omega t))\cos(\frac{\pi x}{2a})\cosh[\frac{\pi(z+h)}{2a}]\end{aligned} \tag{7}$$

where

$$P(t)_n = P_n^1\sin[(\omega+\omega_0)t] + P_n^2\sin[(\omega-\omega_0)t] + P_n^3\sin(2\omega t) + P_n^4\sin(2\omega_0 t) \tag{8}$$

$$B(t) = B^1\sin[(\omega+\omega_0)t] + B^2\sin[(\omega-\omega_0)t] + B^3\sin(2\omega t) + B^4\sin(2\omega_0 t) \tag{9}$$

Only the dominant term of the series solution for Φ_1 is used in Eqs. 4 and 5 when finding Φ_2. By substituting

$$C^i = \begin{cases} 1 & i = 1,2,3 \\ 0 & i = 4 \end{cases} \qquad D^i = \begin{cases} A_0 & i = 1,2,4 \\ C_0 & i = 3 \end{cases} \qquad H^i = \begin{cases} \omega_0^2 & i = 1,2,4 \\ \omega^2 & i = 3 \end{cases} \tag{10}$$

$$F^i = \begin{cases} \omega+\omega_0 & i = 1 \\ \omega-\omega_0 & i = 2 \\ 2\omega & i = 3 \\ 2\omega_0 & i = 4 \end{cases} \qquad G^i = \begin{cases} \omega\omega_0 & i = 1 \\ -\omega\omega_0 & i = 2 \\ \omega^2 & i = 3 \\ \omega_0^2 & i = 4 \end{cases} \qquad E^i = \begin{cases} C_0A_0 & i = 1,2 \\ \frac{C_0^2}{2} & i = 3 \\ \frac{A_0^2}{2} & i = 4 \end{cases} \tag{11}$$

the expressions for the coefficients P_n^i and B^i are found as

$$\begin{aligned} P_n^i &= C^i \frac{AD^i}{a} \frac{\cosh[\frac{\pi h}{2a}]}{\cosh[\frac{n\pi h}{a}]} \frac{1}{[\frac{n\pi g}{a}\tanh[\frac{n\pi h}{a}] - (F^i)^2]} \cdot \\ &\left(\frac{(-1)^n(1+4n^2)}{(1+2n)^2(1-2n)^2} \frac{\omega(2aH^i \tanh[\frac{\pi h}{2a}] - \pi g)}{g\pi} \right. \\ &+ \left. \frac{(-1)^{n+1}}{(2n-1)(2n+1)} \left[2F^i + \frac{-(F^i)^2 + \frac{\pi g}{2a}\tanh[\frac{\pi h}{2a}]}{\omega} \right] \right) \qquad (12) \\ &+ J^n \frac{E^i F^i \pi}{16ga^2} \frac{\cosh^2[\frac{\pi h}{2a}]}{\cosh[\frac{\pi h}{a}]} \cdot \frac{(3\pi g - 2aG^i \tanh(\frac{\pi h}{2a}) - 2\pi g \tanh^2(\frac{\pi h}{2a}))}{-(F^i)^2 + \frac{g\pi}{a}\tanh[\frac{\pi h}{a}]} \quad i = 1 \cdots 4 \end{aligned}$$

where $J^n = 1$ for $n = 1$ and $J^n = 0$ for $n > 1$. Further

$$\begin{aligned} B^i &= -\frac{AD^i\omega}{2g\pi a} \frac{\cosh[\frac{\pi h}{2a}]}{(F^i)^2} (2aH^i \tanh[\frac{\pi h}{2a}] - \pi g) - \frac{AD^i}{a(F^i)} \cosh[\frac{\pi h}{2a}] \\ &+ \frac{AD^i}{2a\omega} \cosh[\frac{\pi h}{2a}](1 - \frac{g\pi}{2a(F^i)^2} \tanh[\frac{\pi h}{2a}]) \qquad (13) \\ &- \frac{E^i}{16ga^2(F^i)} \pi \cosh^2[\frac{\pi h}{2a}] \left(\pi g + 2aG^i \tanh(\frac{\pi h}{2a}) + 2\pi g \tanh^2(\frac{\pi h}{2a}) \right) \quad i = 1, 2, 3 \end{aligned}$$

$$B^4 = -\frac{E^i}{16ga^2(F^i)} \pi \cosh^2[\frac{\pi h}{2a}](\pi g + 2aG^i \tanh(\frac{\pi h}{2a}) + 2\pi g \tanh^2(\frac{\pi h}{2a})) \qquad (14)$$

The B^3 coefficient contains an additional term $-A^2/(4\omega^2)$. The solution has been verified by checking that Φ_2 satisfies the boundary conditions. The presented solution satisfies $\Phi_2 = 0$ for $t = 0$ while ζ_2 is initially non-zero. A more general solution for Φ_2 can be obtained by adding solutions that satisfy the homogeneous free surface condition and body boundary conditions.

Fig. 2 shows a cross-section of the tank used in the experiments. The tank was forced to oscillate in the horizontal direction in the cross-sectional plane. The length of the tank was 0.20 m, and as long as no plunging wave breaking occurred, the flow was close to two-dimensional even for long time simulations. The excitation was sinusoidal in time after an initial phase. This initial phase lasted for approximately two oscillation periods. The low damping in the tank made it inconvenient to wait for the motion from the last simulation to die out totally before a new run was started. Measurements of the free surface at the positions shown in Fig. 2 were made, and pictures were taken at registered time instants. The sampled time series are 50 seconds long, but video recordings of longer simulations, as long as 5 minutes, showed that the pronounced beating was still present and steady state oscillations with the forced oscillation period was not achieved. This shows that the damping of the fluid motion is even lower than Keulegan found. One reason may be scale effects. Keulegan assumed laminar flow and used smaller models than us. The Reynolds number associated with the boundary layer flow in our experiments suggests turbulent flow.

As a general comment to the experiments, we note the obvious nonlinearity present in the free surface elevation; the increase in crest height and decrease in wave trough relative to a sinusoidal standing wave. Figs. 3 and 4 show the measured and calculated free surface elevation at wave probe FS3 (see Fig. 2) for $h = 0.5$m, forced oscillation period $T = 1.4$s and $\epsilon_0 = 0.047$m. Fig. 5 shows the position of the tank during the first 20 seconds of this simulation. $t = 0$ corresponds to the same time instant in Figs. 3 and 5. The excitation of the tank started at $t = 7.5$s. The first natural period for this situation is $T_0 = 1.75$s. Fig. 3 shows that the free surface is initially in motion. This gives different initial conditions for the simulation (Fig. 4) and the experiment. Also the excitation with an initial phase of an increasing amplitude will lead to differences in the response. The comparison between the measured and calculated free surface elevation at FS3 shown in Fig. 6 is done for a time window after a few initial oscillations. The calculated values are shifted in time so that the zero-crossings of the fast oscillating part and slowly varying envelope match. The 2. order solution gives a better agreement for both the wave trough and wave crest than the 1. order solution. The influence of initial conditions and non-harmonic excitation will be investigated systematically. We should note that the oscillation amplitude of the free surface is clearly larger than the excitation amplitude.

The free surface profile found from the experiments is compared in Fig. 7 with the 1. order and 2. order approximations and with calculations based on the combined numerical and analytical steady-state solution of Solaas and Faltinsen [2]. Here $h = 0.5$m, $T = 2.0$s and $\epsilon_0 = 0.051$m. The time instant is just before the maximum free surface elevation is reached at the right sidewall. We see a tendency to wavebreaking at the wavecrest. Only the dominant term in the series solution of Φ_1 is included in Eq. 6 when calculating ζ_2. This is consistent with keeping only this term when deriving Φ_2.

The second order solution agrees best with the experiments, but there are differences left to explain. We note spilling wavebreaking in the experiments. According to Penney and Price [4], a criterion for wavebreaking of a standing wave is a vertical downward acceleration larger than 1 g. In the simulation corresponding to Fig. 8, we get a maximum downward acceleration of $1.6g$. Higher order harmonics left out in the theory are more important for acceleration than for displacement.

When the forced oscillation period is close to the highest natural period of the fluid motion inside the tank, the water hits the tank ceiling even for very small excitation amplitudes. A more direct numerical method may then be needed. Since local damage due to water impact on the tank ceiling is of concern and hydroelasticity matters in this context, the chosen numerical method must include the effect of dynamic elastic vibrations of the structure. Since long numerical simulations are needed to get proper statistical estimates of the tank behavior in a seaway, it may be worthwhile to use an analytically based method when the water does not hit the tank ceiling. It implies that the presented analytical solution should be generalized to satisfy arbitrary initial conditions.

Acknowledgements

This work is part of a Ph. D. thesis sponsored by the Research Council of Norway and Det Norske Veritas.

References

[1] Faltinsen, O. M., 'A Nonlinear Theory of Sloshing in Rectangular Tanks', *Journal of Ship Research* Vol. 18, No. 4, Dec. 1974, pp. 224-241

[2] Solaas, F. and Faltinsen, O. M., 'Combined Numerical and Analytical Solution for Sloshing in Two-dimensional Tanks of General Shape', *Journal of Ship Research*, Vol. 41, No. 2, June 1997

[3] Keulegan, G. H., 'Energy Dissipation in Standing Waves in Rectangular Basins', *Journal of Fluid Mechanics*, V ol. 6, 1958

[4] P enney W. G. and Price, A. T., 'Finite P eriodic Stationary Gravity Waves in a P erfect Liquid', *Philosophical T ransactions of the R oyal Society* (London), V ol. A 244, 1952, pp. 254-284

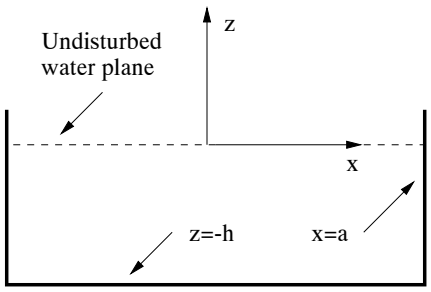

Figure 1: Coordinate system

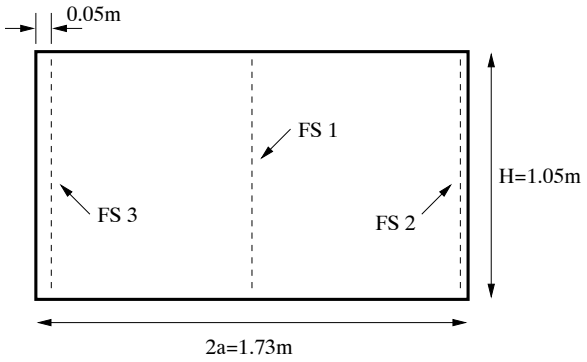

Figure 2: T ank used in the experiments.

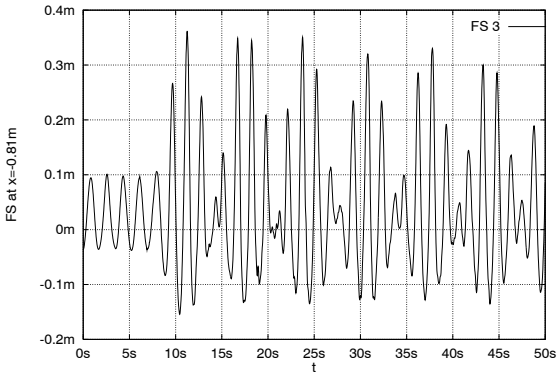

Figure 3: The measured free surface elevation at wave probe FS3 for $h = 0.5$m, $T = 1.4$s and $\epsilon_0 = 0.047$m.

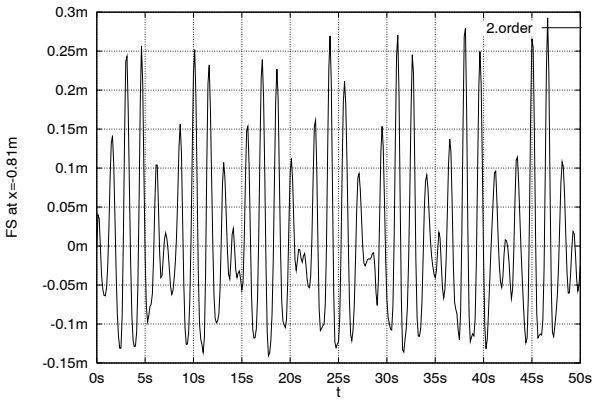

Figure 4: The calculated free surface elevation at the position of w aveprobe FS3 for $h = 0.5$m, $T = 1.4$s and $\epsilon_0 = 0.047$m.

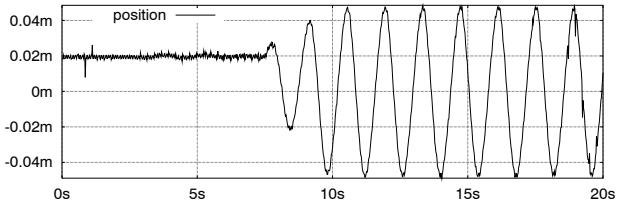

Figure 5: The position of the tank during the measurement presen ted in Fig. 3.

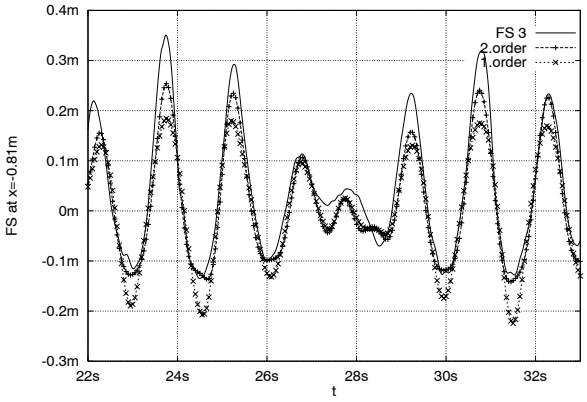

Figure 6: A comparison betw een the measured and calculated free surface. The conditions are as in Fig. 3.

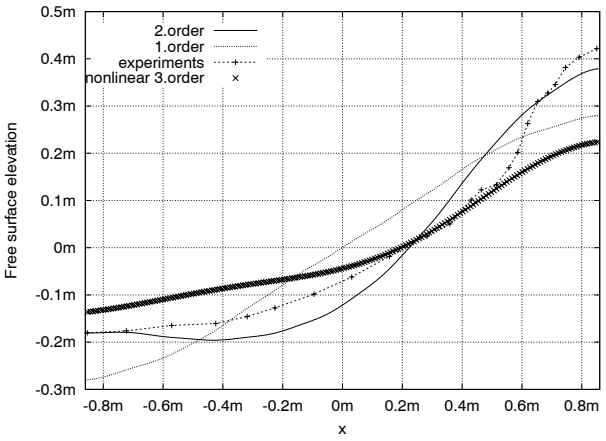

Figure 7: The free surface profile found from the experiments compared with the 1. and 2. order approximations and with calculations based on the combined numerical and analytical solution of Solaas and Faltinsen [2] $h = 0.5$m, $T = 2.0$s and $\epsilon_0 = 0.051$m.

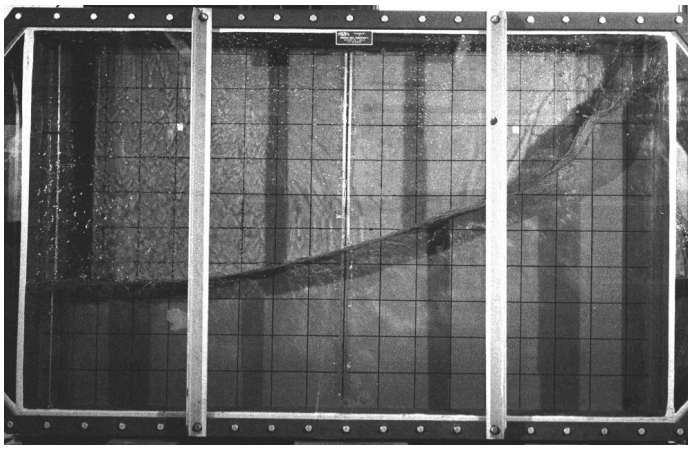

Figure 8: Picture of the sloshing tank for $h = 0.5$m and $T = 2.0$s.

Paper 3

Multidimensional modal analysis of nonlinear sloshing in a rectangular tank with finite water depth

---

Faltinsen, O. M., Rognebakke, O. F., Lukovsky, I. A. and Timokha, A. N.

J. Fluid Mech., **407**, pp. 201-234, 2000

Preface

The nonlinear sloshing models that are applied in the work presented in this thesis are results of theoretical work of Odd M. Faltinsen and Alexander N. Timokha. The first approach that they developed is published in the following paper. The experiments conducted at Det Norske Veritas were used to validate the theory.

Experimental studies of sway sinusoidally excited sloshing validate the modal system for different fluid depths, excitation periods and small excitation amplitudes. Good agreement between theory and experiments is documented.

This asymptotic model has limited applicability in simulating fluid sloshing when the maximum free surface elevation is the order of the tank length l or fluid depth h. This situation occurs when the excitation amplitude is not very small, the depth is close to the critical value $h/l = 0.3374$ or in shallow water.

Some of the shortcomings of this method are addressed by the adaptive multimodal approach by Faltinsen and Timokha (2001). Paper 1 gives an explanation of the differences between the two methods. The adaptive multimodal approach was immediately adopted in the computer code developed by the author for sloshing calculations.

J. Fluid Mech. (2000), *vol.* 407, *pp.* 201–234. Printed in the United Kingdom

Multidimensional modal analysis of nonlinear sloshing in a rectangular tank with finite water depth

By ODD M. FALTINSEN[1], OLAV F. ROGNEBAKKE[1], IVAN A. LUKOVSKY[2] AND ALEXANDER N. TIMOKHA[2]

[1]Department of Marine Hydrodynamics, Faculty of Marine Technology, NTNU, Trondheim, N-7491, Norway

[2]Institute of Mathematics, National Academy of Sciences of Ukraine, Tereschenkivska, 3 str., Kiev, 252601, Ukraine

(Received 29 January 1999 and in revised form 18 October 1999)

The discrete infinite-dimensional modal system describing nonlinear sloshing of an incompressible fluid with irrotational flow partially occupying a tank performing an arbitrary three-dimensional motion is derived in general form. The tank has vertical walls near the free surface and overturning waves are excluded. The derivation is based on the Bateman–Luke variational principle. The free surface motion and velocity potential are expanded in generalized Fourier series. The derived infinite-dimensional modal system couples generalized time-dependent coordinates of free surface elevation and the velocity potential. The procedure is not restricted by any order of smallness. The general multidimensional structure of the equations is approximated to analyse sloshing in a rectangular tank with finite water depth. The amplitude–frequency response is consistent with the fifth-order steady-state solutions by Waterhouse (1994). The theory is validated by new experimental results. It is shown that transients and associated nonlinear beating are important. An initial variation of excitation periods is more important than initial conditions. The theory is invalid when either the water depth is small or water impacts heavily on the tank ceiling. Alternative expressions for hydrodynamic loads are presented. The procedure facilitates simulations of a coupled vehicle–fluid system.

1. Introduction

A main objective is to describe violent fluid motions (sloshing) in a partly filled tank forced to oscillate in a frequency domain close to its lowest natural frequency. The ratio between maximum free surface amplitude and characteristic tank motion amplitude is then high and significant nonlinearities occur. This has practical interest for sloshing in ship tanks. By considering sea states that a ship has to operate in, it is realistic that wave-induced ship motions can cause resonant fluid oscillations. This can lead to large local structural loads in the tank and has an important effect on the global ship motions. It is desirable to develop numerical methods that accurately describe the fluid loading and coupling between ship motions and sloshing. A necessary requirement is that long time simulations can be performed and the proper statistical distribution of response variables obtained for various sea states.

Several studies on different numerical approaches to sloshing have been reported by Su Tsung-Chow (1992), Buechmann (1996), Tanizawa (1996), Chen *et al.* (1997), Pawell (1997) and the Loads Committee of the 13th ISSC (Moan & Berge 1997). A general drawback is the limited ability to perform long time simulations, especially for coupled 'liquid–structure' interactions. It may also be difficult to find water impact loads and local structural response. One reason is that water impact studies would often require a very fine discretization in time and space. Hydroelasticity may also have to be considered. We have instead focused on developing a semi-analytical method based on modal modelling. The present method assumes a smooth tank. This implies that potential theory can be used. The method also requires vertical tank walls near the mean free surface in its equilibrium position. Overturning waves cannot be described. It will be shown that a high degree of analysis can be performed. The consequences are both a time efficient and robust method. Water impact is not studied in detail, but the method can be combined with a local slamming analysis (see Faltinsen & Rognebakke 1999) and applied to coupled 'fluid–tank' simulations. An example is given illustrating the damping effect of forceful water impact on fluid motion.

Modal modelling of nonlinear sloshing implies that the equation of the free surface $\Sigma(t)\colon z = f(x, y, t)$ is expanded in generalized Fourier series by a set of natural modes. The free surface elevation and the unknown velocity potential φ are expressed as

$$\left.\begin{aligned} z = f(x, y, t) &= \sum \beta_i(t)(\text{surfacemode})_i(x, y), \\ \varphi(x, y, z, t) &= \sum R_i(t)(\text{domainmode})_i(x, y, z). \end{aligned}\right\} \tag{1.1}$$

The (x, y, z) coordinate system is fixed relative to the tank; x, y are coordinates in the plane of the unperturbed water surface and t is the time variable. Generally speaking, the surface and volume modes are arbitrary known functions. However, they are typically chosen by the relation

$$(\text{surfacemode})_i(x, y) = (\text{domainmode})_i(x, y, z)|_{\Sigma_0}, \tag{1.2}$$

where Σ_0 is the unperturbed free surface. Since $f(x, y, t)$ is single-valued, (1.1) does not describe overturning waves. Moreover, $(\text{surfacemode})_i(x, y)$ must have a non-varying domain of definition. This means the tank must have vertical walls near the free surface in its equilibrium position.

The generalized coordinates β_i and R_i are found by a coupled system of nonlinear ordinary differential equations (modal system). The derivation of the modal system from the original free boundary problem was first proposed by Narimanov (1957) based on a perturbation technique. It has been further developed by Dodge, Kana & Abramson (1965), Narimanov, Dokuchaev & Lukovsky (1977) and Lukovsky (1990). These and other authors used a perturbation technique combined with variational (Hamilton–Ostrogradsky) projective method and derived small-dimensional models (1–3 degrees of freedom in a vertical circular cylinder) in the generalized coordinates $\beta_i(t)$ or their averaged values (for resonantly excited waves). (See for instance Lukovsky 1976; Miles (1976, 1984*a*, *b*).) Using an averaging technique means that β_i is written as

$$\beta_i = \sum_{j=0}^{\infty} (\langle \beta_i \rangle_j^1(\tau) \sin(j\sigma t) + \langle \beta_i \rangle_j^2(\tau) \cos(j\sigma t)),$$

where σ is the excitation frequency and τ is slowly varying relative to t. The averaged equations of a $\langle \beta_i \rangle^j(\tau)$ have the form of a Duffing equation for a rectangular tank

(see Shemer 1990 and Tsai, Yue & Yip 1990) or a system of four first-order ordinary differential equations for a vertical circular cylindrical tank (see Miles (1984*a*, *b*)). Funakoshi & Inoue (1991) used Miles' model in their detailed simulations. The averaging technique and small-dimensional modal modelling complement each another in the analysis of the steady-state free surface response due to periodic tank excitations. But these methods are questionable in modelling coupled fluid–structure interaction with complicated non-periodic tank motions when transient effects matter. These complex motions are simulated in engineering applications either numerically or by phenomenological (usually pendulum) models (see Chapter 5 of Narimanov *et al.* 1977 or Pilipchuk & Ibrahim 1997). An alternative is to use Narimanov's original technique with the modal representation in the form (1.1) and more general asymptotic assumptions of β_i and R_n in order to reach reasonable dimensions of the modal systems. The successful use of this approach is reported by Limarchenko & Yasinsky (1997) and Lukovsky & Timokha (1995) for simplified models of spacecraft. A similar method was used by Ikeda & Nakagawa (1997) for analysis of damping of vessel motions due to sloshing. This suggests that multidimensional modal analysis can simulate complicated nonlinear wave phenomena coupled with structural vibrations.

The general form of a discrete infinite-dimensional modal system is derived in the first part of this paper by the Bateman–Luke (pressure-integral Lagrangian) variational principle. This idea was proposed independently by Miles (1976) and Lukovsky (1976). They studied forced small-amplitude translatory motions of a vertical circular cylindrical tank. The surfacemodes and domainmodes were obtained by linear theory and related by (1.2). Our derivation of a discrete infinite-dimensional modal system is not restricted to a particular type of body motion. The surface and domain modes are not associated with natural modes and no asymptotic assumptions are introduced in the first stage of the derivation. The infinite-dimensional modal system can be reduced to a finite-dimensional form by assuming small-amplitude forced oscillations and associate order of magnitudes of the different modes. This is done in the second part of the paper to analyse nonlinear sloshing in a two-dimensional rectangular smooth tank with finite water depth. Both forced translatory and rotational body motions are considered. The lowest natural mode is assumed to dominate and the three lowest modes interact nonlinearly with each other. Several modes having higher order are considered by linear theory. The asymptotic theory constructed is a special multidimensional analogue of the model by Ikeda & Nakagawa (1997) and the direct generalization of the third-order hydrodynamic theory by Faltinsen (1974).

Experiments on nonlinear sloshing caused by primary mode resonant excitation have been conducted. The asymptotic modal theory constructed explains the basic observed phenomena including modulated ('beating') waves with a high accuracy of amplitude and 'beating period' characteristics. The beating is a consequence of transients that do not die out on a very long time scale. The reason is the very small damping of the fluid motion inside a smooth tank with no internal structures obstructing the flow and no heavy water impact on the tank ceiling. A consequence is that steady-state response of the fluid motion can have a limited capability to describe sloshing quantitatively. However the steady-state response is valuable to understand important features of the flow like stability and how the response is influenced by water depth, excitation frequency and amplitude. Since it represents a special case of our theory, steady-state solutions are used in the verification process. Examples of steady-state amplitude–frequency response for surge- and pitch-excited nonlinear waves are presented. The results are consistent with the third- and fifth-order steady-state solutions by Faltinsen (1974) and Waterhouse (1994) respectively.

The use of a discrete modal system allows us to calculate various kinematic and dynamic characteristics occurring due to interaction between the fluid and the tank. We present examples of hydrodynamic force and moment on the tank. The structure of the equations describing the fluid motion as a function of the rigid body motions makes it possible to set up an equation system for the coupled tank and fluid motion. An example could be analysis of a ship tank due to wave-induced ship motions. Since the wave conditions that cause violent sloshing may not be extreme, we can use linear time domain theory to describe external hydrodynamic loads acting on the ship. By setting up the equations of motions for the global rigid ship motions together with the equations describing sloshing, complex fluid–structure interaction can be analysed. But the theory does not describe the effect of impact on the tank ceiling. This can easily occur in practical applications and is an area of further research. The asymptotic theory is not applicable to shallow water. This is due to secondary parametric resonance and means that the primary mode is not dominating. The ratio between water depth and breadth of the tank is 0.173 in the example where the finite water depth theory does not work. This is not really shallow water in a hydrodynamic context (see the nonlinear theory by Verhagen & Wijngaarden 1965). What we need is a theory that can combine the present finite water depth theory with a nonlinear shallow water theory.

2. Free boundary value problem

A mobile rigid tank partly filled by an inviscid incompressible fluid is considered. The flow is irrotational. The fluid volume bounded by the free surface $\Sigma(t)$ and the wetted tank surface $S(t)$ is denoted $Q(t)$. Let $O'x'y'z'$ be an absolute coordinate system and $Oxyz$ be a moving coordinate system fixed with respect to the rigid tank. The origin of $Oxyz$ is in the unperturbed free surface and moves with the velocity $\boldsymbol{v}_0$ relative to $O'x'y'z'$. The tank has an angular velocity $\boldsymbol{\omega}$ relative to $O'x'y'z'$. The gravity field has the potential

$$U(x,y,z,t) = -\boldsymbol{g}\cdot\boldsymbol{r}', \qquad \boldsymbol{r}' = \boldsymbol{r}'_0 + \boldsymbol{r}, \tag{2.1}$$

where $\boldsymbol{r}'$ is the radius-vector of a point of the body–fluid system with respect to O', $\boldsymbol{r}'_0$ is the radius-vector of the point O with respect to O', $\boldsymbol{r}$ is the radius-vector with respect to O and $\boldsymbol{g}$ is the gravity acceleration vector.

Since the flow is irrotational, the fluid velocity can be represented as $\boldsymbol{v}_a = \nabla\Phi$, where $\boldsymbol{v}_a$ is the fluid velocity vector at the point (x,y,z) in the moving coordinate system and $\Phi(x,y,z,t)$ is the velocity potential. The velocity potential and the free surface $\Sigma(t)$ can be found from the following nonlinear free boundary problem:

$$\left.\begin{aligned}
&\Delta\Phi = 0 \quad \text{in } Q(t), \qquad \frac{\partial\Phi}{\partial v} = \boldsymbol{v}_0\cdot\boldsymbol{v} + \boldsymbol{\omega}\cdot[\boldsymbol{r}\times\boldsymbol{v}] \quad \text{on } S(t),\\
&\frac{\partial\Phi}{\partial v} = \boldsymbol{v}_0\cdot\boldsymbol{v} + \boldsymbol{\omega}\cdot[\boldsymbol{r}\times\boldsymbol{v}] + \frac{\xi_t}{|\nabla\xi|} \quad \text{on } \Sigma(t),\\
&\frac{\partial\Phi}{\partial t} + \tfrac{1}{2}(\nabla\Phi)^2 - \nabla\Phi\cdot(\boldsymbol{v}_0 + \boldsymbol{\omega}\times\boldsymbol{r}) + U = 0 \quad \text{on } \Sigma(t), \qquad \int_{Q(t)} \mathrm{d}Q = \text{const.}
\end{aligned}\right\} \tag{2.2}$$

Here $\boldsymbol{v}$ is the outer normal to the boundary of $Q(t)$ and $\xi(x,y,z,t) = 0$ is the equation of the free surface $\Sigma(t)$. The last integral condition in (2.2) implies fluid volume conservation and is also the well-known solvability condition for the Neumann boundary value problem.

The free boundary problem (2.2) must be completed by initial or periodicity conditions to get a unique solution. The first type of condition introduces the initial position of the free surface $\Sigma(t_0)$ and the initial distribution of normal derivatives of Φ, i.e.

$$\xi(t_0, x, y, z) = \xi_0(x, y, z), \qquad \frac{\partial \Phi}{\partial v}\Big|_{\Sigma(t_0)} = \phi(x, y, z). \tag{2.3}$$

Here $\xi_0(x, y, z)$ and $\phi(x, y, z)$ are given functions. If the flow starts from rest with sufficiently small tank oscillations, linear theory can be used to formulate the initial conditions. One way of doing this is in terms of impulse conservation. This means

$$\Phi = 0 \quad \text{on } \Sigma_0 \quad \text{and} \quad \text{zero free surface elevation for } t = t_0. \tag{2.4}$$

The last free surface boundary condition (dynamic boundary condition) of (2.2) is obtained by using Lagrange–Cauchy integral for the pressure in the moving coordinate system. It states that the pressure on the free surface is equal to a constant p_0. The hydrodynamic pressure p in $Q(t)$ can be obtained by

$$\frac{\partial \Phi}{\partial t} + \tfrac{1}{2}(\nabla\Phi)^2 - \nabla\Phi \cdot (\boldsymbol{v}_0 + \boldsymbol{\omega} \times \boldsymbol{r}) + U + \frac{p - p_0}{\rho} = 0 \quad \text{in } Q(t). \tag{2.5}$$

Here $\partial\Phi/\partial t$ is calculated in the moving coordinate system, i.e. for a point rigidly connected with the system $Oxyz$.

There is a set of mechanical characteristics (expressed by integrals of Φ and its derivatives), which describes the interaction between the vessel and fluid. They are:

(*a*) the radius-vectors of the mass centre with respect to the points O' and O ($\boldsymbol{r}'_{1C}$ and $\boldsymbol{r}_{1C}$) $\boldsymbol{r}'_{1C} = \boldsymbol{r}'_0 + \boldsymbol{r}_{1C}$, where

$$\rho \int_{Q(t)} U \, \mathrm{d}Q = -\rho \int_{Q(t)} \boldsymbol{g} \cdot \boldsymbol{r}' \, \mathrm{d}Q = -m_1 \boldsymbol{g} \cdot \boldsymbol{r}'_{1C};$$

(*b*) the resulting hydrodynamic forces $\boldsymbol{F}(t)$, and moments $\boldsymbol{N}(t)$ on the tank

$$\boldsymbol{F}(t) = \int_{S(t)} (p - p_0)\boldsymbol{v} \, \mathrm{d}S, \qquad \boldsymbol{N}(t) = \int_{S(t)} \boldsymbol{r} \times ((p - p_0)\boldsymbol{v}) \, \mathrm{d}S. \tag{2.6}$$

3. Derivation of the general modal system by the variational method

Let us consider the boundary value problem (2.2). The unknowns are $\Phi = \Phi(x, y, z, t)$ and $\xi(x, y, z, t)$. We will use a Bateman–Luke variational principle and introduce the pressure in the Lagrangian of the Hamilton principle. The idea of the pressure integral as the Lagrangian in hydrodynamic problems was first proposed by Hargneaves (1908). The canonical formulation of this principle is given by Bateman (1944) and Luke (1967) (for gravity surface waves in infinite basins). We use the formulation given by Lukovsky (1990).

Pressure-integral Lagrangian variational principle. *The boundary value problem given by (2.2) can be described by examining the necessary conditions for the extrema of the functional*

$$W = \int_{t_1}^{t_2} L \, \mathrm{d}t, \tag{3.1}$$

where the Lagrangian L is the pressure integral

$$L = \int_{Q(t)} (p - p_0)\,\mathrm{d}Q = -\rho \int_{Q(t)} \left[\frac{\partial \Phi}{\partial t} + \tfrac{1}{2}(\nabla \Phi)^2 - \nabla \Phi \cdot (\boldsymbol{v}_0 + \boldsymbol{\omega} \times \boldsymbol{r}) + U \right] \mathrm{d}Q; \quad (3.2)$$

and the test functions satisfy

$$\delta\Phi(x, y, z, t_1) = 0, \quad \delta\Phi(x, y, z, t_2) = 0; \quad \delta\xi(x, y, z, t_1) = 0, \quad \delta\xi(x, y, z, t_2) = 0. \quad (3.3)$$

We consider a domain Q having vertical walls in a neighbourhood of the free surface in the equilibrium position. The normal velocity component on the free surface $z = f(x, y, t)$ is given in the body-fixed system by $-\xi_t/|\nabla\xi| = f_t/\sqrt{1 + f_x^2 + f_y^2}$. The velocity potential is expressed as

$$\Phi(x, y, z, t) = \boldsymbol{v}_0 \cdot \boldsymbol{r} + \boldsymbol{\omega} \cdot \boldsymbol{\Omega} + \varphi. \quad (3.4)$$

The vector-function $\boldsymbol{\Omega}(x, y, z) = (\Omega_1, \Omega_2, \Omega_3)$ (Stokes–Zhukovsky potentials) is the solution of the following Neumann boundary value problem:

$$\left.\begin{aligned} &\Delta\boldsymbol{\Omega} = 0 \quad \text{in } Q(t), \\ &\frac{\partial \Omega_1}{\partial v}\Big|_{S(t)+\Sigma(t)} = yv_3 - zv_2, \quad \frac{\partial \Omega_2}{\partial v}\Big|_{S(t)+\Sigma(t)} = zv_1 - xv_3, \\ &\frac{\partial \Omega_3}{\partial v}\Big|_{S(t)+\Sigma(t)} = xv_2 - yv_1, \end{aligned}\right\} \quad (3.5)$$

where v_1, v_2, v_3 are the projections of the outer normal $\boldsymbol{v}$ onto the $Oxyz$-axes. The function φ is a solution of the Neumann boundary value problem

$$\Delta\varphi = 0 \quad \text{in } Q(t), \quad \frac{\partial \varphi}{\partial v}\Big|_{S(t)} = 0, \quad \frac{\partial \varphi}{\partial v}\Big|_{\Sigma(t)} = \frac{f_t}{\sqrt{1 + f_x^2 + f_y^2}}.$$

The Neumann boundary value problems for $\boldsymbol{\Omega}$ and φ have unique solutions since

$$\int_{S(t)+\Sigma(t)} \frac{\partial \Omega_i}{\partial v}\,\mathrm{d}S = 0, \quad \int_{\Sigma(t)} \frac{\partial \varphi}{\partial v}\,\mathrm{d}S = \int_{\Sigma(t)} \frac{f_t}{\sqrt{1 + (\nabla f)^2}}\,\mathrm{d}S = 0$$

are always fulfilled (see Lukovsky & Timokha 1995). These solutions depend parametrically on time. By using (3.4) and the boundary value problems for $\boldsymbol{\Omega}$ and φ it follows that $\boldsymbol{\Phi}$ satisfies the Laplace equation and the Neumann boundary conditions of (2.2). The dynamic condition (pressure balance) on $\Sigma(t)$ gives the final equation connecting $f, \boldsymbol{\Omega}$ and φ.

Let the function $f(x, y, t)$ be expressed as

$$f(x, y, t) = \sum_{i=1}^{\infty} \beta_i(t) f_i(x, y), \quad (3.6)$$

where $f_i(x, y)$ is a complete (to within a constant) orthogonal system of functions satisfying the condition of volume conservation $\int_{\Sigma_0} f_i(x, y)\,\mathrm{d}x\,\mathrm{d}y = 0$. Further,

$$\varphi(x, y, z, t) = \sum_{n=1}^{\infty} R_n(t)\,\varphi_n(x, y, z), \quad (3.7)$$

where the complete system of functions $\varphi_n(x, y, z)$ satisfies the Laplace equation in

the whole tank domain Q and zero Neumann boundary condition on the wetted body surface. Normally, only the wetted body surface below the mean free surface is considered. Since the system $\{\varphi_n(x, y, z)\}$ is complete on any single-connected surface in the tank domain, it is also a complete system on Σ_0. The Stokes–Zhukovsky potentials Ω_i are assumed to be known functions of β_i. Hence, we must only find the unknown functions $\beta_i(t)$ and $R_n(t)$.

Such a family of harmonic functions $\varphi_n(x, y, z)$ can be chosen as a set of solutions of the following boundary spectral problems with spectral parameter λ_n:

$$\Delta\varphi_n = 0 \quad \text{in } Q_0, \quad \frac{\partial\varphi_n}{\partial v} = 0 \quad \text{on } S, \quad \frac{\partial\varphi_n}{\partial v} = \lambda_n\varphi_n \quad \text{on } \Sigma_0, \quad \int_{\Sigma_0} \varphi_n \,\mathrm{d}S = 0. \tag{3.8}$$

This is the same as the linear eigenvalue problem for sloshing. The solutions can be found analytically only for a limited class of tank shapes. Examples are a vertical circular cylinder or a rectangular three-dimensional tank. However, a numerical method can be used to find φ_n for a general tank shape. This was demonstrated by Solaas & Faltinsen (1997), where Moiseev's theory was applied to two-dimensional sloshing. A different approach is to use a patching procedure and consider for instance a tank consisting of a cylindrical part near the free surface. Then the solution in the cylindrical part can be expressed as

$$\varphi_n(x, y, z) = \sum_k (b_{nk} \exp(-\lambda_k z) + a_{nk} \exp(\lambda_k z))\phi_k(x, y) \tag{3.9}$$

with unknown coefficients b_{nk} and a_{nk}. Here λ_k and ϕ_k are the solutions of the following spectral problem:

$$\Delta_2\phi_k(x, y) + \lambda_k^2\phi_k = 0 \quad \text{in } \Sigma_0, \quad \frac{\partial\phi_k}{\partial n} = 0 \quad \text{on } \partial\Sigma_0, \quad \int_{\Sigma_0} \phi_k \,\mathrm{d}S = 0, \tag{3.10}$$

where $\partial\Sigma_0$ is the intersection line between Σ_0 and S. The solution in the non-cylindrical part can be found by a numerical method. When the auxiliary problem (3.10) is formulated in circular (ring-shaped) or rectangular cross-sections Σ_0, the solutions ϕ_k of (3.10) are expressed by Bessel functions and/or sinusoidal functions. Otherwise, a numerical procedure for (3.10) is required.

By substituting (3.4) into (3.2) the Lagrangian L takes the following form:

$$\begin{aligned} L = -\rho \int_{Q(t)} \Big[&\dot{\boldsymbol{v}}_0 \cdot \boldsymbol{r} + \frac{\partial}{\partial t}(\boldsymbol{\omega} \cdot \boldsymbol{\Omega}) + \tfrac{1}{2}\nabla(\boldsymbol{\omega} \cdot \boldsymbol{\Omega}) \cdot \nabla(\boldsymbol{\omega} \cdot \boldsymbol{\Omega}) - \boldsymbol{\omega} \cdot (\boldsymbol{r} \times \nabla(\boldsymbol{\omega} \cdot \boldsymbol{\Omega})) \\ &- \tfrac{1}{2}v_0^2 - \boldsymbol{\omega} \cdot (\boldsymbol{r} \times \boldsymbol{v}_0) - \boldsymbol{\omega} \cdot (\boldsymbol{r} \times \nabla\varphi) + \nabla(\boldsymbol{\omega} \cdot \boldsymbol{\Omega}) \cdot \nabla\varphi \Big] \mathrm{d}Q + L_r, \end{aligned} \tag{3.11}$$

where

$$L_r = -\rho \int_{Q(t)} \left[\frac{\partial\varphi}{\partial t} + \tfrac{1}{2}(\nabla\varphi)^2 + U \right] \mathrm{d}Q. \tag{3.12}$$

The two last integrand terms in square brackets of (3.11) cancel each other from Green's formula, i.e.

$$\int_{Q(t)} (\nabla(\boldsymbol{\omega} \cdot \boldsymbol{\Omega}) \cdot \nabla\varphi - (\boldsymbol{\omega} \times \boldsymbol{r}) \cdot \nabla\varphi) \,\mathrm{d}Q = \int_{S(t)+\Sigma(t)} \left(\frac{\partial(\boldsymbol{\omega} \cdot \boldsymbol{\Omega})}{\partial v} - (\boldsymbol{\omega} \times \boldsymbol{r}) \cdot \boldsymbol{v} \right) \varphi \,\mathrm{d}S = 0.$$

We also introduce the quadratic symmetric inertia tensor $\boldsymbol{J}^1$ with components J_{ij}^1

defined by the equality

$$-\rho\int_{Q(t)}(\tfrac{1}{2}\nabla(\boldsymbol{\omega}\cdot\boldsymbol{\Omega})\cdot\nabla(\boldsymbol{\omega}\cdot\boldsymbol{\Omega})-\boldsymbol{\omega}\cdot(\boldsymbol{r}\times\nabla(\boldsymbol{\omega}\cdot\boldsymbol{\Omega})))\,\mathrm{d}Q$$
$$=-\tfrac{1}{2}\omega_1^2J_{11}^1-\tfrac{1}{2}\omega_2^2J_{22}^1-\tfrac{1}{2}\omega_3^2J_{33}^1-\omega_1\omega_2J_{12}^1-\omega_1\omega_3J_{13}^1-\omega_2\omega_3J_{23}^1.$$

These components J_{ij}^1 can be calculated by Green's formula, i.e.

$$J_{11}^1=\rho\int_{Q(t)}\left(y\frac{\partial\Omega_1}{\partial z}-z\frac{\partial\Omega_1}{\partial y}\right)\mathrm{d}Q=\rho\int_{S(t)+\Sigma(t)}\Omega_1\frac{\partial\Omega_1}{\partial\nu}\,\mathrm{d}S,\tag{3.13a}$$

$$J_{22}^1=\rho\int_{Q(t)}\left(z\frac{\partial\Omega_2}{\partial x}-x\frac{\partial\Omega_2}{\partial z}\right)\mathrm{d}Q=\rho\int_{S(t)+\Sigma(t)}\Omega_2\frac{\partial\Omega_2}{\partial\nu}\,\mathrm{d}S,\tag{3.13b}$$

$$J_{33}^1=\rho\int_{Q(t)}\left(x\frac{\partial\Omega_3}{\partial y}-y\frac{\partial\Omega_3}{\partial x}\right)\mathrm{d}Q=\rho\int_{S(t)+\Sigma(t)}\Omega_3\frac{\partial\Omega_3}{\partial\nu}\,\mathrm{d}S,\tag{3.13c}$$

$$J_{12}^1=J_{21}^1=\rho\int_{Q(t)}\left(z\frac{\partial\Omega_1}{\partial x}-x\frac{\partial\Omega_1}{\partial z}\right)\mathrm{d}Q=\rho\int_{Q(t)}\left(y\frac{\partial\Omega_2}{\partial z}-z\frac{\partial\Omega_2}{\partial y}\right)\mathrm{d}Q$$
$$=\rho\int_{S(t)+\Sigma(t)}\Omega_1\frac{\partial\Omega_2}{\partial\nu}\,\mathrm{d}S=\rho\int_{S(t)+\Sigma(t)}\Omega_2\frac{\partial\Omega_1}{\partial\nu}\,\mathrm{d}S,\tag{3.13d}$$

$$J_{13}^1=J_{31}^1=\rho\int_{Q(t)}\left(x\frac{\partial\Omega_1}{\partial y}-y\frac{\partial\Omega_1}{\partial x}\right)\mathrm{d}Q=\rho\int_{Q(t)}\left(y\frac{\partial\Omega_3}{\partial z}-z\frac{\partial\Omega_3}{\partial y}\right)\mathrm{d}Q$$
$$=\rho\int_{S(t)+\Sigma(t)}\Omega_1\frac{\partial\Omega_3}{\partial\nu}\,\mathrm{d}S=\rho\int_{S(t)+\Sigma(t)}\Omega_3\frac{\partial\Omega_1}{\partial\nu}\,\mathrm{d}S,\tag{3.13e}$$

$$J_{23}^1=J_{32}^1=\rho\int_{Q(t)}\left(x\frac{\partial\Omega_2}{\partial y}-y\frac{\partial\Omega_2}{\partial x}\right)\mathrm{d}Q=\rho\int_{Q(t)}\left(z\frac{\partial\Omega_3}{\partial x}-x\frac{\partial\Omega_3}{\partial z}\right)\mathrm{d}Q$$
$$=\rho\int_{S(t)+\Sigma(t)}\Omega_2\frac{\partial\Omega_3}{\partial\nu}\,\mathrm{d}S=\rho\int_{S(t)+\Sigma(t)}\Omega_3\frac{\partial\Omega_2}{\partial\nu}\,\mathrm{d}S.\tag{3.13f}$$

The Lagrangian L (3.11) can be rewritten as

$$\begin{aligned}L=&-[\dot v_{01}l_1+\dot v_{02}l_2+\dot v_{03}l_3+\dot\omega_1l_{1\omega}+\dot\omega_2l_{2\omega}+\dot\omega_3l_{3\omega}+\omega_1l_{1\omega t}+\omega_2l_{2\omega t}\\&+\omega_3l_{3\omega t}-\tfrac{1}{2}(\omega_1^2J_{11}^1+\omega_2^2J_{22}^1+\omega_3^2J_{33}^1)-\omega_1\omega_2J_{12}^1-\omega_1\omega_3J_{13}^1\\&-\omega_2\omega_3J_{23}^1-\tfrac{1}{2}m_1(v_{01}^2+v_{02}^2+v_{03}^2)+(\omega_2v_{03}-\omega_3v_{02})l_1\\&+(\omega_3v_{01}-\omega_1v_{03})l_2+(\omega_1v_{02}-\omega_2v_{01})l_3]+L_r,\end{aligned}\tag{3.14}$$

where

$$\left.\begin{aligned}&m_1=\rho\int_{Q(t)}\mathrm{d}Q,\quad l_{k\omega}=\rho\int_{Q(t)}\Omega_k\,\mathrm{d}Q,\quad l_{k\omega t}=\rho\int_{Q(t)}\frac{\partial\Omega_k}{\partial t}\,\mathrm{d}Q,\\&l_1=\rho\int_{Q(t)}x\,\mathrm{d}Q,\quad l_2=\rho\int_{Q(t)}y\,\mathrm{d}Q,\quad l_3=\rho\int_{Q(t)}z\,\mathrm{d}Q.\end{aligned}\right\}\tag{3.15}$$

The vectors $\boldsymbol{l}=\{l_k\},\boldsymbol{l}_\omega=\{l_{k\omega}\},\boldsymbol{l}_{\omega t}=\{l_{k\omega t}\}$ depend only on $\beta_i(t)$ and $\dot\beta_i(t)$.

It follows from (3.7) that

$$L_r = -\rho \int_{Q(t)} \left[\sum_{n=1} \dot{R}_n \varphi_n + \tfrac{1}{2} \sum_n \sum_k R_n R_k (\nabla \varphi_n, \nabla \varphi_k) + U \right] \mathrm{d}Q$$
$$= -\left[\sum_n A_n \dot{R}_n + \tfrac{1}{2} \sum_n \sum_k A_{nk} R_n R_k - g_1 l_1 - g_2 l_2 - g_3 l_3 - m_1 \boldsymbol{g} \cdot \boldsymbol{r}_0' \right], \quad (3.16)$$

where

$$A_n = \rho \int_{Q(t)} \varphi_n \, \mathrm{d}Q, \quad A_{nk} = A_{kn} = \rho \int_{Q(t)} (\nabla \varphi_n, \nabla \varphi_k) \, \mathrm{d}Q = \rho \int_{\Sigma(t)+S(t)} \varphi_n \frac{\partial \varphi_k}{\partial \nu} \, \mathrm{d}S \quad (3.17)$$

are functions of $\beta_i(t)$.

The Lagrangian L is originally a function of two independent variables $f(x, y, z, t)$ and $\Phi(x, y, z, t)$. The independent variables become the time-varying functions $\beta_i(t), i \geqslant 1$ and $R_n(t), n \geqslant 1$ after substituting (3.4), (3.6) and (3.7) into the Lagrangian. The variations of the functional (3.1) by $\beta_i(t)$ and $R_n(t)$ for given $\boldsymbol{v}_0(t)$ and $\boldsymbol{\omega}(t)$ are

$$\delta W = \int_{t_1}^{t_2} \left[\sum_n A_n \delta \dot{R}_n + \sum_n \sum_k A_{nk} R_k \delta R_n + \sum_i \left(\sum_n \dot{R}_n \frac{\partial A_n}{\partial \beta_i} \right.\right.$$
$$+ \omega_1 \frac{\partial l_{1\omega t}}{\partial \beta_i} + \omega_2 \frac{\partial l_{2\omega t}}{\partial \beta_i} + \omega_3 \frac{\partial l_{3\omega t}}{\partial \beta_i} + \tfrac{1}{2} \sum_n \sum_k R_n R_k \frac{\partial A_{nk}}{\partial \beta_i}$$
$$+ \dot{\omega}_1 \frac{\partial l_{1\omega}}{\partial \beta_i} + \dot{\omega}_2 \frac{\partial l_{2\omega}}{\partial \beta_i} + \dot{\omega}_3 \frac{\partial l_{3\omega}}{\partial \beta_i} + (\dot{v}_{01} - g_1 + \omega_2 v_{03} - \omega_3 v_{02}) \frac{\partial l_1}{\partial \beta_i}$$
$$+ (\dot{v}_{02} - g_2 + \omega_3 v_{01} - \omega_1 v_{03}) \frac{\partial l_2}{\partial \beta_i} + (\dot{v}_{03} - g_3 + \omega_1 v_{02} - \omega_2 v_{01}) \frac{\partial l_3}{\partial \beta_i}$$
$$\left. - \tfrac{1}{2} \omega_1^2 \frac{\partial J_{11}^1}{\partial \beta_i} - \tfrac{1}{2} \omega_2^2 \frac{\partial J_{22}^1}{\partial \beta_i} - \tfrac{1}{2} \omega_3^2 \frac{\partial J_{33}^1}{\partial \beta_i} - \omega_1 \omega_2 \frac{\partial J_{12}^1}{\partial \beta_i} - \omega_1 \omega_3 \frac{\partial J_{13}^1}{\partial \beta_i} - \omega_2 \omega_3 \frac{\partial J_{23}^1}{\partial \beta_i} \right) \delta \beta_i$$
$$\left. + \left(\omega_1 \frac{\partial l_{1\omega t}}{\partial \dot{\beta}_i} + \omega_2 \frac{\partial l_{2\omega t}}{\partial \dot{\beta}_i} + \omega_3 \frac{\partial l_{3\omega t}}{\partial \dot{\beta}_i} \right) \delta \dot{\beta}_i \right] \mathrm{d}t = 0. \quad (3.18)$$

The following infinite system of nonlinear differential equations (*modal system*) coupling modal functions $R_n(t)$ and $\beta_i(t)$ is obtained by integrating by parts in (3.18) and using (3.3) for test functions:

$$\frac{\mathrm{d}}{\mathrm{d}t} A_n - \sum_k R_k A_{nk} = 0, \quad n = 1, 2, \ldots, \quad (3.19)$$

$$\sum_n \dot{R}_n \frac{\partial A_n}{\partial \beta_i} + \tfrac{1}{2} \sum_n \sum_k \frac{\partial A_{nk}}{\partial \beta_i} R_n R_k + \dot{\omega}_1 \frac{\partial l_{1\omega}}{\partial \beta_i} + \dot{\omega}_2 \frac{\partial l_{2\omega}}{\partial \beta_i} + \dot{\omega}_3 \frac{\partial l_{3\omega}}{\partial \beta_i} + \omega_1 \frac{\partial l_{1\omega t}}{\partial \beta_i} + \omega_2 \frac{\partial l_{2\omega t}}{\partial \beta_i}$$
$$+ \omega_3 \frac{\partial l_{3\omega t}}{\partial \beta_i} - \frac{\mathrm{d}}{\mathrm{d}t} \left(\omega_1 \frac{\partial l_{1\omega t}}{\partial \dot{\beta}_i} + \omega_2 \frac{\partial l_{2\omega t}}{\partial \dot{\beta}_i} + \omega_3 \frac{\partial l_{3\omega t}}{\partial \dot{\beta}_i} \right) + (\dot{v}_{01} - g_1 + \omega_2 v_{03} - \omega_3 v_{02}) \frac{\partial l_1}{\partial \beta_i}$$
$$+ (\dot{v}_{02} - g_2 + \omega_3 v_{01} - \omega_1 v_{03}) \frac{\partial l_2}{\partial \beta_i} + (\dot{v}_{03} - g_3 + \omega_1 v_{02} - \omega_2 v_{01}) \frac{\partial l_3}{\partial \beta_i} - \tfrac{1}{2} \omega_1^2 \frac{\partial J_{11}^1}{\partial \beta_i}$$
$$- \tfrac{1}{2} \omega_2^2 \frac{\partial J_{22}^1}{\partial \beta_i} - \tfrac{1}{2} \omega_3^2 \frac{\partial J_{33}^1}{\partial \beta_i} - \omega_1 \omega_2 \frac{\partial J_{12}^1}{\partial \beta_i} - \omega_1 \omega_3 \frac{\partial J_{13}^1}{\partial \beta_i} - \omega_2 \omega_3 \frac{\partial J_{23}^1}{\partial \beta_i} = 0. \quad (3.20)$$

The system of ordinary differential equations (3.19) can be considered as a linear

system of algebraic equations $\sum A_{nk}(\beta_i)R_k = (\mathrm{d}/\mathrm{d}t)A_n(\beta_i)$. By using a numerical or asymptotic technique we can then find a solution of R_n as a function of β_i. After substituting R_n into (3.20) we get a system of second-order nonlinear differential equations with respect to β_i. The values $\partial l_k/\partial\beta_i$ are given by

$$\frac{\partial l_3}{\partial \beta_i} = \rho \int_{\Sigma_0} f_i^2 \,\mathrm{d}S \;\; \beta_i = \lambda_{i3}\beta_i, \quad \frac{\partial l_2}{\partial \beta_i} = \rho \int_{\Sigma_0} y f_i \,\mathrm{d}S = \lambda_{i2}, \quad \frac{\partial l_1}{\partial \beta_i} = \rho \int_{\Sigma_0} x f_i \,\mathrm{d}S = \lambda_{i1}. \tag{3.21}$$

The constructed infinite-dimensional system of equations (3.19) (3.20) is applicable to any type of rigid body motion. It is necessary that $f(x, y, t)$ given by (3.6) is single-valued. This means that plunging breakers cannot be described. There are no other restrictions on the type of surface wave that can be studied.

4. Modal system for two-dimensional fluid flows

We assume two-dimensional fluid motion in the (x, z)-plane. Then

$$\boldsymbol{v}_0 = (v_{0x}, 0, v_{0z}), \quad \boldsymbol{\omega} = (0, \omega(t), 0), \quad \boldsymbol{r} = (x, 0, z), \quad \boldsymbol{\Omega}(x, 0, z) = (0, \Omega(x, z, t), 0) \tag{4.1}$$

and Ω is the solution of the following boundary value problem:

$$\Delta\Omega = 0 \quad \text{in } Q(t), \qquad \left.\frac{\partial \Omega}{\partial v}\right|_{S(t)+\Sigma(t)} = z v_1 - x v_3. \tag{4.2}$$

The velocity potential $\Phi(x, 0, z, t)$ takes the form

$$\Phi(x, 0, z, t) = v_{0x}x + v_{0z}z + \omega(t)\,\Omega(x, z, t) + \sum_{n=1}^{\infty} R_n(t)\,\varphi_n(x, z), \tag{4.3}$$

where $\varphi_n(x, z)$ is a complete system of harmonic functions satisfying the zero Neumann condition on the bottom and vertical walls and the Laplace equation in Q.

The general infinite-dimensional modal system of ordinary differential equations (3.19), (3.20) has in two dimensions the following form:

$$\frac{\mathrm{d}}{\mathrm{d}t}A_n - \sum_k R_k A_{nk} = 0, \quad n = 1, 2, \ldots, \tag{4.4}$$

$$\sum_n \dot{R}_n \frac{\partial A_n}{\partial \beta_i} + \tfrac{1}{2}\sum_n \sum_k \frac{\partial A_{nk}}{\partial \beta_i} R_n R_k + \dot{\omega}\frac{\partial l_{2\omega}}{\partial \beta_i} + \omega \frac{\partial l_{2\omega t}}{\partial \beta_i} - \frac{\mathrm{d}}{\mathrm{d}t}\left(\omega \frac{\partial l_{2\omega t}}{\partial \dot{\beta}_i}\right)$$
$$+ (\dot{v}_{01} - g_1 + \omega v_{03})\frac{\partial l_1}{\partial \beta_i} + (\dot{v}_{03} - g_3 - \omega v_{01})\frac{\partial l_3}{\partial \beta_i} - \tfrac{1}{2}\omega^2 \frac{\partial J_{22}^1}{\partial \beta_i} = 0. \tag{4.5}$$

5. Asymptotic modal system for a rectangular tank performing arbitrary small-amplitude motions

We consider a mobile rectangular rigid tank filled partly by an inviscid incompressible fluid. The mean water depth is h and l is the tank breadth. The flow is irrotational and two-dimensional (see figure 1). The origin of the coordinate system is in the mean free surface at the centreplane of the tank. The equation $z = f(x, t)$ determines the perturbed free surface $\Sigma(t)$. The fluid domain is

$$Q(t) = \{(x, z) : -h < z < f(x, t); -l/2 < x < l/2\}. \tag{5.1}$$

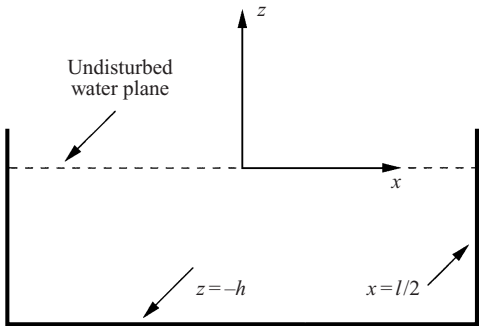

FIGURE 1. Coordinate system.

Since $f(x,t)$ is expressed by (3.6), the complete (to within a constant) orthogonal system of functions $\{f_i(x)\}$ should satisfy the volume conservation condition

$$\int_{-l/2}^{l/2} f_i(x)\,\mathrm{d}x = 0. \tag{5.2}$$

The modal system (4.4), (4.5) can be approximated to surface waves with one primary dominating mode corresponding to the first natural mode. This implies that the body motions are horizontal and/or rotational and quasi-periodic with average frequency close to the first resonance frequency. It is also necessary that the water depth is not shallow and the fluid does not hit the tank ceiling (see, also, physical arguments presented in Faltinsen 1974 and the book by Mikishev 1978). The rigid body motions are assumed small relative to the tank breadth and water depth.

The derivation of the finite-dimensional asymptotic analogue of the system (4.4) and (4.5) requires an asymptotic relation between dominating mode amplitude and excitation amplitude. It is assumed, as in the theory by Faltinsen (1974), that

$$O(\beta_1^3) = O(H) = O(\psi_0) = \epsilon. \tag{5.3}$$

Here H is translatory (surge) motion magnitude and ψ_0 is angular (pitch) magnitude. Further $\beta_2 = O(\epsilon^{2/3}), \beta_3 = O(\epsilon)$. Higher-order terms than ϵ will be neglected in the nonlinear equations. The modes $f_i(x)$ in (3.6) as well as $\varphi_i(x,z)$ in (3.7) can be chosen as the solutions of the spectral problem

$$\left.\begin{aligned} &\Delta\varphi_i = 0 \quad (-l/2 < x < l/2, -h < z < 0), \\ &\left.\frac{\partial\varphi_i}{\partial x}\right|_{x=-l/2,x=l/2} = 0, \quad \left.\frac{\partial\varphi_i}{\partial z}\right|_{z=-h} = 0, \quad \frac{\partial\varphi_i}{\partial z} = \lambda_i\varphi_i \quad (z=0). \end{aligned}\right\} \tag{5.4}$$

This means

$$\left.\begin{aligned} &\lambda_i = \frac{\pi\mathrm{i}}{l}\tanh\left(\frac{\mathrm{i}\pi}{l}h\right), \quad f_i(x) = \cos\left(\frac{\pi\mathrm{i}}{l}(x+l/2)\right), \\ &\varphi_i(x,z) = f_i(x)\frac{\cosh\left((\pi\mathrm{i}/l)(z+h)\right)}{\cosh\left((\pi\mathrm{i}/l)h\right)}. \end{aligned}\right\} \tag{5.5}$$

Equations (3.6) and (3.7) take the following form:

$$f(x,t) = \sum_{i=1}^{\infty}\beta_i(t)f_i(x), \quad \varphi(x,z,t) = \sum_{i=1}^{\infty}R_i(t)f_i(x)\frac{\cosh\left((\mathrm{i}\pi/l)(z+h)\right)}{\cosh\left((\mathrm{i}\pi/l)h\right)}. \tag{5.6}$$

By accounting for the asymptotic relation (5.3) and keeping only terms up to ϵ in

the modal system (4.4) and (4.5) we get

$$\frac{\mathrm{d}}{\mathrm{d}t}A_n - \sum_k R_k A_{nk} = 0, \quad n = 1, 2, \dots, \tag{5.7}$$

$$\sum_n \dot{R}_n \frac{\partial A_n}{\partial \beta_i} + \tfrac{1}{2}\sum_n \sum_k \frac{\partial A_{nk}}{\partial \beta_i} R_n R_k + \dot{\omega}\frac{\partial l_{2\omega}}{\partial \beta_i} + \omega \frac{\partial l_{2\omega t}}{\partial \beta_i} - \frac{\mathrm{d}}{\mathrm{d}t}\left(\omega \frac{\partial l_{2\omega t}}{\partial \dot{\beta}_i}\right) + (\dot{v}_{01} - g_1)\lambda_{i1} + (\dot{v}_{03} - g_3)\beta_i \lambda_{i3} = 0. \tag{5.8}$$

Asymptotic expansions of integrals $A_i, A_{nk}, l_2\omega, l_{2\omega t}$ have to be used in (5.7) and (5.8). Here $A_i, A_{nk}, l_{2\omega}, l_{2\omega t}$ are defined by (3.17) and (3.15) as integrals over the instantaneous fluid volume position. The integrals are divided into integrals over the mean position of fluid volume Q_0 and over the remaining part Q_δ. Q_δ is described by β_i. Further, the integrand of the integrals over Q_δ can be expanded in Taylor series by β_i. Keeping terms up to ϵ gives

$$\left.\begin{aligned} A_1 &= \frac{\rho l}{2}(\beta_1 + E_1(\beta_1\beta_2 + \beta_2\beta_3) + E_0(\beta_1^3 + 2\beta_1\beta_2^2 + \beta_1^2\beta_3)), \\ A_2 &= \frac{\rho l}{2}(\beta_2 + E_2(\beta_1^2 + 2\beta_1\beta_3) + 8E_0\beta_1^2\beta_2), \\ A_3 &= \frac{\rho l}{2}(\beta_3 + 3E_3\beta_1\beta_2 + 3E_0\beta_1^3); \end{aligned}\right\} \tag{5.9}$$

$$\left.\begin{aligned} &A_{11} = \rho l(E_1 + 8E_1E_0\beta_1^2 - (2E_0 - E_1^2)\beta_2), \quad A_{22} = \rho l(2E_2), \\ &A_{12} = A_{21} = \rho l((4E_0 + 2E_1E_2)\beta_1 + (-4E_0 + 2E_1^2)\beta_3), \\ &A_{33} = \rho l(3E_3), \quad A_{13} = A_{31} = 3l\rho(2E_0 + E_1E_3)(\beta_2 + 2E_4\beta_1^2), \\ &A_{23} = A_{32} = 3l\rho(4E_0 + 2E_2E_3)\beta_1, \end{aligned}\right\} \tag{5.10}$$

where

$$E_0 = \frac{1}{8}\left(\frac{\pi}{l}\right)^2, \quad E_i = \frac{\pi}{2l}\tanh\left(\frac{\pi \mathrm{i}}{l}h\right), \quad i \geqslant 1. \tag{5.11}$$

Further, we express R_n as

$$R_n = \sum_i \gamma_i \dot{\beta}_i + \sum_{ij} \gamma_{ij}\dot{\beta}_j\beta_i + \sum_{ijk}\gamma_{ijk}\dot{\beta}_i\beta_j\beta_k + \cdots$$

and substitute it in (5.7). Explicit values of $\gamma_i, \gamma_{ij}, \gamma_{ijk}$ are found by collecting similar terms. The result is

$$\left.\begin{aligned} &R_1 = \frac{\dot{\beta}_1}{2E_1} + \frac{E_0}{E_1^2}\dot{\beta}_1\beta_2 - \frac{E_0}{E_1E_2}\dot{\beta}_2\beta_1 + \frac{E_0}{E_1}\left(-\tfrac{1}{2} + \frac{4E_0}{E_1E_2}\right)\beta_1^2\dot{\beta}_1, \\ &R_2 = \frac{1}{4E_2}\left(\dot{\beta}_2 - \frac{4E_0}{E_1}\beta_1\dot{\beta}_1\right), \quad R_3 = \frac{\dot{\beta}_3}{6E_3} - \frac{E_0}{E_1E_3}\dot{\beta}_1\beta_2 - \frac{E_0}{E_2E_3}\dot{\beta}_2\beta_1 \\ &+\dot{\beta}_1\beta_1^2\left(\frac{3E_2}{2E_3} - \frac{2E_0E_4}{E_1E_3} - E_4 + \frac{4E_0^2}{E_1E_2E_3} + \frac{2E_0E_2}{E_1E_3}\right), \quad R_i = \frac{\dot{\beta}_i}{2iE_i}, \quad i \geqslant 4; \end{aligned}\right\} \tag{5.12}$$

and

$$\left.\begin{aligned}
\dot{R}_1 &= \frac{\ddot{\beta}_1}{2E_1} + \frac{E_0}{E_1^2}\ddot{\beta}_1\beta_2 - \frac{E_0}{E_1E_2}\ddot{\beta}_2\beta_1 + \dot{\beta}_1\dot{\beta}_2\left(\frac{E_0}{E_1^2} - \frac{E_0}{E_1E_2}\right)\\
&\quad + \frac{E_0}{E_1}\left(-\frac{1}{2} + \frac{4E_0}{E_1E_2}\right)\beta_1^2\ddot{\beta}_1 + 2\frac{E_0}{E_1}\left(-\tfrac{1}{2} + \frac{4E_0}{E_1E_2}\right)\dot{\beta}_1^2\beta_1,\\
\dot{R}_2 &= \frac{1}{4E_2}\left(\ddot{\beta}_2 - \frac{4E_0}{E_1}(\beta_1\ddot{\beta}_1 + \dot{\beta}_1^2)\right),\\
\dot{R}_3 &= \frac{\dot{\beta}_3}{6E_3} - \frac{E_0}{E_1E_3}\ddot{\beta}_1\beta_2 - \frac{E_0}{E_2E_3}\ddot{\beta}_2\beta_1 - \left(\frac{E_0}{E_1E_3} + \frac{E_0}{E_2E_3}\right)\dot{\beta}_1\dot{\beta}_2 + (\ddot{\beta}_1\beta_1^2 + 2\dot{\beta}_1^2\beta_1)\\
&\quad \times\left(\frac{3E_2}{2E_3} - \frac{2E_0E_4}{E_1E_3} - E_4 + \frac{4E_0^2}{E_1E_2E_3} + \frac{2E_0E_2}{E_1E_3}\right), \qquad \dot{R}_i = \frac{\ddot{\beta}_1}{2iE_i}, \quad i \geqslant 4.
\end{aligned}\right\} \tag{5.13}$$

By calculating λ_{ij} we get

$$\left.\begin{aligned}
\lambda_{i1} &= \rho\int_{-l/2}^{l/2} x\cos\left(\frac{\mathrm{i}\pi}{l}(x + l/2)\right)\mathrm{d}x = \rho\left(\frac{l}{\mathrm{i}\pi}\right)^2((-1)^i - 1),\\
\lambda_{i3} &= \rho\int_{-l/2}^{l/2}\cos^2\left(\frac{\mathrm{i}\pi}{l}(x + l/2)\right)\mathrm{d}x = \frac{\rho l}{2}.
\end{aligned}\right\} \tag{5.14}$$

$l_{2\omega}$ and $l_{2\omega t}$ (see (3.15)) depend on $\Omega(x, z, t)$ which is the solution of the boundary value problem (4.2). $\Omega(x, z, t)$ depends parametrically on $\beta_i(t)$ due to the free surface $\Sigma(t)$. Since $\partial l_{2\omega}/\partial\beta_i$ and $\partial l_{2\omega t}/\partial\beta_i$ are multiplied by terms of $O(\epsilon)$ in (5.8), it is sufficient to include only linear terms in β_i in the integrals $l_{2\omega}$ and $l_{2\omega t}$. The problem (4.2) in a rectangular tank takes the following form:

$$\left.\begin{aligned}
&\Delta\Omega = 0 \quad \text{in } Q(t), \quad \frac{\partial\Omega}{\partial z} = -x \quad (z = -h),\\
&\frac{\partial\Omega}{\partial x} = z\left(x = \frac{l}{2}, -\frac{l}{2}\right), \quad \frac{\partial\Omega}{\partial v} = -x\frac{1}{\sqrt{1 + (f_x)^2}} - z\frac{f_x}{\sqrt{1 + (f_x)^2}} \quad (z = f(x, t)).
\end{aligned}\right\} \tag{5.15}$$

The solution can be found by a Zhukovsky-type substitution with additional terms for fluctuations of the free surface. This gives

$$\Omega = xz - 2\sum_{i=1}^{\infty} a_i f_i\frac{\sinh((\pi/l)\mathrm{i}(z + h/2))}{\cosh((\pi/2l)\mathrm{i}h)} + \sum_{i=1}^{\infty}\chi_i(t)f_i\frac{\cosh((\pi/l)\mathrm{i}(z + h))}{\cosh((\pi/l)\mathrm{i}h)}. \tag{5.16}$$

The coefficients a_i are found from the condition $\chi_i(t) \equiv 0$, $i \geqslant 1$, if and only if, $\beta_i \equiv 0$, $i \geqslant 1$. Substitution of (5.16) into (5.15) gives

$$\sum_{i=1}^{N} a_i f_i\frac{\mathrm{i}\pi}{l} = x \quad \text{or} \quad a_i = \frac{2l^2}{(\mathrm{i}\pi)^3}[(-1)^i - 1]. \tag{5.17}$$

The functions $\chi_i(t)$ follow from (5.15) after substitution of (5.16) and (5.17) and performing the Taylor series technique for the free surface $\Sigma(t)$ (with respect to β_i). The linear terms of $l_{2\omega}$ and $l_{2\omega t}$ do not depend on $\chi_i(t)$. To show this we substitute

(5.16) in the corresponding integrals

$$l_{2\omega} = -2\rho \sum_{i=1}^{\infty} a_i \tanh\left(\frac{\mathrm{i}\pi}{2l}h\right) \beta_i \int_{-l/2}^{l/2} f_i^2 \,\mathrm{d}x + \rho \sum_{i=1}^{\infty} \chi_i(t) \frac{l}{\mathrm{i}\pi} \tanh\left(\frac{\mathrm{i}\pi}{l}h\right) \int_{-l/2}^{l/2} f_i \,\mathrm{d}x, \tag{5.18}$$

$$l_{2\omega t} = \rho \sum_{j=1}^{\infty} \dot{\chi}(t) \frac{l}{\mathrm{i}\pi} \tanh\left(\frac{\mathrm{i}\pi}{l}h\right) \int_{-l/2}^{l/2} f_i \,\mathrm{d}x. \tag{5.19}$$

It follows from the volume conservation condition (5.2) that

$$l_{2\omega t} = 0, \quad l_{2\omega} = -2\rho \sum_{i=1}^{\infty} \beta_i \left(\frac{l}{\mathrm{i}\pi}\right)^3 [(-1)^i - 1] \tanh\left(\frac{\mathrm{i}\pi}{2l}h\right). \tag{5.20}$$

The derivatives with respect to β_i give

$$\frac{\partial l_{2\omega t}}{\partial \beta_i} = 0, \quad \frac{\partial l_{2\omega}}{\partial \beta_i} = -2\rho \left(\frac{l}{\mathrm{i}\pi}\right)^3 [(-1)^i - 1] \tanh\left(\frac{\mathrm{i}\pi}{2l}h\right), \quad i \geqslant 1. \tag{5.21}$$

Finally, by defining the angular position of the mobile coordinate system $Oxyz$ with respect to $O'x'y'z'$ as $\psi(t)$ we obtain correct to $O(\epsilon)$ that

$$g_3 = -g, \quad g_1 = g\psi(t). \tag{5.22}$$

The terms in (5.8) $\ddot{\psi}\partial l_{2\omega}/\partial\beta_i + (-g_3)\beta_i\lambda_{3i} + (-g_1)\lambda_{1i}$ caused by forced pitch excitation can be rewritten as

$$-\rho \left(\frac{l}{\mathrm{i}\pi}\right)^2 [(-1)^i - 1] \left(\frac{2l}{\mathrm{i}\pi} \tanh\left(\frac{\mathrm{i}\pi}{2l}h\right) \ddot{\psi}(t) + g\psi(t)\right) + g\beta_i. \tag{5.23}$$

When substituting above formula in (5.8), we get the following system of ordinary differential equations describing modal oscillations of a fluid in a rectangular tank performing arbitrary small-magnitude motions (keeping terms up to third order in the nonlinear equations):

$$(\ddot{\beta}_1 + \sigma_1^2\beta_1) + d_1(\ddot{\beta}_1\beta_2 + \dot{\beta}_1\dot{\beta}_2) + d_2(\ddot{\beta}_1\beta_1^2 + \dot{\beta}_1^2\beta_1) + d_3\ddot{\beta}_2\beta_1 + P_1(\dot{v}_{0x} - S_1\dot{\omega} - g\psi) + Q_1\dot{v}_{0z}\beta_1 = 0, \tag{5.24a}$$

$$(\ddot{\beta}_2 + \sigma_2^2\beta_2) + d_4\ddot{\beta}_1\beta_1 + d_5\dot{\beta}_1^2 + Q_2\dot{v}_{0z}\beta_2 = 0, \tag{5.24b}$$

$$(\ddot{\beta}_3 + \sigma_3^2\beta_3) + d_6\ddot{\beta}_1\beta_2 + d_7\ddot{\beta}_1\beta_1^2 + d_8\ddot{\beta}_2\beta_1 + d_9\dot{\beta}_1\dot{\beta}_2 + d_{10}\dot{\beta}_1^2\beta_1 + P_3(\dot{v}_{0x} - S_3\dot{\omega} - g\psi) + Q_3\dot{v}_{0z}\beta_3 = 0. \tag{5.24c}$$

The linear equations describing higher modes are

$$\ddot{\beta}_i + \sigma_i^2\beta_i + P_i(\dot{v}_{0x} - S_i\dot{\omega} - g\psi) + Q_i\dot{v}_{0z}\beta_i = 0, \quad i \geqslant 4. \tag{5.25}$$

Here v_{0x} and v_{0z} are projections of the translational velocity onto axes of Oxz, $\omega(t)$ is the value of the angular velocity of coordinate system $Oxyz$ with respect to $O'x'y'z'$.

The coefficients introduced are calculated by formulas

$$\sigma_i^2 = 2g\mathrm{i}E_i, \quad P_{2i-1} = -\frac{8E_{2i-1}l}{\pi^2(2\mathrm{i}-1)}, \quad P_{2i} = 0, \quad Q_i = 2\mathrm{i}E_i,$$
$$S_i = \frac{2l}{\pi\mathrm{i}} \tanh\left(\frac{\mathrm{i}\pi}{2l}h\right), \quad i \geqslant 1, \tag{5.26}$$

where σ_i is the natural frequency of mode i. Further,

$$\left.\begin{aligned}
&d_1 = 2\frac{E_0}{E_1} + E_1, \quad d_2 = 2E_0\left(-1 + \frac{4E_0}{E_1E_2}\right), \quad d_3 = -2\frac{E_0}{E_2} + E_1,\\
&d_4 = -4\frac{E_0}{E_1} + 2E_2, \quad d_5 = E_2 - 2\frac{E_0E_2}{E_1^2} - \frac{4E_0}{E_1}, \quad d_6 = 3E_3 - \frac{6E_0}{E_1},\\
&d_7 = 9E_0 - 12\frac{E_0E_4}{E_1} - 6E_3E_4 + 24\frac{E_0^2}{E_1E_2} + 3\frac{E_0E_3}{E_1},\\
&d_8 = -6\frac{E_0}{E_2} + 3E_3, \quad d_9 = -6\frac{E_0}{E_1} - 6\frac{E_0}{E_2} - 6\frac{E_0E_3}{E_1E_2} + 3\frac{E_3E_1}{E_2},\\
&d_{10} = 18E_0 - 2E_4\frac{12E_0 + 6E_1E_3}{E_1} + \frac{72E_0^2}{E_1E_2} + 12E_0\left(\frac{E_3}{E_1} - \frac{E_1}{E_2}\right).
\end{aligned}\right\} \tag{5.27}$$

The first two nonlinear equations of (5.24) couple β_1 with β_2 and do not depend on β_3. The third mode component is excited by rigid body motions and the first and the second modes of sloshing. The second mode response becomes infinite if the excitation has frequency content at the natural frequency for the second mode; and similarly for the third and higher modes. The first mode will be finite if it is excited at the natural frequency of the first mode. This is caused by nonlinear effects and will become more evident in the next section on steady-state response.

6. Steady-state sloshing in a rectangular tank with a small-amplitude surge/pitch sinusoidal excitation

The theory of steady-state solutions of the nonlinear sloshing problem in a rectangular tank was created by Faltinsen (1974) based on Moiseev's (1958) method. The constructed asymptotic discrete theory (5.24) makes it possible to generalize the main relations of this theory. For surge-excited steady-state waves we express $\boldsymbol{v}_0$ as $(-H\sigma\sin(\sigma t), 0, 0)$, set $\omega = \psi \equiv 0$ and look for periodic solutions

$$\beta_i(t + 2\pi/\sigma) = \beta_i(t), \qquad \dot{\beta}_i(t + 2\pi/\sigma) = \dot{\beta}_i(t) \tag{6.1}$$

of the discrete model (5.24).

To construct asymptotically the periodic solutions and to derive analytically the amplitude–frequency response of nonlinear sloshing in a rectangular tank caused by forced excitation we express the first approximation of the primary mode in the form

$$\beta_1(t) = A\cos\sigma t + o(A). \tag{6.2}$$

The substitution of (6.2) into (5.24b) with periodicity condition (6.1) yields

$$\beta_1 = A\cos\sigma t + o(A), \qquad \beta_2 = A^2(l_0 + h_0\cos(2\sigma t)) + o(A^2), \tag{6.3}$$

where

$$l_0 = \frac{d_4 - d_5}{2\bar{\sigma}_2^2}, \qquad h_0 = \frac{d_5 + d_4}{2(\bar{\sigma}_2^2 - 4)}, \qquad \bar{\sigma}_i = \frac{\sigma_i}{\sigma}, \quad i = 1, 2. \tag{6.4}$$

The amplitude $A \sim \epsilon^{1/3}$ of the primary mode can be found by substituting (6.3) into the first equation of (5.24) and collecting Fourier terms of lowest order. The equation coupling primary mode amplitude, frequency, breadth and depth will be non-dimensionalized by dividing all length variables by l. This gives

$$\Pi_h(\bar{\sigma}_1, \bar{\sigma}_2, \bar{A}) = (\bar{\sigma}_1^2 - 1)\bar{A} + m_1(\bar{\sigma}_2, \bar{h})\bar{A}^3 - \bar{P}_1\bar{H} = 0, \tag{6.5}$$

$$m_1(\bar{\sigma}_2, \bar{h}) = \bar{d}_1(-\bar{l}_0(\bar{\sigma}_2) + \tfrac{1}{2}\bar{h}_0(\bar{\sigma}_2)) - \tfrac{1}{2}\bar{d}_2 - 2\bar{d}_3\bar{h}_0(\bar{\sigma}_2), \tag{6.6}$$

where the overbar denotes non-dimensionalized value. The coefficient m_1 in equation (6.5) depends on depth–breadth ratio and frequency of excitation ($\bar{\sigma}_i, i = 1, 2$). The last dependence has not been presented earlier for frequency–amplitude response equations. Usually, the corresponding coefficient depends only on h/l. This means that our asymptotic technique differs from Faltinsen–Moiseev's procedure. In order to compare both techniques we need to give the following remark.

Remark. For any asymptotic theory with one dominating mode the nonlinear equation describing the dependence of amplitude–breadth ratio $\bar{A}$ and frequency of excitation σ has the same general form

$$\Pi_h\left(\frac{\sigma_1}{\sigma}, \frac{\sigma_2}{\sigma}, \bar{A}\right) = 0,$$

where σ_1 is the natural frequency of the primary mode.

The function Π can be expanded in a Taylor series. The approach by Moiseev (1958) and Faltinsen (1974) gives the expansion near the point $(\bar{\sigma}_1, \sigma_2/\sigma_1, 0)$ (for fixed $\bar{h}$). Our approach has no asymptotic restriction on the value of frequency σ and, therefore, includes only power series in $\bar{A}$

$$\Pi_h\left(\frac{\sigma_1}{\sigma}, \frac{\sigma_2}{\sigma}, \bar{A}\right) = \Pi\left(\frac{\sigma_1}{\sigma}, \frac{\sigma_2}{\sigma}, 0\right) + \frac{\partial \Pi}{\partial \bar{A}}\left(\frac{\sigma_1}{\sigma}, \frac{\sigma_2}{\sigma}, 0\right)\bar{A} + \frac{1}{2}\frac{\partial^2 \Pi}{\partial \bar{A}^2}\left(\frac{\sigma_1}{\sigma}, \frac{\sigma_2}{\sigma}, 0\right)\bar{A}^2 + \frac{\partial^3 \Pi}{\partial \bar{A}^3}\left(\frac{\sigma_1}{\sigma}, \frac{\sigma_2}{\sigma}, 0\right)\tfrac{1}{6}\bar{A}^3 + o(\bar{A}^3).$$

Since the value σ_2/σ is used to calculate only m_1 we in fact make a more precise calculation of this coefficient.

Equation (6.5) gives infinite response for $\bar{\sigma}_1 = 1$ and $m_1 = 0$. It implies that the third-order theory is not valid if

$$m_1\left(\frac{\sigma_2}{\sigma_1}, \bar{h}\right) = 0.$$

The root of the last equation gives $\bar{h} = h/l = 0.3374\ldots$. This is called the critical depth and coincides with the known value (see Waterhouse 1994). The response changes from being a 'hard-spring' to a 'soft-spring' at the critical depth. The detailed asymptotic analysis of the response near critical depth was done by Waterhouse (1994) by fifth-order theory based on Faltinsen–Moiseev's technique. It was shown that the branches in the amplitude–frequency plane coincide with a third-order theory only for small amplitude. New turning points on the branches occur at a critical value of the amplitude/frequency.

In our case $m_1 = m_1(\sigma_2/\sigma, \bar{h})$ which means that m_1 is a function of σ and $\bar{h}$. If a fixed σ is close to the natural frequency σ_1, but $\sigma \neq \sigma_1$ the equation

$$m_1\left(\frac{\sigma_2}{\sigma}, \bar{h}\right) = 0 \tag{6.7}$$

gives a different value of the critical depth. This means that the critical depth is a function of σ. If a pair $(\sigma, \bar{h})$ satisfies (6.7), then $\bar{A}$ tends to infinity. This effect is illustrated in figures 2 and 3.

Figure 2 shows the positive and negative solutions (branches P_+, P_-) of the secular algebraic equation (6.5) for different values of the water depth h and fixed amplitude of excitation H. The choice of H corresponds to the experimental values reported later in the paper. Branch O is the set of solutions of (6.5) for $H = 0$ (no vibration of

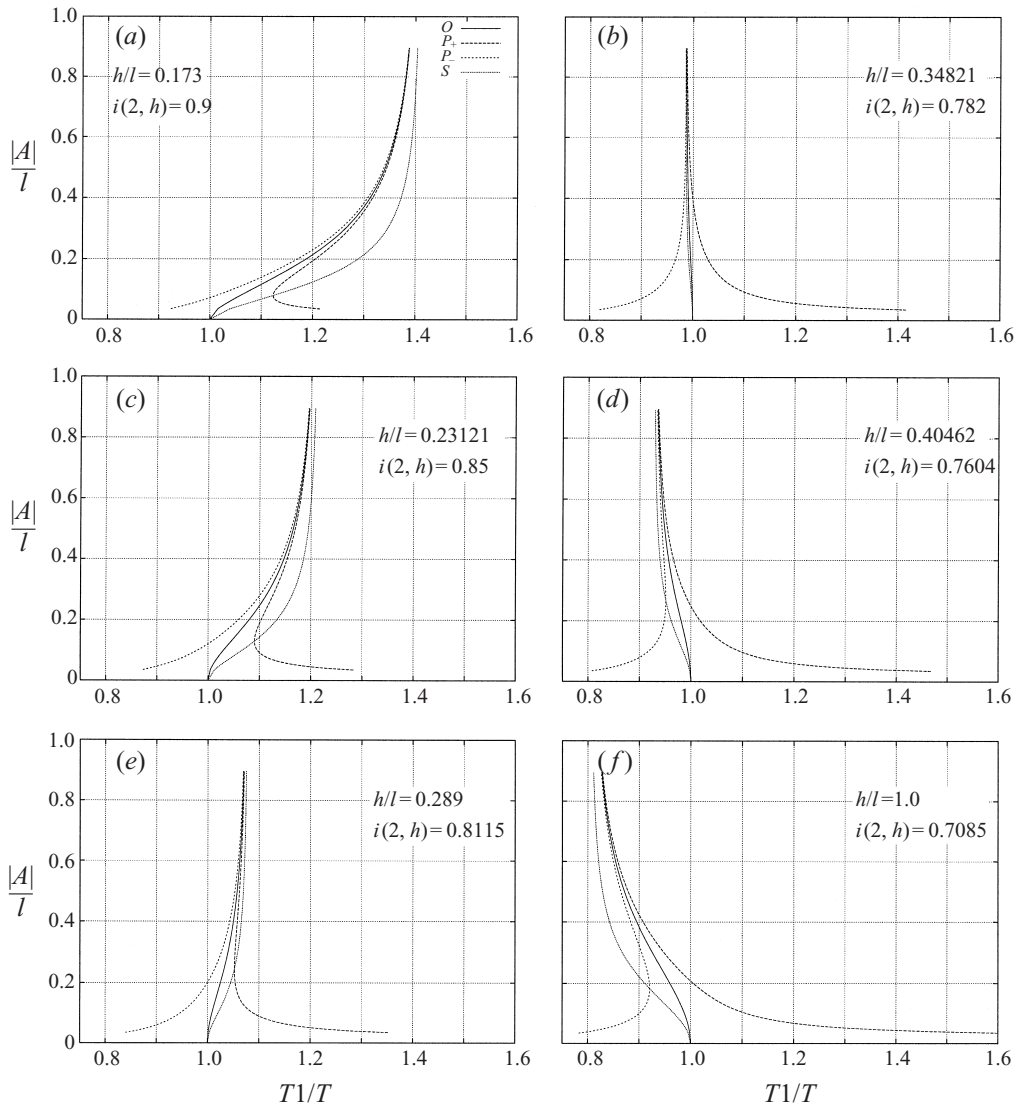

FIGURE 2. Amplitude (A)–frequency (σ) response for nonlinear sloshing due to surge excitation ($\sigma/\sigma_1 = T1/T$). h is the mean water depth, l is the tank breadth, H is the surge amplitude. $i(2, \bar{h})$ is defined by (6.9). $H/l = 0.0173$.

the tank). This can be interpreted as the amplitude–frequency dependence of free nonlinear (periodic) sloshing. The branches presented differ from diagrams obtained by Faltinsen's theory only for large values of $|A|/l$ and far away from the main resonance $\bar{\sigma}_1 = 1$. The last difference is due to the change of m_1 when varying σ. The results agree with the fifth-order theory by Waterhouse (1994) for sufficiently small amplitudes.

Similar results are obtained for steady-state sloshing in a rectangular tank excited by sinusoidal pitch motions. Let us assume the tank is pitching around the point $(0, 0, -z_0)$ of the mobile coordinate system. We can correct to $O(\epsilon)$ express that

$$\psi(t) = \psi_0 \cos(\sigma t), \quad \dot{v}_{0x} = z_0 \ddot{\psi}(t), \quad \dot{v}_{0z} = 0.$$

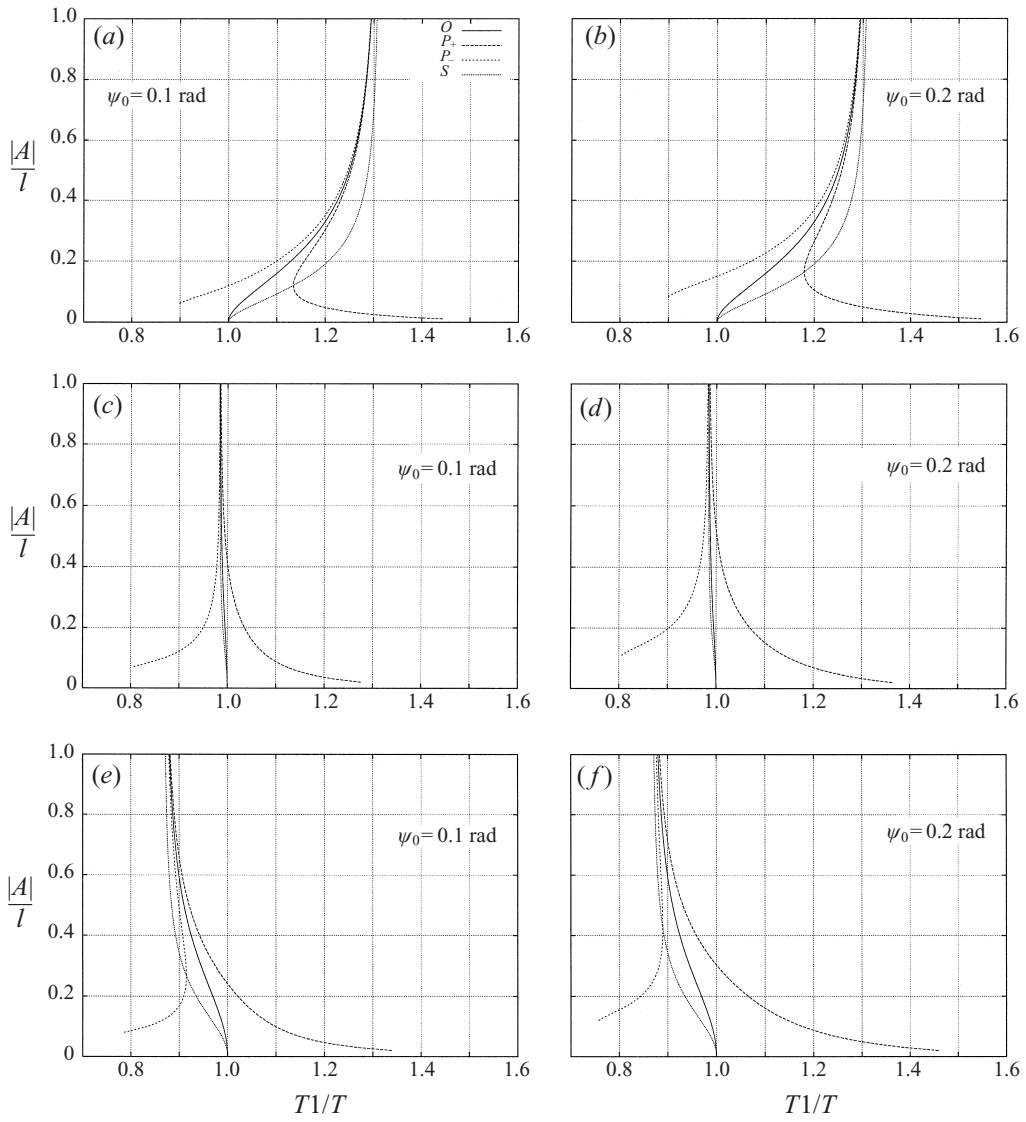

FIGURE 3. Amplitude (A)–frequency (σ) response for nonlinear sloshing due to pitch excitation ($\sigma/\sigma_1 = T1/T$). h is the mean water depth, l is the tank breadth, ψ_0 is the pitch amplitude, $(0, -z_0)$ is the position of pitch axis. $i(2, \bar{h})$ is defined by (6.9). (a, b) $z_0/l = 0$, $h/l = 0.2$, $i(2, \bar{h}) = 0.874$; (c, d) $z_0/l = 0.15$, $h/l = 0.35$, $i(2, \bar{h}) = 0.78$; (e, f) $z_0/l = 0.3$, $h/l = 0.5$, $i(2, \bar{h}) = 0.737$.

The algebraic governing equation for the frequency–amplitude response takes the following form:

$$(\bar{\sigma}_1^2 - 1)\bar{A} + m_1(\bar{\sigma}_2, \bar{h})\bar{A}^3 - \bar{P}_1\psi_0\left(\frac{z_0}{l} - \frac{S_1}{l} + \frac{g}{l\sigma^2}\right) = 0. \tag{6.8}$$

It differs from the equation of forced surge steady-state sloshing (6.5) only by the last inhomogeneous term and agrees with the corresponding equation of Faltinsen (1974).

All the results are based on the assumption that $O(\beta_1^2) = O(\beta_2)$. However, even for periodic solutions we can find a critical value of σ/σ_1 for which the amplitude

of the second mode tends to infinity. It can happen for small h, or for $\bar{\sigma}_2^2 \to 4$ (see the asymptotic solution (6.3), (6.4)). In terms of σ the condition of the secondary resonance takes the form

$$\frac{\sigma}{\sigma_1} \to \sqrt{\frac{\tanh(2\pi h/l)}{2\tanh(\pi h/l)}} = i(2,\bar{h}). \tag{6.9}$$

The value $i(2,\bar{h})$ characterizes the applicability of the theory constructed (see figures 2 and 3). The ratio $T_1/T = \sigma/\sigma_1$ must be close to 1 and not close to $i(2,\bar{h})$.

Similarly, we can introduce for the third mode

$$i(3,\bar{h}) = \sqrt{\frac{\tanh(3\pi h/l)}{3\tanh(\pi h/l)}}. \tag{6.10}$$

However since $i(3,\bar{h}) < i(2,\bar{h})$, the secondary resonance is the most dangerous.

The trend of the distribution of $i(2,\bar{h})$ shows for $\bar{h}$ small enough (but large for shallow water theory) that $i(2,\bar{h}) \to 1$ as $\bar{h} \to 0$. This means that the secondary parametric resonance can occur for small depths and implies that the asymptotic theory presented is not applicable for shallow water.

The stability analysis for surge/pitch excited waves in a rectangular container was done by Faltinsen (1974). We can give reliable new treatment of the stability by introducing branches O and S in figures 2 and 3. The branch O is the relation for the frequency and amplitude for nonlinear free sloshing, which can be found from the equation

$$\text{branch } O\text{: } (\bar{\sigma}_1^2 - 1) + m_1(\bar{\sigma}_2,\bar{h})\bar{A}^2 = 0. \tag{6.11}$$

The branch O is also the asymptotic curve for P_- and P_+ as $A \to \infty$.

The branch S is the set of all turning points of the branch P_+ (or P_- for different depths) for various amplitudes $\bar{H}$ (surge excitation) or ψ_0 (pitch excitation). The turning points correspond to when (6.5) has only two solutions. The condition of two roots of equation (6.5) can be found by differentiating (6.5) with respect to A. This gives

$$\text{branch } S\text{: } (\bar{\sigma}_1^2 - 1) + 3m_1(\bar{\sigma}_2,\bar{h})\bar{A}^2 = 0. \tag{6.12}$$

The branch S does not depend on the value of the excitation amplitude and is only a function of depth–breadth ratio.

Due to the theory of bifurcations the turning point divides the branch P_+ or P_- into stable and unstable sub-branches. It was shown by Faltinsen (1974) that the upper sub-branch of P_+/P_- corresponds to unstable solutions and the lower sub-branch to stable solutions. The branch P_-/P_+ without a turning point corresponds to stable solutions. When repeating the averaging asymptotic analysis given by Faltinsen for our solutions, we arrive at the same result if $\bar{A} \ll 1$.

When varying the values of the excitation amplitude, the sub-branch situated between S and O will always correspond to unstable solutions.

7. Comparison between theory and experiments

A series of experiments on nonlinear sloshing in a smooth rectangular tank due to horizontal (surge) excitation were conducted. Figure 4 shows the tank used in the experiments. The tank has a front plate made of Plexiglas which is stiffened by two vertical L-beams. The tank was placed on a wagon that could slide back and forth

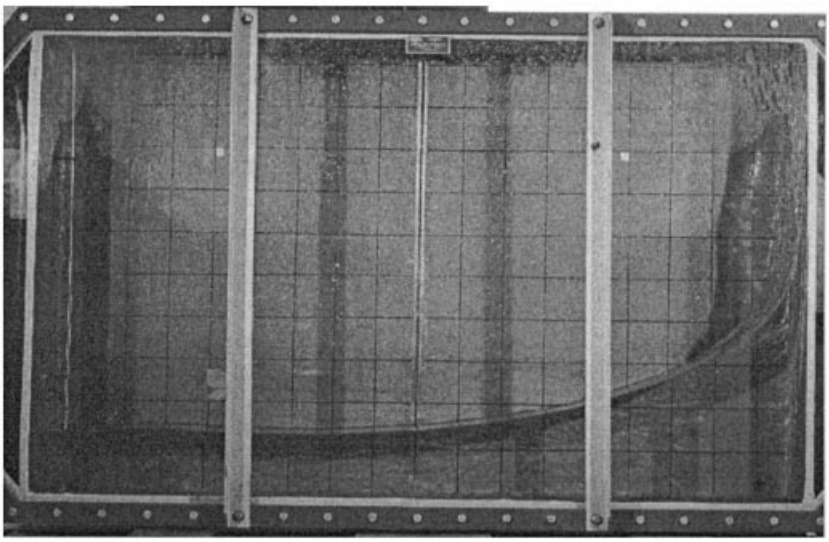

FIGURE 4. Picture of the tank.

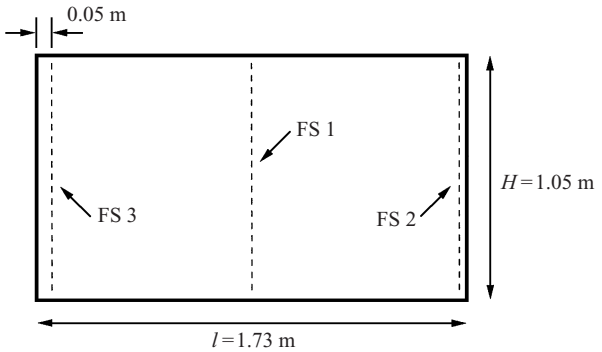

FIGURE 5. Tank dimensions and wave probe positions used in the experiments.

controlled by a hydraulic cylinder. The hydraulic system was strong enough to ensure that the motion inside the tank had little or no effect on the tank motion.

The tank height, breadth and length were respectively 1.05, 1.73 and 0.2 m. The observed free surface elevation did not vary in the length direction. The amplitude of surge excitation was between 0.02 and 0.08 m. The water depth was varied between 0.2 and 0.6 m. The tank was equipped with three wave probes, referred to as FS1, FS2 and FS3 (see figure 5). Wave probes FS1 and FS2 consist of adhesive copper tape directly placed on the tank wall. FS3 is made of steel wire and is standing 0.05 m from the left wall. The tank position was measured by a position gauge. The sampling frequency was 50 Hz and the time series were 50 s long. Video recordings and visual observation of longer simulations, up to 5 minutes, showed that steady-state oscillations with the forced oscillation period were not achieved. This implies that the dissipation in the smooth tank is very small even relative to the small damping predicted by Keulegan (1959). A reason may be that the boundary layer flow is laminar in Keulegan's experiments while it is likely to be turbulent in our case. Since transients do not die out, a beating effect occurs. The most interesting stage for

analysis is during the first 50 s. During this time the beating parameters are stabilized. After this time the typical behaviour of the sloshing is repeated. Also, the preliminary analysis has shown that for beating waves of small amplitude the modulated wave is stabilized for even shorter time.

The free surface elevation had small amplitudes in the initial period after the tank was excited. In some of the tests the water was in small-amplitude motion before starting the excitation. Since the proper initial conditions are unknown two different sets are used to investigate the influence of initial conditions. One set of initial conditions is

$$\beta_i(0) = \dot{\beta}_i(0) = 0, \quad i \geqslant 1. \tag{7.1}$$

The other is based on impulse conservation. If $v_{ox} = \sigma H \cos \sigma t$, this gives

$$\beta_i(0) = 0, \quad \dot{\beta}_i(0) = -\sigma P_i H, \qquad i \geqslant 1. \tag{7.2}$$

The numerical time integrations were done by a fourth-order Runge–Kutta method and 11 equations of (5.24) were used. The simulation time on a Pentium II–366 computer was $\frac{1}{300}$ of the real time.

The examples of figures 6–9 show the effect of initial conditions on free surface elevation for different forced excitation periods T, water depth h and excitation amplitude H. So, for example in figure 6 the effect of initial conditions is not important. However, for the case of figure 7 the condition of impulse conservation leads to more reasonable description of free surface elevation. Figures 8 and 9 also demonstrate good agreement between theory and experiments. The agreement is not perfect in figure 8, but the difference between experimental and numerical simulation decreases when initial conditions are based on impulse conservation. Better agreement between theory and experiment can be achieved by realizing that the forced surge oscillation is not harmonic and does not have a constant amplitude during the initial period. This is illustrated in figure 8 where the excitation period T was not a constant during the first 12 s; it varied from 1.76 s to 1.875 s. This is caused by transient rigid body motions. We assume that these transient motions decay exponentially. This effect was simulated by varying the period and the amplitude of forced excitation in the initial phase. Figure 10 shows the effect of only varying the excitation period. A better agreement with the experiment is then achieved. Separate numerical results showed that the amplitude has less effect than variation of the frequency. The effect of varying the frequency can be found qualitatively by examining the steady-state response in figure 2.

Our theory assumes that the water does not hit the ceiling. The water touches the ceiling in the case of figure 8, but this does not have an important effect on the fluid motion. When comparing theoretical and experimental results for a case when forceful impact occurs, it is evident that they do not agree. A possible reason is energy dissipation due to the impact. The impact causes the ceiling to vibrate which represents energy loss for the fluid motion. Since the tank ceiling is very stiff in the model tests, this is unimportant in the comparative study with experiments. Furthermore, as the water hits the ceiling a jet is formed and eventually the free surface overturns and water hits the free surface. This also causes energy dissipation. An estimate of this energy loss can be calculated by using a generalization of Wagner's (1932) theory (Faltinsen & Rognebakke 1999) and assuming that the kinetic and potential energy in the jet is dissipated. An equivalent linear damping based on energy conservation can then be included in the differential equations for the generalized coordinates for the free surface. The damping coefficients $\alpha_1\dot{\beta}_1$, $\alpha_2\dot{\beta}_2$ and $\alpha_3\dot{\beta}_3$ are introduced in (5.24*a*) to

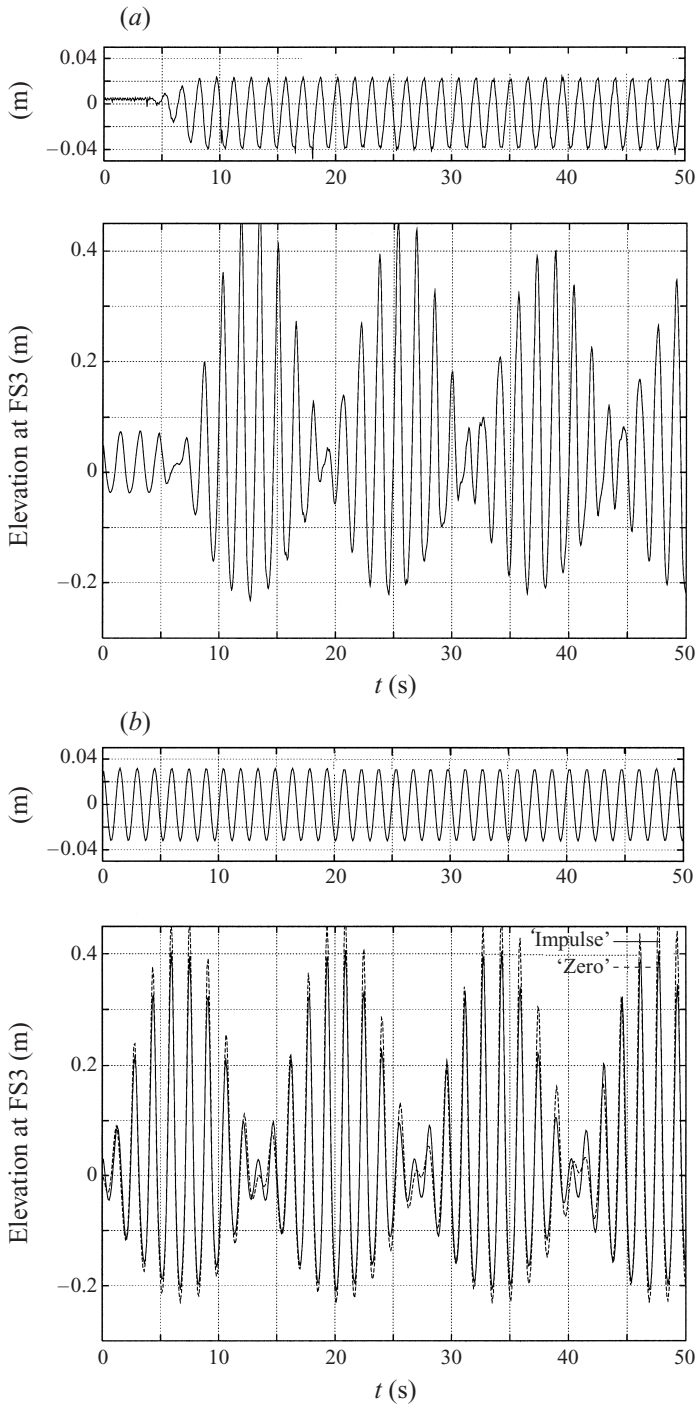

FIGURE 6. (*a*) Measured and (*b*) calculated tank position and free surface elevation at wave probe FS3 ($h = 0.6$ m, $T = 1.5$ s). The curve 'Zero' corresponds to zero initial conditions, 'Impulse' means initial impulse condition.

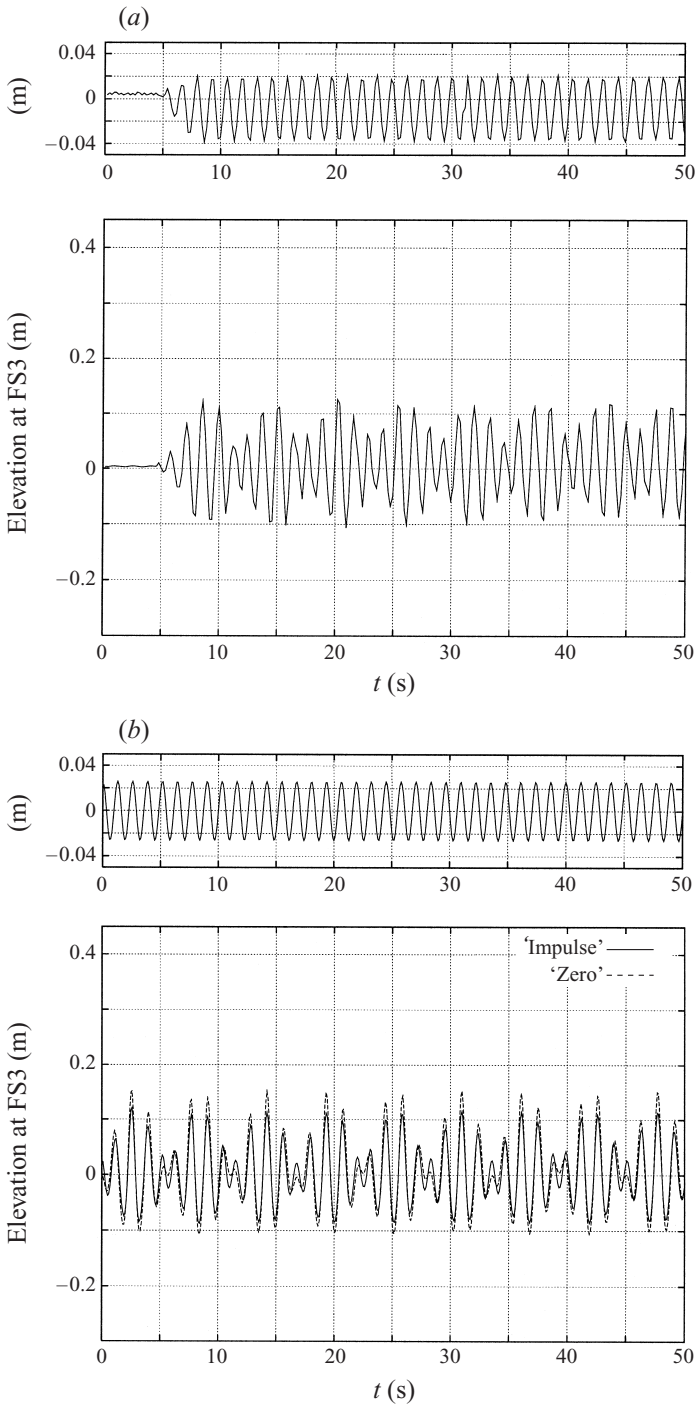

FIGURE 7. As figure 6 but at $T = 1.3$ s.

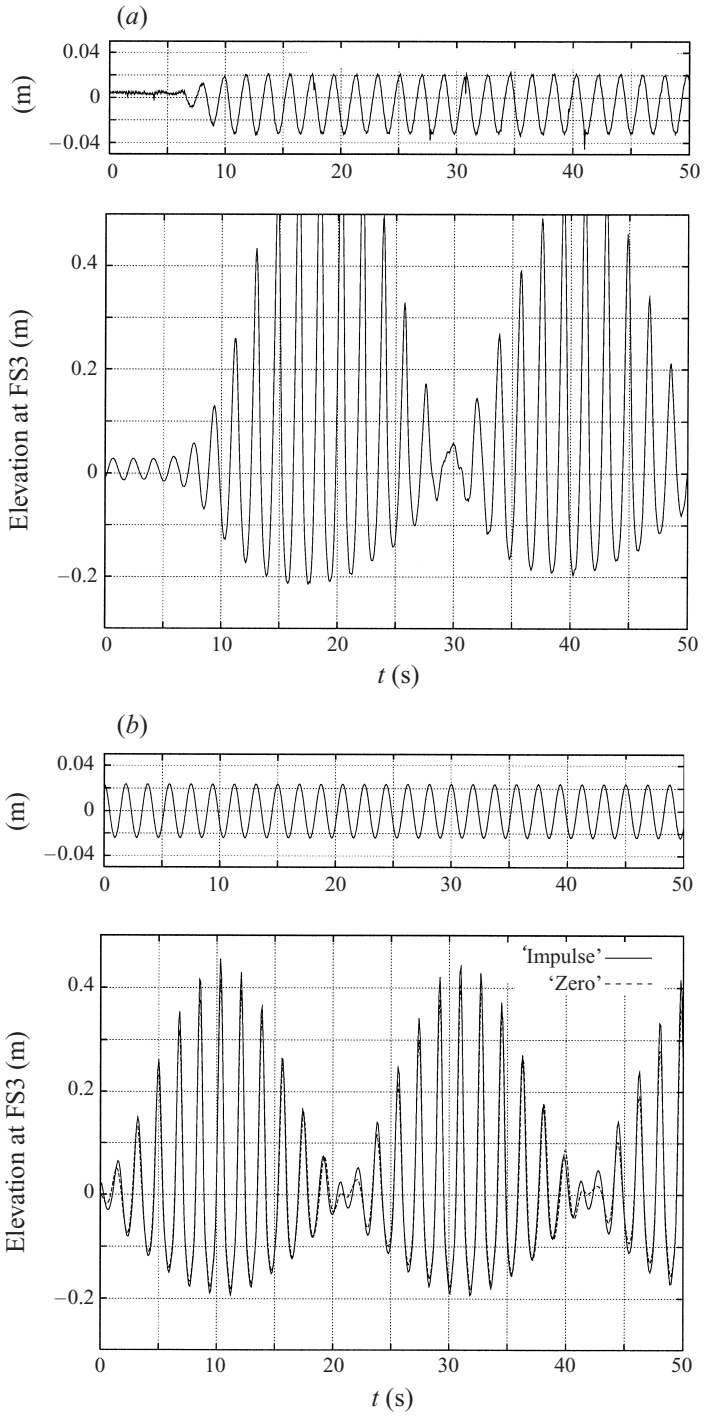

FIGURE 8. As figure 6 but at $h = 0.5\,\mathrm{m}$, $T = 1.875\,\mathrm{s}$.

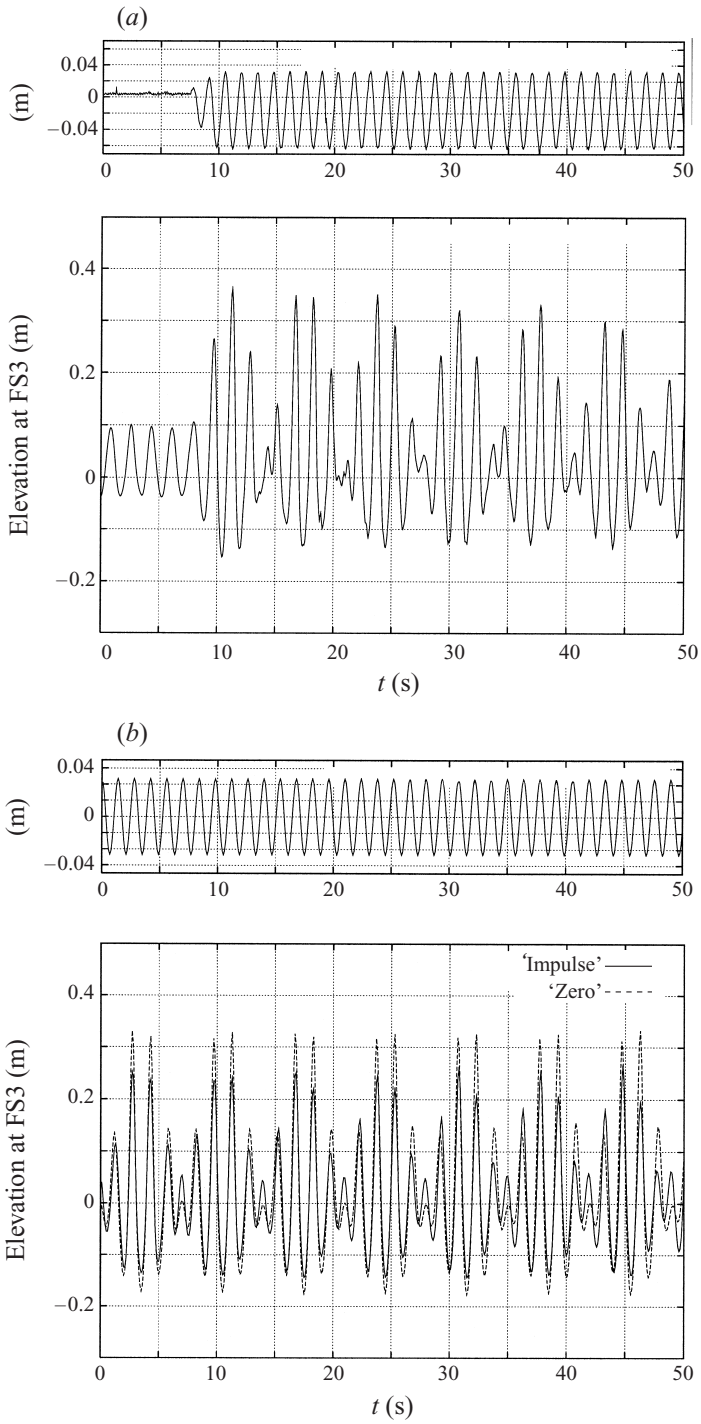

FIGURE 9. As figure 6 but at $h = 0.5\,\mathrm{m}$, $T = 1.4\,\mathrm{s}$.

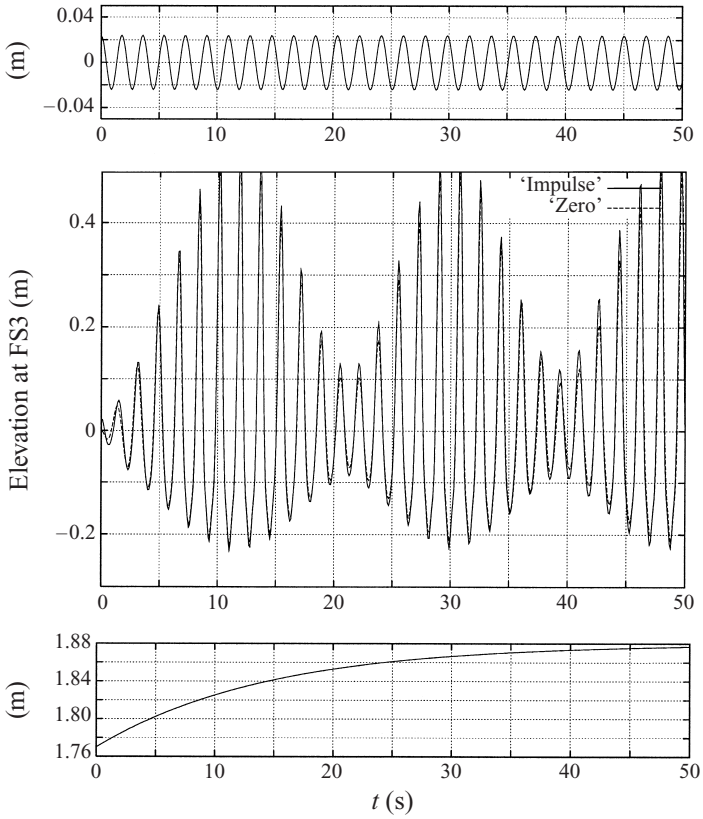

FIGURE 10. Calculated tank position and free surface elevation at wave probe FS3 for $h = 0.5$ m. Effect of varying excitation period exponentially from 1.77 s to 1.875 s.

(5.24*c*), respectively. Since the average forced excitation is close to the lowest natural frequency, it is only α_1 that matters. Figure 11 shows satisfactory agreement between theory and experiments by including damping. The damping will vary from cycle to cycle depending on the severity of the water impact. In the presented case we calculated approximately 40% loss of energy in the tank for every cycle due to the two impacts occurring.

The theory will break down for small water depth. Figure 12 presents experimental data and numerical simulation for $h/l = 0.173$ and $T_1/T = 0.96$. Since $i_2 = 0.9$, the effect of secondary parametric resonance is important. We note that the wave crest is well predicted, while the theoretical value for the trough is clearly lower than in the experiments. In order to improve the theoretical predictions we have to assume that at least the two lowest modes have the same order of magnitude. This means a complete change of the equation system and higher modes have to be introduced in the nonlinear equations. The introduction of the fourth mode in the nonlinear equation system will affect the difference between trough and crest so that the agreement with experiments may improve. The difference between theory and experiments is more evident in figure 13 where $T_1/T = 1.17$ and $h/l = 0.173$. The reason is once again that the primary mode is not dominating. This contradicts our theoretical assumptions. Figure 14 shows that the amplitude of the third mode is higher than the second mode, which is higher than the first mode.

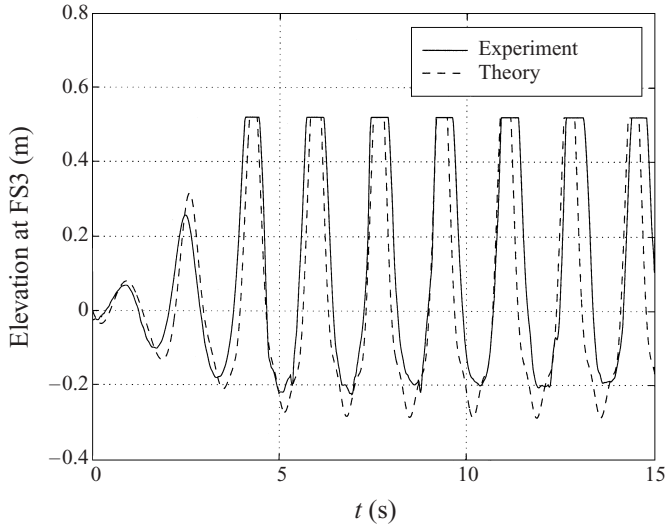

FIGURE 11. Measured and calculated free surface elevation at wave probe FS3 for $T = 1.71$ s, $h = 0.5$ m and $H = 0.05$ m. Calculations account for wave impact on tank ceiling.

8. Calculations of hydrodynamic loads on the tank

How to calculate hydrodynamic loads will be illustrated for the surge-excited rectangular tank. The general expression for the pressure is given by (2.5). By noting that $\Phi = v_{0x}x + \varphi$ and by expressing v_{0x} as $-H\sigma\sin(\sigma t)$ it follows that

$$p = p_0 - \rho\left[\frac{\partial\varphi}{\partial t} + \tfrac{1}{2}(\nabla\varphi)^2 + gz - \sigma^2 H\cos(\sigma t)x - \tfrac{1}{2}H^2\sigma^2\sin^2(\sigma t)\right]. \tag{8.1}$$

Here we use

$$\nabla\varphi = \sum_{i=1}^{N}\frac{\mathrm{i}\pi}{l}R_i(t)\left(-\sin\left(\frac{\mathrm{i}\pi}{l}\left(x+\frac{l}{2}\right)\right)\frac{\cosh((\mathrm{i}\pi/l)(z+h))}{\cosh((\mathrm{i}\pi/l)h)}, 0,\right.$$
$$\left.\cos\left(\frac{\mathrm{i}\pi}{l}\left(x+\frac{l}{2}\right)\right)\frac{\sinh((\mathrm{i}\pi/l)(z+h))}{\cosh((\mathrm{i}\pi/l)h)}\right), \tag{8.2}$$

$$\frac{\partial\varphi}{\partial t} = \sum_{i=1}^{N}\dot{R}_i(t)\cos\left(\frac{\mathrm{i}\pi}{l}\left(x+\frac{l}{2}\right)\right)\frac{\cosh((\mathrm{i}\pi/l)(z+h))}{\cosh((\mathrm{i}\pi/l)h)}, \tag{8.3}$$

where R_i and $\dot{R}_i$ are calculated by (5.12) and (5.13) and N is a number of Fourier terms ($N \geqslant 3$). When applying these formulas above the mean free surface, a Taylor expansion about the mean free surface has to be used.

The force $\boldsymbol{F}$ on the tank due to the fluid can be calculated by direct pressure integration or the compact formula derived by Lukovsky (1990)

$$\boldsymbol{F} = m_l\boldsymbol{g} - m_l[\dot{\boldsymbol{v}}_0 + \boldsymbol{\omega}\times\boldsymbol{v}_0 + \boldsymbol{\omega}\times(\boldsymbol{\omega}\times\boldsymbol{r}_{1C}) + \dot{\boldsymbol{\omega}}\times\boldsymbol{r}_{1C} + 2\boldsymbol{\omega}\times\dot{\boldsymbol{r}}_{1C} + \ddot{\boldsymbol{r}}_{1C}] \tag{8.4}$$

where $\boldsymbol{r}_{1C}$ is radius-vector of the mass centre in mobile coordinate system $Oxyz$ and m_l is fluid mass. We note that $\boldsymbol{F}$ includes the static force component $m_l\boldsymbol{g}$ in addition to hydrodynamic forces.

The formula takes the form

$$\boldsymbol{F} = m_l\boldsymbol{g} - m_l(\dot{\boldsymbol{v}}_0 + \ddot{\boldsymbol{r}}_{1C}) \tag{8.5}$$

in the absence of angular motions ($\omega = 0$).

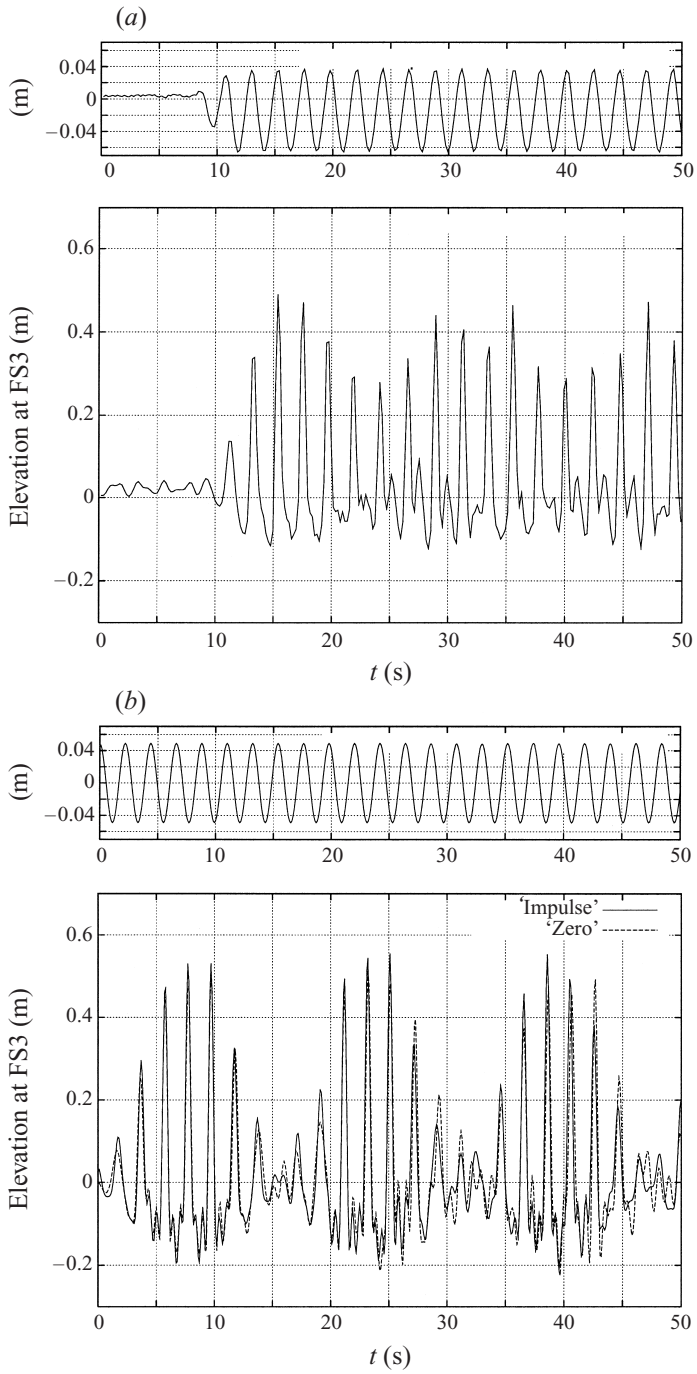

FIGURE 12. (*a*) Measured and (*b*) calculated tank position and free surface elevation at wave probe FS3 ($h = 0.3$ m, $T = 2.2$ s).

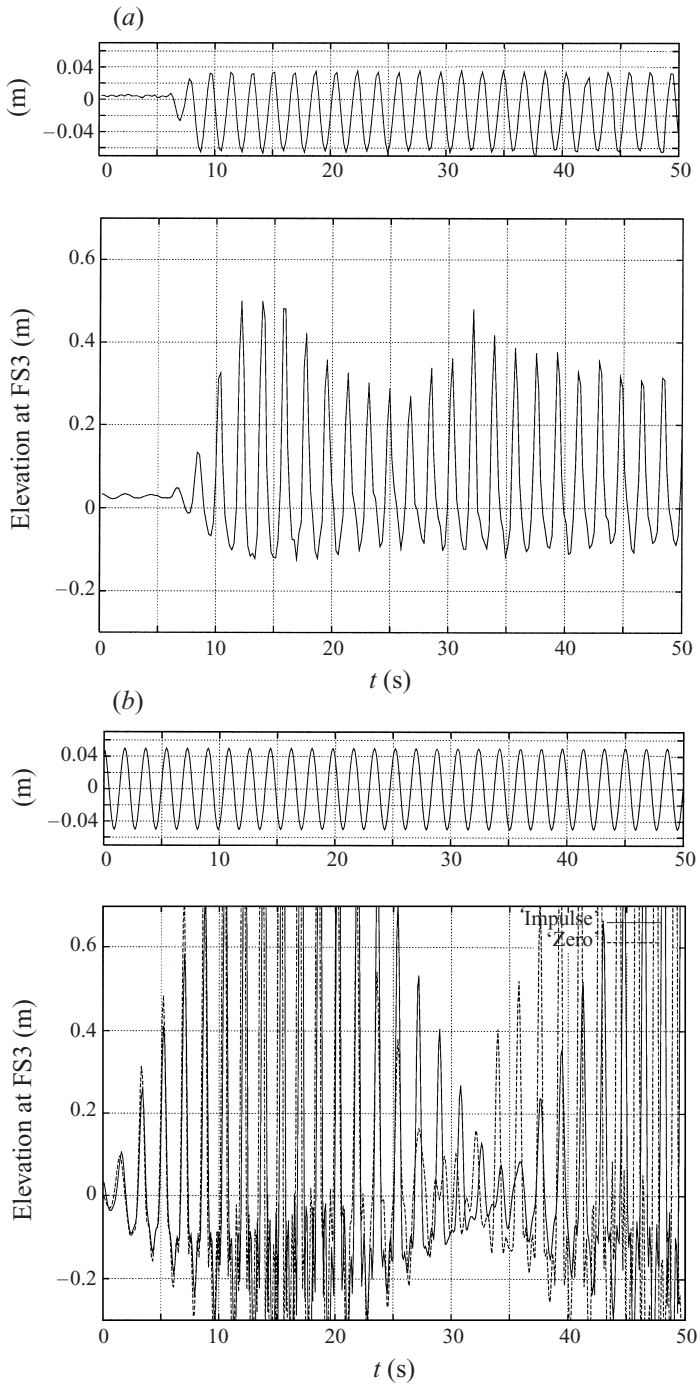

FIGURE 13. As figure 12 but at $T = 1.8$ s.

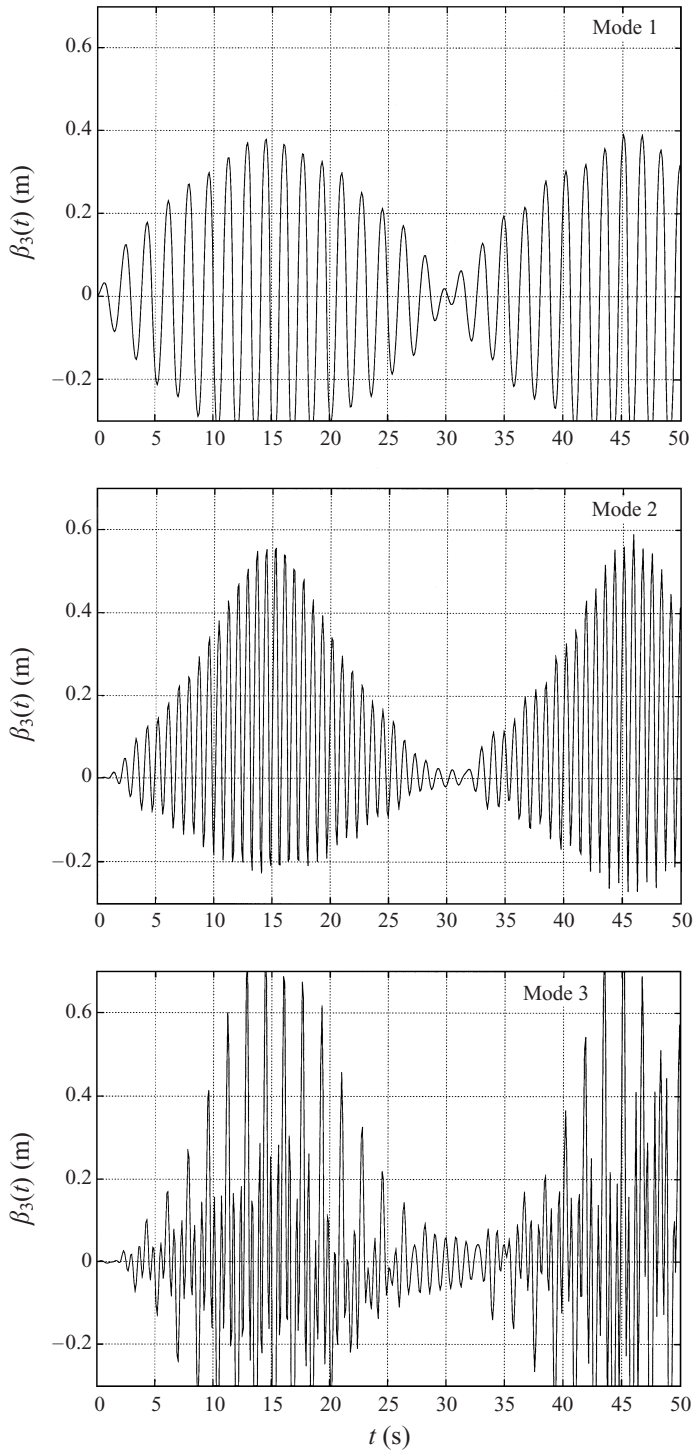

FIGURE 14. Contribution of the three lowest modes to the calculated free surface elevation at wave probe FS3; $h = 0.3$ m, $T = 1.8$ s.

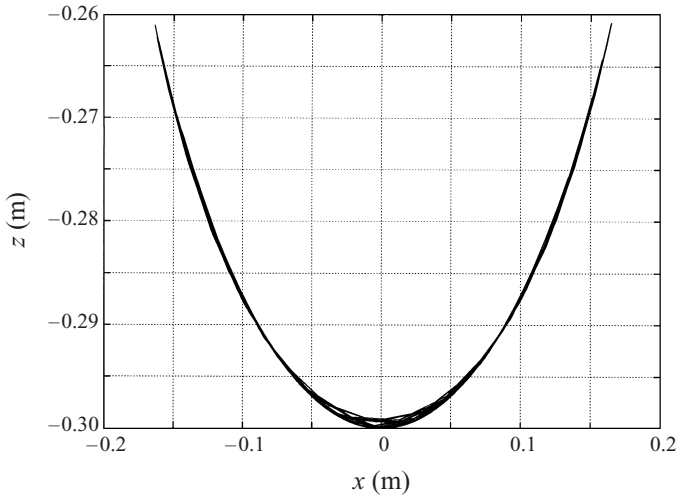

FIGURE 15. The position of mass centre for the case in figure 6.

The calculation shows, that if $\boldsymbol{r}_{1C} = (x_C(t), 0, z_C(t))$, then

$$x_C = -\frac{l}{\pi^2 h}\sum_{i=1}^{N}\beta_i(t)\frac{1}{i^2}(1+(-1)^{i+1}), \qquad z_C = -\frac{h}{2}+\frac{1}{4h}\sum_{i=1}^{n}\beta_i^2(t), \tag{8.6}$$

where the point $(0, -h/2)$ corresponds to mass centre of unperturbed fluid.

By introducing the vector $\boldsymbol{F} = (F_x, 0, F_z)$ we arrive at

$$\left.\begin{aligned} F_x/m_l &= \left(H\sigma^2\cos\sigma t + \frac{l}{\pi^2 h}\sum_{i=1}^{N}\ddot{\beta}_i(t)\frac{1}{i^2}(1+(-1)^{i+1})\right), \\ F_z/m_l &= -\left(g+\frac{1}{2h}\sum_{i=1}^{N}(\ddot{\beta}_i\beta_i+\dot{\beta}_i^2)\right). \end{aligned}\right\} \tag{8.7}$$

Figure 15 shows the trajectory of the mass centre. Figure 16 presents the trajectory of the end of the vector $\boldsymbol{F}/m_l$.

The hydrodynamic moment $\boldsymbol{N}$ on the tank can also be calculated by the special formula derived by Lukovsky (1990) (moment axis coincides with Oy)

$$\begin{aligned} \boldsymbol{N} = m_l\boldsymbol{r}_{1C}\times(\boldsymbol{g}-\boldsymbol{\omega}\times\boldsymbol{v}_0-\dot{\boldsymbol{v}}_0) - \boldsymbol{J}^1\cdot\dot{\boldsymbol{\omega}} - \dot{\boldsymbol{J}}^1\cdot\boldsymbol{\omega} - \boldsymbol{\omega}\times(\boldsymbol{J}^1\cdot\boldsymbol{\omega}) \\ -\ddot{\boldsymbol{l}}_\omega + \dot{\boldsymbol{l}}_{\omega t} - \boldsymbol{\omega}\times(\dot{\boldsymbol{l}}_\omega - \boldsymbol{l}_{\omega t}), \end{aligned} \tag{8.8}$$

where the inertia tensor $\boldsymbol{J}^1$ is defined by (3.13) and $\boldsymbol{l}_\omega, \boldsymbol{l}_{\omega t}$ by (3.15).

For $\boldsymbol{\omega} = \boldsymbol{0}$

$$\boldsymbol{N} = m_l\,\boldsymbol{r}_{1C}\times(\boldsymbol{g}-\dot{\boldsymbol{v}}_0) - \ddot{\boldsymbol{l}}_\omega + \dot{\boldsymbol{l}}_{\omega t}. \tag{8.9}$$

The time-varying functions $\boldsymbol{l}_\omega, \boldsymbol{l}_{\omega t}$ depend on the solutions of the Neumann boundary value problem (3.5) and can be expressed mathematically like the Stokes–Zhukovsky potentials.

By using Green's formula we get

$$N(t) = m_l(x_C g - z_C\dot{v}_0) - \rho\frac{\mathrm{d}}{\mathrm{d}t}\int_{S+\Sigma}(zv_1 - xv_3)\varphi\,\mathrm{d}S, \tag{8.10}$$

where $\boldsymbol{N} = (0, N(t), 0)$.

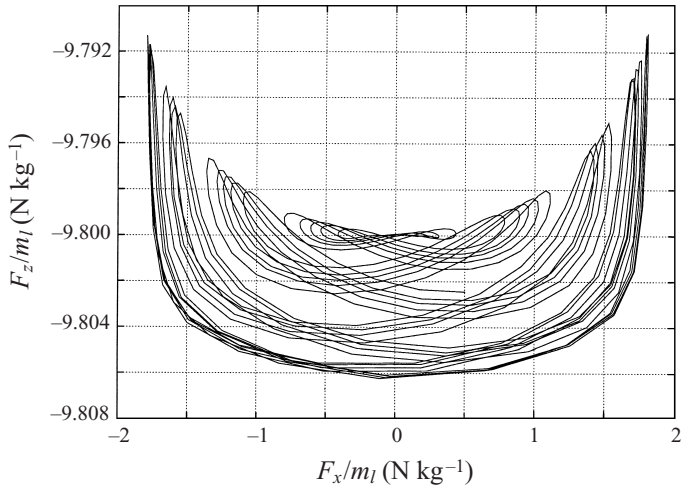

FIGURE 16. The trajectory of the vector of the calculated hydrodynamic force $(F_x/m_l, F_z/m_l)$ on the tank for the case in figure 6.

This is not as simple as the formula (8.7) for the force, but is useful in a verification procedure by comparing with the direct pressure integration of the moment. This should in both cases be derived correct to $O(\epsilon)$.

9. Conclusions

I. Using the Bateman–Luke variational principle, we generalize the procedure proposed by Miles (1976) and Lukovsky (1976) to derive a modal system describing nonlinear sloshing of an incompressible perfect fluid with irrotational flow partly occupying a tank performing an arbitrary three-dimensional motion. If the tank has vertical walls near the mean free surface, this procedure leads to an infinite-dimensional system of nonlinear differential equations coupling the generalized time-dependent coordinates. No assumptions about the order of smallness are made. It applies to any type of rigid body motion. The surface and domain modes do not need to be natural modes. This means that the multidimensional modal discrete system derived has the most general form of the modal equations and can be used for modelling different 'fluid–structure' problems including the problems associated with transient sloshing and coupled 'ship–fluid cargo' motions.

II. Two-dimensional sloshing in a rectangular smooth tank with finite water depth has been studied theoretically. The tank is oscillating with arbitrary rigid body motions of small magnitude with an average frequency close to the lowest natural frequency of the fluid motion. A finite-dimensional asymptotic model with multiple degrees of freedom is derived. This is based on the general discrete infinite-dimensional modal model. The lowest mode is assumed dominant. Each mode has different order of magnitude. The three lowest modes are interacting nonlinearly with each other. An important feature relative to other established nonlinear theories is that transient effects can be described. Since the theory is expressed in terms of a set of nonlinear ordinary differential equations in time, it is considerably simpler than a direct numerical solution of the fluid motion.

Periodic solutions are studied analytically. The amplitude–frequency response is consistent with the fifth-order steady-state solution by Waterhouse (1994).

It is shown that the theory is not valid when the water depth (h) becomes small relative to the tank breadth (l). This is due to secondary parametric resonance. It is then necessary to include nonlinearly interacting modes having the same order of magnitude. This is demonstrated for a tank with $h/l = 0.173$.

III. We have conducted experimental studies of the free surface elevation for forced surge oscillations of two-dimensional flow in a rectangular tank. It is demonstrated experimentally that it takes a very long time for transient fluid motion to die out. This did not occur during an observation period of 5 minutes, which corresponds to the order of 150–200 oscillations in terms of the excitation period. The consequence is that steady-state solutions of nonlinear sloshing in a smooth tank can have limited applicability. Modulated ('beating') waves occurred as a consequence of transient and forced oscillations. The amplitude/'beating' period was stabilized during the first 50 s.

Since we could not exactly state what the initial conditions were in the experiments, a sensitivity study was performed with different initial conditions in the theoretical model. The results were not strongly dependent on this, but better agreement between theory and experiments was in general obtained by using an initial condition based on impulse conservation. For several experiments we observed fluctuations of the excitation frequency in an initial period up to approximately 10 s. This effect was important to include in the theoretical model. There is good agreement with experimental free surface elevation when $h/l \geqslant 0.28$.

IV. The theory was compared with experiments when forceful water impact on the tank ceiling occurred. The theory assumes no tank ceiling. The experimental free surface elevations showed a clear influence of the water impact. It was speculated that this was due to energy dissipation and phenomenological linear damping terms were introduced in the discrete modal system. Good agreement with the experiments was demonstrated. This is an area of future research.

V. It is shown how hydrodynamic forces on the tank can be calculated in a simple way. An alternative formula for the hydrodynamic moment is also presented. The form of the expressions facilities simulations of a coupled 'vehicle–fluid' system.

This work is supported in part by NATO Research Fellowship (Research Council of Norway) at Norwegian University of Science and Technology, Trondheim (fourth author), German Research Council (D.F.G.) (third author). The work by the second author is supported by the Research Council of Norway. The experimental studies were sponsored by Det Norske Veritas.

REFERENCES

Bateman, H. 1944 *Partial Differential Equations of Mathematical Physics.* Dover.

Buechmann, B. A. 1996 2D numerical wave based on a third order boundary element model. In *9th Conf. European Consortium for Mathematics in Industry, Lyngby/Copenhagen, Denmark, June 25–27, 1996*, pp. 417–420.

Chen, Sh., Johnson, D. B., Raad, P. E. & Fadda, D. 1997 Surface marker and micro cell method. *Intl J. Numer. Meth. Fluids* **25**, 749–778.

Dodge, F. T., Kana, D. D. & Abramson, H. N. 1965 Liquid surface oscillations in longitudinally excited rigid cylindrical containers. *AIAA J.* **3**, 685–695.

Faltinsen, O. M. 1974 A nonlinear theory of sloshing in rectangular tanks. *J. Ship. Res.* **18**, 224–241.

Faltinsen, O. M. & Rognebakke, O. F. 1999 Sloshing and slamming in tanks. In *Hydronav'99.–Manoeuvering'99 Gdansk – Ostroda, 1999, Poland*. Technical University of Gdansk.

Funakoshi, M. & Inoue S. 1991 Bifurcations in resonantly forced water waves. *Eur. J. Mech.* B/*Fluids*. **10**, 31–36.

Hargneaves, R. 1908 A pressure–integral as kinetic potential. *Phil. Mag*. **16**, 436–444.

Ikeda, T. & Nakagawa, N. 1997 Non-linear vibrations of a structure caused by water sloshing in a rectangular tank. *J. Sound Vib*. **201**, 23–41.

Keulegan, G. H. 1959 Energy dissipation in standing waves in rectangular basin. *J. Fluid Mech*. **6**, 33–50.

Limarchenko, O. S. & Yasinsky, V. V. 1997 *Nonlinear Dynamics of Constructions with a Fluid*. Kiev Polytechnic University (in Russian).

Luke, J. C. 1967 A variational principle for a fluid with a free surface. *J. Fluid Mech*. **27**, 395–397.

Lukovsky, I. A. 1976 Variational method in the nonlinear problems of the dynamics of a limited liquid volume with free surface. In *Oscillations of Elastic Constructions with Liquid*, pp. 260–264 Moscow: Volna (in Russian).

Lukovsky, I. A. 1990 *Introduction to Nonlinear Dynamics of a Solid Body with a Cavity including a Liquid*. Kiev: Naukova dumka (in Russian).

Lukovsky, I. A. & Timokha, A. N. 1995 *Variational Methods in Nonlinear Dynamics of a Limited Liquid Volume*. Kiev: Institute of Mathematics (in Russian).

Mikishev, G. I. 1978 *Experimental methods in the dynamics of spacecraft*. Moscow: Mashinostroenie (in Russian).

Miles, J. W. 1976 Nonlinear surface waves in closed basins. *J. Fluid Mech*. **75**, 419–448.

Miles, J. W. 1984*a* Internally resonant surface waves in a circular cylinder. *J. Fluid Mech*. **149**, 1–14.

Miles, J. W. 1984*b* Resonantly forced surface waves in a circular cylinder. *J. Fluid Mech*. **149**, 15–31.

Moan, T. & Berge, S. (Eds.) 1997 *Report of Committee 1.2 "Loads"*. In *Proc. 13th Intl Ship and Offshore Structures Congress*, Vol. 1, pp. 59–122. Pergamon.

Moiseev, N. N. 1958 To the theory of nonlinear oscillations of a limited liquid volume of a liquid. *Prikl. Math. Mech*. **22**, 612–621 (in Russian).

Narimanov, G. S. 1957 Movement of a tank partly filled by a fluid: the taking into account of non-smallness of amplitude. *Prikl. Math. Mech*. **21**, 513–524 (in Russian).

Narimanov, G. S., Dokuchaev, L. V. & Lukovsky, I. A. 1977 *Nonlinear Dynamics of Flying Apparatus with Liquid*. Moscow: Mashinostroenie (in Russian).

Pawell, A. 1997 *Free Surface Waves in A Wave Tank. Intl Series Numer. Maths* **124**, 311–320. Birkhauser.

Pilipchuk, V. N. & Ibrahim, P. A. 1997 The dynamics of non–linear system simulating liquid sloshing impact in moving structures. *J. Sound Vib*. **205**, 593–615.

Shemer, L. 1990 On the directly generated resonant standing waves in a rectangular tank. *J. Fluid Mech*. **217**, 143–165.

Solaas, F. & Faltinsen, O. M. 1997 Combined numerical and analytical solution for sloshing in two-dimensional tanks of general shape. *J. Ship Res*. **41**, 118–129.

Su Tsung-Chow 1992 Nonlinear sloshing and the coupled dynamics of liquid propellants and spacecraft. *NASA Tech. Rep*. AD-A250023.

Tanizawa, K. 1996 A nonlinear simulation method of 3D body motions in waves extended formulation for multiple fluid domains. In *11th Intl Workshop on Water Waves and Floating Bodies, March 1996, Hamburg, Germany*. Abstracts.

Tsai, W.-T., Yue, D. K.-P. & Yip, K. M. K. 1990 Resonantly excited regular and chaotic motions in a rectangular wave tank. *J. Fluid Mech*. **216**, 343–380.

Verhagen, J. H. G. & Wijngaarden, L. van 1965 Nonlinear oscillations of fluid in a container. *J. Fluid Mech*. **22**, 737–751.

Wagner, H. 1932 Uber Stoss- und Gleitvorgange an der Oberflache von Flussigkeiten. *Z. Angew. Math. Mech*. **12**, 193–235.

Waterhouse, D. D. 1994 Resonant sloshing near a critical depth. *J. Fluid Mech*. **281**, 313–318.

Paper 4

Sloshing and slamming in tanks

Faltinsen, O. M. and Rognebakke, O. F.
Hydronav'99 and Manouevring'99, Gdansk/Ostrada, Poland, 1999

Preface

Sloshing may lead to slamming when a partially filled tank is excited with a period in vicinity of the highest natural period for the fluid motion. When the water surface hits the roof at one of the upper corners of the tank, large slamming forces with a short duration act on both the tank roof and vertical wall adjacent to the impact position. The impacts will also contribute to the dissipation of energy in the tank.

The base flow is calculated on the basis of the nonlinear sloshing theory by Faltinsen, Rognebakke, Lukovsky, and Timokha (2000), (Paper 3). A generalization of the theory by Wagner (1932) is used to find the slamming induced flow. The impacting surface is approximated by a parabola with radius of curvature R. Wagner's solution is corrected by accounting for the tank walls and bottom. The velocity potential due to impact is expressed as the sum of the velocity potential for infinite fluid and an infinite sum of image velocity potentials. When the impact phase is over, the generalized coordinates of the base flow are modified in order for the free surface to fit the new profile.

An interesting observ ationis that the horizontal slamming induced force is larger than the vertical slamming force on the tank roof.

Energy is dissipated through the jet formed in the impact. The hypothesis is that the kinetic and potential energy in the jet flow caused by the impact is dissipated when the jet flow impacts on the free surface. Thus, fluid damping occurs. The flux of energy is estimated and related to the total energy of the fluid in motion in the tank. A linear damping term is introduced in the base flow formulation. The level of damping is set so that an equal amount of energy is removed over one oscillation cycle as is lost in the jet. Appendix B shows the calculation of change in energy due to a linear damping term. An iterative procedure is follow ed when impacts occur.

Theoretical results are compared with data from experiments conducted in cooperation with Det Norske Veritas. The comparison is limited to the free surface elevation history, since force and pressure measurements are not available. Good agreement between theory and experiments is demonstrated.

SLOSHING AND SLAMMING IN TANKS

Odd M. Faltinsen and Olav F. Rognebakke
Department of Marine Hydrodynamics
Norwegian University of Science and Technology
N-7491 Trondheim, Norway

ABSTRACT

Sloshing and slamming in a smooth rectangular tank forced to oscillate horizontally and harmonically with a period close to the highest natural period are analyzed by including water impact in the nonlinear sloshing theory by Faltinsen et al. [4]. Finite water depth and two-dimensional potential flow is assumed. Generalized coordinates for the free surface elevation are described by a system of nonlinear ordinary differential equations in time. This leads to a time efficient solution. Simple expressions for hydrodynamic loads are derived. The water impact causes damping due to dissipation of the kinetic and potential energy in the jet resulting from slamming. Predicted free surface elevations are compared with model tests. There is a generally good agreement. The slamming causes large loads on the vertical wall adjacent to the impact area in the tank roof.

INTRODUCTION

A partially filled tank will experience violent fluid motion and slamming when the ship motions contain energy in the vicinity of the highest natural period for the fluid motion. The fluid motion is characterized by strong nonlinearities and small damping and is coupled to the ship motions. The external wave induced loads can in many practical cases be described by linear theory.

A theoretical method has to be robust and time efficient. Very long time simulations are needed to obtain statistical estimates of the tank response. Several attempts on direct numerical simulations of the fluid motions in a ship tank have been reported. A difficulty is to achieve long time simulations. Some methods may numerically loose fluid mass on a long time scale. Since the

URN:NBN:no-2322

highest natural period of the fluid motion is strongly dependent on fluid mass, this can result in unphysical numerical simulations. It is also difficult to incorporate slamming in a direct numerical method. The rapid change in time and space requires special treatment.

We have decided to develop a more analytically based approach. The method is both time efficient and robust. It seems easy to combine with the ship motions and external linear wave induced loads. The external and internal problem must then be solved simultaneously by means of the equations of rigid body ship motions. Harmonic forced sway oscillations of a rectangular smooth two-dimensional tank is analyzed in this paper. The water depth is finite and the wave system resembles standing waves. We first describe the theoretical method when no tank roof is present. Since irrotational fluid motion is assumed, internal structures causing flow separation can only be treated empirically by drag formulations. The effect of the tank roof is handled by generalizing Wagner's method [9]. The kinetic and potential energy in the jet caused by water impact is assumed dissipated when the jet impacts on the water surface. This energy loss is represented as a damping of the fluid motion. The study shows that large slamming induced pressures also occur on the vertical wall adjacent to the impact position on the tank roof. Numerical simulations for the free surface elevation are compared with experimental results.

THEORY

Consider a rectangular smooth and rigid tank forced to oscillate harmonically in sway. The fluid is incompressible and the flow is two-dimensional and irrotational. The water depth h is finite. Shallow water phenomena are not included. The forced oscillation frequency σ is close to the lowest natural frequency σ_1 of the fluid motion. The height and the breadth of the tank is H and l. The coordinate system (x,z) is fixed relative to the tank with origin in the mean free surface and in the center of the tank (See Fig. 1).

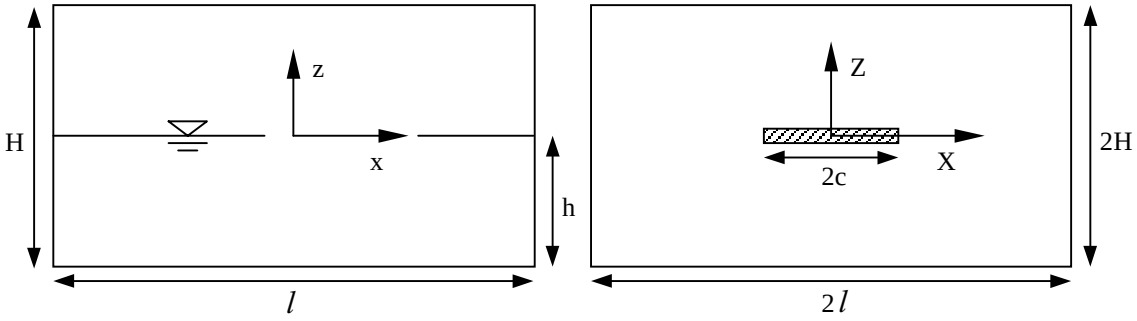

Figure 1: Tank dimensions, coordinate systems and problem configuration in slamming analysis

Violent fluid motion will occur due to resonant motions and small damping. When the fluid does not impact on the tank roof, the damping is very small and mainly due to viscosity in the boundary layers (Keulegan [6]). Nonlinearities are

significant and cause finite amplitudes at resonance. When the fluid motion does not impact the tank roof, ref. [4] is applied. This is based on a Bateman-Luke variational principle and use of the pressure in the Lagrangian of the Hamilton principle. This results in a system of nonlinear ordinary differential equations in time. The unknowns are generalized coordinates β_i of the free surface elevation. The procedure applies to any tank shape as long as the tank walls are vertical near the mean free surface. The equation system for our particular problem will be described. The free surface elevation ζ is written as

$$\zeta = \sum_{i=1}^{N} \beta_i(t)\cos(\pi i(x+0.5l)/l) \tag{1}$$

The forced oscillation amplitude is assumed small and of O(ε). Further $\beta_i = O(\varepsilon^{i/3}), \quad i = 1,3$, Higher order terms than ε are neglected in the nonlinear equations. Forced heave and roll can easily be included ([4]). The following system of ordinary differential equations was derived for forced sway.

$$\begin{aligned}
&(\ddot{\beta}_1 + \sigma_1^2\beta_1) + d_1(\ddot{\beta}_1\beta_2 + \dot{\beta}_1\dot{\beta}_2) + d_2(\ddot{\beta}_1\beta_1^2 + \dot{\beta}_1^2\beta_1) + d_3\ddot{\beta}_2\beta_1 + P_1\dot{v}_{0x} = 0\\
&(\ddot{\beta}_2 + \sigma_2^2\beta_2) + d_4\ddot{\beta}_1\beta_1 + d_5\dot{\beta}_1^2 = 0\\
&(\ddot{\beta}_3 + \sigma_3^2\beta_3) + d_6\ddot{\beta}_1\beta_2 + d_7\ddot{\beta}_1\beta_1^2 + d_8\ddot{\beta}_2\beta_1 + d_9\dot{\beta}_1\dot{\beta}_2 + d_{10}\dot{\beta}_1^2\beta_1 + P_3\dot{v}_{0x} = 0\\
&\ddot{\beta}_i + \sigma_i^2\beta_i + P_i\dot{v}_{0x} = 0, \quad i \geq 4
\end{aligned} \tag{2}$$

Here dots mean time derivatives, v_{0x} is the forced sway velocity of the tank and

$$\begin{aligned}
&\sigma_i^2 = 2gE_i, \quad P_{2i-1} = -8E_{2i-1}l/(\pi^2(2i-1)) \quad i \geq 1\\
&E_0 = (\pi/l)^2/8, \quad P_{2i} = 0, \quad E_i = 0.5\pi\tanh(\pi i h/l)/l \quad i \geq 1
\end{aligned} \tag{3}$$

$$\begin{aligned}
&d_1 = 2E_0/E_1 + E_1 \qquad d_2 = 2E_0(-1 + 4E_0/(E_1E_2)) \qquad d_3 = -2E_0/E_2 + E_1\\
&d_4 = -4E_0/E_1 + 2E_2 \qquad d_5 = E_2 - 2E_0E_2/E_1^2 - 4E_0/E_1 \qquad d_6 = 3E_3 - 6E_0/E_1\\
&d_7 = 9E_0 - 12\frac{E_0E_4}{E_1} - 6E_3E_4 + 24\frac{E_0^2}{E_1E_2} + 3\frac{E_0E_3}{E_1} \qquad d_8 = -6\frac{E_0}{E_2} + 3E_3\\
&d_9 = -6E_0/E_1 - 6E_0/E_2 - 6E_0E_3/(E_1E_2) + 3E_1E_3/E_2\\
&d_{10} = 18E_0 - 12E_4(2E_0 + E_1E_3)/E_1 + 72E_0^2/(E_1E_2) + 12E_0(E_3/E_1 - E_1/E_2)
\end{aligned} \tag{4}$$

Eqs. (2) are solved numerically by a fourth order Runge-Kutta method. Initial conditions on β_i and $\dot{\beta}_i$ have to be specified. Ref. [4] used two sets of initial conditions. One set is $\beta_i(0) = \dot{\beta}_i(0) = 0$. The other set was based on impulse conservation. The results were insensitive to these initial conditions after some oscillation periods. However, since no damping is present, the effect of the initial period is very important and does not die out. It means that fluid motions oscillating with the natural period and the forced oscillation period interact

URN:NBN:no-2322

linearly and nonlinearly and cause a beating effect. Steady state oscillations were not obtained. This was experimentally confirmed.

When the water impacts on the tank roof at either $x=-0.5l$ or $x=0.5l$, Wagner's [9] theory (see also ref. [3]) is generalized to find slamming induced flow. The analysis assumes a small angle between undisturbed free surface and tank roof. This may not be true at the end of an impact. The tank is assumed rigid so possible hydroelastic effects are ignored. The inflow velocity V(t) and the slope of the impacting surface can be found directly from Eq. (1). The impacting surface is approximated by a parabola with radius of curvature R. The wetted length c(t) follows from Wagner's integral equation. Wagner's solution is corrected by accounting for the tank walls and bottom. $c(t)/H$ and $c(t)/l$ are assumed small. A local coordinate system (X,Z) is used (see Fig. 1). If the water impacts at $x=-0.5l$, then $X=x+0.5l$ and $Z=z-(H-h)$. The wetted part of the tank roof is then from X=0 to X=c. The dynamic free surface condition is $\varphi=0$ on Z=0. Here φ is the velocity potential caused by slamming. The flow for either $X>0, Z\le 0$ or $X<0, Z\le 0$ is of interest. This can be found by studying cross-flow past a flat plate of length 2c in a rectangular box of breadth $2l$ and height 2H (see Fig. 1). The velocity potential due to impact is expressed as the sum of the velocity potential for infinite fluid and an infinite sum of image velocity potentials

$$\varphi_{mn}=0.5Vc^2(Z-2mH)(-1)^{|m|}/\left[(X-2nl)^2+(Z-2mH)^2\right] \tag{5}$$

All possible combinations of negative and positive integers m and n except simultaneously m=0, n=0 should be summed. The sum over m for m≠0 is

$$\begin{aligned}\varphi_n=\frac{Vc^2}{2}\frac{\partial}{\partial Z}\,&[0.5\ln[0.5(\cosh(\pi(X-2nl)/(2H))-\cos(\pi Z/(2H)))\,]\\&-0.5\ln[0.5(\cosh(\pi(X-2nl)/(2H))+\cos(\pi(Z-2H)/(2H)))\,]\,]\end{aligned} \tag{6}$$

When n=0, φ_0 can be written as Eq. (6) minus $-0.5Vc^2Z/(X^2+Z^2)$. It can be shown that conservation of fluid mass is correct to O(c^2).

When the impact phase is over, the free surface is fitted to Eq. (1), i.e. new values β_i^n are introduced. When impact occurs at $x=-0.5l$, the free surface elevation is written as

$$\varsigma=\begin{cases}H-h & \text{when } -0.5l<x<-0.5l+c_{\max}\\ \sum_{i=1}^{N}\beta_i\cos(\pi i(x+0.5l)/l)+\eta & \text{when } -0.5l+c_{\max}<x<0.5l\end{cases} \tag{7}$$

Here η is found by a Wagner's analysis for infinite fluid. This means

$$\eta=0.5(x+0.5l)\left\{(x+0.5l)-\sqrt{(x+0.5l)^2-c_{\max}^2}\right\}/R-0.25c_{\max}^2/R \tag{8}$$

URN:NBN:no-2322

Due to the orthogonality of $\cos(\pi i(x+0.5l)/l)$, explicit formulas for β_i^n are found. Since V(t)=0 at c=c_{max}, the slamming induced free surface η has zero vertical velocity. This implies $\dot{\beta}_i^n = \dot{\beta}_i$. When the water impacts at $x = 0.5l$, the procedure is similar.

The hydrodynamic force on the tank can be calculated by conservation of fluid momentum. It follows by Eq. 5.7 in Faltinsen [3] that

$$\frac{\mathrm{d}\vec{M}}{\mathrm{d}t} = -\int_{S_B} p\vec{n}\,\mathrm{d}s - \rho g \int_{S_B+S_F} z\vec{n}\,\mathrm{d}s \tag{9}$$

where the normal vector $\vec{n}$ is positive out of the fluid. S_B and S_F are wetted body surface and free surface respectively. $\vec{M}$ is the fluid momentum, p is hydrodynamic pressure, ρ is mass density of fluid and g is acceleration of gravity. By writing the fluid velocity as $v_{0x}\vec{i} + \nabla\varphi$ it follows by Eq. (9) and Gauss theorem that the hydrodynamic force is

$$\vec{F} = -\vec{i}\,m_l\dot{v}_{0x} - m_l g\vec{k} - \frac{\mathrm{d}}{\mathrm{d}t}\iiint_{\Omega}\rho\nabla\varphi\,\mathrm{d}\tau = -\vec{i}\,m_l\dot{v}_{0x} - m_l g\vec{k} - \frac{\mathrm{d}}{\mathrm{d}t}\rho\int_{S_B+S_F}\varphi\vec{n}\,\mathrm{d}s \tag{10}$$

where Ω is the fluid volume and m_l is the fluid mass. Green's second identity is used to rewrite the surface integral. Auxilliary velocity potentials $\Psi_1 = x$, $\Psi_3 = z$ that satisfy $\partial\Psi_i/\partial n = n_i$ on S_B + S_F are introduced. Since $\partial\varphi/\partial n = 0$ on S_B, it follows that

$$\vec{F} = -\vec{i}\,m_l\dot{v}_{0x} - m_l g\vec{k} - \frac{\mathrm{d}}{\mathrm{d}t}\rho\int_{S_F}\vec{r}\,\frac{\partial\varphi}{\partial n}\mathrm{d}s \tag{11}$$

where $\vec{r} = x\vec{i} + z\vec{k}$. Since the integral of $\partial\varphi/\partial n$ over S_F is zero from mass conservation, the result is independent of the origin of the position vector. The following horizontal force correct to $O(c^2)$ has been derived

$$\begin{aligned} F_x = {} & -m_l\dot{v}_{0x} + \rho\left(\frac{l}{\pi}\right)^2\sum_{i=1}^{N}\ddot{\beta}_i(t)\frac{1}{i^2}\left[(-1)^{i+1}+1\right] \\ & \pm\frac{d}{dt}\left\{\frac{\rho V c^2}{2}\left[\ln\left(\frac{\pi c}{8H}\right) - \frac{1}{2} - \ln\left(\tanh\left(\frac{\pi l}{4H}\right)\right)\right] - \sum_{n=1}^{\infty}\ln\left[\frac{\tanh(A)\tanh(B)}{\tanh\left(\frac{\pi nl}{2H}\right)\tanh\left(\frac{\pi nl}{2H}\right)}\right]\right\} \end{aligned} \tag{12}$$

Here A=$\pi(2n-1)l/(4H)$ and B=$\pi(2n+1)l/(4H)$. The plus and minus sign apply when the water impacts close to $x = -0.5l$ and $0.5l$, respectively. When no impact occurs, Eq. (12) agrees with Lukovsky's formula [7], [8]. The slamming part of Eq. (12), i.e. the last term, has been controlled by direct pressure

URN:NBN:no-2322

integration. The slamming induced pressure is written as $p=-\rho\dfrac{\partial}{\partial t}\left(\varphi_\infty+\varphi_0+\sum_{n=1}^{\infty}(\varphi_n+\varphi_{-n})\right)$. Here φ_n are given by Eq. (6) and the subsequent text. φ_∞ is the slamming induced velocity potential in infinite fluid. When impact occurs at $x=-0.5l$, this can be written as

$$\varphi_\infty=\begin{cases}-V\left(c^2+Z^2\right)^{1/2}-VZ & x=-0.5l,\quad Z\le 0\\ -0.5Vc^2Z/\left[l^2+Z^2\right] & x=0.5l,\quad Z\le 0\end{cases} \tag{13}$$

Similar formulas apply for impact at $x=0.5l$. The image potentials φ_n have a secondary effect relative to φ_∞. The impact pressure on the roof is given by $p=\rho\dfrac{\mathrm{d}}{\mathrm{d}t}\left[V\left(c^2-X^2\right)^{1/2}\right]$. This is singular at $|X|=c$. Here $X=x+0.5l$ when the water impacts at $x=-0.5l$. Similar for impact close to $x=0.5l$. The singularity at $|X|=c$ can be removed by matching with a local jet flow at the spray root $\left(|X|\approx c\right)$ (Zhao & Faltinsen [10]). The maximum pressure is $0.5\rho\dot{c}^2$. Since the image potentials satisfy $\varphi=0$ at $Z=0$, they do not contribute to the slamming induced pressure on the tank roof. The vertical slamming force on the tank roof and bottom are respectively

$$\begin{aligned}F_Z^{SR}&=\frac{\mathrm{d}}{\mathrm{d}t}\left(\rho V\frac{\pi}{4}c^2\right)\\ F_Z^{SB}&=-\frac{\mathrm{d}}{\mathrm{d}t}\left[\frac{\rho Vc^2}{2}\left\{\sum_{n=1}^{\infty}\sin^{-1}\left(\tanh\left(\frac{\pi(1-2n)l}{2H}\right)\right)+\sum_{n=0}^{\infty}\sin^{-1}\left(\tanh\left(\frac{\pi(1+2n)l}{2H}\right)\right)\right\}\right]\end{aligned} \tag{14}$$

The vertical force due to the ambient sloshing motions follows from Eq. (11) as $F_Z=-m_lg-0.5l\sum\left(\dot{\beta}_i^2+\beta_i\ddot{\beta}_i\right)$. Eq. 12 shows that the horizontal slamming induced force is logarithmically singular when $c\to 0$ and hence larger than the vertical slamming force on the tank roof. A reason is that the large slamming pressures act on a finite length on the vertical wall adjacent to the impact position while they act on a small wetted surface on the tank roof.

Compressibility will limit the pressure and the force in a very small initial phase of the impact. Air cushion and bubbles may also be present and influence the slamming pressure. But hydroelasticity may be far more important to account for in a local structural analysis (Faltinsen [1], [2]).

The previous analysis neglects dissipative forces. When the water impacts on the tank roof, fluid damping is believed to occur. The hypothesis is that the kinetic and potential energy in the jet flow caused by the impact is dissipated when the jet flow impacts on the free surface. This idea is used to introduce damping. The kinetic and potential energy loss during impact can be estimated as respectively (Faltinsen & Zhao [5])

$$E_{KE} = \frac{\rho\pi}{4}\int_0^{t_s} V^2 c\dot{c}\,\mathrm{d}t \quad , \; E_{PE} = \rho g(H-h)\frac{\pi}{8}\int_0^{t_s}\frac{V^2 c}{\dot{c}}\,\mathrm{d}t \tag{15}$$

where t_s is the duration of the impact. This energy loss can be related to the total energy E in the system. This is found by noting that the time rate of energy without any loss is $\mathrm{d}E/\mathrm{d}t = F_x v_{0x}$. Here F_x is given by Eq. (12). When studying one oscillation period, the previous loss of kinetic and potential energy is subtracted from E. The energy loss ΔE during one oscillation period is related to a damping ratio ξ by $\Delta E / E = 4\pi\xi$. The linear damping term $2\xi\sigma_i\dot{\beta}_i$ is introduced in each of Eqs. (2). An iterative procedure is followed. A simulation over one period is started with no damping. A first estimate of ξ is found. The simulation is repeated. This results in a new ΔE and thereafter a new ξ. This is done for iteration i>1 as $0.5(\Delta E_i + \Delta E_{i-1})/E = 4\pi\xi$. Convergence is typically achieved after 5 iterations.

RESULTS

A series of experiments has been conducted in cooperation with Det Norske Veritas. The tank height was 1.02m, breadth 1.73m and length 0.2m. The tank was forced to oscillate in the horizontal direction in the cross-sectional plane. The observed free surface elevation did not vary in the length direction. Wave probes were used to measure the free surface elevation at the two side walls and in the middle of the tank and a position gauge was used to measure the instantaneous position of the tank.

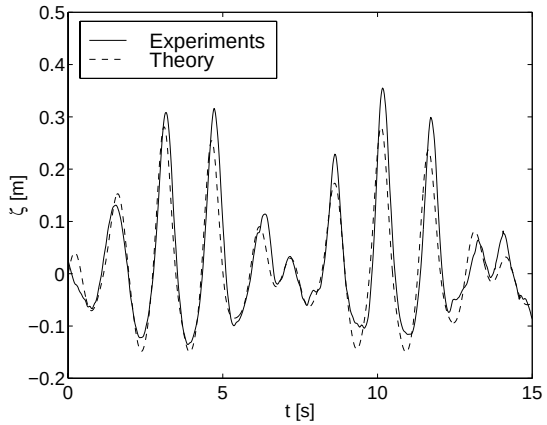

Figure 2: Free surface elevation ζ at the tank wall. T=1.4s, h=0.5m and ε_0=0.048m. h/l =0.289 and T/T$_n$=0.798

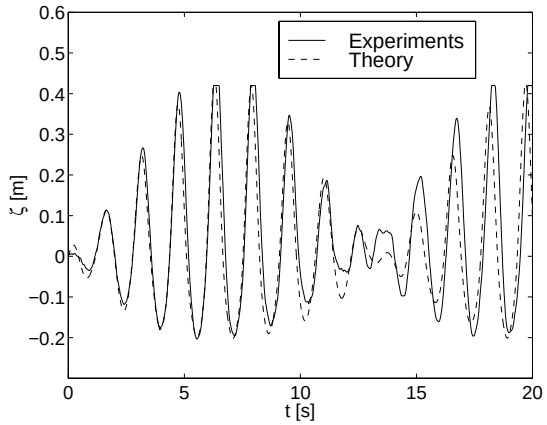

Figure 3: Free surface elevation ζ at the tank wall. T=1.5s, h=0.6m and ε_0=0.032m. h/l =0.347 and T/T$_n$=0.899

URN:NBN:no-2322

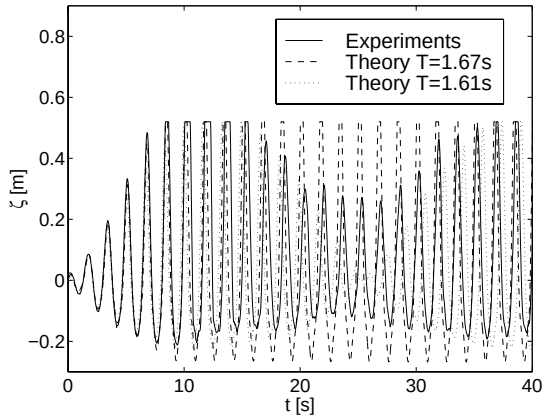

Figure 4: Free surface elevation ζ at the tank wall. T=1.67s, h=0.5m and ε_0=0.0252m. h/l =0.289 and T/T$_n$=0.952

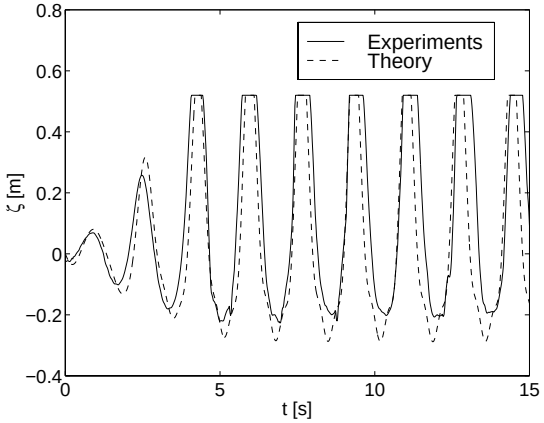

Figure 5: Free surface elevation ζ at the tank wall. T=1.71s, h=0.5m and ε_0=0.05m. h/l =0.289 and T/T$_n$=0.975

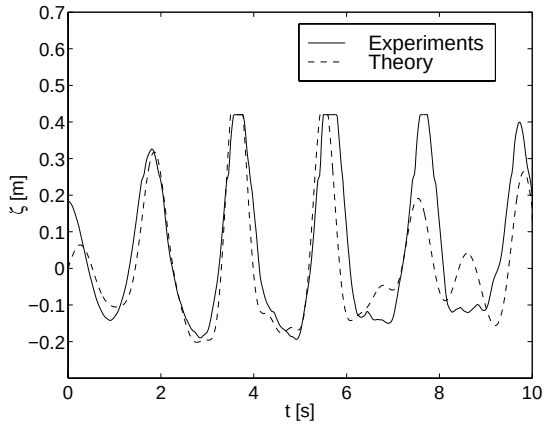

Figure 6: Free surface elevation ζ at the tank wall. T=2.03s, h=0.6m and ε_0=0.085m. h/l =0.347 and T/T$_n$=1.22

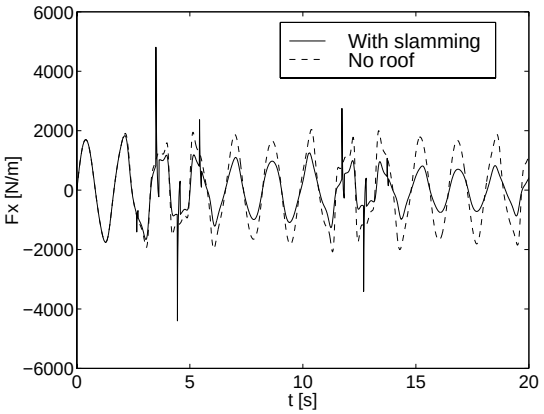

Figure 7: Horizontal force on the tank T=2.03s, h=0.6m and ε_0=0.085m. h/l =0.347 and T/T$_n$=1.22

The following comparisons between theory and experiments are for h/l close to the critical depth $h/l = 0.337$. The amplification of theoretical fluid response at the highest resonance period is largest at the critical depth. Fig. 2 shows an example on the good agreement between theory and experiments when no tank roof impact occurs. ε_0 means forced sway amplitude. Since the damping is zero in the theory and very small in reality, response at the natural period T_n does not die out and beating occurs. This is evident in Fig. 2 and was observed as long as the experiments lasted, i.e. up to 5 minutes. The initial time $t = 0$ in Fig. 2 and subsequent figures corresponds to the start up of the experiments. Fig. 3 shows an example with light roof impact. Good agreement between theory and experiments is demonstrated. Maximum theoretical

amplitude $\zeta_{\infty m}$ with no tank roof is 0.45m. Fig. 4 shows a case with heavier roof impact. Here $\zeta_{\infty m}$ is 1.78m. There is good agreement for maximum values and the initial phase. But the beating is not correctly predicted. Actually it has been theoretically shown that the beating can be strongly sensitive to both frequency and oscillation amplitude, i.e. nonlinearities matter. Fig. 4 shows that by sligthly changing the oscillation period there is good predictions of the beating. Fig. 5 shows a case with very heavy roof impact. $\zeta_{\infty m}$ is in this case 1.8m. Good agreement is demonstrated. When predicting slamming loads we have to evaluate the impact velocity, i.e. $\mathrm{d}\zeta/\mathrm{d}t$. Fig. 5 suggests that this can be satisfactorily estimated by theory. Fig. 6 shows another case with roof impact. We note some difficulties in correctly predicting beating. Here $\zeta_{\infty m}$ is 0.67m. Fig. 7 shows corresponding theoretical values for the horizontal hydrodynamic force. The influence of impact is clearly evident. Actually the force is logarithmically singular at time of impact. The slamming induced force in Fig. 7 is calculated from 0.002s after initial impact. We have also presented what the horizontal force would be without tank roof. This demonstrates the damping effect of roof impact. We can illustrate the damping in another way. In the first oscillation period where impact occurs, the following values are calculated after 6 iterations:

Mean energy in the tank:		316.5 Nm/m
First impact:	Potential energy loss	1.0 Nm/m
	Kinetic energy loss	1.3 Nm/m
Second impact:	Potential energy loss	36.9 Nm/m
	Kinetic energy loss	58.2 Nm/m

This gives a damping coefficient ξ = 0.0246 which means that 30% of the mean energy in the tank is lost due to the two impacts.

CONCLUSIONS

Sloshing and slamming in a smooth rigid rectangular tank forced to oscillate horizontally and harmonically with a period close to the highest natural period are analyzed by including water impact in the nonlinear sloshing theory by Faltinsen et al. [4]. Finite water depth and two-dimensional potential flow is assumed. Nonlinear effects are significant. Generalized coordinates for the free surface elevation are described by a system of nonlinear, ordinary differential equations in time. Water impact is included by combining Wagner's [9] method with an infinite set of image potentials. The image system has a secondary effect. The water impact causes damping due to dissipation of the kinetic and potential energy in the jet resulting from slamming. An equivalent linear damping based on energy conservation is introduced. This damping is important. Viscous damping in a smooth tank is insignificant. The solution procedure is time efficient and robust. Simple expressions for hydrodynamic forces are derived based on conservation of fluid momentum. The formulas are

URN:NBN:no-2322

verified by direct pressure integration. When the water does not impact the tank roof, the formulas agree with Lukovsky [7], [8].

Predicted free surface elevations are compared with model tests. Steady-state oscillations are not obtained even after very long simulations. This is due to linear and nonlinear combinations of fluid flow oscillating with the natural period and the forced oscillation period.

The importance of damping due to tank roof impact is demonstrated. There is generally good agreement between theory and experiments. Cases with unsatisfactory predictions of beating are demonstrated. This is due to high sensitivity between beating and oscillation period and amplitude.

The slamming causes large loads on the vertical wall adjacent to the impact area in the tank roof.

REFERENCES

[1] Faltinsen, O.M., (1999). Water entry of a wedge by orthotropic plate theory, Accepted for publication in Journal of Ship Research.

[2] Faltinsen, O.M., (1997). The effect of hydroelasticity on ship slamming, *Phil. Trans. R. Soc. A.*, 355, 1-17.

[3] Faltinsen, O.M., (1990). *Sea Loads on Ships and Offshore Structures*, Cambridge, England: Cambridge University Press.

[4] Faltinsen, O.M., Rognebakke, O.F., Lukovsky, I.A., Timokha, A.N., (1999). Multidimensional modal analysis of nonlinear sloshing in a tank. Part I: Variational method. Part II: Sloshing in rectangular tank with finite water depth. Submitted for publication.

[5] Faltinsen, O.M., Zhao, R., (1997). Water entry of ship sections and axisymmetric bodies, AGARD FDP and Ukraine Institute of Hydromechanics Workshop on 'High-Speed Body Motion in Water', Kiev, Ukraine, AGARD Reprt. 818, Paper no. 24, 11p.

[6] Keulegan, G.H., (1959). Energy dissipation in standing waves in rectangular basin*, J. Fluid Mech*., 6, pp. 33-50

[7] Lukovsky, I.A., (1995). *Introduction to nonlinear dynamics of a solid body with a cavity including a liquid*, Kiev: Naukova dumka, 296p (in Russian)

[8] Lukovsky, I.A., Timokha, A.N., (1995). *Variational methods in nonlinear dynamics of a limited liquid volume*, Kiev: Naukova dumka, 400p (in Russian)

[9] Wagner, H., (1932). Über Stoss- und Gleitvorgänge an der Oberflache von Flussigkeiten, Zeitschr. F. Angew. *Math. und Mech*., Vol. 12, No. 4, pp. 193-235.

[10] Zhao, R., Faltinsen, O.M., (1993). Water entry of two-dimensional bodies, *J. Fluid Mech*., 246, pp. 593-612.

Paper 5

Damping of sloshing due to tank roof impact

Rognebakke, O. F. and Faltinsen, O. M.

15th International Workshop on Water Waves and Floating Bodies,
Ceasarea, Israel, 2000

Preface

This extended abstract was presented at the 15th International Workshop on Water Waves and Floating Bodies in Ceasarea, Israel.

In Paper 4, the damping effect of sloshing motion from impacts in a smooth rectangular tank was discussed. In reality, tanks are often chamfered. The impact angle between the rising free surface and roof is thus increased relative to a flat roof, and the impact pressures and forces decrease. The calculation of energy dissipated during the impact is based on the theory of Wagner (1932). Appendix C. contains details of the derivation of energy loss in a chamfered tank.

Wagner's analysis assumes a small angle between the undisturbed free surface and the tank roof. For a chamfered roof, this assumption is invalidated. A correction factor based on the similarity solution by Dobrovol'skaya (1969) is introduced. Zhao and Faltinsen (1993) used the similarity solution and present numerical calculations for a triangular wedge entering through an initially undisturbed free surface with a constant downward velocity. These results are used in the present study to correct the energy estimates for large impact angles. An alternative is to use the generalized Wagner's theory developed by Faltinsen (2001). Figures 4.1 and 4.2 show the mass flux, M_{flux}, and kinetic energy flux, $\mathrm{d}E_{kin}/\mathrm{d}t$, through the jet calculated by means of Wagner's theory, the similarity solution and the generalized Wagner's theory. V is the constant impact velocity, β is the wedge deadrise angle and ρ is the density of the fluid. The curves based

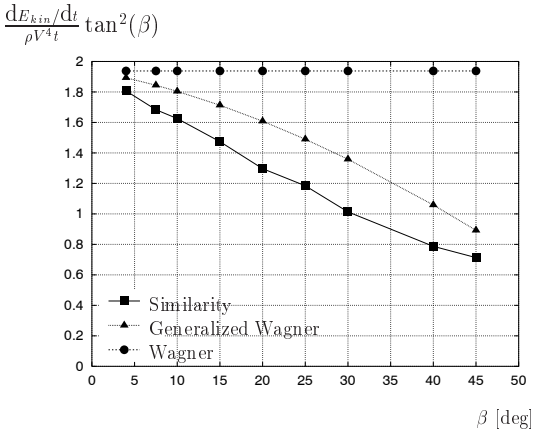

Figure 4.1: Kinetic energy flux through the jet

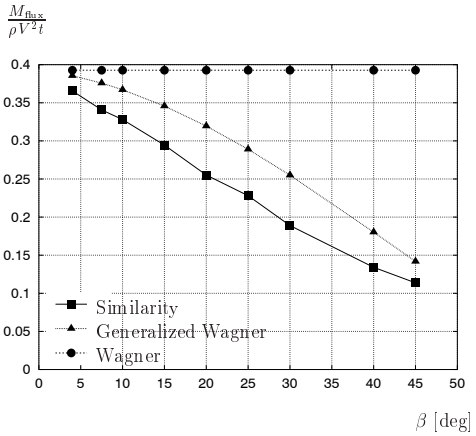

Figure 4.2: Mass flux through the jet

on the similarity solution are not smooth. The values are estimated from printed plots in Zhao and Faltinsen (1993). Since the similarity solution does not give the location of the spray root explicitly, there is a certain ambiguity in finding the exact location.

DAMPING OF SLOSHING DUE TO TANK ROOF IMPACT

Olav F. Rognebakke and Odd M. Faltinsen
Department of Marine Hydrodynamics
Norwegian University of Science and Technology
N-7034 Trondheim, Norway

Introduction

Sloshing in a smooth tank leads to violent fluid motion for an excitation frequency close to the lowest natural frequency of the fluid motion. When the free surface hits the tank roof, a water impact similar to slamming occurs, and energy is dissipated. A statistical treatment of sloshing demands time efficient calculations. Thus, the analytic approach proposed by Faltinsen et al. [1] is well suited for the task. However, the analytical model does not account for the impact of the water on the roof. By estimating the kinetic and potential energy loss in the jet generated during the impact and relating this to the total energy in the fluid, an equivalent damping term can be introduced in the analytical model. A Wagner's method [2] is applied. When the impact angle between the rising free surface and the tank wall or roof is large, results from a similarity solution are utilized to correct the estimated energy loss. Numerical simulations for the free surface elevations without impact are compared with experimental results. Numerical force calculations and experimental data for different fluids are presented for a LNG tank model.

Theory

Consider a rectangular smooth and rigid tank forced to oscillate harmonically in sway. The fluid is incompressible and the flow is two-dimensional and irrotational. The height and the breadth of the tank is H and l. The coordinate system (x, z) is fixed relative to the tank with origin in the mean free surface and in the center of the tank, Fig. 1.

Violent fluid motion will occur due to resonant motions and small damping. When the fluid does not impact on the tank roof, the damping is very small and mainly due to viscosity in the boundary layers [3]. Nonlinearities are significant and cause finite amplitudes at resonance. When fluid motion does not impact the tank roof, [1] is applied.

This is based on a Bateman-Luke variational principle and use of the pressure in the Lagrangian of the Hamilton principle. This results in a system of nonlinear ordinary differential equations in time. The unknowns are generalized coordinates β_i of the free surface elevation. The procedure applies to any tank shape as long as the tank walls are vertical near the mean free surface. The equation system for the rectangular tank excited in sway follows. The free surface elevation ζ is written as

$$\zeta = \sum_{i=1}^{N} \beta_i(t) \cos(\frac{\pi i(x + 0.5l)}{l})$$

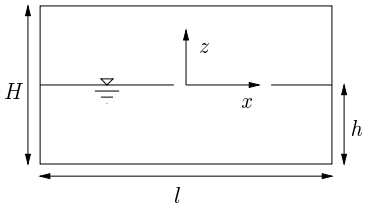

Figure 1: Coordinate system and tank dimensions.

The forced oscillation amplitude is assumed small and of $O(\epsilon)$. Further $\beta_i = O(\epsilon^{\frac{i}{3}})$, $i = 1, 3$. Higher order terms than ϵ are neglected in the nonlinear equations. The following system of nonlinear ordinary differential equations for the generalized coordinates describing the free surface are derived for forced motions

$$\begin{aligned}
&(\ddot{\beta}_1 + 2\xi\sigma_1\dot{\beta}_1 + \sigma_1^2\beta_1) + d_1(\ddot{\beta}_1\beta_2 + \dot{\beta}_1\dot{\beta}_2) + d_2(\ddot{\beta}_1\beta_1^2 + \dot{\beta}_1^2\beta_1) \\
&\quad + d_3\ddot{\beta}_2\beta_1 + P_1(\dot{v}_{0x} - S_1\dot{\omega} - g\psi) + Q_1\dot{v}_{0z}\beta_1 = 0, \\
&(\ddot{\beta}_2 + 2\xi\sigma_2\dot{\beta}_2 + \sigma_2^2\beta_2) + d_4\ddot{\beta}_1\beta_1 + d_5\dot{\beta}_1^2 + Q_2\dot{v}_{0z}\beta_2 = 0, \\
&(\ddot{\beta}_3 + 2\xi\sigma_3\dot{\beta}_3 + \sigma_3^2\beta_3) + d_6\ddot{\beta}_1\beta_2 + d_7\ddot{\beta}_1\beta_1^2 + d_8\ddot{\beta}_2\beta_1 + d_9\dot{\beta}_1\dot{\beta}_2 \\
&\quad + d_{10}\dot{\beta}_1^2\beta_1 + P_3(\dot{v}_{0x} - S_3\dot{\omega} - g\psi) + Q_3\dot{v}_{0z}\beta_3 = 0 \\
&\ddot{\beta}_i + 2\xi\sigma_i\dot{\beta}_i + \sigma_i^2\beta_i + P_i(\dot{v}_{0x} - S_i\dot{\omega} - g\psi) + Q_i\dot{v}_{0z}\beta_i = 0, \quad i \geq 4.
\end{aligned} \tag{1}$$

Here v_{0x} and v_{0z} are projections of translational velocity onto axes of Oxz, $\omega(t)$ is the value of angular velocity of coordinate system $Oxyz$ with respect to $O'x'y'z'$. The calculation formulas for the coefficients σ_i, P_i, S_i, Q_i, $i \geq 1$ and d_j, $j = 1, \ldots, 10$ are given in [1]. The equation system is solved numerically by a fourth order Runge-Kutta method.

The linear damping term $2\xi\sigma_i\dot{\beta}_i$ is included in each of eq. 1. The damping is found as an equivalent damping so that the energy removed from the system during one full cycle is equal to the energy lost in the impact, $\xi = \frac{1}{4\pi}\frac{\Delta E}{E}$

When the water impacts on the tank roof, fluid damping is believed to occur. The hypothesis is that the kinetic and potential energy in the jet flow caused by the impact is dissipated. Fig. 2 shows the evolution of an impact in the upper left corner of a LNG ship tank. The formation and overturning of the jet is evident.

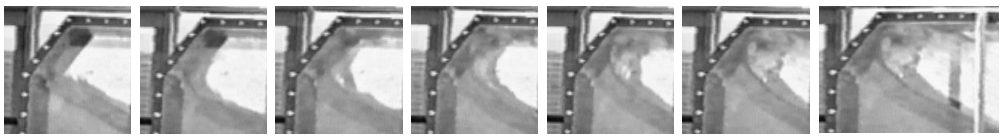

Figure 2: Snapshots of upper left corner of LNG tank during impact

This energy loss is related to the total energy E in the system, which is found from $\dot{E} = F_x v_{0x}$ for forced sway. When studying one oscillation period, the previous loss of kinetic and potential energy is subtracted from E. An iterative procedure is followed. A

simulation over one period is started with no damping. A first estimate of ξ is found. The simulation is repeated, results in a new ΔE and thereafter a new ξ. This is done for iteration $i > 1$ as $0.5\frac{\Delta E_i + \Delta E_{i-1}}{E} = 4\pi\xi$. Typically, 5 iterations are sufficient for convergence.

The impact model is based on a generalized Wagner's approach [2]. The tank is assumed rigid so possible hydroelastic effects are ignored. The inflow velocity $V(t)$ and the slope of the impacting surface can be found directly from Eq. . The impact velocity is approximated by a linear function $V(t) = V_0 + V_1 t$. $t = 0$ is the time of impact. The impacting surface is approximated by a parabola with radius of curvature R. The wetted length $c(t)$ follows from Wagner's integral equation. This solution can be corrected by accounting for the tank walls and bottom. Details can be found in [5]. However, this effect is not important and thus is not included here. The Wagner's analysis assumes a small angle between undisturbed free surface and tank roof. A similarity solution presented by Zhao and Faltinsen [4] valid for large angles is applied to correct the energy estimates when this is not the case. The energy estimates obtained from Wagner's analysis are multiplied by a reduction factor. Fig. 3 gives the definitions of symbols used in the slamming analysis. $c(t)$ is the horizontal distance from $x = 0$ to the spray root, δ is the thickness of the jet, u_c is the velocity of the control surface following the spray root and u_a is the absolute fluid velocity at the spray root. Fig. 4 introduces symbols applied in the similarity solution. s_j is the length of the jet, β is the deadrise angle of the wedge, β_0 is the angle of the triangular jet and ζ_L and ζ_B are the vertical distance to the jet root and tip of the jet, respectively.

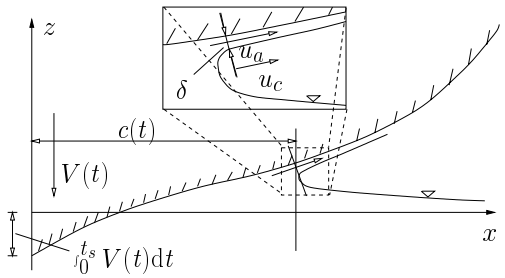

Figure 3: Definitions for the slamming analysis

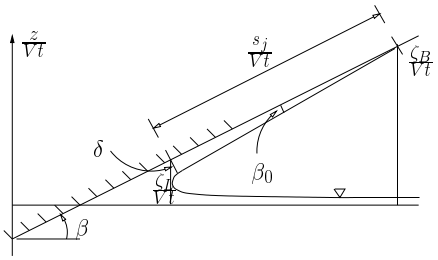

Figure 4: Definitions used in the similarity solution

The similarity solution is derived for a constant impact velocity. However, the reduction factor found for the energy loss for a constant speed is also applied for the linearly decreasing impact velocity.

The kinetic energy flux into the jet is calculated for both the similarity solution and Wagner's approach for a wedge and constant impact speed. The kinetic and potential energy flux through the jet can generally be found as

$$\frac{\mathrm{d}E_{kin}}{\mathrm{d}t} = \frac{\rho}{2} u_a^2 \delta u_f \quad , \quad \frac{\mathrm{d}E_{pot}}{\mathrm{d}t} = \rho g (H - h) M_{\text{flux}} \tag{2}$$

when a constant velocity across the jet is assumed and the potential energy loss is estimated as the potential energy the mass of the water has relative to the level of the mean

free surface. u_f is the relative velocity betw een the fluid velocity and the control surface velocity, $u_f = u_a - u_c$. M_{flux} is the flux of mass into the jet. Wagner's solution gives [4]

$$u_a = 2\frac{\mathrm{d}c}{\mathrm{d}t}\ , \quad u_c = \frac{\mathrm{d}c}{\mathrm{d}t}\ , \quad \delta = \frac{\pi V^2 2c}{16(\frac{\mathrm{d}c}{\mathrm{d}t})^2}\ , \quad c = \frac{\pi V t}{2\tan(\beta)}\ , \quad \delta = \frac{\tan(\beta) V t}{4} \tag{3}$$

and the kinetic energy flux and mass flux

$$\left.\frac{\mathrm{d}E_{kin}}{\mathrm{d}t}\right|_W = \frac{\rho V^4 \pi^3 t}{16\tan^2(\beta)}\ , \quad M_W = \frac{\mathrm{d}c}{\mathrm{d}t}\delta = \frac{\pi V^2}{8}t \tag{4}$$

The jet in the similarity solution is assumed to be triangular, giving

$$\frac{s_j}{Vt} = \frac{\xi_B - \xi_L}{Vt\sin(B)}\ , \quad \frac{\delta}{Vt} = \frac{s_j}{Vt}\tan(\beta_0) \tag{5}$$

The mass flux into the jet is then equal to

$$M_S = \frac{\mathrm{d}}{\mathrm{d}t}\left[\frac{1}{2}s_j\delta\right] = \frac{\mathrm{d}}{\mathrm{d}t}\left[\frac{1}{2}(\frac{\zeta_B - \zeta_L}{\sin(\beta)})^2\tan(\beta_0)\right] = \left[\frac{\zeta_B - \zeta_L}{Vt\sin(\beta)}\right]^2\tan(\beta_0)V^2 t \tag{6}$$

A constant flux velocity in the similarity solution is found as $u_f = \frac{M_S}{\delta}$. By observing that the z component of u_c must be equal to $\frac{\mathrm{d}\zeta_L}{\mathrm{d}t}$ plus the constant downward velocity V, u_c can be estimated as

$$u_c = \frac{\frac{\mathrm{d}\zeta_L}{\mathrm{d}t}}{\sin(\beta)} + \frac{V}{\sin(\beta)} \tag{7}$$

Again, substituting in Eq. 2, the kinetic energy flux for the similarity solution is

$$\left.\frac{\mathrm{d}E_{kin}}{\mathrm{d}t}\right|_S = \frac{\rho V^4 t\tan(\beta_0)}{2\sin^4(\beta)}\left[(\frac{\frac{\mathrm{d}\zeta_L}{\mathrm{d}t}}{V}) + 1 + \frac{\zeta_B - \zeta_L}{Vt}\right]^2\left[\frac{\zeta_B - \zeta_L}{Vt}\right]^2 \tag{8}$$

Fig. 5 shows the difference in kinetic energy and mass flux for Wagner's approach and the similarity solution. The numerical results are based on numbers presented in [4]. When $\beta \to 0$, the results by the similarity solution and Wagner agree.

Results and discussion

The free surface elevation is compared with experimental results for a heavy impact case in Fig. 6. The tank is rectangular with $l = 1.73$m, a filling height $h = 0.5$m and a total height of $H = 1.02$m. The period and amplitude of the sway excitation are $T = 1.71$s and $\epsilon_0 = 0.05$m, respectively. ϵ_0 means forced sway amplitude. The figure suggests that a satisfactory estimate of the impact velocity $\frac{\mathrm{d}\zeta}{\mathrm{d}t}$ can be calculated. This value is important in the prediction of slamming loads.

Fig. 7 shows the dimensions of the prismatic LNG tank model for which computational and experimental results of horizontal forces are presented in Fig. 8. d is the width of the

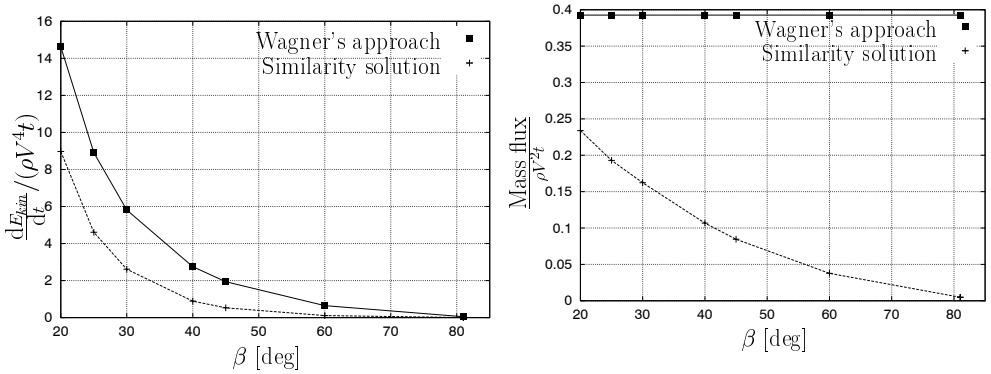

Figure 5: Kinetic energy and mass flux

tank. The chamfer angle is 45. This gives a reduction factor for the kinetic energy loss of 0.27 and a factor of 0.22 for the potential energy loss. Wagner's approach over-predict the energy loss for large angles. A good agreement is seen for results away from resonance, where the current approach predicts too large forces. Sources of error are discussed below.

The energy loss through the jet and evolution of the wetted length $c(t)$ are shown in Fig. 9. In this special case, approximately 1/4 of the total energy in the fluid is lost during the two impacts of one cycle. The kinetic and potential energy loss are of the same magnitude. The main part of the energy loss is generated during the initial phase of the impact. Hence, the errors due to an assumption of a linearly decreasing impact velocity and constant free surface curvature should not be large. At $t = 35.425$ the impact moves past the chamfered part of the roof.

There are several uncertainties and sources of error in the presented methodics, of which some have been discussed already. The accuracy of the nonlinear flow model is of great importance. Missing nonlinear effects can for an excitation close to resonance result in a large misprediction of the maximum free surface elevation, leading to an even larger error in the estimation of the damping level. Local downward vertical accelerations above 1g are calculated for some impact cases. According to Penney and Price [6] this is a criterion for breaking of a standing wave. The only back-coupling from the impact to the analytic model is through damping. When the duration and spatial extent of the impact are large this simplification may no longer suffice.

Further work will focus on the continued development of a nonlinear boundary element method designed for calculating the impact jet flow. This approach will serve to validate the current methodics, as well as provide an alternative damping estimat for heavy impact situations. The wish to still use the nonlinear analytical method for the non-impact flow is motivated by the dramatic difference in simulation time. The energy loss through the jet is important. Thus, a state of the art volume of fluids program must have a very fine discretization both in time and space in order to capture this.

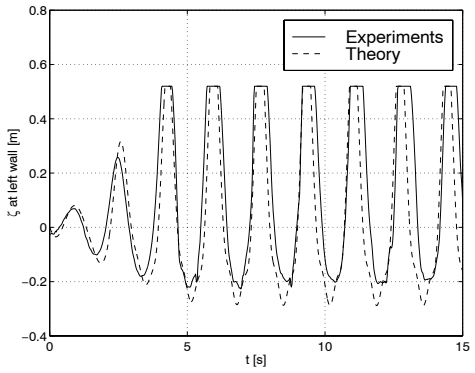

Figure 6: Free surface elevation for a case of heavy roof impact

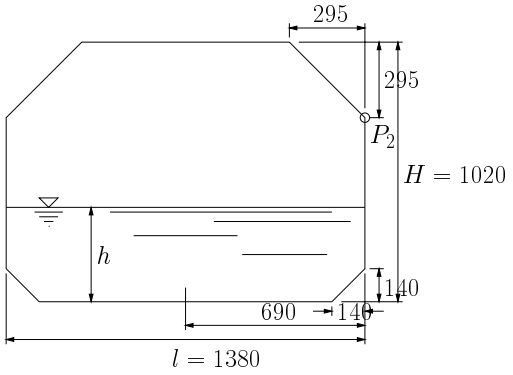

Figure 7: Prismatic LNG tank model

Acknowledgements

This work is part of a Ph. D. thesis sponsored by the Research Council of Norway and Det Norske Veritas.

References

[1] Faltinsen, O. M., Rognebakke, O. F., Lukovsky, I. A., Timokha, A. N. Multidimensional modal analysis of nonlinear sloshing in a rectangular tank with finite water depth. Accepted for publication in *J. Fluid Mech.*.

[2] Wagner, H. (1932) Über Stoss- und Gleitvorgänge and der Oberflache von Flussigkeiten. Zeitsdhr. F. Angew. *Math. und Mech.* **12**, 193-235

[3] Keulegan, G. H. (1958) Energy dissipation in standing waves in rectangular basins. *J. Fluid Mech.* **6**, 33-50

[4] Zhao, R., Faltinsen, O. M. (1993) Water entry of two-dimensional bodies. *J. Fluid Mech.* **246**, 593-612

[5] Faltinsen, O. M., Rognebakke, O. F. (1999) Sloshing and slamming in tanks. *HYDRONAV'99-MANOEUVERING'99* Gdansk-Ostrada, Poland

[6] Penney, W. G., Price, A. T. (1952) Finite Periodic Stationary Gravity Waves in a Perfect Liquid. *Phil. Trans. Royal Soc.* (London) **A 244**, 254-284

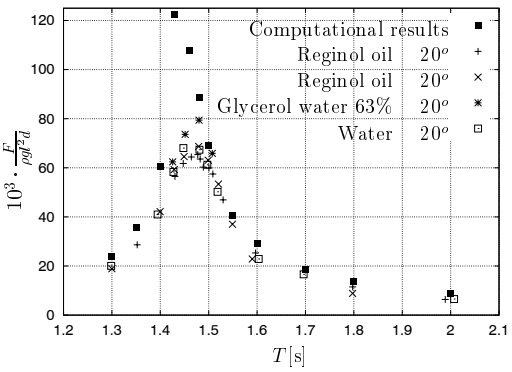

Figure 8: LNG tank $\frac{h}{l} = 0.4$, $\frac{\epsilon_0}{l} = 0.01$. Computational results and experimental data for various fluids

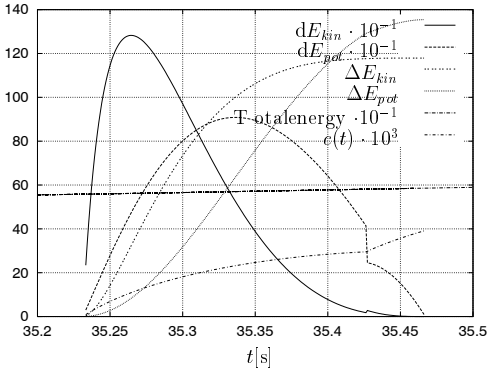

Figure 9: LNG tank $\frac{h}{l} = 0.4$, $\frac{\epsilon_0}{l} = 0.01$ and $T = 1.43$s. Change of energy during an impact

Paper 6

Effect of sloshing on ship motions

Rognebakke, O. F. and Faltinsen, O. M.
16th International Workshop on Water Waves and Floating Bodies,
Hiroshima, Japan, 2001

Preface

This extended abstract was presented at the 16th International Workshop on Water Waves and Floating Bodies in Hiroshima, Japan.

Sloshing in the context of marine engineering usually happens when a tank is excited by ship motions. The sloshing induced forces will influence the ship motion. A coupled system of ship dynamics and sloshing was next topic in line for study. The nonlinear sloshing method including an impact model was an ideal starting point, since the structure of the method readily facilitates coupling. A high computational efficiency is also a significant advantage.

Two-dimensional experiments were conducted for a box-shaped hull section excited by regular beam sea. The experiments are used to validate the calculation of a coupled system.

A commercial linear frequency- and time-domain ship motions program was used in the calculations, with the inclusion of a sloshing module programmed by the author. This module gives as output the sloshing force, either based on a linear or nonlinear sloshing model, with the rigid body tank motions as input. Iterative calculations in the frequency domain were used when linear sloshing was considered. In the case of nonlinear sloshing, the sloshing model did not work properly with the time domain version of the commercial program. Instead, the hydrodynamic coefficients were calculated by the program and used as input for an integration routine where the equation of motion for the coupled system, Eq. (1) in the paper, was integrated in time. The use of constant coefficients as opposed to a convolution formulation was deemed relevant since steady-state motions were studied and the experiments showed almost no trace of the higher order sloshing force harmonics in the sway motion of the coupled system.

A strong sensitivity of the calculated sway response to the damping level of the internal sloshing flow was discovered for sway frequencies in the vicinity of the first linear eigenperiod for the fluid motion in the tank. A quasi-linear approach was applied to explain this effect.

Figure 2 illustrates the relationship between the wave amplitude and wave frequency used in the experiments. The values indicate the input to the wave-maker. Later investigation showed that the calibration transfer function in the control system of the wavemaker is not perfectly accurate for low frequencies. This influences the normalization of the experimental results. However, the discrepancy between input amplitude and the amplitude of the resulting wave is minimal in the frequency range covered in Fig. 6.

The top left plot of Fig. 6 shows wrong results for the sway motions when a linear sloshing model is applied. The results valid for two filled tanks were used by mistake. Fig. 5 presents the correct values.

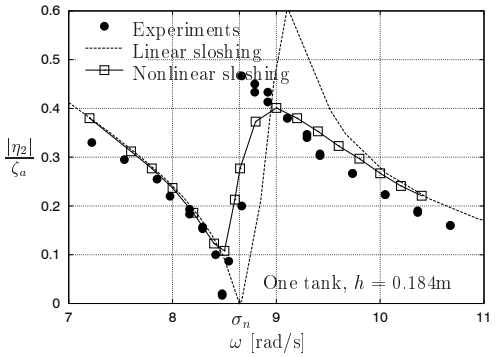

Figure 5.1: Comparison betw een experiments and calculations

EFFECT OF SLOSHING ON SHIP MOTIONS

Olav F. Rognebakke and Odd M. Faltinsen
Department of Marine Hydrodynamics
Norwegian University of Science and Technology
N-7491 Trondheim, Norway

When a ship carrying liquid cargo moves in waves, sloshing may occur. The ship motions excite sloshing which in return affects the ship motions. 2-D experiments on a box-shaped ship section excited by regular beam sea have been conducted to study this coupling effect. The section contains two tanks and can only move in sway. The external ship motion problem may be solved by using a standard linear strip theory program, while the sloshing must be described by a nonlinear method. The adaptive multimodal approach by Faltinsen and Timokha [1] has been used. This method has been extensively validated for forced tank motions. The present study represents a first validation for coupled internal and external flows.

The experiments were carried out in the wave flume of the Department of Marine Hydrodynamics at NTNU. The flume has an overall length of 13.5 m and is 0.6 m wide. It is equipped with an electronically operated, computer controlled, single flap wavemaker, calibrated for a water depth of 1.03 m. The side walls and the bottom of the flume are made of glass.

Fig. 1 shows model parameters. The ship section with an overall length of 596 mm has 2 mm clearance from the flume walls. The breadth is 400 mm and the draft 200 mm. The two identical tanks have breadth b of 376 mm, a length of 150 mm and a height of 288 or 388 mm depending on the position of the deck. The deck may be lowered when sloshing induced water impact on the tank roof is desirable. No tank roof impact occurred in the reported examples. Weights are added to the model so that the total weight equals the buoyancy for the fixed draft and different amounts of water in the tanks. The section slides along two rails where low friction bearings are used. It is restrained from drifting off by springs with a total stiffness of 30.9 N/m. The springs cause an eigenfrequency well below the studied wave frequencies. The steepness of the waves was kept below a certain threshold value to prevent breaking. Fig. 2 gives the chosen relation between frequency ω and amplitude ζ_a of the generated regular waves.

A typical time series for the sway motion of the section with water in one tank, is shown in Fig. 3. A transient phase precedes a steady state for the system. A beating period of ≈ 5 s is evident during the transient phase. This is the eigenperiod of the system consisting of the springs and the ship model. A shift in mean position of the section occurs due to 2nd order drift force. The steady state motions show almost no higher order harmonics. This indicates that the higher order part of the sloshing force is filtered out by the system. The steady state phase is short for long waves and consequently the uncertainties in measured sway amplitude increase. For wave periods very close to the first natural period of the fluid in the tanks an unstable situation may occur. The sway amplitude shifts and thus two steady state responses take place during one run. In the experimental data presented later where one tank is filled with $h = 0.184$ m, this can be seen as two very different

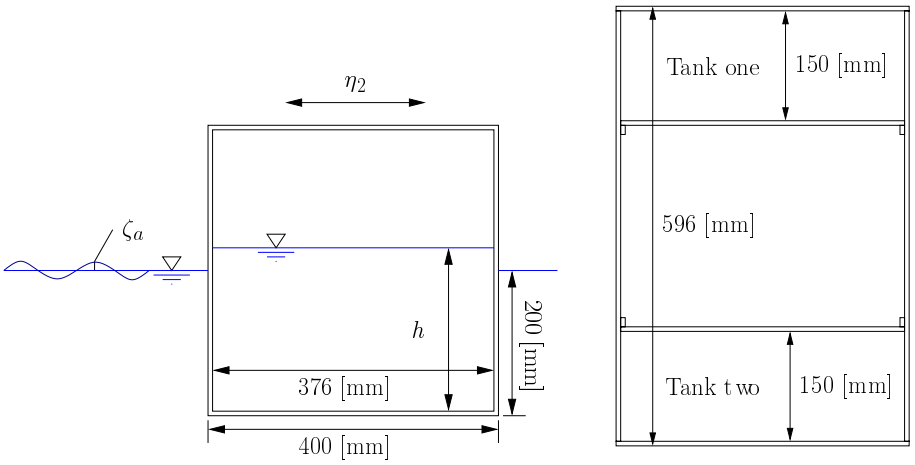

Figure 1: Bo x-shaped ship section, side and top view

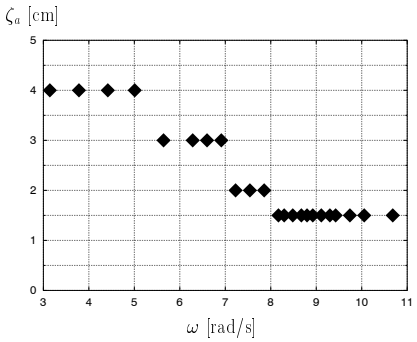

Figure 2: Relationship betw een wave amplitude and wave frequency

measured sway amplitudes for a wave frequency$\omega = 8.65$ rad/s. This is associated with jumps between different branches of the steady-state sloshing solution [2]. The steady state ends when waves reflected from the wavemaker and the beach reach the model.

Measured and calculated sway amplitudes for empty tanks have been compared to validate the accuracy of the measurements, (see Fig. 4). A standard linear seakeeping program was used in the calculations. The experimental results for rigid mass agree well with the computed values.

Fig. 4 illustrates the large effect of the fluid motion inside the tanks. When ω is smaller or sligh tly higher than the low est linear eigenfrequencyσ_n of the fluid motion in the tanks, a sway response lower than for a rigid fluid mass is observed for half-filled tanks. The force resulting from the fluid motion in the tanks acts against the sway excitation force in this case. When $\omega \approx \sigma_n$ the sway motion is almost zero. For ω sligh tly abov e σ_n the sway motion increases due to the fluid in the tanks. This behaviour can be qualitatively

explained by using a linear model for the sloshing. The phase of the sloshing force shifts 180° when the excitation frequency moves from below to above the first natural frequency.

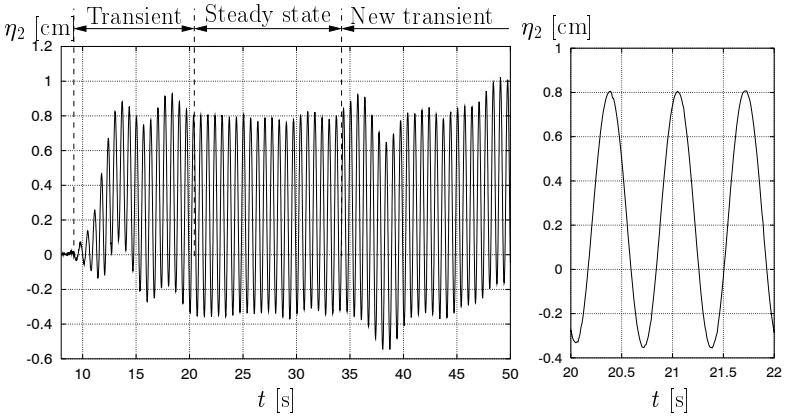

Figure 3: Example of time history of the sway motion of the ship section. $\omega = 9.42$ rad/s and $\zeta_a = 0.015$m

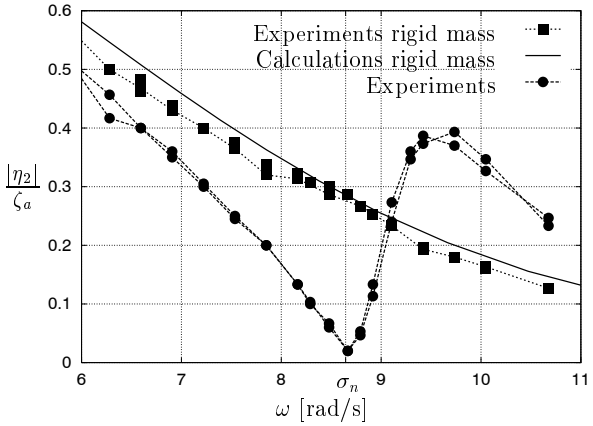

Figure 4: Sway amplitude for rigid mass and for two tanks filled with $h = 0.184$ m

The change with wave frequency of the phasing between the forces acting on the model is visually apparent from Fig. 5. The right plot in this figure gives the experimental values for sway motion when one of the tanks is filled with $h = 0.184$ m. Snapshots show the instantaneous position of the free surface both inside the tank and outside the ship section, for three different wave frequencies. The phasing between the internal and

external fluid motion permits to qualitatively understand why the internal fluid motion can either amplify or reduce the ship motion. The phasing is evident from the relative vertical motion of the free surfaces inside and outside the model.

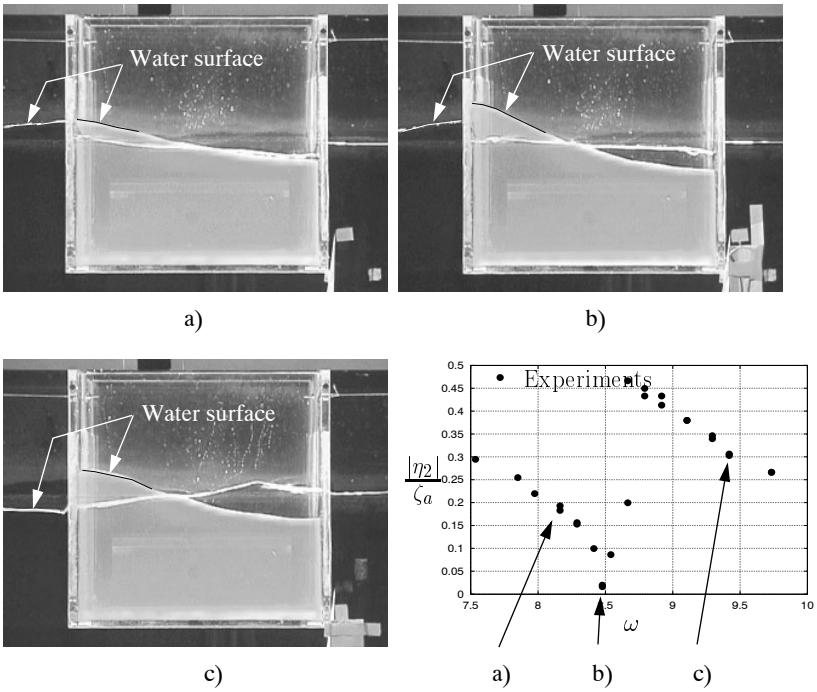

Figure 5: Motion of fluid inside and outside the tank. $h = 0.184$ m. One tank is filled

An interesting phenomenon is observed for wave frequencies close to the resonance for the fluid motion in the tanks. When the wavefront hits the model, a significant sway motion is initiated. This in turn excites sloshing in the tanks, and thus a sloshing force starts to counteract the excitation force from the waves. The sway motion decreases until an equilibrium is reached. At this stage the sway induced sloshing force almost balances the excitation force from the waves. However, since $\omega \approx \sigma_n$ a very small sway motion causes a violent sloshing response.

Fig. 6 shows experimental and computed values of the sway motion of the model for different filling levels of one or two tanks. The first linear eigenfrequency σ_n is indicated in the plots. Calculated values found by using an analytical linear and nonlinear sloshing solution and a standard linear seakeeping program for the external flow are presented for all cases. The calculations based on the linear sloshing model follow the general trend of the experiments. However, the sway amplitude is consistently over-predicted for frequencies right above σ_n. The reason is that the linear sloshing force is either in phase or exactly 180° out of phase with the position of the model. Actually, the phase transition occurs over a certain range of frequencies. Furthermore, when a large percentage of the

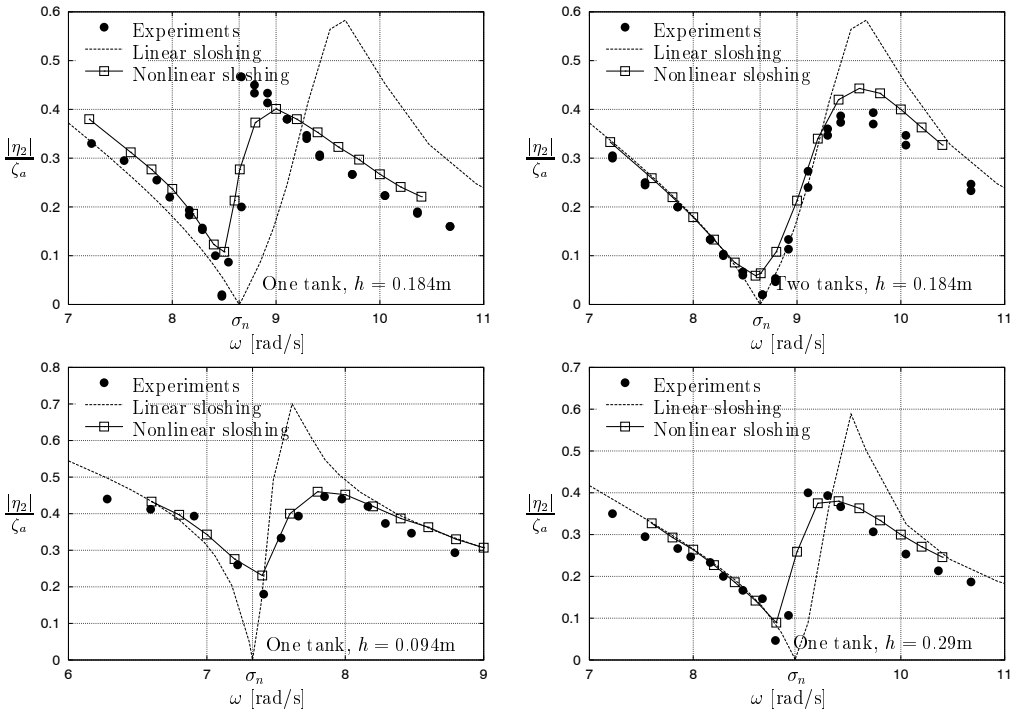

Figure 6: Comparisons between experiments and calculations

sloshing force acts in phase with the mass and added mass forces and works against them, the increased motion results in an increased sloshing force amplitude. When the frequency is equal to σ_n in the linear sloshing model the resulting sloshing force is infinite for finite sway motion. The combination of the linear sloshing force with the dynamics of the model cause zero sway for $\omega = \sigma_n$, while in reality the sway motion will have a minimum different from zero in the vicinity of σ_n.

The linear sloshing model fails in predicting the frequency of minimum sway motion for the three cases when only one tank is filled, since the large amplitude sloshing at resonance invalidates the assumption of a constant natural frequency for the internal fluid motion. In [2] it is shown how the first natural frequency varies as a function of the sloshing amplitude. When the filling height h is below the critical value $h/b = 0.3374$, σ_n increases as the amplitude increases. This explains the discrepancy in minimum sway by the linear sloshing model for $h = 0.094$ m. For $h = 0.29$ m and 0.184 m, the water level is above the critical depth and consequently the experiments show a minimum below σ_n. When $h = 0.184$ m and two tanks are filled, the amplitude of the sloshing motion at $\omega \approx \sigma_n$ is rather small. Hence the linear sloshing model gives an acceptable result.

In the computational results where the nonlinear model is included, the equation of motion Eq. (1) is solved in time and coupled with the nonlinear sloshing model.

$$(M + A_{22})\,\ddot{\eta}_2 + B_{22}\dot{\eta}_2 + C_{22}\eta_2 - F_{\text{exc}}(\zeta_a) - F_{\text{slosh}}(\eta_2) = 0 \qquad (1)$$

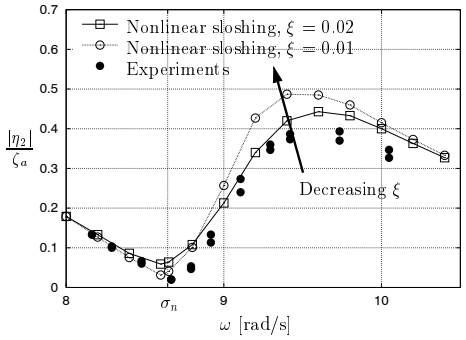

Figure 7: Experimental and computed sway amplitudes for two tanks, $h = 0.184$ m. Effect of sloshing damping ξ

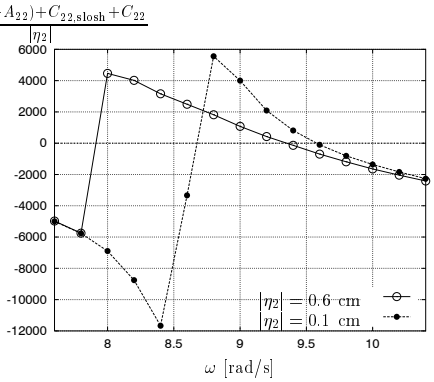

Figure 8: Mass terms - in phase with sway acceleration $\ddot{\eta}_2$

In (1) M is structural mass excluding internal fluid mass, A_{22} and B_{22} are the frequency dependent added mass and damping due to the external linear flow, C_{22} is the linear spring coefficient, F_{exc} is the horizontal linear wave excitation force and F_{slosh} is the horizontal force caused by sloshing. The simulations are prolonged until steady state sway motion is achieved. The external flow model needs justification. A proper linear external model should be based on the methodology presented by Cummins [3] which implies that the radiation force is a function of convolution integrals. This would be needed in order to calculate the transient phase of the external flow and sloshing induced higher order harmonic motions. But several authors, e.g. Adegeest [4], report difficulties in applying such a formulation in practice. Actually the influence of higher harmonics in the sloshing force is negligible. This can be seen from spectral analysis of the sway motion time history. In our case, since we focus on the steady-state motions, the present external force model represents a satisfactory approximation.

By including a nonlinear sloshing model a better agreement between the calculations and the experiments is obtained. For instance a much improved prediction of the minimum sway motion is achieved.

The computed sway amplitudes for two tanks and $h = 0.184$ m were found to be sensitive to the level of damping chosen for the sloshing motion. Fig. 7 shows how the damping of the internal flow affects the results when a variation from 2% to 1% the critical damping is considered. A description of how damping is included in the sloshing model can be found in [2]. This damping may represent e.g. viscous effects or local breaking and is not rationally predicted. The effect of external vortex shedding at the sharp corners was studied and found to be small. For $\omega > \approx \sigma_n$ the sway amplitudes increase with a decreasing damping, while around sloshing resonance the motion becomes smaller. In order to explain this phenomenon, the balance between the different terms in the equation of motion was studied. A quasi-linear approach was applied. The sum of the terms in or 180° out of phase with the sway accelerations are presented in Fig. 8. The contribution from the sloshing force is expressed as a frequency dependent restoring term

$C_{22,\mathrm{slosh}}$. By making an analogy with a linear system the zero of this sum corresponds to an eigenfrequency for the sway motion. The sum is close to zero just above or below $\omega = 9.5$ rad/s for the two amplitudes of steady state sway motion presented. Further, the sloshing force is large and nearly 180° out of phase with the acceleration in the vicinity of this frequency. Thus a small change in the phasing will lead to an important alteration of the part of the sloshing force which can be considered as a damping term for the coupled system. The damping terms are in this case all that balances the external force. For the example presented in Fig. 7 a phase change of 5° for F_{slosh} at $\omega = 9.4$ rad/s leads to a change of 10% in the sway motion. The phase is a function of the damping of the fluid motion inside the tanks. This explains the observed theoretical behaviour. If heavy tank roof impact had occurred, the damping of the internal fluid motion would be dominated by tank roof impact damping, [5]. Since the latter damping component can be rationally calculated, the ambiguity in selecting ξ demonstrated in Fig. 7 would be unimportant.

Further work will include the effect of tank roof impact. A natural next step is to include the roll and heave motion in the 2-D model before starting on a 3-D analysis to avoid that too many physical effects are included simultaneously in a complicated dynamic system.

Acknowledgements

This work is part of a Ph. D. thesis sponsored by the Research Council of Norway.

References

[1] Faltinsen, O. M. and Timokha, A. N. (2001) Adaptive multimodal approach to nonlinear sloshing in a rectangular tank., *J. Fluid Mech.*

[2] Faltinsen, O. M., Rognebakke, O. F., Lukovsky, I. A., Timokha, A. N. (2000) Multidimensional modal analysis of nonlinear sloshing in a rectangular tank with finite water depth., *J. Fluid Mech.*. **407**, 201-234

[3] Cummins, W. E. (1962), The impulse-response function and ship motions. *Schiffstechnik 9*(47), 101-109

[4] Adegeest, L. J. M. (1995), Nonlinear hull girder loads, Ph.D. thesis, Delft University of Technology, Faculty of Mechanical Engineering and Marine Technology

[5] Rognebakke, O. F. and Faltinsen, O. M (2000), Damping of sloshing due to tank roof impact, *15th International Workshop on Water Waves and Floating Bodies*, Caesarea, Israel

Paper 7

Coupling of sloshing and ship motions

Rognebakke, O. F. and Faltinsen, O. M.
Under submission to *J. Ship Research*

Is not included due to copyright

Appendix A

Program for sloshing calculations

A computer program has been developed for calculation of sloshing in rectangular or chamfered tanks forced to move in sway. The core of the program is an implementation of the adaptive multimodal approach of Faltinsen and Timokha (2001). Impact calculations are included, and an iterative procedure is applied when impacts occur. The calculation of damping due to impacts follows Rognebakke and Faltinsen (2000), (Paper 5).

Figure A.1 presents the program flow diagram. Note that only the main steps in the series of computations are included. The concept of 'oscillation period' is important. It is necessary to monitor changes in energy throughout one such period to relate the fractional loss of energy to the artificial linear damping term. A new oscillation period begins when the water surface rises above the initial undisturbed water level at one side of the tank. At the same instant, the water surface should have a downward velocity at the other side. This criterion seems to be robust, and it also works when the free surface motion is different from a standing wave.

The time stepping loop starts with solving the nonlinear system of ordinary differential equations for the β_i that represent the amplitudes of the free surface modes.

When a new oscillation period starts, the change in energy during last period is checked. If some energy is lost due to impacts, a new damping coefficient is calculated. The current iteration number is compared with the maximum allowed. If the maximum is reached, a counter is reset and all the, hopefully, converged flow variables are saved. This event is referred to as 'Save state'. If the iteration is to be continued, the previously saved state is retrieved, the iteration number increased and the calculation continues with the new damping coefficient.

In case of no lost energy, the iteration loop is skipped.

When the free surface hits the roof at one side of the tank, the initial impact velocity V_0 and the radius of curvature of the free surface R are calculated. After a while, the vertical velocity

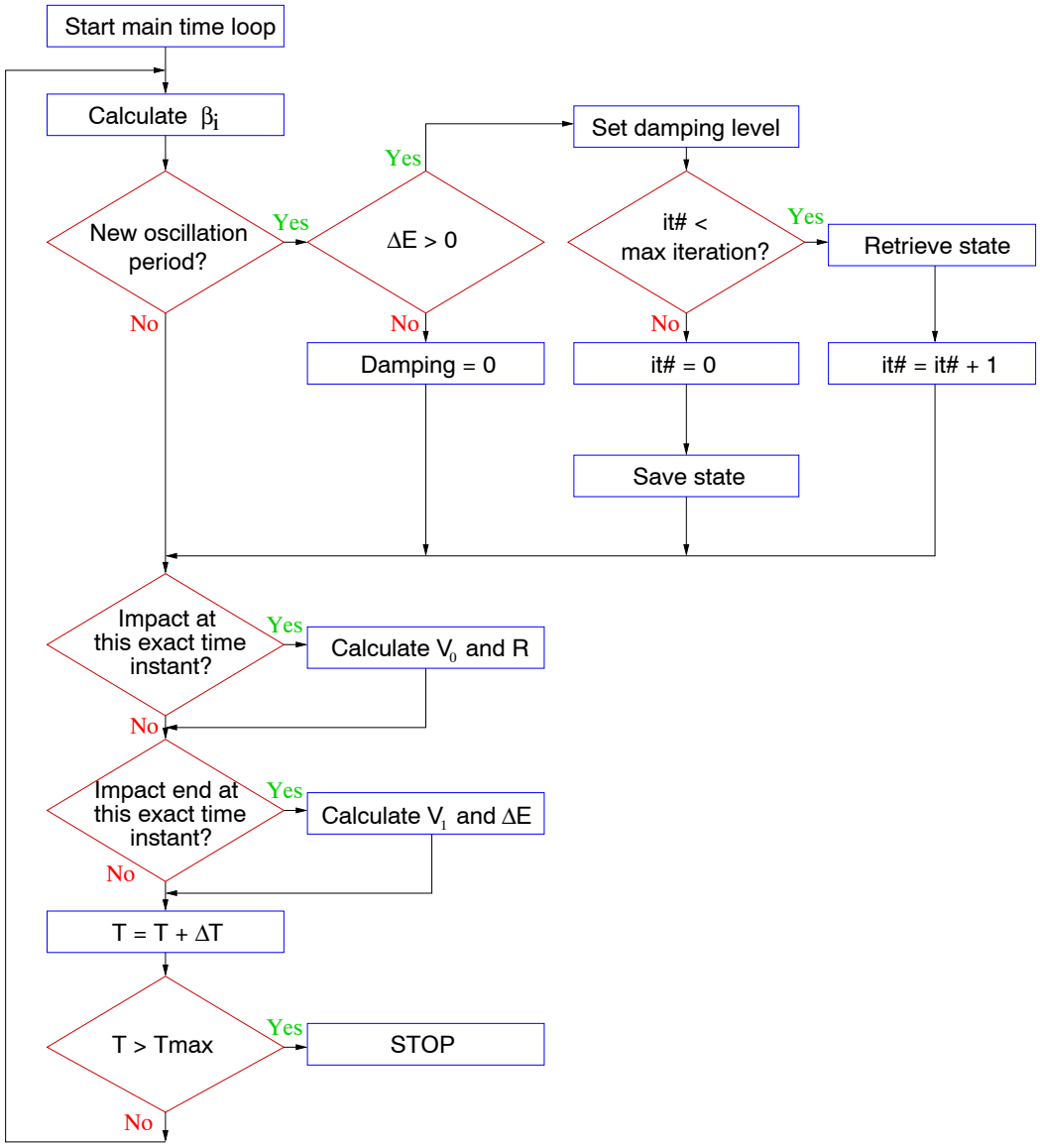

Figure A.1: Program flow diagram

of the free surface is zero, and the impact is at an end. Now that the duration of the impact is known, the negative acceleration V_1 and, finally, the energy lost during the impact are found.

Appendix B

Energy change from linear damping term

B.1 Linear damping of mass-spring system

Consider a one degree of freedom linear mass-spring system with mass M, damping coefficient B and stiffness C. The system is excited by a harmonically oscillating force F. The period of oscillation is T. The displacement variable is x. The equation of motion for this system is

$$M\ddot{x} + B\dot{x} + Cx = F \tag{B.1}$$

where dots denote time derivatives. The critical damping $B_{\text{crit}} = 2M\sigma$, where $\sigma = \sqrt{C/M}$. The change of energy in the system is given as

$$\frac{\mathrm{d}}{\mathrm{d}t}E(x, \dot{x}) = F\dot{x} - B\dot{x}^2 \tag{B.2}$$

The removal of energy from the system during one period of oscillation due to damping is

$$\Delta E = \int_0^T B\dot{x}^2 \mathrm{d}t \tag{B.3}$$

The response can be written as $x = x_a e^{i\omega t}$. This gives

$$\Delta E = \frac{1}{2}x_a^2 T\sigma^2 B \tag{B.4}$$

The total energy of the system is denoted E. When all the energy is in the form of kinetic energy , the total energy is

$$E = \frac{1}{2} M x_a^2 \sigma^2 \tag{B.5}$$

The fraction of the total energy being removed during one period is

$$\frac{\Delta E}{E} = \frac{x_a^2 T \sigma^2 B}{M x_a^2 \sigma^2} = \frac{TB}{M} \tag{B.6}$$

The damping coefficient ξ is introduced. $\xi = 1$ for a critically damped system.

$$B = 2\sigma M \xi \tag{B.7}$$

This gives

$$\frac{\Delta E}{E} = 2\sigma \xi T \tag{B.8}$$

Assume that the period of excitation is close to the undamped eigenperiod of the system

$$T \approx \frac{2\pi}{\sigma} \tag{B.9}$$

The relation between the fraction of energy removed and ξ is found as

$$\xi = \frac{1}{4\pi} \frac{\Delta E}{E} \tag{B.10}$$

B.2 Relation between ξ and Keulegan's 'modulus of decay'

Keulegan (1958) introduces a 'modulus of decay', α, for a standing wave of initial amplitude a_0 oscillating with a period T as

$$\frac{a}{a_0} = e^{-\frac{\alpha t}{T}} \tag{B.11}$$

where a is the amplitude of the wave after time t. He reports that the relation between the fractional change in energy of the standing wave and the modulus of decay over one period of oscillation is

$$\alpha = \frac{\Delta E}{2E_{\text{mean}}} \tag{B.12}$$

where ΔE is the change of energy in the wave and E_{mean} is the mean energy of the wave during the oscillation period. Assume that the change in energy is small compared to the total energy in the tank, so that $E_{\text{mean}} \approx E$. A comparison between Eqs. (B.12) and (B.10) gives

$$\xi = \frac{\alpha}{2\pi} \tag{B.13}$$

Appendix C

Impact energy loss in chamfered tank

C.1 Problem description

When the free surface inside the tank hits the tank roof, a simplified method based on a generalized Wagner's slamming approach (Wagner (1932)) is used to calculate the loss of energy. The rising surface is approximated by a parabola with radius of curvature R, and the impact velocity is linearly decreasing and is expressed as $V(t) = V_0 + V_1 t$ where $V_1 < 0$. The time of impact is $t = 0$. For a chamfered tank, the vertical distance, $\eta_b(x)$, from any point on our idealized, frozen surface at $t = 0$ to the chamfer part of the roof is given by the radius of curvature R and the chamfer angle β. Figure C.1 shows the direction of the x-axis.

$$\eta_b(x) = \tan(\beta)x + \frac{x^2}{2R} \tag{C.1}$$

When a heavy impact occurs, the wetted length may exceed the horizontal length of the chamfer, $C_{\max}$, and the last part of the impact may be considered as a flat roof impact. In Fig. C.1 the idealized situation is shown for a two phase impact. The curved lines drawn out for three different time steps represent the frozen free surface, and additional lines give an impression of how the uprise of water may look. The jet is not shown. The impact is in the first phase when $t = t_1$ and $c(t) < C_{\max}$, while for $t = t_2$ the second phase has just started. These two phases will be treated in the following.

Figure C.2 gives the definitions of symbols used in the slamming analysis. $c(t)$ is the horizontal distance from $x = 0$ to the spray root, δ is the thickness of the jet, u_c is the velocity of the control surface following the spray root and u_a is the fluid velocity in the jet direction at the spray root. Define u_f as the difference in velocity between the fluid and the control surface,

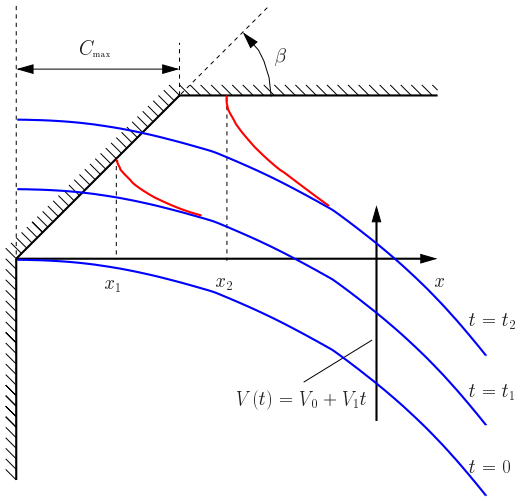

Figure C.1: Heavy impact on chamfered roof

$u_f = u_a - u_c$. The kinetic and potential energy flux through the jet can generally be found as

$$\frac{\mathrm{d}E_{\mathrm{kin}}}{\mathrm{d}t} = \frac{\rho}{2} u_a^2 \delta u_f \quad , \quad \frac{\mathrm{d}E_{\mathrm{pot}}}{\mathrm{d}t} = \rho g (H - h) M_{\mathrm{flux}} \tag{C.2}$$

Here H is the total height of the tank and h is the water filling level. $M_{\mathrm{flux}} = \delta u_f$ is the flux of mass into the jet. Wagner's solution (see Zhao and Faltinsen (1993)) gives

$$u_a = 2\frac{\mathrm{d}c}{\mathrm{d}t} \, , \quad u_c = \frac{\mathrm{d}c}{\mathrm{d}t} \, , \quad \delta = \frac{\pi V^2 2c}{16(\frac{\mathrm{d}c}{\mathrm{d}t})^2} \tag{C.3}$$

The flux of energy in the jet is known if the rate of change of the wetted length is found.

C.2 Finding the wetted length

The procedure for solving Wagner's integral equation and finding the wetted length is described in Faltinsen (1990).

Wagner's impact analysis is based on the assumption of irrotational and incompressible fluid so that potential theory is valid.

The classical impact problem with the dynamic free surface condition $\phi = 0$ on $z = 0$ and the body boundary condition $\partial\phi/\partial z = -V(t)$ on $z = 0$ is illustrated in Fig. C.3. The resulting velocity potential on the body is

$$\phi = -V(t)\sqrt{c^2(t) - x^2}, \quad |x| > c(t) \tag{C.4}$$

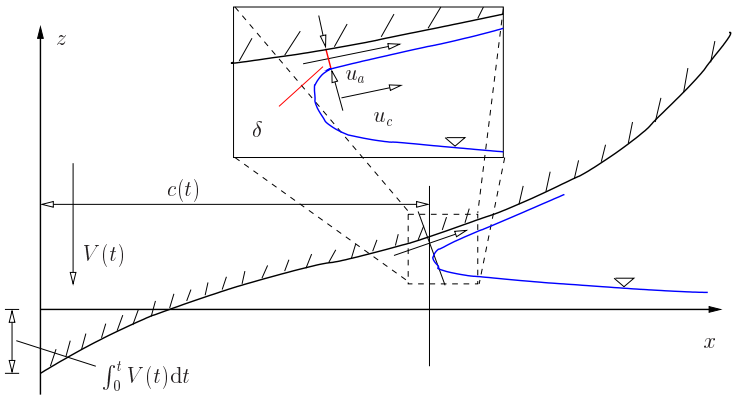

Figure C.2: Definitions for the slamming analysis

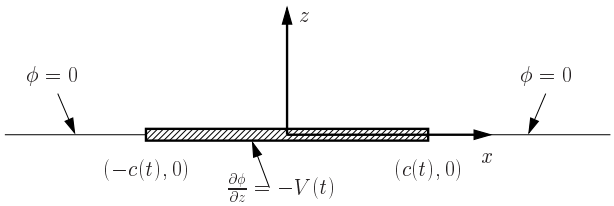

Figure C.3: Boundary value problem for simplified analysis of impact between a tw o-dimensional body and water

while the vertical v elocity at the free surface is

$$\frac{\partial \phi}{\partial z} = \frac{V(t)x}{\sqrt{x^2 - c^2(t)}} - V(t) \quad \text{at} \quad z = 0\ ,\ |x| > c(t) \tag{C.5}$$

The free surface elevation, η, relative to the bottom of the impacting body can be written as

$$\eta = \int_0^t \frac{V(t)x}{\sqrt{x^2 - c^2(t)}} \mathrm{d}t \tag{C.6}$$

The vertical distance traveled b y a particle on the initially calm free surface has to be equal to the v ertical coordinateof a point on the impacting body, $\eta_b(x)$, relativ e to the bottom ofthe body. We then get an integral equation where both c and t are unknowns

$$\eta_b(x) = \int_0^x \frac{x\mu(c)}{\sqrt{x^2 - c^2(t)}} \mathrm{d}c \tag{C.7}$$

where

$$\mu(c) = V(t)\frac{\mathrm{d}t}{\mathrm{d}c} \tag{C.8}$$

The unknown function $\mu(c)$ relating c and t is substituted in the integral equation, and the integration limits are changed. The idea is now to approximate $\mu(c)$ by a polynomial in c

$$\mu(c) = A_0 + A_1 c \tag{C.9}$$

where A_0 and A_1 are constants to be determined. The right hand side of Eq. (C.7) can be integrated to give

$$\eta_b(x) = A_0 \frac{\pi}{2} x + A_1 x^2 \tag{C.10}$$

$\eta_b(x)$ is known for a given impact problem, and thus the coefficients A_0 and A_1 can be found. Eq. (C.8) is then used to find $c(t)$

$$(A_0 + A_1 c)\,\mathrm{d}c = V(t)\mathrm{d}t \tag{C.11}$$

Integration gives

$$A_0 c + \frac{A_1 c^2}{2} = \int_0^t V(t)\mathrm{d}t \tag{C.12}$$

Assuming a linearly changing impact velocity, $V(t) = V_0 + V_1 t$, the expression for the wetted length becomes

$$c = -\frac{A_0}{A_1} + \frac{\sqrt{A_0^2 + 2A_1 V_0 t + A_1 V_1 t^2}}{A_1} \tag{C.13}$$

The expression for $\mathrm{d}c/\mathrm{d}t$ is also useful

$$\frac{\mathrm{d}c}{\mathrm{d}t} = \frac{V_0 + V_1 t}{A_0 + A_1 c} \tag{C.14}$$

C.3 Phase 1: Impact on chamfer

Until the spray root has reached the top of the chamfer, $\eta_b(x)$ is found from Eq. (C.1) and Eq. (C.10)

$$\eta_b(x) = \tan(\beta)x + \frac{x^2}{2R} = A_0 \frac{\pi}{2} x + A_1 x^2 \tag{C.15}$$

This gives $A_0 = 2\tan\beta)/\pi$ and $A_1 = 1/(2R)$. By combining Eqs. (C.2), (C.3), (C.13) and (C.14) the flux of kinetic and potential energy through the jet are found to be

$$\frac{\mathrm{d}E_{\mathrm{kin}}^{\mathrm{phase\ 1}}}{\mathrm{d}t} = \rho(V_0 + V_1 t)^3 \pi R \frac{-\frac{2\tan(\beta)}{\pi} + \sqrt{\frac{4\tan^2(\beta)}{\pi^2} + \frac{V_0 t}{R} + \frac{V_1 t^2}{2R}}}{2\sqrt{\frac{4\tan^2(\beta)}{\pi^2} + \frac{V_0 t}{R} + \frac{V_1 t^2}{2R}}} \tag{C.16}$$

$$\frac{\mathrm{d}E_{\mathrm{pot}}^{\mathrm{phase\ 1}}}{\mathrm{d}t} = \frac{\rho g(H-h)\pi(V_0+V_1t)}{4}R\left(-\frac{2\tan(\beta)}{\pi}+\sqrt{\frac{4\tan^2(\beta)}{\pi^2}+\frac{V_0t}{R}+\frac{V_1t^2}{2R}}\right) \cdot\sqrt{\frac{4\tan^2(\beta)}{\pi^2}+\frac{V_0t}{R}+\frac{V_1t^2}{2R}} \tag{C.17}$$

The loss of kinetic and potential energy during phase 1 of the impact is found as

$$\Delta E_{\mathrm{kin}}^{\mathrm{phase\ 1}} = \int_0^{t_{\mathrm{end}}} \frac{\mathrm{d}E_{\mathrm{kin}}^{\mathrm{phase\ 1}}}{\mathrm{d}t}\mathrm{d}t \tag{C.18}$$

$$\Delta E_{\mathrm{pot}}^{\mathrm{phase\ 1}} = \int_0^{t_{\mathrm{end}}} \frac{\mathrm{d}E_{\mathrm{pot}}^{\mathrm{phase\ 1}}}{\mathrm{d}t}\mathrm{d}t \tag{C.19}$$

where $t_{\mathrm{end}} = -V_0/V_1$ if $V(t) < 0$, and $t_{\mathrm{end}} = t_{\mathrm{max}}$ if $c = C_{\mathrm{max}}$. These integrals are solved numerically

C.4 Phase 2: Impact on flat roof

When the spray root at $x = c(t)$ has moved past the chamfer, the vertical distance $\eta_b(x)$ is approximated by

$$\eta_b(x) = \frac{x^2}{2R} = A_0\frac{\pi}{2}x + A_1x^2 \tag{C.20}$$

This gives $A_0 = 0$ and $A_1 = 1/(2R)$. Again, use that $t = t_{\mathrm{max}}$ when $c = C_{\mathrm{max}}$. The wetted length is now given by

$$c = \sqrt{2R\left[2V_0(t-t_{\mathrm{max}}) + V_1(t-t_{\mathrm{max}})^2\right] + C_{\mathrm{max}}^2} \tag{C.21}$$

while the rate of change of the wetted length is

$$\frac{\mathrm{d}c}{\mathrm{d}t} = \frac{2R(V_0+V_1t)}{\sqrt{2R\left(2V_0(t-t_{\mathrm{max}}) + V_1(t-t_{\mathrm{max}})^2\right) + C_{\mathrm{max}}^2}} \tag{C.22}$$

The thickness of the jet is

$$\delta = \frac{\pi\left(2R\left[2V_0(t-t_{\mathrm{max}}) + V_1(t-t_{\mathrm{max}})^2\right] + C_{\mathrm{max}}^2\right)^{3/2}}{32R^2} \tag{C.23}$$

This gives for the flux of energy

$$\frac{\mathrm{d}E_{\mathrm{kin}}^{\mathrm{phase\ 2}}}{\mathrm{d}t} = \frac{\rho(V_0+V_1t)^3\pi R}{2} \tag{C.24}$$

$$\frac{\mathrm{d}E_{\mathrm{pot}}^{\mathrm{phase\ 2}}}{\mathrm{d}t} = \frac{\rho g(H-h)\pi(V_0+V_1t)}{16R}\left(2R\left[2V_0(t-t_{\mathrm{max}}) + V_1(t-t_{\mathrm{max}})^2\right] + C_{\mathrm{max}}^2\right) \tag{C.25}$$

$\Delta E_{\text{kin}}^{\text{phase 2}}$ and $\Delta E_{\text{pot}}^{\text{phase 2}}$ can be found by analytical integration. This is straightforward although the resulting expressions are large.

$$\Delta E_{\text{kin}}^{\text{phase 2}} = \int_{t_{\max}}^{-V_0/V_1} \frac{\mathrm{d}E_{\text{kin}}^{\text{phase 2}}}{\mathrm{d}t}\mathrm{d}t \tag{C.26}$$

$$\Delta E_{\text{pot}}^{\text{phase 2}} = \int_{t_{\max}}^{-V_0/V_1} \frac{\mathrm{d}E_{\text{pot}}^{\text{phase 2}}}{\mathrm{d}t}\mathrm{d}t \tag{C.27}$$

The total energy loss is

$$\Delta E_{\text{kin}} = \Delta E_{\text{kin}}^{\text{phase 1}} + \Delta E_{\text{kin}}^{\text{phase 2}} \tag{C.28}$$

$$\Delta E_{\text{pot}} = \Delta E_{\text{pot}}^{\text{phase 1}} + \Delta E_{\text{pot}}^{\text{phase 2}} \tag{C.29}$$

Appendix D

2. order initial value solution

A two dimensional rectangular tank is excited in sway. A second order initial value solution of the resulting sloshing motion is derived. The response is assumed to be of the same order as the excitation. The tank geometry and the coordinate system is shown in Fig. D.1. The coordinate system is fixed in space. The tank motion relative to equilibrium is $\eta = \epsilon_0 \sin(\omega t)$.

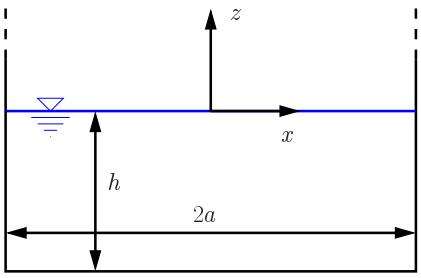

Figure D.1: Tank geometry and coordinate system

D.1 First order solution

The boundary value problem that is solved is illustrated in Fig. D.2. The initial conditions $\Phi_1 = 0$ and $\partial\Phi_1/\partial t = 0$ on the mean free surface are used. Faltinsen (1978) presents a solution to this problem. The total first order potential is given as

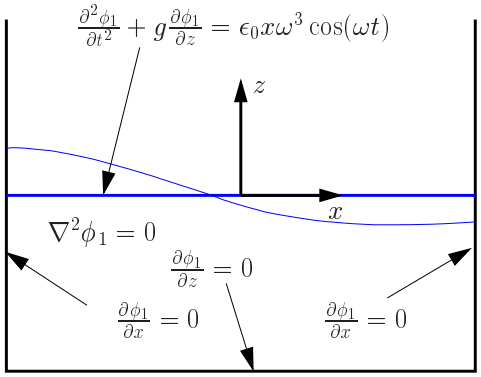

Figure D.2: First order boundary value problem

$$\Phi_1 = \phi_1 + \phi_c$$

where

$$\phi_c = A\cos(\omega t)x \quad , \quad A = \epsilon_0\omega$$

ϕ_1 is found as a series solution. The total first order potential is

$$\begin{aligned}\Phi_1 \;=\; & \sum_{n=0}^{\infty}\sin\left(\frac{(2n+1)\pi}{2a}x\right)\left\{A\cos(\omega t)\left(\frac{2}{a}\right)\left(\frac{2a}{(2n+1)\pi}\right)^2(-1)^n\right. \\ & \left.+\cosh\left(\frac{(2n+1)\pi}{2a}(z+h)\right)\left[A_n\cos(\omega_n t)+C_n\cos(\omega t)\right]\right\}\end{aligned}$$

where the coefficients are expressed as follows

$$K_n = \frac{\omega A}{\cosh\left\{\frac{(2n+1)\pi}{2a}h\right\}}\left(\frac{2}{a}\right)\left[\frac{2a}{(2n+1)\pi}\right]^2(-1)^n$$

$$C_n = \frac{\omega K_n}{\omega_n^2-\omega^2} \quad , \quad A_n = -C_n - \frac{K_n}{\omega}$$

The eigenfrequencies of the system are found from

$$\omega_n^2 = g\frac{(2n+1)\pi}{2a}\tanh\left\{\frac{(2n+1)\pi}{2a}h\right\}$$

Only the first term in the series solution for the ϕ_1 part of the first order sloshing potential is used in the derivation of the second order potential.

$$\phi_1 = \left[A_0\cos(\omega_n t)+C_0\cos(\omega t)\right]\sin(\frac{\pi x}{2a})\cosh(\frac{\pi(z+h)}{2a})$$

The constants are given by the following expressions

$$K_0 = \frac{\omega A}{\cosh(\frac{\pi h}{2a})}\frac{8a}{\pi^2}\ ,\ C_0 = \frac{\omega K_0}{{\omega_0}^2 - \omega^2}\ ,\ A_0 = -C_0 - \frac{K_0}{\omega}$$

The square of the lowest eigenfrequency of the system is

$$\omega_0^2 = \frac{g\pi}{2a}\tanh\left(\frac{\pi h}{2a}\right)$$

D.2 Second order solution

The second order boundary value problem is illustrated in Fig. D.3. The right hand sides of the

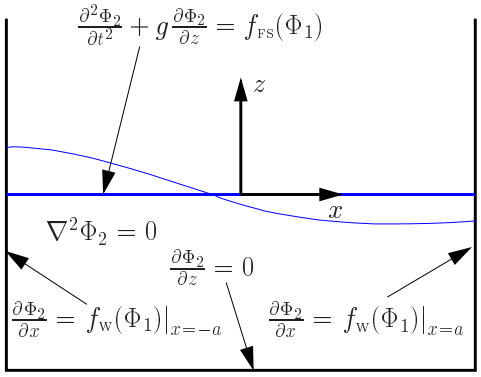

Figure D.3: Second order boundary value problem

free surface condition and wall conditions are respectively

$$f_{\rm FS} = -\frac{\partial}{\partial t}\left[\left(\frac{\partial\Phi_1}{\partial x}\right)^2 + \left(\frac{\partial\Phi_1}{\partial z}\right)^2\right] + \frac{1}{g}\frac{\partial\Phi_1}{\partial t}\frac{\partial}{\partial z}\left(\frac{\partial^2\Phi_1}{\partial t^2} + g\frac{\partial\Phi_1}{\partial z}\right)\Big|_{z=0}$$

and

$$f_{\rm W} = -\epsilon_0\sin(\omega t)\frac{\partial^2\Phi_1}{\partial x^2}\Big|_{x=\pm a}$$

The total second order potential is expressed as

$$\Phi_2 = \phi_2^* + \phi_2$$

The separation of the potential in two parts is convenient when treating the boundary conditions. The boundary condition ensuring zero flow through the bottom gives

$$\frac{\partial\phi_2^*}{\partial z}\Big|_{z=-h} = 0 \quad , \quad \frac{\partial\phi_2}{\partial z}\Big|_{z=-h} = 0$$

while the boundary conditions on the walls are

$$\left.\frac{\partial \phi_2^*}{\partial x}\right|_{x=\pm a} = -\epsilon_0 \sin(\omega t) \left.\frac{\partial^2 \phi_1}{\partial x^2}\right|_{x=\pm a} \quad , \quad \left.\frac{\partial \phi_2}{\partial x}\right|_{x=\pm a} = 0$$

The combined dynamic and kinematic free surface condition is separated into a homogeneous part

$$\frac{\partial^2 \phi_2^*}{\partial t^2} + g\frac{\partial \phi_2^*}{\partial z} = 0 \quad , z = 0$$

and an inhomogeneous part

$$\begin{aligned}
\frac{\partial^2 \phi_2}{\partial t^2} + g\frac{\partial \phi_2}{\partial z} &= -\frac{\partial}{\partial t}\left[\left(\frac{\partial \Phi_1}{\partial x}\right)^2 + \left(\frac{\partial \Phi_1}{\partial z}\right)^2\right] + \frac{1}{g}\frac{\partial \Phi_1}{\partial t}\frac{\partial}{\partial z}\left(\frac{\partial^2 \Phi_1}{\partial t^2} + g\frac{\partial \Phi_1}{\partial z}\right) \\
&= -\frac{\partial}{\partial t}\left[\left(\frac{\partial \phi_1}{\partial x}\right)^2 + 2A\frac{\partial \phi_1}{\partial x}\cos(\omega t) + A^2\cos^2(\omega t) + \left(\frac{\partial \Phi_1}{\partial z}\right)^2\right] \\
&\quad + \frac{1}{g}\left(\frac{\partial \phi_1}{\partial t} - Ax\omega\sin(\omega t)\right)\frac{\partial}{\partial z}\left(\frac{\partial^2 \phi_1}{\partial t^2} - Ax\omega^2\cos(\omega t) + g\frac{\partial \phi_1}{\partial z}\right) \quad , z = 0 \\
&= \mathrm{HS}
\end{aligned}$$

ϕ_2 is found by first writing out the right hand side HS. The following ordering of the resulting equation is used

$$\begin{aligned}
\mathrm{HS} &= \mathrm{HS1}\cdot\cos(\frac{\pi x}{2a}) + \mathrm{HS2}\cdot x\sin(\frac{\pi x}{2a}) + \mathrm{HS3}\cdot\cos^2(\frac{\pi x}{2a}) \\
&+ \mathrm{HS4}\cdot\sin^2(\frac{\pi x}{2a}) + \mathrm{HS5}
\end{aligned}$$

The following relationships are used in HS

$$\sin^2(\frac{\pi x}{2a}) = \frac{1}{2} - \frac{1}{2}\cos(\frac{\pi x}{a}) \ , \ \cos^2(\frac{\pi x}{2a}) = \frac{1}{2} + \frac{1}{2}\cos(\frac{\pi x}{a})$$

The parts of HS3 and HS4 proportional to $\cos(\frac{\pi x}{a})$ are combined and denoted HS6, while terms of HS3 and HS4 independent of x constitute HS7.

$$\mathrm{HS6} = \frac{1}{2}(\mathrm{HS3} - \mathrm{HS4})$$

$$\mathrm{HS7} = \frac{1}{2}(\mathrm{HS3} + \mathrm{HS4})$$

The total right hand side of the inhomogeneous free surface condition is then

$$\mathrm{HS} = \mathrm{HS1}\cdot\cos(\frac{\pi x}{2a}) + \mathrm{HS2}\cdot x\sin(\frac{\pi x}{2a}) + \mathrm{HS6}\cdot\cos(\frac{\pi x}{a}) + (\mathrm{HS5} + \mathrm{HS7})$$

where

$$
\begin{aligned}
\text{HS1} &= 8g\pi aA(A_0(\omega_0+\omega)\sin[(\omega_0+\omega)t]+A_0(\omega_0-\omega)\sin[(\omega_0-\omega)t] \\
&+ 2C_0\omega\sin(2\omega t))\cosh(\frac{\pi h}{2a}) \\
\text{HS2} &= 2\pi A\omega\cosh(\frac{\pi h}{2a})(\\
&- A_0(2a\omega_0^2\tanh(\frac{\pi h}{2a})-\pi g)\sin[(\omega_0+\omega)t] \\
&+ A_0(2a\omega_0^2\tanh(\frac{\pi h}{2a})-\pi g)\sin[(\omega_0-\omega)t] \\
&- C_0(2a\omega^2\tanh(\frac{\pi h}{2a})-\pi g)\sin[2\omega t] \quad) \\
\text{HS5} &= A^2\sin(2\omega t) \\
\text{HS6} &= 16ga^2(\\
&- A_0^2\omega_0\pi\cosh^2(\frac{\pi h}{2a})(2g\pi\tanh^2(\frac{\pi h}{2a})+2\omega_0^2 a\tanh(\frac{\pi h}{2a})-3\pi g)\sin(2\omega_0 t) \\
&+ C_0^2\omega\pi\cosh^2(\frac{\pi h}{2a})(2g\pi\tanh^2(\frac{\pi h}{2a})+2\omega^2 a\tanh(\frac{\pi h}{2a})-3\pi g)\sin(2\omega t) \\
&+ C_0A_0(\omega-\omega_0)\pi\cosh^2(\frac{\pi h}{2a})(3\pi g+2a\omega_0\omega\tanh(\frac{\pi h}{2a})-2\pi g\tanh^2(\frac{\pi h}{2a}))\sin[(\omega-\omega_0)t] \\
&+ C_0A_0(\omega+\omega_0)\pi\cosh^2(\frac{\pi h}{2a})(3\pi g-2a\omega_0\omega\tanh(\frac{\pi h}{2a})-2\pi g\tanh^2(\frac{\pi h}{2a}))\sin[(\omega+\omega_0)t] \quad) \\
\text{HS7} &= 16ga^2(\\
&- A_0^2\omega_0\pi\cosh^2(\frac{\pi h}{2a})(2g\pi\tanh^2(\frac{\pi h}{2a})+2\omega_0^2 a\tanh(\frac{\pi h}{2a})+\pi g)\sin(2\omega_0 t) \\
&+ C_0^2\omega\pi\cosh^2(\frac{\pi h}{2a})(2g\pi\tanh^2(\frac{\pi h}{2a})+2\omega^2 a\tanh(\frac{\pi h}{2a})+\pi g)\sin(2\omega t) \\
&+ C_0A_0(\omega-\omega_0)\pi\cosh^2(\frac{\pi h}{2a})(\pi g-2a\omega_0\omega\tanh(\frac{\pi h}{2a})+2\pi g\tanh^2(\frac{\pi h}{2a}))\sin[(\omega-\omega_0)t] \\
&+ C_0A_0(\omega+\omega_0)\pi\cosh^2(\frac{\pi h}{2a})(\pi g+2a\omega_0\omega\tanh(\frac{\pi h}{2a})+2\pi g\tanh^2(\frac{\pi h}{2a}))\sin[(\omega+\omega_0)t] \quad)
\end{aligned}
$$

The following Fourier-series expansions are utilized

$$x\sin(\frac{\pi x}{2a}) = \frac{8a}{\pi^2}\left(\frac{1}{2}+\sum_{n=1}^{\infty}\frac{(-1)^n(1+4n)}{(1+2n)^2(1-2n)^2}\cos(\frac{n\pi x}{a})\right)$$

$$\cos(\frac{\pi x}{2a}) = \frac{4}{\pi}\left(\frac{1}{2}+\sum_{n=1}^{\infty}\frac{(-1)^n}{(2n-1)(2n+1)}\cos(\frac{n\pi x}{a})\right)$$

The part of HS $\propto x\sin(\frac{\pi x}{2a})$ is now studied. Assume the following form of ϕ_2^2, where superscript 2 refers to HS2,

$$\phi_2^2 = \sum_{n=0}^{\infty}A(t)_n^2\cos(\frac{n\pi x}{a})\cosh[\frac{n\pi(z+h)}{a}]$$

$$A(t)_n^2 = A_n^{21}\sin[(\omega+\omega_0)t] + A_n^{22}\sin[(\omega-\omega_0)t] + A_n^{23}\sin(2\omega t)$$

This is inserted into the free surface condition and compared to the right hand side HS2 where the series expression for $x\sin(\frac{\pi x}{2a})$ is used. The terms with time dependency $\sin[(\omega+\omega_0)t]$ are denoted ϕ_2^{21}.

$$\begin{aligned}
\left(\frac{\partial^2\phi_2^{21}}{\partial t^2} + g\frac{\partial\phi_2^{21}}{\partial z}\right)_{z=0} &= \sum_{n=0}^{\infty} A_n^{21}\cos[\frac{n\pi x}{a}]\cosh[\frac{n\pi h}{a}]\{-(\omega+\omega_0)^2 \\
&+ \frac{g\pi n}{a}\tanh[\frac{n\pi h}{a}]\}\sin[(\omega+\omega_0)t] \\
&= \mathrm{HS2}^1 \\
&= \frac{AA_0\omega}{g\pi a}\cosh[\frac{\pi h}{2a}]\left(2a\omega_0^2\tanh[\frac{\pi h}{2a}] - \pi g\right)\cdot \\
&\quad \frac{8a}{\pi^2}\left(\frac{1}{2} + \sum_{n=1}^{\infty}\frac{(-1)^n(1+4n)}{(1+2n)^2(1-2n)^2}\cos(\frac{n\pi x}{a})\right)\sin[(\omega+\omega_0)t]
\end{aligned}$$

Superscript 1 in $\mathrm{HS2}^1$ indicates the time dependency $\sin[(\omega+\omega_0)t]$. in a similar way as A_n^{21},

$$\begin{aligned}
A_0^{21} &= -\frac{AA_0\omega}{g\pi a}\frac{\cosh[\frac{\pi h}{2a}]}{(\omega+\omega_0)^2}(2a\omega_0^2\tanh[\frac{\pi h}{2a}] - \pi g) \\
A_n^{21} &= \frac{AA_0\omega}{g\pi a}\frac{\cosh[\frac{\pi h}{2a}]}{\cosh[\frac{n\pi h}{a}]}\frac{(-1)^n(1+4n^2)}{(1+2n)^2(1-2n)^2}\frac{(2a\omega_0^2\tanh[\frac{\pi h}{2a}] - \pi g)}{[\frac{n\pi g}{a}\tanh[\frac{n\pi h}{a}] - (\omega+\omega_0)^2]} \qquad n>0 \\
A_0^{22} &= -\frac{AA_0\omega}{g\pi a}\frac{\cosh[\frac{\pi h}{2a}]}{(\omega-\omega_0)^2}(2a\omega_0^2\tanh[\frac{\pi h}{2a}] - \pi g) \\
A_n^{22} &= \frac{AA_0\omega}{g\pi a}\frac{\cosh[\frac{\pi h}{2a}]}{\cosh[\frac{n\pi h}{a}]}\frac{(-1)^n(1+4n^2)}{(1+2n)^2(1-2n)^2}\frac{(2a\omega_0^2\tanh[\frac{\pi h}{2a}] - \pi g)}{[\frac{n\pi g}{a}\tanh[\frac{n\pi h}{a}] - (\omega-\omega_0)^2]} \qquad n>0 \\
A_0^{23} &= -\frac{AC_0}{4g\pi a\omega}\cosh[\frac{\pi h}{2a}](2a\omega_0^2\tanh[\frac{\pi h}{2a}] - \pi g) \\
A_n^{23} &= \frac{AC_0\omega}{g\pi a}\frac{\cosh[\frac{\pi h}{2a}]}{\cosh[\frac{n\pi h}{a}]}\frac{(-1)^n(1+4n^2)}{(1+2n)^2(1-2n)^2}\frac{(2a\omega^2\tanh[\frac{\pi h}{2a}] - \pi g)}{[\frac{n\pi g}{a}\tanh[\frac{n\pi h}{a}] - 4\omega^2]} \qquad n>0
\end{aligned}$$

The part of HS $\propto\cos(\frac{\pi x}{2a})$ is next in line. Assume the following form of ϕ_2^1 where superscript 1 refers to HS1,

$$\phi_2^1 = \sum_{n=0}^{\infty} A(t)_n^1\cos(\frac{n\pi x}{a})\cosh[\frac{n\pi(z+h)}{a}]$$

$$A(t)_n^1 = A_n^{11}\sin[(\omega+\omega_0)t] + A_n^{12}\sin[(\omega-\omega_0)t] + A_n^{13}\sin(2\omega t)$$

The terms with the time dependency $\sin[(\omega+\omega_0)t]$ are denoted ϕ_2^{11},

$$\begin{aligned}\left(\frac{\partial^2\phi_2^{11}}{\partial t^2}+g\frac{\partial\phi_2^{11}}{\partial z}\right)_{z=0} &= \sum_{n=0}^{\infty}A_n^{11}\cos[\frac{n\pi x}{a}]\cosh[\frac{n\pi h}{a}]\{-(\omega+\omega_0)^2\\ &+ \frac{g\pi n}{a}\tanh[\frac{n\pi h}{a}]\}\sin[(\omega+\omega_0)t]\\ &= \mathrm{HS1}^1\\ &= \frac{AA_0\pi}{2a}(\omega+\omega_0)\cosh[\frac{\pi h}{2a}]\cdot\\ &\quad \frac{4}{\pi}\left(\frac{1}{2}+\sum_{n=1}^{\infty}\frac{(-1)^{n+1}}{(2n-1)(2n+1)}\cos(\frac{n\pi x}{a})\right)\sin[(\omega+\omega_0)t]\end{aligned}$$

This procedure is repeated for the other time dependencies, resulting in the following coefficients

$$\begin{aligned}A_0^{11} &= -\frac{AA_0}{a(\omega+\omega_0)}\cosh[\frac{\pi h}{2a}]\\ A_n^{11} &= \frac{2AA_0}{a}(\omega+\omega_0)\frac{(-1)^{n+1}}{(2n-1)(2n+1)}\frac{\cosh[\frac{\pi h}{2a}]}{\cosh[\frac{n\pi h}{a}]}\frac{1}{-(\omega+\omega_0)^2+\frac{n\pi g}{a}\tanh[\frac{n\pi h}{a}]} \qquad n>0\\ A_0^{12} &= -\frac{AA_0}{a(\omega-\omega_0)}\cosh[\frac{\pi h}{2a}]\\ A_n^{12} &= \frac{2AA_0}{a}(\omega-\omega_0)\frac{(-1)^{n+1}}{(2n-1)(2n+1)}\frac{\cosh[\frac{\pi h}{2a}]}{\cosh[\frac{n\pi h}{a}]}\frac{1}{-(\omega-\omega_0)^2+\frac{n\pi g}{a}\tanh[\frac{n\pi h}{a}]} \qquad n>0\\ A_0^{13} &= -\frac{AC_0}{2\omega a}\cosh[\frac{\pi h}{2a}]\\ A_n^{13} &= \frac{4AC_0}{a}\omega\frac{(-1)^{n+1}}{(2n-1)(2n+1)}\frac{\cosh[\frac{\pi h}{2a}]}{\cosh[\frac{n\pi h}{a}]}\frac{1}{-4\omega^2+\frac{n\pi g}{a}\tanh[\frac{n\pi h}{a}]} \qquad n>0\end{aligned}$$

The part of HS $\propto\cos(\frac{\pi x}{a})$ is now studied. Assume the following form of ϕ_2^6 where superscript 6 refers to HS6,

$$\phi_2^6 = A(t)^6\cos(\frac{\pi x}{a})\cosh[\frac{\pi(z+h)}{a}]$$

$$A(t)^6 = A^{61}\sin[(\omega+\omega_0)t]+A^{62}\sin[(\omega-\omega_0)t]+A^{63}\sin(2\omega t)+A^{64}\sin(2\omega_0 t)$$

Start out with terms with the time dependency $\sin[(\omega+\omega_0)t]$ denoted ϕ_2^{61}.

$$\begin{aligned}\left(\frac{\partial^2\phi_2^{61}}{\partial t^2}+g\frac{\partial\phi_2^{61}}{\partial z}\right)_{z=0} &= A^{61}\cos[\frac{\pi x}{a}]\cosh[\frac{\pi h}{a}]\{-(\omega+\omega_0)^2\\ &+ \frac{g\pi}{a}\tanh[\frac{\pi h}{a}]\}\sin[(\omega+\omega_0)t]\\ &= \mathrm{HS6}^1\\ &= 16ga^2C_0A_0(\omega+\omega_0)\pi\cosh^2[\frac{\pi h}{2a}]\cdot\\ &\quad (3\pi g-2a\omega_0\omega\tanh(\frac{\pi h}{2a})-2\pi g\tanh^2(\frac{\pi h}{2a}))\sin[(\omega+\omega_0)t]\end{aligned}$$

This procedure is repeated for the other time dependencies, and the following coefficients result.

$$\begin{aligned}
A^{61} &= 16ga^2C_0A_0(\omega+\omega_0)\pi\frac{\cosh^2[\frac{\pi h}{2a}]}{\cosh[\frac{n\pi h}{2a}]}\cdot \\
&\quad \frac{(3\pi g-2a\omega_0\omega\tanh(\frac{\pi h}{2a})-2\pi g\tanh^2(\frac{\pi h}{2a}))}{-(\omega+\omega_0)^2+\frac{g\pi}{a}\tanh[\frac{\pi h}{a}]} \\
A^{62} &= 16ga^2C_0A_0(\omega-\omega_0)\pi\frac{\cosh^2[\frac{\pi h}{2a}]}{\cosh[\frac{n\pi h}{2a}]}\cdot \\
&\quad \frac{(3\pi g-2a\omega_0\omega\tanh(\frac{\pi h}{2a})-2\pi g\tanh^2(\frac{\pi h}{2a}))}{-(\omega-\omega_0)^2+\frac{g\pi}{a}\tanh[\frac{\pi h}{a}]} \\
A^{63} &= 16ga^2C_0^2\omega\pi\frac{\cosh^2[\frac{\pi h}{2a}]}{\cosh[\frac{n\pi h}{2a}]}\cdot \\
&\quad \frac{(3\pi g-2a\omega^2\tanh(\frac{\pi h}{2a})-2\pi g\tanh^2(\frac{\pi h}{2a}))}{-4\omega^2+\frac{g\pi}{a}\tanh[\frac{\pi h}{a}]} \\
A^{64} &= 16ga^2A_0^2\omega_0\pi\frac{\cosh^2[\frac{\pi h}{2a}]}{\cosh[\frac{n\pi h}{2a}]}\cdot \\
&\quad \frac{(3\pi g-2a\omega_0^2\tanh(\frac{\pi h}{2a})-2\pi g\tanh^2(\frac{\pi h}{2a}))}{-4\omega_0^2+\frac{g\pi}{a}\tanh[\frac{\pi h}{a}]}
\end{aligned}$$

The only part left of HS at this stage in the deriv ations, is independent of x. Assume the follo wing form of ϕ_2^7 where superscript 7 refers to HS7 and HS5.

$$\phi_2^7 = A(t)^7$$

This part of the second order potential is independent of x and z.

$$A(t)^7 = A^{71}\sin[(\omega+\omega_0)t] + A^{72}\sin[(\omega-\omega_0)t] + A^{73}\sin(2\omega t) + A^{74}\sin(2\omega_0 t)$$

First the terms with the time dependency $\sin[(\omega+\omega_0)t]$ denoted ϕ_2^{71}.

$$\begin{aligned}
\frac{\partial^2\phi_2^{71}}{\partial t^2} &= -(\omega+\omega_0)^2A^{71}\sin[(\omega+\omega_0)t] \\
&= \mathrm{HS7}^1 \\
&= 16ga^2C_0A_0(\omega+\omega_0)\pi\cosh^2(\frac{\pi h}{2a})\cdot \\
&\quad (\pi g+2a\omega_0\omega\tanh(\frac{\pi h}{2a})+2\pi g\tanh^2(\frac{\pi h}{2a}))\sin[(\omega+\omega_0)t]
\end{aligned}$$

This procedure is repeated for the other time dependencies, giving the following coefficients

$$\begin{aligned}
A^{71} &= -\frac{16ga^2C_0A_0}{(\omega+\omega_0)}\pi\cosh^2[\frac{\pi h}{2a}](\pi g+2a\omega_0\omega\tanh(\frac{\pi h}{2a})+2\pi g\tanh^2(\frac{\pi h}{2a})) \\
A^{72} &= -\frac{16ga^2C_0A_0}{(\omega-\omega_0)}\pi\cosh^2[\frac{\pi h}{2a}](\pi g-2a\omega_0\omega\tanh(\frac{\pi h}{2a})+2\pi g\tanh^2(\frac{\pi h}{2a})) \\
A^{73} &= -\frac{A^2}{4\omega^2}-16ga^2C_0^2\omega\pi\cosh^2[\frac{\pi h}{2a}](\pi g+2a\omega^2\tanh(\frac{\pi h}{2a})+2\pi g\tanh^2(\frac{\pi h}{2a})) \\
A^{74} &= 16ga^2A_0^2\omega_0\pi\cosh^2[\frac{\pi h}{2a}](\pi g+2a\omega_0^2\tanh(\frac{\pi h}{2a})-2\pi g\tanh^2(\frac{\pi h}{2a}))
\end{aligned}$$

The first term in the expression for A^{73} comes from HS5. The total expression for ϕ_2 is now in place.

T o find the remaining part of Φ_2, ϕ_2^*, the boundary conditions on the walls are basis.

$$\begin{aligned}\left.\frac{\partial\phi_2^*}{\partial x}\right|_{x=\pm a} &= -A\sin(\omega t)\left.\frac{\partial^2\phi_1}{\partial x^2}\right|_{x=\pm a} \\ &= \pm\frac{\pi^2 A}{8a^2}\left(A_0\sin[(\omega+\omega_0)t]+A_0\sin[(\omega-\omega_0)t]+C_0\sin(2\omega t)\right)\cosh(\frac{\pi h}{2a})\end{aligned}$$

This gives for ϕ_2^*

$$\phi_2^* = \frac{\pi A}{4a}\left(A_0\sin[(\omega+\omega_0)t]+A_0\sin[(\omega-\omega_0)t]+C_0\sin(2\omega t)\right)\cos(\frac{\pi x}{2a})\cosh(\frac{\pi(z+h)}{2a})$$

This potential does not satisfy the combined free surface condition, and another potential must be added so that the total in sum satisfies this condition. The additional potential $\phi_2^{'}$ must satisfy

$$\left.\frac{\partial\phi_2^{'}}{\partial x}\right|_{x=\pm a} = 0 \quad , \quad \left.\frac{\partial\phi_2^{'}}{\partial z}\right|_{z=-h} = 0$$

$$\frac{\partial^2\phi_2^{'}}{\partial t^2}+g\frac{\partial\phi_2^{'}}{\partial z} = -\left(\frac{\partial^2\phi_2^*}{\partial t^2}+g\frac{\partial\phi_2^*}{\partial z}\right) \quad , z=0$$

The right hand side of this last equation is written out and the Fourier series expansion of $\cos(\frac{\pi x}{2a})$ is utilized. The following form is assumed for $\phi_2^{'}$

$$\phi_2^{'} = \sum_{n=0}^{\infty} B(t)_n\cos(\frac{n\pi x}{a})\cosh[\frac{n\pi(z+h)}{a}]$$

$$B(t)_n = B_n^1\sin[(\omega+\omega_0)t]+B_n^2\sin[(\omega-\omega_0)t]+B_n^3\sin(2\omega t)$$

The equation originating from the free surface condition is

$$\begin{aligned}\left(\frac{\partial^2\phi_2^{'}}{\partial t^2}+g\frac{\partial\phi_2^{'}}{\partial z}\right)_{z=0} &= \frac{A\pi}{4a}\cos(\frac{\pi x}{2a})\cosh(\frac{\pi h}{2a})\cdot \\ &\{[-A_0(\omega+\omega_0)^2\sin[(\omega+\omega_0)t]-A_0(\omega-\omega_0)^2\sin[(\omega-\omega_0)t] \\ &-4C_0\omega^2\sin(2\omega t)] \\ &+\tanh(\frac{\pi h}{2a})\frac{\pi g}{2a}\left[A_0\sin[(\omega+\omega_0)t]+A_0\sin[(\omega-\omega_0)t]+C_0\sin(2\omega t)\right]\}\end{aligned}$$

The terms with the time dependency $\sin[(\omega+\omega_0)t]$ are denoted $\phi_2^{`1}$.

$$\begin{aligned}\left(\frac{\partial^2\phi_2^{`1}}{\partial t^2}+g\frac{\partial\phi_2^{`1}}{\partial z}\right)_{z=0} &= \sum_{n=0}^{\infty}B_n^1\cos[\frac{n\pi x}{a}]\cosh[\frac{n\pi h}{a}]\{-(\omega+\omega_0)^2\\ &\quad +\frac{g\pi n}{a}\tanh[\frac{n\pi h}{a}]\}\sin[(\omega+\omega_0)t]\\ &= \frac{AA_0\pi}{4a}\cosh(\frac{\pi h}{2a})(-(\omega+\omega_0)^2+\frac{g\pi}{2a}\tanh[\frac{\pi h}{2a}])\cdot\\ &\quad \frac{4}{\pi}\left(\frac{1}{2}+\sum_{n=1}^{\infty}\frac{(-1)^n}{(2n-1)(2n+1)}\cos(\frac{n\pi x}{a})\right)\sin[(\omega+\omega_0)t\end{aligned}$$

This procedure is repeated for the other time dependencies, and the coefficients are found to be

$$\begin{aligned}B_0^1 &= \frac{AA_0}{2}\cosh[\frac{\pi h}{2a}](1-\frac{g\pi}{(\omega+\omega_0)^2}\tanh[\frac{\pi h}{2a}])\\ B_n^1 &= AA_0\frac{(-1)^{n+1}}{(2n-1)(2n+1)}\frac{\cosh[\frac{\pi h}{2a}]}{\cosh[\frac{n\pi h}{a}]}\frac{-(\omega+\omega_0)^2+\frac{\pi g}{2a}\tanh[\frac{\pi h}{2a}]}{-(\omega+\omega_0)^2+\frac{n\pi g}{a}\tanh[\frac{n\pi h}{a}]} \quad n>0\\ B_0^2 &= \frac{AA_0}{2}\cosh[\frac{\pi h}{2a}](1-\frac{g\pi}{(\omega-\omega_0)^2}\tanh[\frac{\pi h}{2a}])\\ B_n^2 &= AA_0\frac{(-1)^{n+1}}{(2n-1)(2n+1)}\frac{\cosh[\frac{\pi h}{2a}]}{\cosh[\frac{n\pi h}{a}]}\frac{-(\omega-\omega_0)^2+\frac{\pi g}{2a}\tanh[\frac{\pi h}{2a}]}{-(\omega-\omega_0)^2+\frac{n\pi g}{a}\tanh[\frac{n\pi h}{a}]} \quad n>0\\ B_0^3 &= \frac{AC_0}{2}\cosh[\frac{\pi h}{2a}](1-\frac{g\pi}{\omega^2}\tanh[\frac{\pi h}{2a}])\\ B_n^3 &= AC_0\frac{(-1)^{n+1}}{(2n-1)(2n+1)}\frac{\cosh[\frac{\pi h}{2a}]}{\cosh[\frac{n\pi h}{a}]}\frac{-4\omega^2+\frac{\pi g}{2a}\tanh[\frac{\pi h}{2a}]}{-4\omega^2+\frac{n\pi g}{a}\tanh[\frac{n\pi h}{a}]} \quad n>0\end{aligned}$$

The total second order potential is

$$\Phi_2=\phi_2+\phi_2^*+\phi_2^{`}$$

Appendix E

Sloshing experiments DNV

This appendix is meant to show the availabilit y of experimental data after the series of experiments conducted at Det Norske Veritas at Høvik during the spring of 1998.

A rectangular tank with dimensions given in Fig. E.1 was forced to oscillate harmonically in the horizontal direction in the cross-sectional plane, referred to as sway. The width of the tank is 0.2m.

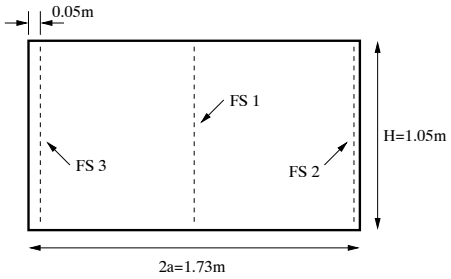

Figure E.1: Rectangular tank

The collected data consists of the horizontal motion of the tank and the free surface elevation at three positions, denoted FS1, FS2 and FS3. These are indicated in Fig. E.1. The sampling frequency was 50Hz. The sloshing motion was captured on video, and at specific time instances pictures were taken. The instantaneous free surface elev ation shown in the pictures can be related to the time history for the sw aymotion and w aveprobe measurements. Figure E.2 sho ws an example of the time history for the sway motion of the tank and free surface elevation

at the right tank wall. The moment the camera was triggered is also indicated in the plot. The camera shutter is opened and a picture taken after a delay of 0.226s. The tank is filled with 50cm of water and the sway period is 1.54s.

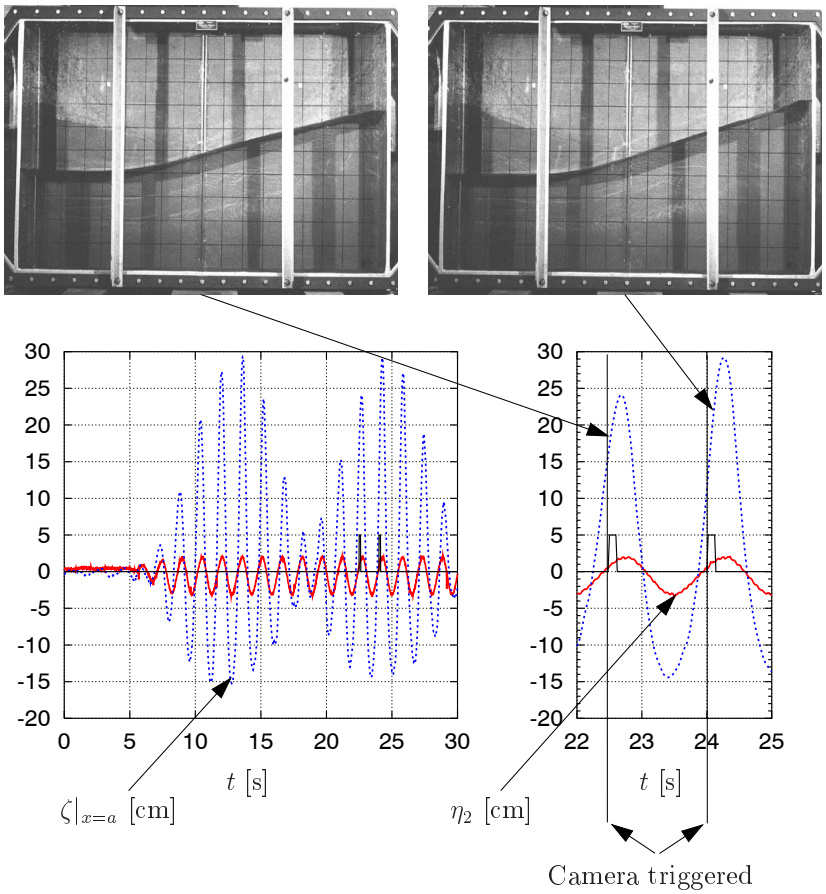

Figure E.2: Typical measurement of free surface elevation at the right tank wall $\zeta|_{x=a}$, the sway motion η_2 and instances for triggering the camera. $x = 0$ in the middle of the tank.

The waveprobes used in the tank are a combination of a cylindrical sensor, FS3, of 3mm diameter and sensors, FS1 and FS2, made by two parallel 5mm wide strips of metal tape. They are capacitive sensors and give as output the instantaneous elevation of the free surface. The sensors made from tape are fixed to the tank wall, while FS3 stands vertically 5cm from the left wall. The surface tension effects matter close to the probes. For the circular probe, an error in the free surface elevation measurements within $\approx$ 1mm is expected. Adherence of water to the wall and metal tape was not found to be a problem for the other probes. The calibration of the probes was performed by gradually emptying and filling the tank while collecting data. The

calibration factor was found to be stable, but a slow drift of the zero value was discovered. This is not a problem since the series of measurements always start with a calm free surface so that the zero level is known. The availability of pictures and video gives the opportunity to control the free surface measurements.

E.1 Set of parameters studied

Tables E.1 present the set of parameters for which runs with data sampling were made. A measure of the effect used as input to the sway motion mechanism is included. The sway amplitude in centimeters is roughly 6.4 times this number, but the relation is not perfectly linear and the factor also varies slightly with filling level. The most used effect of 0.8 results in a sway amplitude of ≈ 5.1cm. The exact time history of the sway motion is as mentioned a part of the sampled data for each run. Video was taken at a different time and thus separate tables, E.2, are presented where the combination of filling level, sway amplitude and sway period captured on video is given.

T able E.1: Run parameters for sloshing experiments

50 cm filling		
P eriod [s]	**Effect**	**# Pics**
0.91	0.8	4
1.0	0.4	4
1.0	0.8	5
1.1	0.8	2
1.25	0.4	3
1.25	1.0	6
1.4	0.8	2
1.43	0.2	2
1.43	0.4	5
1.43	0.8	7
1.5	0.8	2
1.54	0.4	3
1.6	0.8	2
1.667	0.1	4
1.667	0.2	7
1.667	0.3	9
1.667	0.4	7
1.7	0.8	2
1.74	0.1	7
1.74	0.8	3
1.82	0.1	6
1.82	0.2	2
1.89	0.2	4
1.89	0.4	4
1.9	0.8	1
2.0	0.4-0.7	7
2.0	0.7	3
2.0	0.9	9
2.0	0.5	4
2.2	0.8	2
2.22	0.4	2
2.22	0.8	3
2.5	1.0	5

20 cm filling		
Period [s]	**Effect**	**# Pics**
1.9	0.8	2
2.0	0.8	1
2.1	0.8	5
2.2	0.8	2
2.3	0.8	6
2.4	0.8	1
2.5	0.8	11
2.7	0.8	5
3.0	0.8	3

30 cm filling		
Period [s]	**Effect**	**# Pics**
1.5	0.8	3
1.6	0.8	2
1.7	0.8	6
1.8	0.8	6
1.9	0.8	6
2.0	0.8	5
2.1	0.8	5
2.2	0.8	6
2.3	0.8	4
2.4	0.8	1

60 cm filling		
Period [s]	**Effect**	**# Pics**
1.1	1.32	2
1.2	1.32	4
1.3	1.32	2
1.4	1.32	3
1.5	1.32	4
1.6	1.32	8
1.7	1.32	8
1.9	1.32	2
2.0	1.32	3
2.1	1.32	5
2.3	1.32	3

T able E.2: Run parameters for sloshing experiments - only video taken

10 cm filling		
P eriod[s]	**Effect**	**Video [m:s]**
3.5	0.8	1:45

20 cm filling		
P eriod[s]	**Effect**	**Video [m:s]**
1.33	08	1:08
1.8	0.8	1:33
2.0	0.8	1:20
2.1	0.8	1:22
2.2	0.8	1:22
2.3	0.8	1:10
2.4	0.8	1:30
2.5	0.8	1:29
2.7	0.8	1:20
3.0	0.8	1:11

30 cm filling		
P eriod[s]	**Effect**	**Video [m:s]**
1.1	0.8	1:30
1.17	0.8	1:00
1.6	0.8	1:15
1.7	0.8	1:15
1.8	0.8	1:06
1.9	0.2	2:00
1.9	0.8	3:09
2.0	0.8	3:08
2.1	0.8	3:08
2.2	0.8	3:13
2.3	0.8	1:07
2.5	0.8	1:19

50 cm filling		
P eriod[s]	**Effect**	**Video [m:s]**
1.0	0.5	1:30
1.0	1.0	1:30
1.0	1.5	1:30
1.666	0.3	1:0
1.666	0.4	5:0
1.75	0.05	1:30
1.82	0.05	2:0
1.82	0.1	2:0
1.82	0.15	2:0
2.0	0.4	3:00
2.0	0.6	3:00
2.0	0.8	3:00
2.22	0.8	2:00
2.22	1.2	2:00
2.5	1.0	0:30
2.5	1.4	1:0

60 cm filling		
P eriod[s]	**Effect**	**Video [m:s]**
1.0	1.32	2:0
1.1	1.32	2:0
1.2	1.32	2:0
1.3	1.32	2:0
1.4	1.32	2:0
1.5	1.32	2:0
1.6	1.32	2:0
1.8	1.32	1:0
2.0	1.32	2:0
2.1	1.32	2:0
2.3	1.32	1:0
1.6	0.50	2:0
1.9	0.50	2:0
2.1	0.50	2:0